ELECTRONIC DEVICE FABRICATION FROM THIN FILM DIAMOND: SURFACE PREPARATION, PATTERNING, METALLISATION AND CHARACTERISATION

Simon Sui Man Chan

This thesis is submitted for the degree of Doctor of Philosophy.

Department of Electronic and Electrical Engineering
University College
University of London
JULY 1996

UNIVERSITY OF LONDON

Abstract of Thesis

ELECTRONIC DEVICE FABRICATION FROM THIN FILM DIAMOND: SURFACE PREPARATION, PATTERNING, METALLISATION AND CHARACTERISATION

The unique combination of the material properties of diamond as predicted by theory suggests that numerous fields of applications may benefit from its development. Natural and synthetic crystals grown within the extreme conditions required for crystallisation in the thermodynamically stable regime results in material where the size, shape and expense has proved to be prohibitive for many applications. The synthesis of diamond by the technique of chemical vapour deposition in the metastable phase permits thin films of this material to be deposited over sufficient substrate areas and geometries for new applications to be considered. Of particular interest in this thesis is the electronic properties of semiconducting thin films of diamond, and the development of elements essential towards the routine fabrication of reliable devices based on standard integrated circuit fabrication techniques. With this aim, the theoretical properties of diamond pertaining to electronic applications are summarised; investigations within the literature considering the superiority over present semiconducting materials are also discussed. Such levels of performance are compared to the current status of semiconducting thin film diamond.

Characterisation of thin film diamond with particular emphasis on the electronic properties of current state-of-the-art material has been carried out via the surface and bulk analytical techniques of Auger electron spectroscopy, Raman scattering spectroscopy, scanning electron microscopy and Hall-effect measurements; the limitations of this material are identified. Surface investigations undertaken show that the as-deposited state of such films may be graphitic in nature; proper material preparation prior to the fabrication of electronic devices is considered a pre-requisite in order to achieve reliable device behaviour. Contact metallisations on properly prepared material display a bulk dependence; the requirements for rectification are demonstrated and discussed. Both rectifying and non-rectifying electrical contacts have been developed to a state where stable operation at room and elevated temperatures prevail. In view of the present lack of a routine patterning method, the excimer-laser based technique of projection patterning has been studied in terms of operational parameters, and both surface features and bulk microstructures have been created. The nature of the material after laser processing is fully characterised. Thin film diamond field-effect transistors capable of operation under high temperature ambients have been designed and fabricated based on the principles derived here; the performance of future electronic device structures is discussed in view of required improvements in fabrication technique and material requirements.

ACKNOWLEDGEMENTS

In the memory of my father, and to my mother, brothers and sisters (+in-laws), cousins (LWT, YCC), and the extended family; this is for you guys and I hope you flick through the pages one of these days!

Financial considerations fortunately, or not, always come foremost to mind, and so the assistance of the government in the guise of the Engineering and Physical Sciences Research Council (originally Science and Engineering Research Council) or whatever the powers that be choose to call themselves is gratefully acknowledged for supporting my extended period in higher education. A British Vacuum Council's travel grant has enabled a presentation at the Diamond Films '95 European Conference in Barcelona.

All those with whom I have been connected at the Rutherford Appleton Laboratory (another institution going through many name changes) via my CASE award have been of immense help (at least two chapters worth!); most notable have been Graham Arthur who provided a wealth of advise on practical issues with the laser system, Frank Raybould for his much appreciated assistance, and to my CASE supervisor Francis Goodall. Many other establishments have provided their equipment, expertise and effort in some capacity; the Semiconductor IRC at Imperial College (Jeff Harris *et al.*) have kindly allowed access to Hall equipment, and the Defence Research Agency (Malvern) via the late Don Rodway, a genuinely helpful man, for Raman facilities and diamond wafers. Of special mention are Paul Chalker and Colin Johnston of AEA Technology (Harwell) for their useful discussions/comments regarding aspects connected with this work, and for all the diamond wafers that they have provided over the past few years.

Closer to home, the expertise of various staff at UCL have made the progress of my work move at a more steady pace; these include the 9th floor clean room staff of Kevin Lee, David Prescott and to Fred Stride for their helpful advice. Others include Alan and Trevor of the workshop, Manju, Tony Kenyon for scanning facilities and "my woman" and the Big-Man at Senate House for those chips. All the keen footballers past and present with whom I have scrapped with in Regents Park, the Lard Society ("by invitation only"), and all other bods (*e.g.* Sagar Patel) who have shown that it is OK to talk non-scientifically while being a postgrad.

My colleagues and friends (going a bit far here...) who form the ever-changing Diamond Electronics Group (formerly the DESSG!) have provided, at very selective times, a good environment in which to conduct scientific research; these include Robert McKeag (for his special brand of jokes), Mike Whitfield (for social-political discussions with Iain Davies, and for knowing the X-section of.....well, *barns*), Bhaswar Baral for making dud paper planes and Lisa Pang for believing in those transistors. The original 'the boy' Lye-Hing Chua for Senate House discussions and for showing that there really is life after UCL. Duncan Marshall, a short-haired easy-to-beat-up guy for beating me once or possibly twice at those games of chess which took place after office hours, obviously; cheers Duncs for showing me my data-logging/stamp-collecting position in life with "Katz '35", and looking forward to those 20 pints, mate!

And finally, to how it all began, a short talk with Richard B Jackman, the team leader and my "Boss"; a man of endless enthusiasm and energy bordering on hyperactivity, couldn't catch up with him on the stairwells on day one....and still can't. Once told me in true proverbial fashion "research isn't easy, but it's fun"...well, that's another story. Here's to semi-colons; ; ; ; ; ; ; ;!

SC, June 1996 (London).

CONTENTS

2. PROPERTIES AND POTENTIAL OF DIAMOND FOR ELECTRONIC APPLICATIONS

3. SYNTHESIS AND CURRENT STATUS OF SEMICONDUCTING THIN FILM DIAMOND

4. EXPERIMENTAL METHODS: CHARACTERISATION, PROCESSING & DEVICE FABRICATION

5. SURFACE PREPARATION AND CHARACTERISATION OF THIN FILM DIAMOND

6. ELECTRICAL CHARACTERISATION OF SEMICONDUCTING THIN FILM DIAMOND

7. NON-RECTIFYING Ti-BASED CONTACT METALLISATIONS TO THIN FILM DIAMOND

8. RECTIFYING CONTACT METALLISATIONS TO OXIDISED THIN FILM DIAMOND

9. PATTERNING OF DIAMOND FILMS BY EXCIMER LASER PROJECTION

10. CHARACTERISATION OF EXCIMER LASER PROCESSED DIAMOND FILMS

11. THIN FILM DIAMOND FIELD EFFECT TRANSISTOR

1: INTRODUCTION

Wide energy bandgap semiconductors such as 3C-SiC (E_g= 2.2 eV) and GaN (E_g= 3.39 eV) are currently under intense study as a result of their basic material properties. These materials are forecast to make significant inroads into a number of specific applications where present semiconductors such as Si (E_g= 1.1 eV) and GaAs (E_g= 1.4 eV) are limited. On current technological trends, increasing demands are being made on electronic device components capable of operating under higher temperature ambients, chemically harsh environments, higher power levels, and as optical materials active in the blue and UV wavelengths. The aerospace, automotive, petroleum and multimedia industries will benefit directly from such developments [*Special Issue*, 1991]. Wide energy bandgap materials may enable these demands to be met as a result of their ability to sustain higher electric fields, and their lower intrinsic charge carrier densities at a given temperature. The investigation of SiC and GaN has led to the development of specific applications: high temperature and high power transistors, ultra-violet photodetectors, and commercial blue light-emitting diodes have been produced from SiC, with potentially superior GaN-based device applications expected to follow [Morkoc, 1994].

The general classification of diamond as an insulator arises from its wide energy bandgap of 5.5 eV. However, the semiconducting properties of a small subset of natural crystals [Custers, 1952] has led to predictions of diamond being a superior wide bandgap semiconductor. The wide bandgap nature and the many favourable mechanical and thermal properties may only provide significant advantages if further understanding of this material is gained. With this aim, practical investigations into the properties of natural crystals have demonstrated good comparisons with predictions from theoretical analysis; however, for the realisation of diamond as an electronic material, the natural form poses many restrictions in terms of economics, quality, functionality and reproducibility. Diamond crystals may also be synthesised by high-pressure high-temperature (HPHT) techniques; these are based on the conversion of various forms of carbon within the thermodynamically stable regime for diamond (*e.g.* 5 GPa, 1500 °C [Bakon, 1993]) but produces material similar to that found in nature. The demonstration of diamond growth within the metastable phase by the technique of chemical vapour deposition (CVD) though, has been of particular significance in the development of diamond as a semiconducting material [see Plano, 1995 for a historical summary]. When compared with HPHT techniques, the requirements of CVD in terms of equipment set-up and operating conditions are minimal: a mixture of methane and hydrogen gas flowing over a heated filament (2000 °C) onto a heated substrate (900 °C) within an evacuated chamber (20 mbar) is sufficient. Furthermore, CVD techniques permit the synthesis of uniform and continuous thin films of diamond over a greater surface area than has been previously achieved. Thus, together with the possible incorporation of acceptor impurities during crystal growth, semiconducting diamond films may be synthesised to allow the formation of electronic applications in a commercially viable manner.

In order to assess the potential of this material for electronic applications, this thesis aims to explore the current state-of-art, and to develop some of the required tools based as far as possible on very-large-scale-integration (VLSI) techniques [Sze, 1988] for the fabrication of reliable electronic devices from thin film diamond. The performance of such prototype devices may subsequently identify the areas required for further development if commercial applications from this material are to be realised. However, for the processing of electronic devices from a "new" material, various aspects have to be considered; these include determination of current properties, post-deposition material treatments, electrical contact formation, device and substrate delineation. Therefore to begin such a work, chapter 2 reviews the "ultimate" properties relevant to electronic applications to provide an indication of the levels of achievement that may be expected. Theoretical predictions within the literature based on these values have also been included. Since many of these properties have yet to be achieved, a review is given of a range of growth techniques together with the electronic properties of films produced by these methods. Chapter 4 is a description of the experimental techniques employed in this thesis for the characterisation and processing of the material and associated test structures and devices. The wide range of growth techniques and conditions have resulted in films with a large variation in the state of the as-deposited surface with consequences on the electrical characteristics; chapter 5 presents results of a surface study of various post deposition treatments and assesses their suitability for fabrication of devices from thin film diamond. Chapter 6 is a study of state-of-the-art diamond films and their corresponding electronic transport characteristics; these are compared with values for natural crystals and theoretical predictions. In chapters 7 and 8, electrical contacts on diamond films are studied as a pre-requisite for active electronic devices; both non-rectifying (chapter 7) and rectifying (chapter 8) are presented with emphasis on their dependence on material properties and their reliability at elevated temperatures. Chapter 9 presents a study of the potential of excimer laser as a source for the patterning of diamond films and explores various process dependent parameters. The non-reactivity of diamond to wet etching demands that dry etching techniques be developed for such pattern delineation. The results of chapter 9 are developed in chapter 10 which characterises the chemical nature of diamond films exposed to deep ultra-violet excimer laser radiation. The techniques developed in many of these chapters have been employed in the design and fabrication of thin film transistor structures operating under the field-effect principle at elevated temperatures: the results of this are presented in chapter 11. Finally, chapter 12 provides an overall summary with proposed further work and discusses the required improvements in device fabrication techniques and material quality.

REFERENCES

Custers, J.F.H., [1952]. *Physica,* **18**, 489.

Morkoc, H., Strite, S., Gao, G.B., Lin, M.E., Sverdlov, B. and Burns, M., [1994]. *J. Appl. Phys.,* **76**, 1363.

Plano, L.S., [1995]. in Diamond: Electronic Properties and Applications, L.S. Pan and D.R. Kania (eds.) (Kluwer Academic Press) Boston, USA.

Special Issue on Wide-bandgap Semiconductors, [1991]. *Proc. IEEE*, **79**.

Sze, S.M. (ed), [1988]. *VLSI Technology*, 2nd edition (McGraw-Hill) New York, USA.

2: PROPERTIES AND POTENTIAL OF DIAMOND FOR ELECTRONIC APPLICATIONS

2.1 INTRODUCTION

The unique combination of extreme properties possessed by diamond have been acknowledged for many centuries; these attributes have been applied to a diversity of applications which have ultimately depended on the size, shape and economic costs of the diamond available at the time, together with the ability to control and modify these parameters to the desired effect. Traditionally, the market consumption for both natural and synthetic industrial diamond (grown by high-pressure high temperature (HPHT) methods) has been estimated to be 65% for abrasives, 20% for micron-sized powders, 10% for drilling diamonds, and 5% for toolstones [Bakon, 1993]. Such applications have typically exploited the excellent mechanical properties of diamond which include it being the hardest known material possessing the highest mechanical strength and room temperature thermal conductivity. The general properties of diamond are summarised in Table 2.1 [extracted from Bachmann, 1991].

The utilisation of either natural or HPHT synthetic diamond is, however, limited by variations in its geometrical dimensions and quality, together with the restrictions imposed by economic costs. The advent of chemical vapour deposition (CVD) methods for the synthesis of diamond *films* at low pressures and temperatures (typically 20 mbar, 1000 °C) though, promises to overcome the difficulties inherent in the more traditional sources of diamond. Diamond films permit the design of applications possessing greater active area with the possibility of wider integration of other material systems. Applications employing these extreme properties either in prototype form or envisaged include wear-resistant tool coatings, multichip module (MCM) packaging [Napolitano, 1993], and optical coatings for lenses and windows [Yoder, 1993]. Further general applications for diamond films have been well documented [Davidson, 1994].

However, it is the potential of diamond as a electronic, semiconducting material which is of interest here. Two developments have been paramount in the current interest for the realisation of applications of diamond in the electronics field; the discovery of semiconducting properties in natural type IIb diamond, together with the ability to deposit doped thin films by CVD techniques over a sufficiently large area amenable to present-day integrated circuit fabrication technology. Indeed, the improvement in thin film diamond growth over the past decade, as discussed in the next chapter, has in part been driven by the desires of the electronic engineer with an aim of circumventing limitations in present day semiconductor technology. Characteristics such as high thermal conductivity, large breakdown field and comparable electron and hole mobilities have been reported. Accepted values for these parameters are displayed in Table 2.2 together with typical values for the more established semiconductors Si and GaAs and values for other wide bandgap materials SiC and GaN; diamond may ultimately possess many superior properties. These electronic properties have led to predictions for order of magnitude improvements in the areas of high power, high frequency and high temperature electronics. The aim of this chapter is to discuss some of the properties of diamond which are relevant for the realisation of electronic applications. Simulation studies which have been carried out by others for the intended purpose of revealing the ultimate potential of diamond as a material for future electronic related applications will be discussed.

Property	Diamond	Notes / comparison
Knoop's Hardness (kg mm^{-2})	7000	hardest material known SiC (2480), Si (850), stainless steel (660)
Coefficient of friction	0.1 (in air)	very low in air
Young's Modulus (10^{11} N m^{-2})	10.35	highest mechanical strength SiC (7), Si (1.9), stainless steel (2)
Sound propagation velocity (km s^{-1})	18.2	1.6 x value of alumina
Chemical inertness		inert to all acids, bases and solvents at room temperature
Range of high transmittance (μm)	0.22-2.5 & > 6	orders of magnitude lower than other materials in infra-red
Refractive index	2.41	1.6 x value of silica
Thermal conductivity @ 300 K (Wcm^{-1}K^{-1})	20	highest value at 300 K Si (2.3), SiC (3.2), Cu (5)
Thermal expansion (10^6 K^{-1})		Si (2.33), SiC (3.3), stainless steel (17.3)

Table 2.1 Selected properties of diamond [extracted from Bachmann, 1991].

Property	Diamond	Si	GaAs	3C-SiC	GaN
Bandgap (eV)	5.45	1.1	1.43	2.2	3.39
Electron mobility (cm^{2}V^{-1}s^{-1})	2000	1500	8500	1000	900
Hole mobility (cm^{2}V^{-1}s^{-1})	1800	600	400	40	150
Breakdown (10^6 Vcm^{-1})	10	0.3	0.4	4	5
Intrinsic resistivity (Ωcm)	10^{16}	10^3	10^9	$>10^9$	$>10^9$
Saturation electron velocity (10^7cms^{-1})	2.7	1	2	2	2.7
Dielectric constant	5.7	11.9	12.8	9.7	9
Work function (eV)	•4.8 (p-type) •-ve ({111} surface)	4.8	4.7	-	-

Table 2.2 Electronic properties of diamond compared with other semiconductors [extracted from Yoder, 1993; Morkoc; 1994].

2.2 CRYSTAL STRUCTURE OF DIAMOND

Carbon is the sixth element in the periodic table and, with an atomic structure of $(1s)^2(2s)^2(2p)^2$, occupies a site in the Group IV column along with the semiconductors silicon and germanium. Rather than be distributed with two electrons in the *s* orbital, it may energetically be more favourable for the 4 valence electrons to be evenly distributed with 1 electron in the *s* orbital and in each of the three *p* orbitals [Kittel, 1986]; this leads to the possibility where the sublevels may form hybridised orbitals capable of covalent bonding. Depending on external conditions, bonding between carbon atoms may then result in the sp^3 hybridised configuration which is the classic "diamond structure" as favoured in crystalline silicon and germanium. However the crystallised carbon may also exist in a number of other allotropic forms depending on the hybridisation favoured *e.g.* graphite (sp^2) or carbyne (sp) [Bakon, 1993]. Mixed bonding within carbon solids may also exist; the class of diamond-like carbons (DLC) consists of sp^2 and sp^3 hybridisations.

The diamond crystal structure is shown in Figure 2.1. The location of six atoms (shaded) in the centre of the faces of the cube along with the corner atoms lead to the face-centred cubic lattice (fcc). The other carbon atoms (unshaded) may be viewed as part of another fcc lattice resulting in the idea of diamond being composed of two inter-penetrating fcc cubic lattices displaced from one another by one quarter of the cube diagonal [Kittel, 1986]. The carbon to carbon bond length and the lattice constant, *a*, have been quoted at 298 K to be 0.154450 nm and 0.356683 nm respectively [Bakon, 1993].

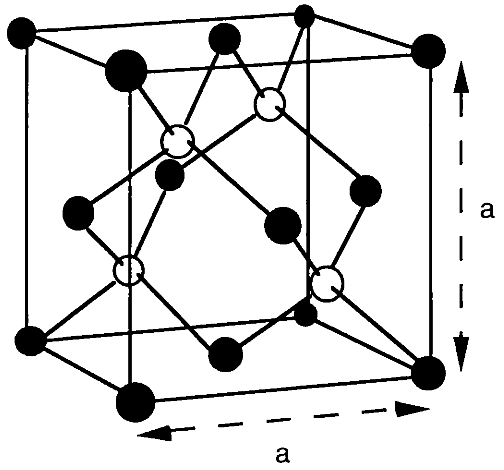

Figure 2.1 Crystal structure of diamond; the shaded circles (centre of atoms) indicate carbon atoms of one fcc lattice structure, whilst the clear circles show carbon atoms of a second inter-penetrating fcc lattice [redrawn from Kittel, 1986]. "a" is the lattice constant.

2.3 ELECTRONIC BAND STRUCTURE OF DIAMOND

The band structure of diamond has been investigated by a number of workers as summarised by Fong and Klein [1995]. The absence of a complete shell between the core and valence states enables carbon to be well represented by the tight-binding model [Wolfe, 1989]; this model, which may be realised by the LCAO (linear combination of atomic orbitals) method, is based on the hypothesis that much of the atomic nature is maintained in the solid. This approximation has been employed by Painter *et al.* [1971] to derive the band structure of diamond as shown in Figure 2.2.

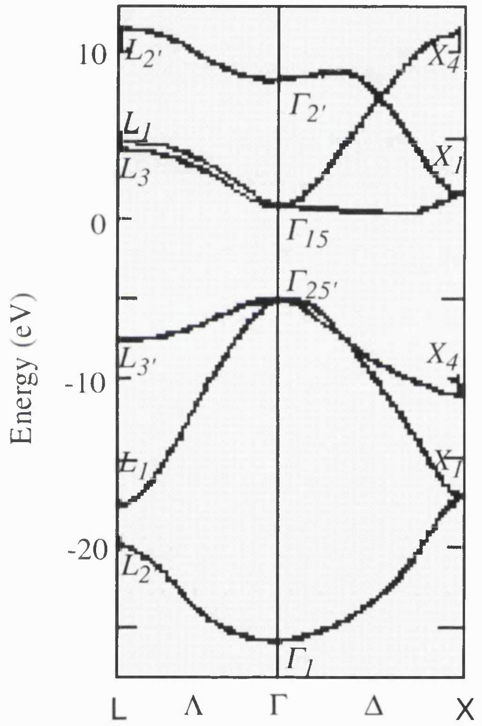

Figure 2.2 Energy-band structure of diamond [redrawn from Painter, 1971].

The structure is characterised by a fairly broad set of 4 valence bands composed of carbon $2s$ and $2p$ orbitals; the lower set of the 4 bands are primarily s-like in nature, with the upper valence band states p-like and the central set displaying the sp^3 hybridization nature [Fong, 1995]. The calculations by Painter *et al.* [1971] which show the valence band maximum, $\Gamma_{25'}$ consisting of two bands (Figure 2.2) has ignored the interaction between the spin and magnetic moment of the orbital motion of electrons. This spin-orbit coupling tends to remove the degeneracy of states [Painter, 1971]; the upper branch of the valence band maximum is then split into two doubly degenerate subbands known as the bands of the "heavy" and "light" holes [Wolfe, 1989]. The degeneracy is then lifted except at the centre of the Brillouin zone *i.e.* at Γ. The lower of the two bands in Figure 2.2 may then shift to lower energies, being termed the split-off band. The excited states of electrons formed by anti-bonding between the valence orbitals [Kittel, 1986] result in a narrow set of conduction bands (~10 eV wide) with an energy separation of 5.4 eV between the valence band maximum at Γ and the conduction band minima sited ~ (0.7, 0, 0) in the **ΓX** direction [Painter, 1971]. Thus, in order for an electron to travel from the valence band maximum to the conduction band minimum requires the interaction of a lattice phonon for the conservation of momentum to be satisfied; hence diamond is an indirect bandgap material. Experimentally the indirect bandgap transition has been measured by Himpsel *et al.* [1980] to be (5.5 +/- 0.05) eV by employing photoemission techniques. The energy separation in the Γ direction between the valence band maximum and the first set of conduction bands was found to be (6.0 +/- 0.2) eV [Himpsel, 1980].

From optical absorption data taken from natural diamond with radiation in the range 5-6 eV, Clark *et al.* [1964] found the indirect band separation to be 5.47 +/- 0.005 eV; this band separation around 600 K was found to display the following temperature dependence:

$$\frac{\partial E_g}{\partial T} = 5.40 - 2.6 \times 10^{-4} eV.K^{-1} \qquad (2.1)$$

2.4 EFFECTIVE MASS OF ELECTRONS AND HOLES

With knowledge of the band structure of a material, the electronic transport properties of the charge carriers within their respective bands, *i.e.* electrons in the conduction band and holes in the valence band, may be approximated. The transport properties, *i.e.* the response of the charge carriers to an applied force (*e.g.* external field) may be determined from a knowledge of the energy of an electron (or hole) within the periodic potential of the lattice; this is given by Wolfe *et al.* [1989]:

$$E(k) = \frac{\hbar^2 k^2}{2m^*} \qquad (2.2)$$

where

$$m^* = \frac{\hbar^2}{{}^{\partial^2 E}\!/\!{}_{\partial k'^2}\Big|_{k=k_0}}. \qquad (2.3)$$

Equation 2.3 is defined as the "effective mass" of electrons at k_0 which is designated the minimum of the of the *E(k)* relation *i.e.* the bottom of the conduction band. In the case of diamond, where the surfaces of equal energy of the conduction band minima are ellipsoidal in nature, the electron effective mass is given in terms of the longitudinal (m_l^*) and transverse (m_t^*) effective masses representing components of the ellipsoid of revolution [Wolfe, 1989]. Table 2.3 compares electron effective mass values for diamond with other semiconductors. The theoretical values by Nava and co-workers [1980] and Fong and Klein [1995] have been derived from band structure calculations. The experimental values have been obtained from a time-of-flight technique for measurement of the ohmic mobility (ratio of drift velocity and applied field) together with the anisotropic nature of the drift velocity at high fields observed along different crystal planes of a type IIa diamond crystal [Nava, 1980].

With six equivalent energy minima in the conduction band, the electron conductivity effective mass (an average value of the electron mass within the conduction band minima) may be estimated from [Hess, 1988]:

$$\frac{1}{m_{e,c}^*} = \frac{1}{3}\left[\frac{1}{m_l^*} + \frac{2}{m_t^*}\right]. \qquad (2.4(a))$$

The density of states electron effective mass, which averages over the whole of the conduction band may be obtained from:

$$m_{e,dos}^* = (m_l m_t^2)^{1/3} \ . \qquad (2.4(b))$$

Material	$(m_l^*) / m_o$	$(m_t^*) / m_o$	$(m_e^*) / m_o$	Reference
Diamond^{theo}	1.24	0.25	-	[Nava, 1980]
Diamond^{theo}	1.665	0.290	-	[Fong, 1995]
Diamond^{expt}	1.4	0.36	-	[Nava, 1980]
Si	0.98	0.19	-	[Shur, 1990]
Ge	1.64	0.082	-	"
GaAs	-	-	0.067	"
InP	-	-	0.08	"
InSb	-	-	0.014	"

Table 2.3 Electron effective mass of selected semiconducting materials including theoretical (^{theo}) and experimental (^{expt}) values for diamond, where m_l^* and m_t^* are the longitudinal and transverse components of the effective mass. m_e^* is the effective mass of materials wherein the constant energy surface of the conduction band minima is spherical in nature. m_o is the free space electron mass.

In a similar manner, the effective mass may be developed for hole carriers at the top of the valence band maxima. Removal of the degeneracy at the top of the valence band maxima leads to values for the upper band designated the heavy hole band (m_{hh}^*), and the light hole band (m_{lh}^*). Some values which have been determined for diamond are summarised in Table 2.4; the values presented by Dean *et al*. [1965] and Williams [Collins, 1979] are experimentally determined average values employing temperature dependent Hall measurements. The effective mass of holes in the split-off band has been estimated by Reggiani *et al.* [1983] to be $0.15m_o$ based on band structure calculations.

Material	m_{hh}^* / m_o	m_{lh}^* / m_o	Reference
Diamond^{expt}	1.1	0.3	[Reggiani, 1979]
Diamond^{theo}	0.614	0.208	[Fong, 1995]
Diamond^{theo}	0.40	0.28	[Lawaetz, 1971]
Diamond^{expt}	1.1	(average value)	[Dean, 1965]
Diamond^{expt}	0.75	(average value)	[Collins, 1979]
Si	0.53	0.16	[Shur, 1990]
Ge	0.35	0.043	"
GaAs	0.62	0.074	"
InP	0.85	0.089	"
InSb	0.47	0.015	"

Table 2.4 Hole effective mass of selected semiconductors , where m_{hh}^* and m_{lh}^* are the effective masses of holes in the heavy hole and light hole bands respectively. m_o is the mass of the electron in free space.

Assuming that the shape of the valence band extreme is spherical in nature, then the conductivity and density of states effective hole mass may be approximated by Equation 2.5(a) and (b) respectively [Han, 1995].

$$m_{h,c}^* = \left(m_{hh}^{3/2} + m_{lh}^{3/2}\right) \Big/ \left(m_{hh}^{1/2} + m_{lh}^{1/2}\right) \tag{2.5(a)}$$

$$m_{h,dos}^* = \left(m_{lh}^{3/2} + m_{hh}^{3/2}\right)^{2/3} \tag{2.5(b)}$$

However, interaction between the two degenerate valence bands and the split-off band results in distortion from this spherical shape; better approximations may be obtained by modelling the valence band as an warped energy surface and details for this have been presented by Han *et al.* [1995] and references quoted therein.

2.5 LOW-FIELD ELECTRON AND HOLE MOBILITY

In a semiconductor, the application of an external electric field produces a shift in the distribution of the equilibrium electron (hole) velocities; when the field is modest, only a small perturbation to this equilibrium occurs [Blakemore, 1986]. The resultant average drift velocity of the charge carriers is then proportional to the applied electric field with the constant of proportionality called the low-field, or ohmic mobility. The mobility of the electron (hole) is given by Equation 2.6(a), and is connected to the electrical conductivity of a material by the expression given in Equation 2.6(b).

$$\mu_{n,p} = \frac{e\langle \tau_m \rangle}{m_{n,p}^{*}} \qquad (2.6(a))$$

$$\sigma = e(n\mu_n + p\mu_p) \qquad (2.6(b))$$

where e is the electronic charge, $\langle \tau_m \rangle$ the momentum relaxation time (mean free time between scattering collisions) averaged over the energy distribution of the carriers, and $m_{n,p}^{*}$ the conductivity effective mass of the electron (n) or hole (p) within the medium. The mobility, or the ability in which charge carriers may move in the application of an electric field, is determined in a perfect crystal (*i.e.* in the absence of structural defects such as dislocations, vacancies and grain boundaries) only by collisions of the charge carriers by any intentionally introduced extrinsic impurities or crystal vibrations (phonons) within the lattice. These scattering mechanisms are incorporated in the mobility definition via the relaxation time in an inverse additive form; for a covalently bonded, non-polar semiconductor like diamond, these may include the following scattering processes: ionised impurity scattering, neutral impurity scattering, and phonon (both acoustic and optical) scattering [Shur, 1990]. At room temperature and low field strengths, the dominant scattering mechanisms in a semiconductor such as silicon (particularly with impurity concentrations greater than 10^{17} cm^{-3}) are those by acoustic phonons and ionised impurities [Hess, 1988]. However, neutral impurity scattering may also have to be accounted for at room temperature if a low ionisation population occurs for extrinsic dopants as is the case for boron introduced into diamond. Calculations such as that by Ferry [1975] has taken these scattering mechanisms into account as well as scattering due to equivalent intervalley phonons; the results for electron and hole mobilities are summarised in Table 2.5. It is interesting to note that the electron mobility value for diamond are at least comparable to those for silicon, and possess a superior hole mobility; furthermore this hole mobility has a comparable value to that for the electron with implications for electronic application identified by *e.g.* Shenai *et al.* [1989] and will be discussed later.

Material	μ_e (cm^{2}V^{-1}s^{-1})	μ_h (cm^{2}V^{-1}s^{-1})	Reference
Diamond^{theo}	2000	-	[Ferry, 1975]
Diamond^{expt}	2300	-	[Nava, 1980]
Diamond^{theo}	-	2100	[Reggiani, 1979]
Diamond^{expt}	2000	1850	[Konorova, 1967]
Diamond^{expt}	1850	1200	[Redfield, 1954]
Si	1350	450	[Smith, 1978]
GaAs	8500	400	[Shur, 1990]
Ge	3900	1900	[Smith, 1978]
InSb	78000	750	[Smith, 1978]
InP	4600	150	[Shur, 1990]
InAs	33000	450	[Shur, 1990]

Table 2.5 Electron and hole low-field mobilities (300 K) of selected materials.

Table 2.5 shows that a reasonably good agreement exists between the experimentally and theoretically determined values of mobility for charge carriers in diamond; the experimental measurements have been obtained using high quality natural crystals though, in such materials, low concentrations of impurities such as nitrogen may be expected(see table 3.1). The limitation in the mobility due to acoustic phonon interaction μ_l and that due to impurity scattering μ_i have been shown to follow the relationships given in Equation 2.7 [Sze, 1981], where m^* is the conductivity effective mass and N_i is the ionised impurity concentration. The dependence of both the electron and hole mobilities thus depend not only on the level of impurities within the crystal lattice but also on the temperature. A comparison of reports has previously been made by Han and co-workers [1995] summarising the temperature dependence of the mobility parameter; in the main, the T$^{-3/2}$ variation was observed by the original authors up to ~400 K indicating the dominance of acoustic phonon scattering. However, at temperatures greater than ~400 K, a more significant deterioration in the mobility has been observed by some authors including Collins [1989] who reported a T$^{-2.9}$ variation.

$$\mu_l \approx (m^*)^{-5/2} T^{-3/2} \tag{2.7(a)}$$

$$\mu_i \approx (m^*)^{-1/2} N_i^{-1} T^{+3/2} \tag{2.7(b)}$$

2.6 HIGH-FIELD CARRIER TRANSPORT

In a semiconductor under the influence of low electric field intensities, the drift velocity of carriers is directly proportional to the applied field in a manner as described by the carrier mobility factor. The energy which the carrier distribution gains from the electric field under low-field intensity conditions is transferred efficiently to the crystal lattice through collisions with low energy acoustic phonons and impurities. This allows both the average energy of the carriers to remain close to the thermal equilibrium value of 3/2kT, with the low-field mobility remaining independent of the applied field [Wolfe, 1989]. However as each electron-phonon collision makes only a small change in the energy of the carrier [Blakemore, 1985], the application of a moderate electric field leads to a situation wherein the effective temperature of the carriers, T_e, is greater than that of the lattice temperature T_{lat}. In such an event, the drift velocity begins to vary in a non-linear fashion as $\sqrt{T_{lat} / T_e}$ [Sze, 1981], and the carriers may then be referred to as "warm". As the electric field is further increased, a saturation of carrier drift velocity is observed due to "hot" carriers possessing sufficient energy to excite a high energy optical phonon mode. A slight increase in the slope of the velocity-field characteristics thereafter is indicative of carriers maintaining an energy greater than the optical phonon mode for an interval of time [Blakemore, 1986].

In the case of diamond, calculations have shown the potential for superior saturated carrier velocities at high fields when compared with other semiconductors of interest; evaluations such as that by Ferry [1975] shows the promise of electron drift velocity of 2.3 x 10^7 cms^{-1} at field strengths of 20-30 $kVcm^{-1}$, a value twice that of silicon and comparable to that of GaAs. Experimental measurements on highly resistive natural diamond has resulted in values saturated carrier velocities of 1.5 x 10^7 cms^{-1} (electrons) and 1.1 x 10^7 cms^{-1} (holes) [Nava, 1980]. The velocity-field characteristics for electrons and holes in various semiconducting systems are shown in Figure 2.3 [Trew, 1991]. The curves show the cases of GaAs and InP where, due to transfer between non-equivalent minima in the conduction band, the value of drift velocity is actually lower than at intermediate electric fields.

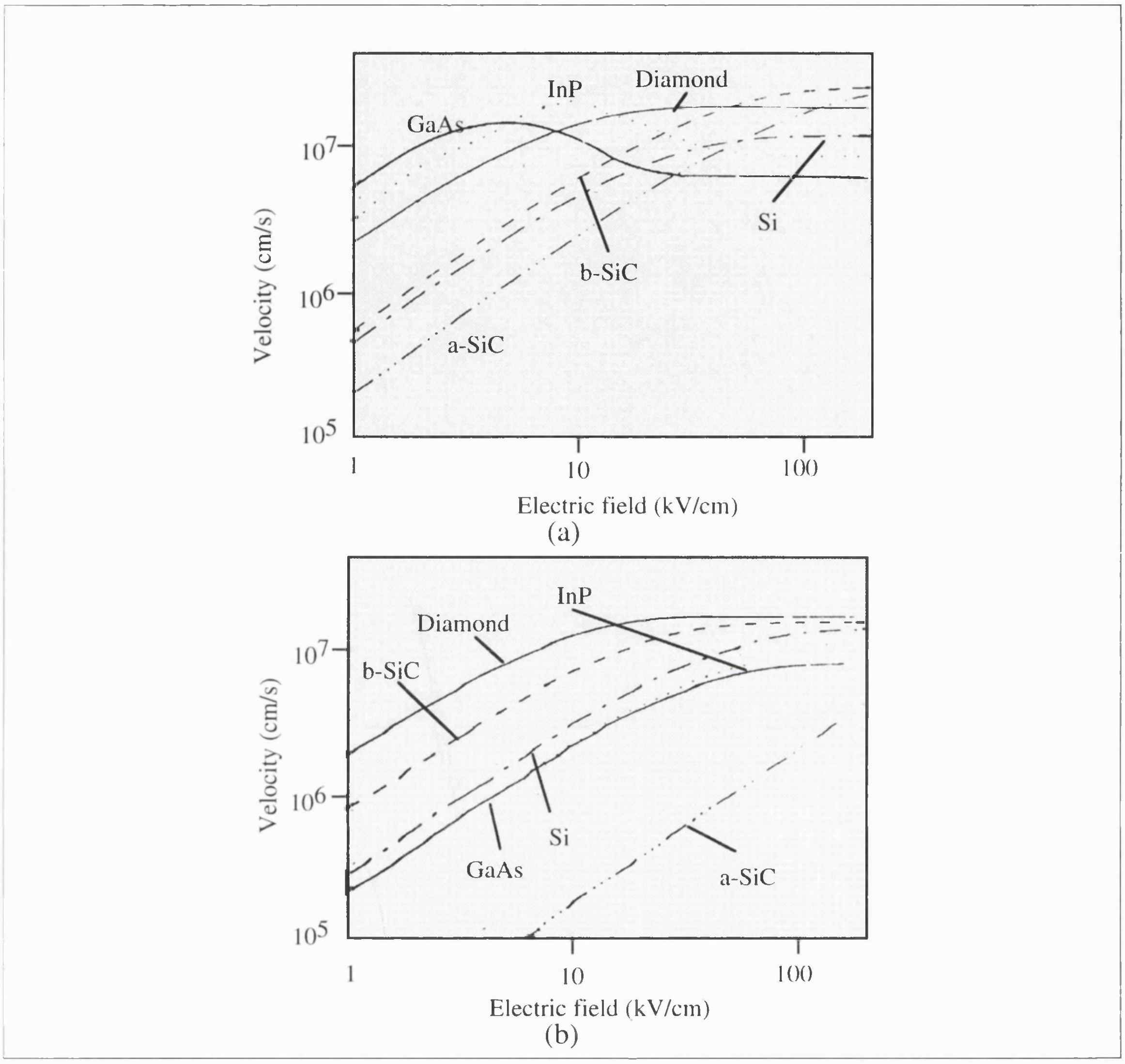

Figure 2.3 Velocity-field characteristics for (a)electrons and (b)holes for various semiconductors at doping levels of 10^{17}cm^{-3} [redrawn from Trew, 1991].

In the event of an increase in the electric field, the possibility exists for some carriers to avoid the optical phonon mode and, instead, gain sufficient energy for the generation of electron-hole pairs in the process of impact ionisation. This breakdown mechanism sets the upper limit of permissible applied voltages in semiconductor devices employing junctions. The breakdown field in diamond has been quoted to exceed 10^6 Vcm^{-1} [Trew, 1991]; this may be compared with characteristic values for Si and GaAs of 3 and 4 x 10^5 Vcm^{-1}, respectively [Sze, 1981]. A large value for the critical breakdown field enables device designs for carriers to be maintained at their saturation velocity, and also allows for the increased output power levels of RF devices as will be discussed later.

2.7 THERMAL PROPERTIES

The thermal conductivity of diamond being 20 $Wcm^{-1}K^{-1}$ at room temperature represents the highest value of any known material; this is demonstrated by the values given in Table 2.6 [Jones, 1992; Eden, 1993]. The thermal conductivity over a range of temperatures has been experimentally determined previously and this is re-presented in Figure 2.4 [Geis, 1988].

Material	Thermal conductivity ($Wm^{-1}K^{-1}$)	Thermal expansion coefficient (wt.ppm K^{-1})	Electrical insulator ?
Diamond (CVD)	700 - 2000	1 - 1.5	Y
Polyimide	0.2	> 50	Y
BeO	223	6.4	Y
AlN	70 - 230	3.3	Y
Si	149	2.6	N
GaAs	45	5.9	Semi
Mo	146	5.1	N
Cu	396	16.8	N

Table 2.6 Thermal properties at 300 K [extracted from Jones, 1992; Eden, 1993].

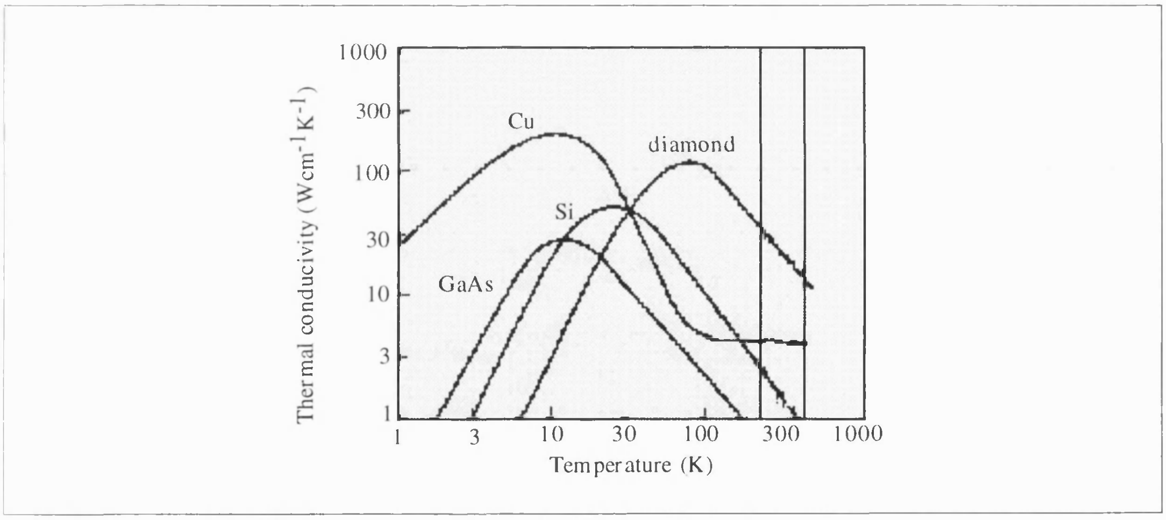

Figure 2.4 Measured thermal conductivity values versus temperature for Ge, Si, GaAs, Cu, SiO_2 and type II diamond [redrawn from Geis, 1988].

For the potential of CVD diamond to be realised, a more comprehensive understanding of the properties of actual films needs to be acquired; the thermal conductivity *K* of a dielectric crystal is dependent on the various phonon scattering mechanisms which include defects resulting from points, lines and surfaces [Anthony, 1994]. Anthony *et al.*

synthesised diamond by a two stage CVD/high pressure process to obtain diamond containing only 0.1 % ^{13}C (as opposed to the 1.1 % typical in natural crystals) with a thermal conductivity value of 33 Wcm^{-1}K^{-1} thus demonstrating that superior properties may be acquired from synthetic material if the process is controlled. However in CVD material, it is the polycrystalline nature of the material which may be of prime concern [Seal, 1994]. Thermal conductivity has been shown to vary as a function of the grain size of crystallites within the films; a value of 21 Wcm^{-1}K^{-1} at the growth surface of a 350 μm thick film has been measured compared with 7 Wcm^{-1}K^{-1} near the substrate interface [Graebner, 1992]. These authors also demonstrated an anisotropy in thermal conductivity in the parallel and perpendicular directions to the film plane (50% higher in the perpendicular plane) as well as an inverse proportionality to the Raman linewidth.

2.8 THE POTENTIAL OF DIAMOND FOR ELECTRONIC APPLICATIONS

The unique combination of properties of diamond have been considered by others [Shenai, 1989; Geis, 1991; Baliga, 1982; Collins, 1989] for the potential introduction into a wide range of applications encompassing the areas of high power, high frequency and high temperature electronics. In order to appreciate the extent of this potential advantage of diamond over other material systems for electronic applications, various parameters and figures of merit have been devised as a measurement of the ultimate performance possible. Investigations of such nature have tended to focus on the Johnson, Keyes and Baliga figure of merits, relating various issues of concern including the operating frequency, output power, and possible thermal limitations. Other features previously considered by workers within the field include both the ultimate temperature of operation as dictated by material properties in device components such as pn junctions and Schottky rectifiers, and the probable performance at these conditions.

2.8.1 Figures of merit: Johnson, Keyes, and Baliga

A system for predicting the performance limits of transistors as determined solely by the physical properties of a semiconducting material and independent of design details has been proposed by E.O. Johnson [1965]. The investigation was based on a model of charge carriers traversing the base region of a transistor and resulted in an expression which relates the operating power and frequency in such a device structure; this was found to be related to the dielectric breakdown field of the semiconductor E_M and the saturated carrier velocity v_s of the charge carriers. The Johnson figure of merit (JFOM) is given in

Equation 2.8; where P_M is the maximum operating power at the cut-off frequency, f_T, and X_C is the channel reactance at this frequency. The JFOM stipulates that there is a maximum operating power at a chosen frequency of operation and that this relationship is governed by material parameters.

$$JFOM = P_M X_C f_T^{\ 2} = \left[\frac{E_M v_s}{2\pi}\right]^2 \qquad (2.8)$$

Instead of the power-frequency considerations as discussed by Johnson, a figure of merit was developed by Keyes (KFOM) which considers the thermal limitations of a material system on the high frequency performance of devices. In the consideration of circuit parameters such as the desired operating power and the maximum permissible temperature rise, it is possible for a minimum device size to be dictated and, through a dependence of drift region length and the time of traversal of charge carriers, a maximum frequency of operation may be specified which is dependent on material parameters in the following manner [Keyes, 1972]:

$$KFOM = \lambda\left[\frac{c v_s}{4\pi\varepsilon_r}\right]^{1/2} \qquad (2.9)$$

; where λ is the material thermal conductivity, ε_r the relative permittivity of the material, c the speed of light in free space and v_S the saturation velocity of the carriers.

Values for both the Johnson and Keyes figure of merit have been calculated and tabulated in a normalised form by Shenai *et al.* [1991] for various semiconductors at 300 K; this is reproduced in Table 2.7.

Material	ε_r	E_M	v_S	λ	JFOM	KFOM
Si	1	1	1	1	1	1
Ge	1.36	0.54	0.60	0.40	0.1	0.27
GaAs	1.09	1.08	2.0	0.31	4.67	0.41
GaP	0.94	1.89	2.0	0.33	14.3	0.49
6H-SiC	0.85	8.1	2.0	3.3	262	5.1
Diamond (n)	0.47	18.9	2.7	13.3	2601	32

Table 2.7 Johnson [1965] (JFOM) and Keyes [1972] (KFOM) figures of merit (300 K) normalised against silicon for a number of semiconducting materials. The symbols are defined in the text [reproduced from Shenai, 1989].

In power semiconductor based systems, the power MOSFET (metal-oxide-semiconductor filed-effect transistor) has become popular in many applications due to its inherent high switching speed and high input impedance. Baliga [1982] proposed a figure of merit (BFOM) as a theoretical guideline to determine the physical properties of a material which govern the power losses in such devices; the sole element of loss was considered to be the conduction loss in the ON-state. Subsequently a modified expression, the Baliga high-frequency FOM [Baliga, 1989], included switching losses due to the charging and discharging of device input capacitance during high frequency operation, and is based on a junction field-effect transistor (JFET) though is also applicable for the MOSFET structure provided the gate oxide capacitance greatly exceeds the depletion capacitance. The BFOM and the BHFFOM are given in Equations 2.10(a,b) respectively; where E_G is the energy bandgap, V_G the gate voltage, μ the low field mobility, ε_r the relative permittivity, E_M and V_B the field and voltage at breakdown. Baliga [1989] also estimated the minimum power loss (P_{min}) and corresponding active JFET structure device area (A_{min}) based on the dominant power loss mechanisms being conduction and switching; these values are reproduced in Table 2.8.

$$BFOM = \varepsilon_r \mu E_G^{\,3} \qquad (2.10(a))$$

$$BHFFOM = \frac{\mu E_M^{\,2} V_G^{\,1/2}}{2 V_B^{\,3/2}} \qquad (2.10(b))$$

Material	E_M	μ	BFOM	BHFFOM	A_{min}	P_{min}
Si	1	1	1	1	1	1
GaAs	1.29	5.7	13.3	9.5	0.241	0.325
6H-SiC	8.1	0.2	106.3	13.1	0.037	0.276
Diamond (n)	18.9	1.27	8574	453.7	0.004	0.047
Diamond (p)	18.9	1.00	6751	357.2	0.004	0.053

Table 2.8 Baliga (BFOM, BHFFOM) figures of merit at 300K for a number of semiconductors, with the values being normalised to that of silicon. The symbols are defined in the text [reproduced from Baliga, 1989].

A study carried out by Shenai *et al.* [1989] to investigate the drift region conductance, the ultimate frequency of operation and the thermal limitations in power devices based on abrupt p-n junctions reached similar conclusions; for devices with identical breakdown levels, the drift region conductance was found to be 3 orders of magnitude greater than that of silicon in accordance with Baliga [1989]. A feature considered of particular relevance for electronics was that of the comparable values shown for both n- and p-type material;

such a property, as indicated by the comparable hole and electron mobilities, may allow for the possibility of high performance complementary power devices as well as simplifying the design of control circuitry [Shenai, 1989]. Shenai *et al.* [1989] further proposed that although the maximum frequency of operation of power devices with equal area may be increased sevenfold for GaAs over Si devices, a fifty-fold improvement may be projected for diamond. Such figures compare well with those obtained by the Keyes figure of merit which predicted slightly lower values, though in that case the effect of thermal conductivity was accounted for.

Trew *et al.* [1991] have taken the specific example of the metal semiconductor field-effect transistor (MESFET) and modelled its performance with diamond, SiC and GaAs as the active substrate material. The model accounted for device dimensions, operation in the saturated carrier velocity regime, matching of the device to an external circuit, and the effect of temperature rise on the thermal resistance of the device. A specific contact resistivity for the source and drain of 10^{-4} Ωcm^2 was considered sufficient for operation in the microwave regime (approximately 3-300 GHz). The predictions for diamond and SiC are shown in Figure 2.5 together with experimental data for GaAs. In the X-band (8-12 GHz), diamond MESFETs are predicted to be capable of producing 200 W of power as compared with 8 W for comparable GaAs devices. At higher frequencies of 100 GHz, diamond may produce up to 1 W.

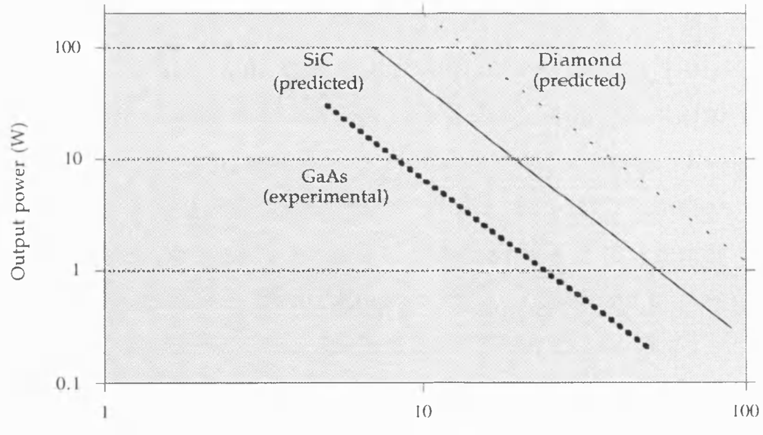

Figure 2.5 RF power performance versus frequency for diamond, SiC and GaAs MESFETs [redrawn from Trew, 1991].

2.8.2 Considerations for high temperature operation

The wide bandgap and high thermal conductivity of diamond promises the potential for high temperature electronic applications; the temperature at which a material becomes intrinsic, *i.e.* at thermal energies wherein electrons may be excited across the bandgap, has been calculated for a range of materials including Si (600 K), GaAs (900 K), 6H-SiC (1300 K), and diamond (3000 K) [Shenai, 1989]. Si-based power semiconductor devices are limited in their operating capability to temperatures of ~200 °C [Shenai, 1989], with GaAs power devices predicted to extend this by a factor ~1.3, due to limitations imposed by the thermal conductivity of the material [Baliga, 1981]. In fact, in order for high temperature operation to be realised, two further considerations have been identified by Shenai *et al.* [1989]. These are (i) the effect of high ambient temperatures on device conductivity in the ON-state of a device arising from possible material changes; and (ii) the effect of intrinsic thermal leakage currents on power dissipation in the OFF-state. The conductance of a material is dependent not only on the mobility of the charge carriers in the system, but also on the number of charge carriers (Equation 2.4). Thus in order to investigate the temperature variation of the electrical conductance of a material, a knowledge of the variation of these two factors with temperature are required.

The temperature variation of carrier mobility has been modelled by many groups *e.g.* [Ferry, 1975; Nava, 1980; Reggiani, 1979; 1981; Collins, 1989] based on curve fitting to experimental results on natural diamond crystals. Ferry [1975] and Nava *et al.* [1980] both found the theoretically predicted $T^{-3/2}$ electron mobility dependence for temperatures less than 400 K, indicating a mobility characterised by acoustic phonon scattering as suggested by Equation 2.5. However at temperatures >400 K, a more severe degradation of the mobility was observed; this was suggested to be the onset of intervalley phonon scattering [Nava, 1980]. The mobility of the hole carriers has also been observed to display such a tendency for degradation at elevated temperatures; Reggiani *et al.* [1979; 1981] have observed in natural diamond a $T^{-1.5}$ acoustic phonon limited mobility dependence up to 400 K, followed by a $T^{-2.8}$ relationship at greater temperatures. A similar result has been reported by Collins [1989]. Near room temperature mobility (electron/hole) dependence have been quoted for Si and GaAs as ($T^{-2.42}/T^{-2.2}$) and ($T^{-1.0}/T^{-2.1}$), respectively [Sze, 1981, p28].

Although the rate of this decrease in the mobility of charge carriers at higher temperatures has a significant effect for proposed applications, the implication on high temperature operation may in fact be partially compensated by the relatively deep acceptor levels in boron doped material (activation energy of 0.37 eV). Whereas in a system containing shallow dopants the extrinsic carrier population is near fully ionised at room temperature and any reduction in the carrier mobility leads to an overall reduction in the electrical conductance of the system, in boron doped diamond at higher temperatures the increase in ionised impurities leads to an increase in the population of charge carriers. The overall effect of this on the electrical conductance of a semiconducting system has been modelled by Collins [1992] accounting for this deep level acceptor state. Using a mobility value for diamond of 290 $cm^2V^{-1}s^{-1}$ (acceptor concentration of $8x10^{17}$ cm^{-3}) together with a mobility deterioration of $T^{-2.9}$ from 290 K, the conductance of one-sided diodes made from Si, GaAs and diamond with respective gate lengths of 5, 5.4 and 0.3 μm was found by Collins [1993] to follow that depicted in Figure 2.6. From this result, it is evident that the material resistance at room temperature is greater than that for silicon, and it is not until temperatures of 350 K and 450 K that the conductance of the diamond device is superior to similar Si and GaAs devices, respectively. Indeed, in the temperature range 450-1000 K, the conductance level is shown to be greater than, or at least equal to that of the conductance levels of GaAs at room temperature. In this view, specific diamond electronic applications such as power devices operating at the condition of saturated velocity in the high temperature regime (at least to 700 °C), are not expected to be limited by the decrease in mobility at elevated temperatures. In the design of diamond electronic applications at temperatures greater than 100-200 °C when the mobility starts to decline at $T^{-2.8}$, it would thus be appropriate to ensure operation the saturated velocity regime with the application of sufficient field strengths. Trew *et al.* [1991] have shown that the shortening of the gate length for a fixed drain-source bias (*i.e.* increasing the electric field across the device) in power MESFET devices results in a less stringent requirement in the material mobility to prevent limitations in the output power efficiency; for operation at 10 GHz and 10 V drain-source bias, a 1 μm gate length requires a mobility value of 1500 $cm^2V^{-1}cm^{-1}$ whereas for a 0.5 μm gate length a mobility of 400 $cm^2V^{-1}cm^{-1}$ is required.

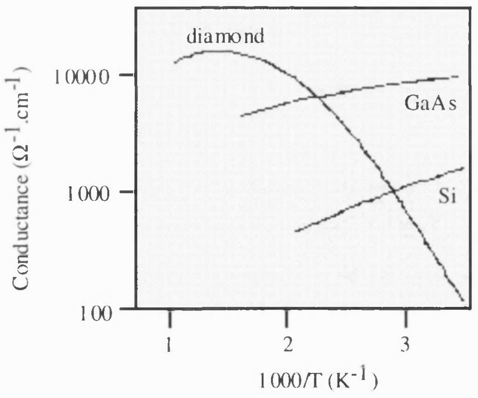

Figure 2.6 Drift region conductance versus temperature in one sided diodes made from Si, GaAs and diamond of respective gate lengths 5.4, 5, 0.3 μm (derived from the depletion layer thickness at breakdown) [redrawn from Collins, 1992].

The second factor as identified by Shenai [1989] for high temperature operation is the effect on the thermal leakage currents in typical components of systems such as Schottky-barrier rectifying junctions. Taking the ideal Schottky diode leakage current which is a function of the metal-semiconductor barrier height [Sze, 1981, p258], the temperature for which the reverse current was equal to 1% of the forward current was calculated to be in excess of 700 °C for diamond compared with 230 °C and 410 °C for GaAs diodes, respectively.

2.9 SUMMARY

The properties presented in this chapter indicate the many potential benefits which may be gained from employing diamond as the active substrate materials in specifically targeted applications. From the established figures of merits such as Johnson and Keyes, the potential exists for active diamond electronic devices to operate with a higher "power-frequency" product *i.e.* a greater power output is expected at a given frequency of operation. The wide bandgap nature of diamond coupled with the excellent thermal conductivity predicts a greater temperature range of operation than is possible with currently established semiconductors such as Si or GaAs. Indeed, Geis and co-workers [1987] have demonstrated transistor action and power gain with a point contact transistor (HPHT single crystal synthetic diamond) operating at 510 °C. This ability of the material to maintain its integrity under extreme conditions also extends the possibility of operation to other extremities such as chemically or radiation harsh environments. Radiation detectors have been constructed out of diamond since the fifties due to it possessing the strongest chemical bonding of all semiconductors rendering it the most immune to radiation damage [Yoder, 1991]; it was also emphasised that in such application it is the charge carrier with the lowest mobility (*i.e.* the hole) which dominates the response time of the device. Interest has also recently been concentrated on sensoring devices for use in specific applications encompassing not only electronic but also mechanical requirements [Petersen, 1981]. The construction of micro-electromechanical systems (MEMS) such as accelerometers and pressure sensors from diamond is foreseen to benefit immensely from the unique combination of properties of diamond including such attributes as extreme chemical inertness. A property of diamond which is currently of much interest is the possibility of efficient electron emission from diamond. The wide bandgap of diamond means that the conduction band of the material is close to the vacuum level, with the possibility of a negative electron affinity (NEA) being present; indeed on the (111) surface of diamond this has been demonstrated to be the case [Himpsel, 1979]. Vacuum microelectronic devices have been suggested [Davidson, 1993] as well as the possibility of field emission displays which are currently under active research.

With the demonstration of many of the theoretically predicted properties of diamond by the use of natural single crystals, the ability of CVD diamond films has to be investigated and compared to such achievements. The concerns raised by Collins [1989; 1992] regarding the superiority in terms of electronic properties over more established semiconductors like Si and GaAs are legitimate and careful assessment of potential applications are required. Nevertheless, the calculations by Collins [1992] may now appear to be pessimistic with the improvements acquired in growth technology; carrier mobilities have increased from the value of 290 cm^{2}V^{-1}s^{-1} used by Collins as typical for natural diamond crystals to greater than 1000 cm^{2}V^{-1}s^{-1} for homoepitaxial films at similar doping concentrations [Fox, 1995]. This improvement in the electronic properties of the chemically vapour deposited films over many previous reports regarding natural crystals was considered by Fox and co-workers [1995] a result of lowering of compensation of active carriers. Indeed, the superior thermal properties of synthetic material over the best results from natural material suggests that further improvements may be made.

REFERENCES

Anthony, T.R., [1994]. in *Thin Film Diamond,* ed. Lettington, A. and Steeds, J.W., (Chapman & Hall), London, UK.

Bachmann, P., [1991]. *Physics World*, **April**, 32.

Baliga, B.J., [1982]. *J. Appl. Phys.,* **53**, 1759.

Baliga, B.J., [1989]. *IEEE Electron Device Lett.*, **10** , 455.

Bakon, A. and Szymanski, A., [1993]. *Practical Uses of Diamond,* (Ellis Horwood), New York, USA.

Blakemore, J.S., [1986]. *Solid State Physics*, 2nd Edition, (Cambridge University Press), Cambridge, UK.

Clark, C.D., Dean, P.J. and Harris, P.V., [1964]. *Proc. R. Soc. (London),* **A277**, 312.

Collins, A.T. and Lightowlers, E.C., [1979]. in *The Properties of Diamond,* ed. J.E. Field (Academic Press) London, UK.

Collins, A.T., [1989]. *Semicon. Sci. Technol.*, **4**, 669.

Collins, A.T., [1992]. *Materials Sci. Engin.*, **B11**, 257.

Davidson, J.L., [1994]. in *Synthetic Diamond: Emerging CVD Science and Technology,* ed. K.E. Spear and J.P. Dismukes (John Wiley) New York, USA.

Dean, P.J., Lightowlers, E.C. and Wight, D.C., [1965]. *Phys Rev.,* **140**, 352.

Eden, R.C., [1993]. *Diamond Relat. Mater.,* **2**, 1051.

Ferry, D.K., [1975]. *Phys. Rev.,* **B12** , 2361.

Fong, C.Y. and Klein, B.M., [1995]. in *Diamond: Electronic Properties and Applications*, ed. L.S. Pan and D.R. Kania (Kluwer Academic Press) Massachusetts, USA.

Fox, B.A., Hartsell, M.L., Malta, D.M., Wynands, H.A., Kao, C.-T., Plano, L.S., Tessmer, G.J., Henard, R.B., Holmes, J.S., Tessmer, A.J. and Dreifus, D.L., [1995]. *Diamond Relat. Mater.,* **4**, 622.

Geis, M.W., Rathman, D.D., Ehrlich, D.J., Murphy, R.A. and Lindley, W.T., [1987]. *IEEE Electron Device Lett.,* **8**, 341.

Geis, M.W., Efremow, N.N. and Rathman, D.D., [1988]. *J. Vac. Sci. Technol.,* **A6**, 1953.

Geis, M.W., [1991]. *Proc. IEEE,* **79** , 669.

Grabner, J.E., Jin, S., Kammlott, G.W., Herb, J.A. and Gardinier, C.F., [1992]. *Appl. Phys. Lett.,* **60**, 1576.

Han, S., Pan, L.S. and Kania, D.R., [1995]. in *Diamond: Electronic Properties and Applications*, ed. L.S. Pan and D.R. Kania (Kluwer Academic Press) Massachusetts, USA.

Hess, K., [1988]. *Advanced Theory of Semiconductor Devices*, (Prentice-Hall), New Jersey, USA.

Himpsel, F.J., Knapp, J.A., vanVechten, J.A. and Eastman, D.E., [1979]. *Phys. Rev.,* **B20**, 624.

Himpsel, F.J., van der Veen, J.F. and Eastman, D.E., [1980]. *Phys. Rev.,* **B22** , 1967.

Johnson, E.O., [1965]. *RCA Review,* **26**, 163.

Jones, B.L., [1992]. *Industrial Diamond Rev.*, **4**, 175.

Keyes, R.W., [1972]. *Proc. IEEE,* **2**, 225.

Kittel, C., [1986]. *Introduction to Solid State Physics,* (John Wiley & Sons), New York, USA.

Konorova, E.A. and Shevchenko, S.A., [1967]. *Sov. Phys. Semicon.*, **1** ,299.

Lawaetz, P., [1971]. *Phys Rev.,* **B4**, 3460.

Morkoc, H., Strite, WS., Gao, G.B., Lin, M.E., Sverdlov, B. and Burns, M., [1994]. *J. Appl. Phys.,* **76**, 1363.

Napolitano, L.M., Jr., Meeks, E., Robles, J.E., Johnson, D., Daily, M.R., Miller, D., Norwood, D.P., Peterson, D.W., Reber, C.A. and Worobey, W., [1993]. *Int. J. Microcircuits Electronic Packaging,* **16**, 271.

Nava, F., Canali, C., Jacobani, C., Reggiani, L. and Kozlov, S.F., [1980]. *Solid State Comm*, **33**, 475.

Painter, G.S., Ellis, D.E. and Lubinsky, A.R., [1971]. *Phys. Rev.,* **B4** , 3610.

Petersen, K.E., [1982]. *Proc. IEEE,* **70**, 420.

Redfield, A.G., [1954]. *Phys. Rev.*, **94** , 526.

Reggiani, L., Bosi, S., Canali, C., Nava, F. and Kozlov, S.F., [1979]. *Solid State Comm.*, **30**, 333.

Reggiani, L., Waechter, D. and Zukotynski, [1983]. *Phys. Rev.,* **B28**, 3550.

Seal, M. [1994]. in *Thin Film Diamond,* ed. Lettington, A. and Steeds, J.W., (Chapman & Hall), London, UK.

Shenai, K., Scott, R.S. and Baliga, B.J., [1989]. *IEEE Trans. Electron Devices*, **36** , 1811.

Shur, M., [1990]. *Physics of Semiconductor Devices*, (Prentice-Hall), New Jersey, USA.

Smith, R.A., [1978]. *Semiconductors*, 2nd Edition, (Cambridge University Press), Cambridge, UK.

Sze, S.M., [1981]. *Physics of Semiconductor Devices*, 2nd Edition, (John Wiley & Sons), New York, USA.

Trew, R.J., Yan, J.-B. and Mock, P.M., [1991]. *Proc. IEEE*, **79**, 598.

Wolfe, C.M., Holonyak Jr., N. and Stillman, G.E., [1989]. *Physical Properties of Semiconductors*, (Prentice-Hall), New Jersey, USA.

Yoder, M.N., [1991]. In *Diamond and Diamond-Like Films and Coatings*, eds. R.E. Clausing *et al*, (Plenum Press), New York, USA.

Yoder, M.N., [1993]. In *Diamond Films and Coatings,* ed. R.F. Davis, (Noyes Publications,) New Jersey, USA.

3: SYNTHESIS AND CURRENT STATUS OF SEMICONDUCTING THIN FILM DIAMOND

3.1 INTRODUCTION

The ability to synthesise continuous thin films of diamond in a routine fashion by chemical vapour deposition techniques has permitted investigations to be made into the likely performance of diamond based electronic devices. Although the demonstration of both passive and active electronic applications such as Schottky diodes [Kiyota, 1995] and field-effect transistors [Tessmer, 1993] on CVD diamond films have been promising, many difficulties remain to be clearly identified and successfully tackled. The fact that all deposited diamond films on commercially viable non-diamond substrates is polycrystalline in nature means that the required characterisation is complicated by a combination of structural defects and grain boundaries. It is therefore the primary aim of this chapter to describe the more commonly practised techniques of growth of thin film diamond, as well as identifying current limitations and immediate aims in the chemical vapour deposition of diamond. The current status of the electronic properties of such films will be examined with emphasis on the state of dopant incorporation and on observed values of electrical resistivity and carrier mobility. Natural and homoepitaxial diamond have been included not only as a suitable comparison, but also as an indication of the possible levels of future achievement. The more recent introduction of state of the art oriented, textured diamond films will also be considered though fewer reports are currently available.

3.2 NATURAL AND SYNTHETIC DIAMOND

Naturally occurring diamond which comes primarily from Africa (Zaire, Republic of South Africa, Botswana) and the USSR [Bakon, 1993], display a range of differing characteristics; this variation allows the generalisation of diamond into "types" as summarised in Table 3.1 [Wilks, 1991]. Type I refers to diamonds that contain nitrogen impurities leading to a characteristic absorption edge at 330 nm instead of band edge absorption at 220 nm. However, in diamonds classified as type II which contain very low nitrogen levels, a subset labelled as type IIb was found to display semiconducting properties; this has subsequently been attributed to the presence of boron acceptor centres [Collins, 1971].

The discovery in the late 18th century of diamond being a crystalline form of carbon together with the subsequent development of chemical thermodynamic theory led to a more scientific approach in the synthesis of the material. The culmination of such efforts led to the announcement in 1955 by Bundy and co-workers at General Electric of a reproducible process for the synthesis of diamond [Davidson, 1994 and references therein]. This, and subsequent modifications have been based on the principle of synthesis in the thermodynamically stable region for diamond, and may be appreciated from the diamond-graphite phase diagram of which the Berman-Simon curve is one such example [Wilks, 1991]; this is reproduced in Figure 3.1. Growth methods based in this regime are commonly referred to as high-pressure, high-temperature (HPHT) techniques and the product as synthetic diamond.

Type	Abundance	Edge of UV absorption	Edge of IR absorption	Nitrogen content
Ia	ca. 98% (natural)	ca. 330nm	2.5µm to 10µm	N to 0.3% A and B aggregates; low levels of single N atoms ($<10^{16}cm^{-3}$)
Ib	ca. 0.1% (natural) main HPHT			N in single substitutional sites
IIa	ca. 2%	220nm	2.5µm to 6µm; transparent>6µm	Very low N level.
IIb				Extremely low N level; semiconducting (B acceptors)

Table 3.1 Classification of natural diamond crystals [extracted from Wilks, 1991].

Presently, HPHT techniques are based on the conversion of various forms of carbon (typically graphite) into the crystalline form of diamond and may be classified as follows: (i) direct conversion; (ii) synthesis using molten transition metal solvent catalyst; (iii) shock wave direct conversion; and (iv) growth using diamond seed crystals. These methods differ due to a combination of economic costs and the desired application of the final product *e.g.* the use of a molten catalyst such as copper, iron or nickel sufficiently improves both the rate and yield of the graphite to diamond conversion. However, diamond obtained from both the catalyst and the shock wave methods are generally defective and small (typically less than 1 mm). The addition of seeds allow the growth of crystals of quality comparable to the best natural stones with growth rates of 2-3 mg.h^{-1} [Bakon, 1993].

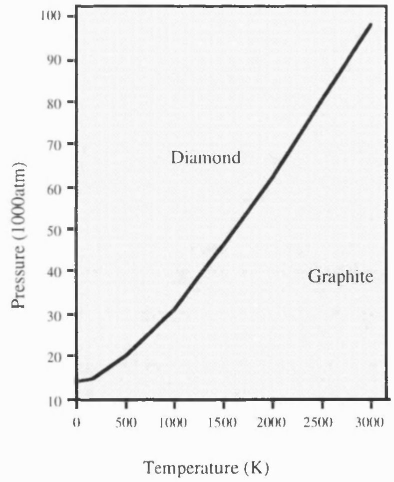

Figure 3.1 Berman and Simon curve for diamond-graphite thermodynamic stability [redrawn from Wilks, 1991].

3.3 DIAMOND SYNTHESIS IN THE METASTABLE PHASE

Diamond synthesis in the metastable phase (with respect to graphite) was first reported by Eversole of the Union Carbide Corporation in the early 1950s. Further breakthroughs were subsequently achieved by Angus in 1962 with the use of atomic hydrogen in the growth process, Deryagin in 1976 and Spitsyn in 1981 with growth on non-diamond substrates, and the NIRIM group (Setaka, Sato, Kamo, Matsumoto) with descriptions of the hot-filament, microwave and DC methods of low-pressure growth [see Davidson, 1994 and references therein]. This has resulted in the field now generally known as chemical vapour deposition (CVD) of diamond and has been the most popular and successful method of producing diamond in this thermodynamic regime. The importance of metastable CVD growth in the context of electronic applications include:

(i) the ability to grow uniform films of diamond over sufficient area for the current technology of processing electronic applications to be applicable;
(ii) the ability for material synthesis to occur onto commercially viable substrates within a set-up which is not economically prohibitive;
(iii) the allowance of a controllable method for the incorporation of impurity atoms for the realisation of semiconducting behaviour in the material; and
(iv) the use of growth conditions which may be non-destructive to other material systems.

3.4 THE VIABILITY AND CONDITIONS FOR METASTABLE GROWTH

As a result of the small value of free energy difference between diamond and graphite (0.03 eV/atom at 298 K and atmospheric pressure [Angus, 1989]), there is always a finite possibility of the formation of both phases in any attempt at synthesis. Hence, formation of diamond in the metastable phase can be assumed to depend on the selection of growth conditions wherein the competing rate of nucleation together with further growth of graphite (or indeed other non-diamond carbon), and spontaneous graphitisation of the diamond surface is low. Crystallisation and growth of diamond can therefore be taken as a combination of thermodynamic, kinetic and chemical factors. The following requirements for CVD growth of diamond have been considered by Koba [1993]:

(i) bulk transport and subsequent activation of a carbon-containing reactant gas phase for the formation of film precursors;
(ii) the presence of a driving force to transport activated species from the gas phase onto the substrate surface followed by adsorption of the precursors onto the substrate surface,

diffusion of the precursors to the growth sites and reaction of the film precursor for incorporation of film constituents;
(iii) the active presence of a species which suppresses the formation of the graphite; the critical role of atomic hydrogen in the growth process has been established where it is believed to etch graphite 50 times faster than diamond [Bachmann, 1991] and may be active in the prevention of the reconstruction of the diamond surface into non-diamond elements, as well as an aid for the creation of free radical sites on the hydrogen saturated growth surface [Angus, 1989].

3.5 CHEMICAL VAPOUR DEPOSITION OF DIAMOND FILMS

3.5.1 Growth techniques

Many techniques for the chemical vapour deposition (CVD) of diamond thin films have been developed; these techniques have been reviewed extensively in the literature *e.g.* [Zhu, 1991; Bachmann, 1993], and the most common of these may be categorised into the following: (i) hot-filament CVD; (ii) plasma enhanced CVD; and (iii) combustion flame.

(i) Hot-filament chemical vapour deposition (HFCVD)

The chemical vapour deposition of diamond employing hot filaments of suitable metals, as originally detailed by Matsumoto *et al.* [1982], is one of the simplest demonstrations of a routine growth technique; a schematic diagram of the apparatus is given in Figure 3.2. In this experimental set-up, a refractory metal filament (*e.g.* tantalum, tungsten) is heated to temperatures ~2000 °C for the purpose of dissociating the precursor gas mixture. A substrate situated about 1 cm from the filament is independently heated to ~1000 °C. Typically, a gas mixture of 1% hydrocarbon (most commonly methane) in hydrogen is admitted at a rate of 100 sccm (standard cubic cm per minute) into a deposition chamber at a pressure of 40-100 Torr. Within such an environment, growth rates have been shown to vary between 1-10 $\mu m.h^{-1}$ depending on the various deposition parameters, over areas limited only by the filament shape and design. The possibility for the fabrication of three-dimensional structures such as the coating of fibres by following filaments round substrates have been demonstrated [May, 1995].

One of the major problems associated with HFCVD has been practical difficulties concerning the filament; within the carbonaceous atmosphere of the deposition zone, refractory metals form carbides which leads to warpage and embrittlement of the filament with the subsequent degradation in film uniformity. Consideration for the filament include lifetime, impurity emission, functional abilities and economic cost; Matsubara [1990] and Jansen [1990] have reported on such aspects.

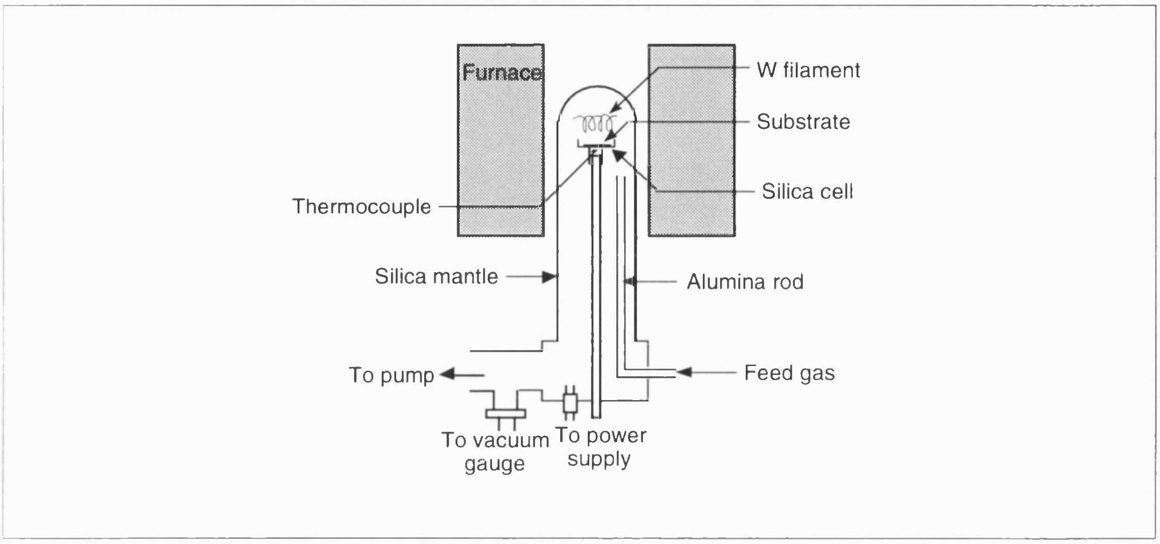

Figure 3.2 Schematic diagram of hot-filament chemical vapour deposition apparatus [redrawn from Matsumoto, 1982].

(ii) Plasma enhanced chemical vapour deposition

Spitsyn [1981] suggested that both hydrogen and the hydrocarbon precursors may be efficiently radicalised by the employment of electric fields to form neutral mixtures of molecules, charged particles (electrons, positive and negative ions) and photons. In the event, various plasma systems have been investigated including microwave (MW), radio frequency (RF) and direct current (DC). Plasma systems may further be sub-divided into low (<200 Torr) and high (200-760 Torr) pressure techniques. At the higher pressures, greater power levels are required to maintain the existence of the plasma, resulting in a much higher gas temperature or "thermal" plasmas where near-unity dissociation of molecules into atoms and radicals may occur [Bachmann, 1993].

(a) Microwave plasma enhanced chemical vapour deposition (MPCVD)

The use of high frequency radiation (2.45 GHz) [Kamo, 1983] has become one of the most popular methods for plasma excitation in the deposition of diamond; Figure 3.3 shows various equipment set-ups. Typical deposition conditions are similar to that of the hot filament method; chamber pressures of 40-100 Torr, substrate temperature 800 °C, 1% methane in hydrogen results in growth rates of 1-5 $\mu m.h^{-1}$ with 1 kW microwave power. In the tubular design (Figure 3.3(a)), the substrate is placed directly in the path of the microwaves which can lead to severe contamination of the deposited films due to plasma etching of the silica tube. This design has been largely superseded by the resonant cavity design (Figure 3.3(b)) where larger uniform deposition areas are achievable with less contamination from chamber walls [Bachmann, 1993]. Electron cyclotron resonance (ECR) systems, where the frequency of the electron gyration is equal to that of the microwaves, have been investigated at 2.45 GHz by Kawarada [1987] in the aim of achieving large, uniform and higher density plamas (Figure 3.3(c)). However at pressures of less than 0.1 mbar, where true ECR conditions are satisfied, deposition rates and crystal sizes were observed to be reduced considerably.

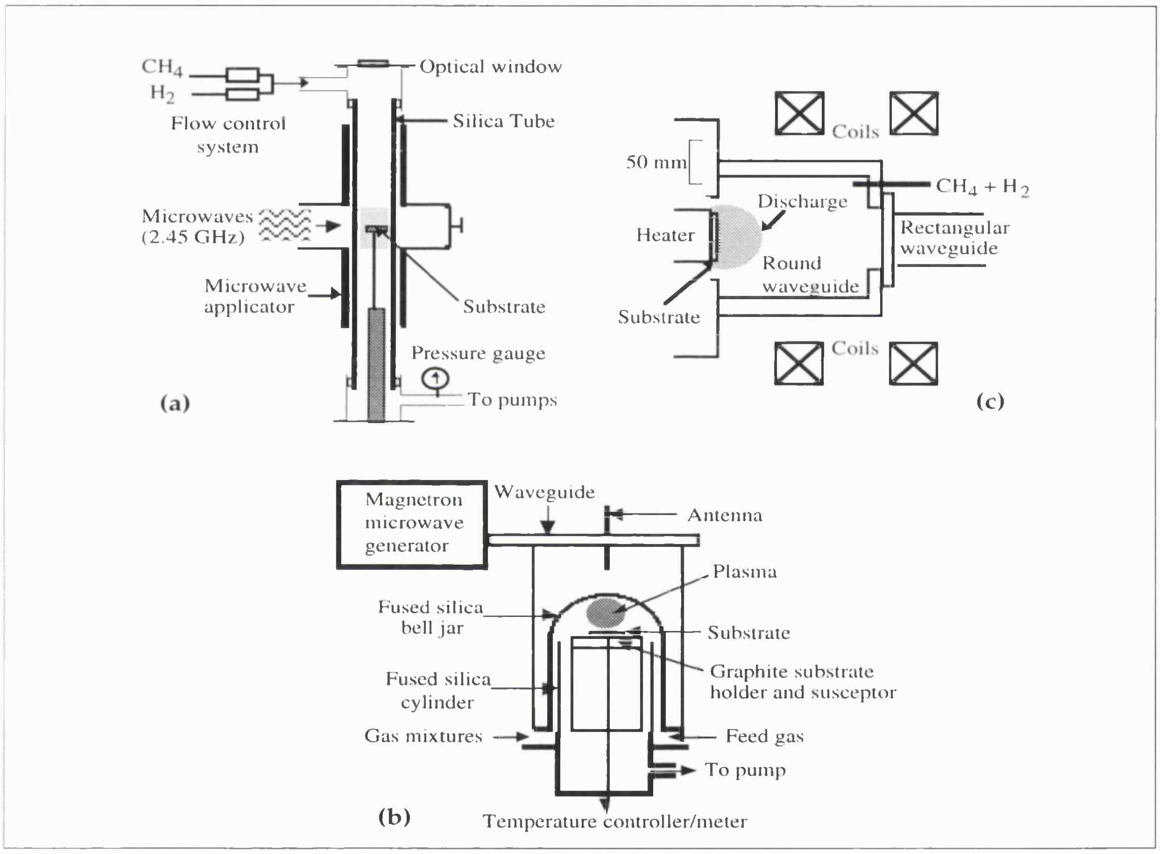

Figure 3.3 Schematic diagrams of microwave plasma CVD systems in the configuration of (a) tubular; (b) bell-jar; and (c) magneto-microwave [redrawn from Zhu, 1991].

(b) Radio frequency plasma chemical vapour deposition (RFCVD)

The existence of RF plasma technology in the microelectronics industry makes it an attractive possibility for the low pressure deposition of diamond. Both the parallel plate and the inductively coupled (Figure 3.4) low pressure plasmas have been investigated from 100 Hz to the more common 13.56 MHz [Zhu, 1991]. Deposition conditions are similar to that used in microwave discharge systems but the quality of deposited material have been inferior [Bachmann, 1993].

The introduction of an atmospheric pressure inductively coupled thermal plasma torch by Matsumoto [1987] using frequencies 3-30 MHz and RF powers of 40-80 kW has resulted in diamond deposition with high growth rates (60-180 $\mu m.h^{-1}$). However the sophistication, high power consumption and large gas volume requirements are still drawbacks of this type of system.

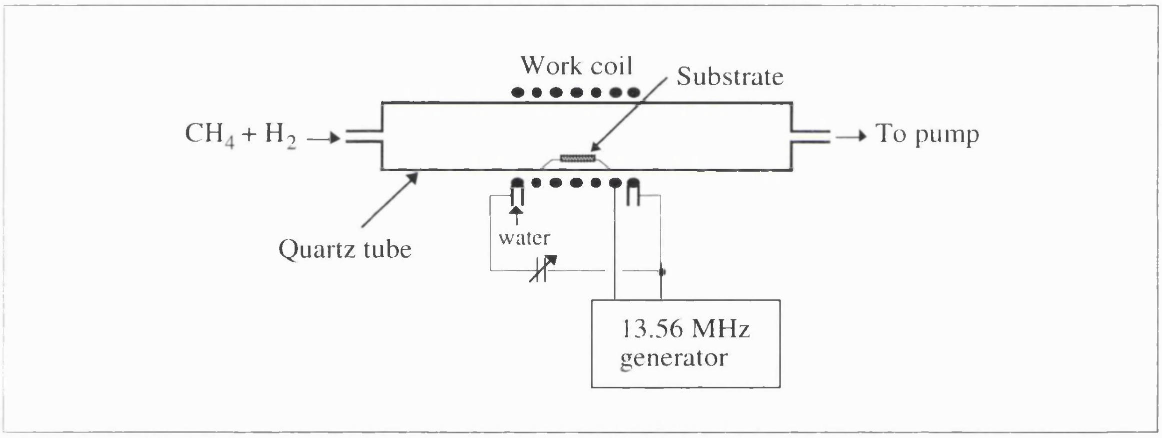

Figure 3.4 Schematic diagram of inductively-coupled radio frequency (RF) CVD apparatus [redrawn from Matsumoto, 1987].

(c) Direct current plasma chemical vapour deposition (DCCVD)

The formation of direct current (DC) discharge plasma at the higher gas pressure of 200 Torr has also been successful in diamond deposition [Suzuki, 1987]; Figure 3.5(a) shows such a set-up. A modification of the low pressure DC plasma system is the DC plasma jet introduced by Matsumoto [1987] as shown below in Figure 3.5(b); the gas mixture is fed into a conventional plasma torch at 3k-70k sccm where temperatures of around 4000 °C allow for complete gas dissociation. Good quality diamond films may be achieved by this method with extremely high deposition rates (20-1000 $\mu m.h^{-1}$) [Bachmann, 1993]. However problems still exist with small deposition areas, sophisticated and expensive equipment, high power consumption and film non-uniformity.

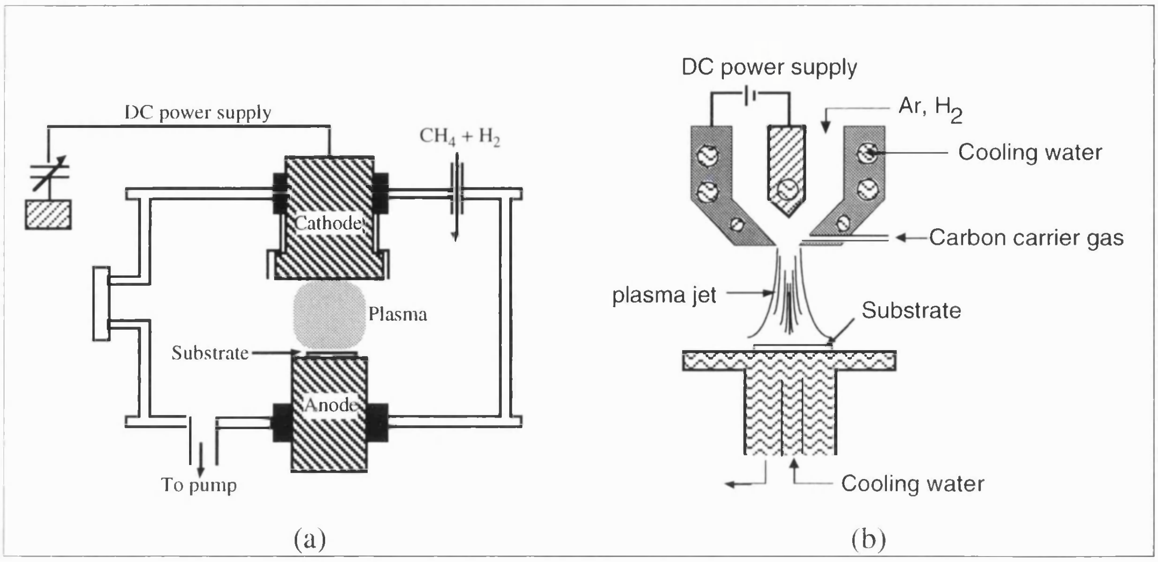

Figure 3.5 Schematic diagram of (a) direct current (DC) plasma CVD reactor [redrawn from Suzuki, 1987] and (b) direct current (DC) plasma jet system [redrawn from Matsumoto, 1987].

(iii) Combustion flame chemical vapour deposition

The use of an oxy-acetylene (welding) torch was first demonstrated by Hirose *et al.* [1988] to deposit diamond from various parts of the flame when a mixture of 50% acetylene in oxygen was used. Deposition occurs around the tip of the acetylene feather and is believed to have a gas phase temperature of 3000 °C. Although this technique may allow extremely high growth rates (30-200 $\mu m.h^{-1}$) with good film quality at the lower rates, many practical problems exist. Temperature fluctuations and hence film uniformity is difficult to control, with the vast amounts of gas employed (500-1000 sccm) difficult to recycle into the reactive zone.

3.5.2 Comparison of CVD diamond growth techniques

A summary of the present status of the many existing diamond CVD techniques has been presented in a review by Bachmann [1993] and is reproduced here in Table 3.2. The importance of higher plasma densities and temperatures engendered by the high power techniques are reflected in the greater growth rates achieved in the atmospheric and thermal plasma techniques as well as by combustion flame. Nevertheless, the high power requirements of high pressure plasmas necessitates elaborate substrate cooling schemes as well as more sophisticated controlling schemes. Furthermore, the performance requirements of the diamond films which may include a combination of good substrate adhesion, high optical transparency, low impurity content and high thermal conductivity together with economic considerations will ultimately dictate the deposition method.

Method	Rate /μm/h	Area/cm^2	Quality	Advantages	Drawbacks
Hot filament	0.3-2	100	+++	simple large area	contamination stability
Combustion flame	30-100	<1	+++	simple	area stability
DC discharge (low P)	<0.1	70	+	simple large area	quality rate
DC discharge (medium P)	20-250	<2	+++	rate quality	area
DC plasma jet	930	<2	+++	highest rate quality	area, stability homogeneity
RF (low P)	<0.1	?	-/+	scale-up	quality, rate
RF (thermal)	180	2	+++	rate	area, stability homogeneity
Microwave (2.45GHz)	1(low P) 30(high P)	40	+++	quality stability	rate area
Microwave (ECR, 2.45 GHz)	0.1	>40	-/+	area low P	quality rate

Table 3.2 Comparison of some CVD diamond deposition methods [extracted from Bachmann, 1992].

3.6 PROGRESS TOWARDS DIAMOND HETEROEPITAXY

Although much progress has been made on the development of techniques for the synthesis of diamond films in the metastable phase, the goal of heteroepitaxy, *i.e.* the formation of single-crystalline diamond as an extension of a single-crystalline non-diamond substrate over a large area remains a major task. The methods of growth described above almost invariably leads to deposited thin films on non-diamond substrates to be of a polycrystalline nature. The existence of sharply angled grain boundaries arising from the randomly oriented crystallites results in a severe degradation of the electronic transport properties when compared to theoretical values. However, two areas of scientific investigation may lead to the hope of a future possibility for the heteroepitaxial growth of diamond over an appreciable lateral area. Firstly, the growth of diamond as an extension of a diamond substrate (crystal), homoepitaxy, has been demonstrated in the metastable regime employing the same chemical vapour deposition techniques [*e.g.* Chu, 1992]. Furthermore, heteroepitaxial growth of diamond by these conditions has also been demonstrated, albeit to a very limited extent, on very small areas ($<10^{-4}$ cm^2) of single crystalline cubic boron nitride, nickel, copper, silicon carbide and silicon [see Geis, 1991 and references therein); these have lattice constants of 3.615 Å, 3.524 Å, 3.61 Å, 4.36 Å and 5.43 Å, respectively compared with 3.567 Å of diamond.

Significant work has been concentrated on the growth of diamond films on silicon substrates as opposed to *e.g.* c-BN or SiC due to availability and economic considerations. It has also been found though, that the diamond nucleation rate on carbide-forming substrates such as silicon, molybdenum or tungsten is one or two orders of magnitude higher than on non-carbide forming substrates [Spitsyn, 1981]. Furthermore, nucleation on polycrystalline substrates has been found to be enhanced when compared with growth on single-crystalline substrates. Such observations suggested that controlled nucleation was a key issue towards more acceptable growth rates. Whereas before, an induction period of 1-2 hours was required for sparse nucleation, pre-treating the substrates by scratching with micron-sized diamond particles resulted not only in a reduction of this induction period but also in the coalescence of the individual crystallites and subsequent formation of continuous films. Although it may be postulated that residual particles left on the surface from the scratching medium may act as diamond nucleation sites, it has also been found that the abrading of the substrate surface with non-diamond particles such as c-BN, SiC and stainless steel also leads to enhanced nucleation densities. This may be due to the possibility of nucleation being enhanced by the effect of a high surface defect density acting as preferential nucleation sites [Stoner, 1992]. Although such understanding is still not conclusive, the abrading of surfaces for the purpose of increased nucleation is not seen as the path towards the goal of heteroepitaxy. Furthermore, the nature of scratching with random particulates leads to a combination of both randomly oriented particles lying on the substrate surface, and randomly dispersed defect sites which could inherently result in the growth of randomly oriented crystallites and hence sharp grain boundaries in continuous films. The density of nucleation due to scratching is approximated to be on the order of 10^7 cm^{-2} [Stoner, 1992].

Two areas of progress have been recognised towards the improvement of the first generation of CVD diamond thin films. By controlling the growth competition between the different orientation of the individual grains, certain directions of growth may be enhanced and a preferential state of the surface may subsequently be obtained (van Der Drift evolution theory). Wild *et al.* [1994] demonstrated films with surfaces consisting of rectangular, nearly coplanar {100} facets by controlling film morphology via growth temperature and methane concentration; these "fibre-textured" films which show random in-plane orientation is shown in Figure 3.6(a). The introduction of the process of bias-enhanced nucleation by workers including Stoner *et al.* [1992] resulted in the increase of nucleation density on unscratched silicon surfaces to 10^{11} cm^{-2}, an improvement of 3-4 orders over conventionally scratched substrates. The development of a three stage process involving an initial carburization step speculated to form an epitaxial conversion layer of b-SiC on silicon, followed by the placing of a negative bias of 250 VDC on the substrate for nucleation and finally textured growth led to an in-plane orientation of individual crystallites in registration with the substrate [Wolter, 1993]. Although such films are still polycrystalline in nature, the fact that in-plane orientation of individual diamond crystallites exists may result in a less significant presence of the grain boundaries. Furthermore, coalescence of individual grains may be observed with increasing film thickness (Figure 3.6(b)).

Another promising development has been the demonstration by Geis *et al.* [1991] who introduced a method for the controlled seeding on morphologically pattern-etched silicon surfaces. In this case, oriented single-crystal diamond seeds about 100 μm in size were deposited via a liquid medium onto etched pits or grooves on the silicon substrate. Continuous films of thickness 250 μm have been grown employing this method [Geis, 1992] resulting in films that contain low-angled grain boundaries; such boundaries are due to the fact that the starting crystals are never perfectly aligned. It is envisaged that near single-crystalline "substrates" created by this technique may be used as "templates" for further growth of thin films which may then be "lifted off" [Geis, 1994; Janssen, 1995].

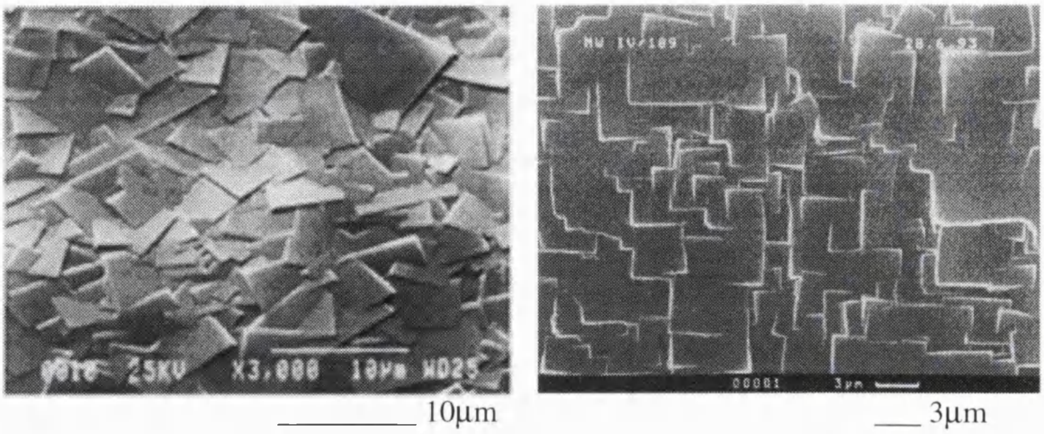

(a) (b)

Figure 3.6 Diamond films grown by CVD techniques employing (a)van Der Drift evolution theory to obtain textured polycrystalline film, and (b)bias-enhanced nucleation and texturing for oriented polycrystalline material [Wild, 1994].

3.7 CONSIDERATIONS FOR THE INCORPORATION OF DOPANTS

Among the diamond crystals found naturally, nitrogen is by far the most common impurity present. Semiconducting properties due to boron acceptor centres in Type IIb diamond have also been extensively examined [Collins, 1971]. For the incorporation of electrically active dopant impurities into diamond, various aspects which include geometric and energetic factors have to be taken into account. The tetrahedral configuration of diamond results in an inter-atomic distance of only 0.154 nm requires any prospective impurity atom to be of this dimension if it is to be incorporated into the lattice as an electrical dopant. In this sense, boron (group III) and nitrogen (group V), being potential acceptor and donor atoms respectively may be immediately viewed as suitable dopant candidates due to their relative positions in the periodic table.

At present, the doping of diamond is being actively investigated via the gas phase, ion implantation and to a lesser extent, by solid state in-diffusion. It is generally accepted that the doping of diamond films in which electrically active impurities are distributed through the lattice has only been successful with boron. The presence of boron atoms at substitutional sites have been found to create acceptor centres with an activation energy of 0.37 eV in natural diamond with doping concentrations up to 8 x 10^{16} cm^{-3} [Collins, 1971]. This large ionisation barrier results in an activation of less than 1% of the introduced dopant concentration at room temperature [Geis, 1992]; the implications on the electrical properties have been described in the previous chapter. Boron doping has been demonstrated by the introduction of diborane (B_2H_6) into the feed gas in a standard microwave plasma system [Fujimori, 1986;1990]; non-toxic boron trioxide (B_2O_3) has also been reported by Okano *et al.* [1990; 1993] where it was dissolved in methyl alcohol (CH_3OH) and diluted with acetone to be vaporised and used as a reactant gas.

Ion implantation has also been investigated as a means of incorporating boron atoms into the diamond lattice. Although the technology is mature for silicon processing, the fact that diamond is metastable leads to possible graphite formation during implantation or in the subsequent post-annealing process, which has been found to be necessary in order to activate the boron atoms [Prins, 1992]. Many parameters have been investigated such as the substrate temperature during implantation; Prins [1992] reported of the beneficial results obtained by implanting natural diamonds at 77 K at energies up to 120 keV with total B doses of 4.5×10^{15} cm^{-2}. At this temperature it was proposed that vacancies created in the lattice are "frozen", allowing suitable post-implant annealing (up to 1750 °C) to activate the boron dopants; the dopants exhibited an electrical activation energy of 0.37 eV. Implantation of polycrystalline films have also been demonstrated by Kalish *et al.* [1994] who compared B and C implanted films done at -30 °C at an ion energy of 60 keV and dose of 2×10^{16} cm^{-2}. After subsequent annealing at 1000 °C and the removal of a graphitic surface layer, conductive nature was only observed with the B implanted film. Fontaine *et al.* [1994] demonstrated by Raman spectroscopy that the integrity of CVD polycrystalline films remain only up to a B dosage threshold of 3×10^{15} cm^{-2} at an implant energy of 90 keV.

A solid state diffusion technique has been demonstrated by Tsai *et al.* [1991] to create an ultra-shallow p-channel field-effect transistor in natural diamond. In this case, cubic boron nitride was used as the p-type dopant and was diffused into the diamond lattice to a depth of 50 nm by rapid thermal processing (RTP) at 1400°C. A concentration of 3×10^{19} boron atoms.cm^{-3} was reported at 50 nm but a similar concentration of nitrogen profile was found (in the highest quality CVD diamond films, isolated substitutional nitrogen may be less than 0.01 ppm [Collins, 1993]).

The promise of well controlled n-type impurity doping has thus far not replicated the success of boron incorporation as a p-type dopant. Nitrogen, which is common in natural diamond, exists in isolated substitutional sites (Type Ib) and would thus suggest its suitability as an impurity for n-type doping. However, the energy band of the impurity centre is about 2 eV below the conduction band [Collins, 1989] and, with such a large activation energy requirement, results in nitrogen being of little consequence in the electronic behaviour of diamond films. Theoretical calculations for phosphorus doping in diamond predicts the possibility of a shallow (0.2 eV) donor occupying substitutional sites albeit with a low solubility factor [Kajihara, 1993]. Investigations into this have been conducted particularly by Okano *et al.* [1990; 1993] using diphosphorus pentaoxide (P_2O_5). In this case, due to the low solubility of phosphorus in the diamond lattice, concentrations of less than 10^{17} atoms.cm^{-3} were observed, along with the fact that gas concentration appeared to have little influence on film resistivity (~100 Ωcm). Similar observations by Flemish *et al.* [1994] have been made using PH_3 in the gas mix; the belief there was that incorporation was preferentially at the grain boundaries.

Of the metallic elements in Group I, lithium and sodium have been studied as possible donors for diamond. Theoretical calculations by Kajihara *et al.* [1993] have shown the preference for both elements to occupy interstitial sites with the possibility of being shallow dopants with activation energies of 0.1 eV (Li) and 0.3 eV (Na). However, the high energy of formation of both elements suggests possible difficulties in incorporation during either growth or in-diffusion [Kajihara, 1993]. Therefore, the more energetic method of ion implantation has been studied by groups including Prawer *et al.* [1993] with implantation of Li and Na ions into natural diamond. Electrical conductance of the implanted films was believed to related to the presence of the implanted ions since similar implantation with other ions of comparable mass did not result in a reduction in the resistivity of the diamond crystal; activation energies of 0.2 eV (Li) and 0.13 eV (Na) were obtained with sheet resistance in region of 10^9 Ω/square.

3.8 PROPERTIES OF B-DOPED P-TYPE DIAMOND

The introduction of boron impurity atoms into the diamond crystal lattice as a source of acceptor centres in substitutional sites by the methods described previously is now considered to be a controllable process. Typically, measurements are made by the technique of secondary ion mass spectroscopy (SIMS) to evaluate the impurity concentration as a function of the film outgrowth. A representative SIMS depth profile to a depth of 0.7 μm is reproduced in Figure 3.7 along with the corresponding Raman spectra as an indication of the effect of boron incorporation on diamond film quality from gas-phase boron-doped polycrystalline CVD diamond films.

The smooth SIMS profile indicates a uniform incorporation of boron dopants in the bulk, with the relative increase in concentration almost proportional to the boron/carbon (B/C) ratio in the reactant gas mixture. Electrically, the resistivity of these films demonstrated an inverse proportionality to the B/C ratio over the 4 orders of magnitude investigated (10^2-10^{-2} Ω.cm). However the broadening in the Raman peaks shows that as the magnitude of boron atoms is increased, an adverse effect on film quality may be experienced. It has also been observed by Mort *et al.* [1989] that the film quality as judged by Raman spectra may remained unchanged with boron concentrations up to 6 x10^{19} cm^{-3} boron atoms. A study carried out by Graham *et al.* [1994] on oriented (100) textured films employing the technique of cathodoluminescence (CL) from a transmission electron microscope allowed direct correlation of CL emission with specimen microstructure; this reported of an increase in the density of dislocations after the introduction of boron dopants. The doping efficiency, defined in terms of the actual number of boron atom incorporated in the films with that present in the gas phase, has been shown to display a level of disparity; Mort *et al.* 1989] proposed a doping efficiency of about 20% over a range of B/C concentrations, and Fujimori *et al.* [1990] 6% (40 ppm), 34% (100 ppm) and 57% (1000 ppm) with both using diborane sources.

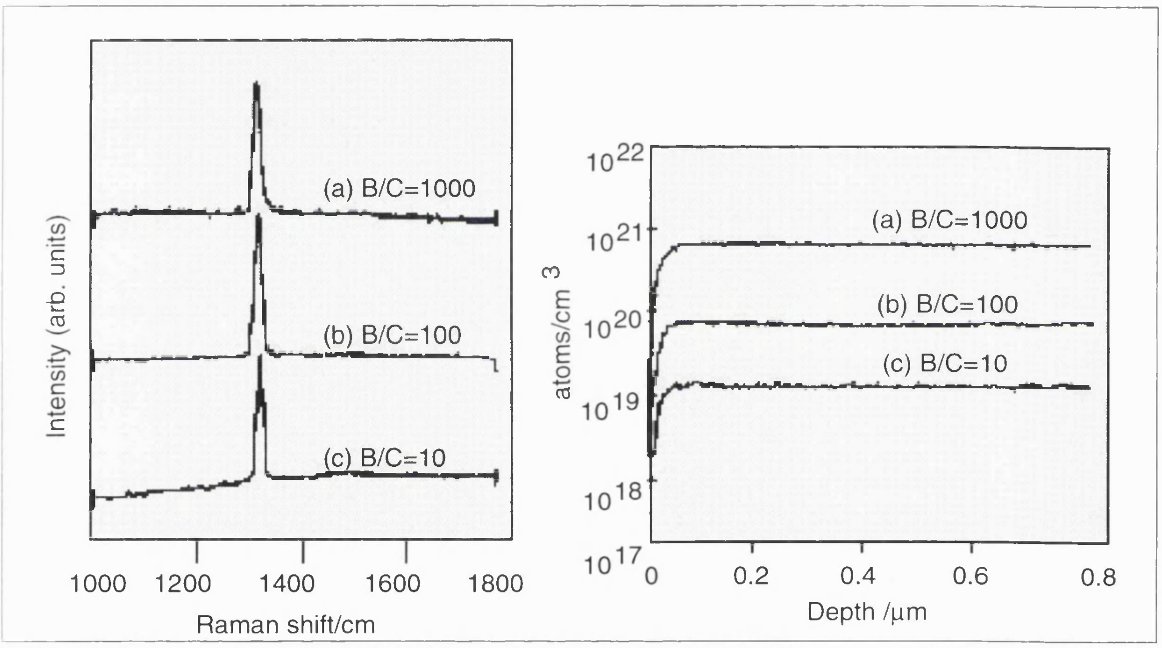

Figure 3.7 SIMS depth profile and associated Raman spectra of boron doped polycrystalline diamond films [redrawn from Okano, 1993].

The activation energy of boron dopant impurities in natural and synthetic diamond single crystals has been found to be 368.5 +/- 1.5 meV [Collins, 1971]; the boron concentration of these crystals were later determined by the technique of prompt particle nuclear microanalysis to be 1-5 x 10^{16} cm^{-3} [Lightowlers, 1976]. In the case of polycrystalline CVD diamond, Okano *et al.* [1993] investigated the activation energy of boron dopants for concentrations as judged by SIMS analysis of 1 x 10^{19} cm^{-3}, 7 x 10^{19} cm^{-3} and 8 x 10^{20} cm^{-3}; the corresponding activation energies measured over the temperature range of 253-333 K were found to be 0.38 eV, 0.34 eV and 0.26 eV. This appears to be in reasonable agreement with the work by Fujimori *et al.* [1990] on homoepitaxial (100) diamond who found boron activation values of 0.43 eV, 0.34 eV and 0.22 eV over a temperature range of 373-773 K for doping levels of 1 x 10^{17} cm^{-3}, 6 x 10^{18} cm^{-3} and 1 x 10^{20} cm^{-3}, respectively. It may be seen from this data that as the dopant concentration present in the films is increased, the activation energy is observed to decrease; this trend has been confirmed in compilation of results by Nishimura *et al.* [1991] for a range of natural/synthetic single crystals and polycrystalline samples. This is reproduced in Figure 3.8.

It has been suggested by Nishimura [1991] that if the above figure was extrapolated then, at a boron concentration of around 10^{21} atoms cm^{-3}, a zero activation energy for the ionisation of the dopant would result, *i.e.* the material would become degenerate and display metallic properties. Indeed, synthetic semiconducting diamonds have been observed to become degenerate at approximately 7 x 10^{20} boron atoms cm^{-3} [Vishnevskii, 1981]. Similar values have been observed for the onset of this condition on both CVD homoepitaxial and polycrystalline diamond; dopant concentrations of 3 x 10^{20} cm^{-3} [Shiomi, 1991] and 1 x 10^{21} cm^{-3} [Werner, 1994] were found for the respective types of material. These figures may be compared with the value calculated from the Mott metal/insulator transition of 1.2 x 10^{20} cm^{-3} [Mott, 1993; Shiomi, 1991]; in such a situation, it is believed that the wave function of the neighbouring boron acceptor atoms overlap, and conduction takes place within a broadened impurity band.

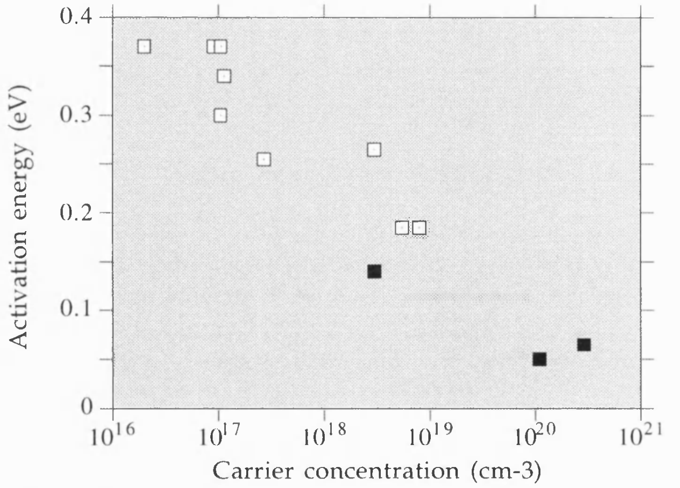

Figure 3.8 Boron activation energy versus carrier concentration for natural/ synthetic diamond (open circles) and CVD polycrystalline diamond films (shaded circles) [redrawn from Nishimura, 1991].

3.9 CARRIER TRANSPORT PROPERTIES OF P-TYPE DIAMOND FILMS

In order to further consider the current status of chemically vapour deposited semiconducting diamond films, a comparison of various parameters determining the electronic transport characteristics of boron-doped diamond films has been made here of typical and state of the art material; polycrystalline, randomly oriented diamond has been compared to single-crystalline material in the form of homoepitaxial films and natural crystal (Table 3.3). Furthermore, from the limited literature available, data on textured and oriented diamond has been included. From this compilation, it may be seen that, for the polycrystalline samples, Hall mobility values of approximately 30-50 cm^{2}V^{-1}s^{-1} may be achieved for an atomic boron concentration of approximately 10^{18} cm^{-3}. As the concentration of boron dopant is increased (with a corresponding increase in active carrier concentration), the hole carrier mobility has been observed to decrease in a near-monotonic fashion; this has been observed by Masood et *al.* [1992] for a polycrystalline sample at room temperature and similarly in homoepitaxial films [*e.g.* Grot, 1991; Mori, 1993; Fujimori, 1990] (see Chapter 6).

Nature	Resistivity (Ω cm)	Carrier Conc.(cm^{-3})	Atomic B Conc.(cm^{-3})	E_A (eV)	Hall Mobility	Reference
Poly	20-100	$9x10^{15}$-$2x10^{17}$	10^{17}-10^{21}	0.30-0.38	2-32	Masood [1992]
Poly	0.15-5	$3x10^{18}$-$3x10^{20}$	$6x10^{19}$-$2x10^{20}$	0.1	0.22-0.6	Nishimura[1991]
Poly	100	$1x10^{14}$-$2x10^{16}$	$2x10^{18}$-$5x10^{18}$	0.05	2.8-10	vonWindheim[1993]
Poly	-	$6.8x10^{14}$	$4x10^{18}$	0.356	47.8	Fox [1994]
Poly	600	$3x10^{14}$	$2x10^{18}$	-	33.3	Malta [1993]
T&O	644	$5.9x10^{13}$	-	0.346	165	Stoner [1993]
T&O	-	$2.4x10^{14}$	$2x10^{18}$	0.356	135	Fox [1994]
Homo	-	$2x10^{14}$-$1x10^{17}$	-	0.22-0.43	7.8-470	Fujimori [1990]
Homo	80	$2x10^{14}$	$2x10^{18}$	0.349	519	Malta [1993]
Homo	0.15-7	$2x10^{15}$-$4x10^{17}$	-	0.28-0.38	110-450	Mori [1993]
Homo	-	10^{14}	$2.7x10^{18}$	-	590	Visser [1992]
Homo	0.14-216	$1x10^{14}$-$1x10^{18}$	-	-	33-290	Grot [1991]
Natural	-	$2x10^{13}$	$1.5x10^{16}$	0.361	564	vonWindheim[1993]

Table 3.3 Comparison of electronic properties of diamond thin films and natural crystal, where Poly= polycrystalline; T&O= textured and oriented; Homo= homoepitaxial; Natural= natural crystal. Hall mobility values (cm^{2}V^{-1}s^{-1}) are taken at room temperature.

From Table 3.3, it may be seen that for similar levels of atomic boron concentration *e.g.* 10^{14} cm^{-3}, the corresponding hole mobility value obtained for polycrystalline diamond films (33.3 $cm^2V^{-1}s^{-1}$, [Malta, 1993]) is significantly lower than that obtained for homoepitaxial material (590 $cm^2V^{-1}s^{-1}$, [Visser, 1992]). The higher mobility value (5 times that of polycrystalline films) in textured, (100) oriented films have been proposed to be a consequence of the low angle grain boundaries (< 5°). However, the measured mobility is still less than that of similarly doped homoepitaxial films which is seen to suggest that the boundaries remain a deleterious factor in electronic transport [Stoner, 1993]. This difference may be a result of many potential physical differences as identified by Malta *et al.* [1993]; the effect of grain boundaries, the possibility of different conduction mechanisms (*e.g.* impurity band conduction), compensation by donor impurity atoms or radiation induced defects (*e.g.* by microwave plasma).

3.10 SUMMARY

The advent of chemical vapour deposition of thin films of diamond by the techniques summarised in this chapter enables the many properties of this material to be studied in the view of future commercial applications. In particular, in the interest of electronic applications, intentional p-type doping by boron impurities of CVD films replicating the semiconducting properties found in type IIb natural stones has been demonstrated; gas-phase doping has been shown to control the resistivity of diamond films over many orders of magnitude. In addition, the possibility of controlling the growth environment suggests that a major source of compensation of active charge carriers in natural diamond, believed to be a configuration of nitrogen (contributing typically 17% [vonWindheim, 1993a]), may be reduced in CVD films in much the same way as isotope reduction has resulted in superior thermal properties [Fox, 1995]. However, the fact that n-type doping has not been demonstrated imposes a significant limitation to the device engineer's repertoire. The polycrystalline nature of diamond when deposited on economically viable substrates has been shown to lead to poor electronic properties arising from factors including the granular nature. Nevertheless, progress has been achieved over the past number of years resulting in the development of textured films with oriented grains; the electronic properties of such films have to be more fully investigated in order to ascertain the origins of the benefits to the transport characteristics.

The sheer range of techniques of growth and practices employed within the field has also tended to increase uncertainties surrounding polycrystalline diamond films. As-deposited diamond films have been demonstrated to possess unexpectedly high conductivity values which may be decreased by up to six orders of magnitude by annealing at temperatures as low as 100 °C; within the rich hydrogen atmosphere of the growth chamber, hydrogen passivation of traps has been suggested a cause of this [Landstrass, 1989]. Such a phenomenon poses implications for certain applications, high temperature devices being foremost. In addition, conductive layers have been reported to exist on as-deposited films [Mori, 1992; Plano, 1994]; this will be further addressed in Chapter 5. Hence, electronic device fabrication on CVD films has to account for a number of factors including various post-deposition preparatory steps if reliable device characteristics are to be achieved.

REFERENCES

Angus, J.C., Buck, F.A., Sunkara, M., Groth, T.F., Hayman, C.C. and Gat, R., [1989]. *MRS Bulletin*, **October**, 38.

Bachmann, P., [1991]. *Physics World*, **April**, 32.

Bachmann P., [1993]. In *Thin Film Diamond*, edited by A.Lettington and J.W.Steeds (Chapman & Hall), London, UK.

Bakon, A. and Szymanski, A., [1993]. *Practical Uses of Diamond*, (Ellis Horwood), West Sussex, UK.

Chu, C.J., Hauge, R.H., Margrave, J.L. and D'Evelyn, M.P., [1992]. *Appl. Phys. Lett.*, **61**, 1393.

Collins, A.T. and Williams, A.W.S., [1971]. *J. Phys. C: Solid St. Phys.,* **4**, 1789.

Collins, A.T., [1989]. *Semicon. Sci. Technol.*, **4**, 605.

Collins, A.T., [1993]. In *Thin Film Diamond*, edited by A.Lettington and J.W.Steeds (Chapman &Hall), London.

Davidson, J.L., [1994]. in *Synthetic Diamond: Emerging Science and Technology*, ed. K.E. Spear, J.P. Dismukes, (John Wiley), New York, USA.

Flemish, J.R., Schauer, S.N., Wittstruck, R., Landstrass, M.I. and Plano, M.A., [1994]. *Diamond Relat. Mater.*, **3**, 672.

Fontaine, F., Deneuville, Gheeraert, E., Gonon, P., Abello, L. and Lucazeau, G. [1994], *Diamond Relat. Mater.*, **3**, 623.

Fox, B.A., Stoner, B.R., Malta, D.M., Ellis, P.J., Glass, R.C. and Sivazlian, F.R., [1994]. *Diamond & Relat. Mater.*, **3**, 382.

Fox, B.A., Hartsell, M.L., Malta, D.M., Wynands, H.A., Kao, C.-T., Plano, L.S., Tessmer, G.J., Henard, R.B., Holmes, J.S., Tessmer, A.J., and Dreifus, D.L., [1995]. *Diamond & Relat. Mater.*, **4**, 622.

Fujimori, N., Imai, T. and Doi, A., [1986]. *Vacuum*, **6**, 99.

Fujimori, N., Nakahata, H. and Imai, T., [1990]. *Jpn. J. Appl. Phys.*, **29**, 824.

Geis, M.W., Smith, H.I., Argoitia, A., Angus, J., Ma, G.-H.M., Glass, J.T., Butler, J.T., Robinson, C.J. and Pryor, R., [1991]. *Appl. Phys. Lett.*, **58**, 2485.

Geis, M. and Angus, J.C., [1992]. *Scientific American*, **October**, 64.

Geis, M.W., Efremow, N.N., Susalka, R., Twichell, J.C., Snail, K.A., Spiro, C., Sweeting, B. and Holly S., [1994]. *Diamond Relat. Mater.,* **4**, 76.

Graham, R.J., Shaapur, F., Kato, K. and Stoner, B.R., [1994]. *Appl. Phys. Lett.,* **65**, 292.

Grot, S.A., Hatfield, C.W., Gildenblat, G.Sh., Badzian, A.R. and Badzian, T., [1991]. *Appl. Phys. Lett.*, **58** , 1542.

Hirose, Y., Amanuma, S. and Komaki, K., [1988; 1990]. *J. Appl. Phys.,* **68**, 6401.

Jansen, F., Machonkin, M.A. and Kuhman, D.E., [1990]. *J. Vac. Sci. Technol.,* **B8,** 3785.

Janssen, G. and Giling, L.J., [1995]. *Diamond Relat. Mater.,* **4**, 1025.

Kajihara, S.A., Antonelli, A. and Bernholc, J., [1993]. *Physica B*, **185**, 144.

Kalish, R, Uzan-Saguy, C., Samoiloff, A., Locher, R. and Koidl, P. [1994]. *Appl. Phys. Lett.,* **64**, 2532.

Kamo, M., Sato, Y., Matsumoto, M. and Setaka, N., [1983]. *J. Crystal Growth*, **62**, 642.

Kawarada, M., Mar, K. and Kiraki, A., [1987]. *Jpn. J. Appl. Phys.*, **26**, L1032.

Kiyota, H., Matsushima< Sato, K., Okushi, H, Ando, T., Kamo, M., Sato, Y. and Iida, M., [1995]. *Appl. Phys. Lett.,* **67**, 3596.

Koba, R.J., [1993]. In *Diamond Films and Coatings*, edited by R.F.Davis, (Noyes Publications), Park Ridge, USA.

Landstrass, M.I. and Ravi, K.V., [1989]. *Appl. Phys. Lett.*, **55**, 975.

Lightowlers, E.C. and Collins, A.T., [1976]. *J. Phys. D: Appl. Phys.,* **9**, 951.

Malta, D.M., von Windheim, J.A. and Fox, B.A., [1993]. *Appl. Phys. Lett.*, **62**, 2926.

Masood, A. and Aslam, M., [1992]. *Appl. Phys. Lett.*, **61**, 1832.

Matsubara, H. and Sakuma, T., [1990]. *J. Mater. Science*, **25**, 4472.

Matsumoto, S., Sato, Y., Tsutsumi, M. and Setaka, N., [1982]. *J. Mater. Science*, **52**, 219.

Matsumoto, S., Hino, M. and Kokayashi, T., [1987]. *Appl. Phys. Lett.*, **51**, 737.

May, P.W., Rego, C.A., Ashfold, N.M.R., Rosser, K.N., Lu, G., Walsh, T.D., Holt, L., Everitt, N.M. and Partridge, P.G., [1995.] *Diamond & Relat. Mater.,* **4**, 794.

Mori Y., Eimori, N., Hatta, A., Ito, T. and Hiraki, A., [1992]. *Jpn. J. Appl. Phys.*, **31**, L1718.

Mori, Y., Yagi, H., Deguchi, M., Sogi, T., Yokota, Y., Eimori, N., Yagyu, H., Ohnishi, H., Kitabatake, M., Nishimura, K., Hatta, A., Ito, T., Hirao, T., Sasaki, T. and Hiraki, A., [1993]. *Jpn. J. Appl. Phys.*, **32**, 4661.

Mort, J., Kuhman, D., Machonkin, M., Morgan, M., Jansen, F., Okumura, K., LeGrice, Y.M. and Nemanich, R.J., [1989]. *Appl. Phys. Lett.*, **55**, 1121.

Mott, N., [1993]. *Conduction in non-crystalline materials,* (Clarendon Press), Oxford, UK.

Nishimura, K., Das, K. and Glass, J.T., [1991]. *J. Appl. Phys.*, **69**, 3142.

Okano, K., Kiyota, H., Iwasaki, T., Nakamura, Y., Akiba, Y., Kurosu, T., Iida, M. and Nakamura, T., [1990]. *Appl. Phys. A.*, **51**, 344.

Okano, K., Kiyota, H., Kurosu, T. and Iida, M., [1993]. *Diamond Relat. Mater.*, **3**, 35.

Plano, M.A., Zhao, S., Gardinier, C.F., Landstrass, M.I., Kania, D.R., Kagan, H., Gan, K.K., Kass, R., Pan, L.S., Han, S., Schnetzer, S. and Stone, R., [1994]. *Appl. Phys. Lett.*, **64**, 193.

Prawer, S., Uzan-Saguy, C., Braunstein, G. and Kalish, R., [1993]. *Appl. Phys. Lett.*, **63**, 2502.

Prins, J.F., [1992]. *Thin Solid Films*, **212**, 11.

Shiomi, H., Nishibayashi, Y. and Fujimori, N. [1991]. *Jpn. J. Appl. Phys.*, **30**, 1363.

Spitsyn, B.V., Bouilov, L.L. and Derjaguin, B.V., [1981]. *J. Crystal Growth*, **52**, 219.

Stoner, B.R., Ma, G.-H.M., Wolter, S.D. and Glass, J.T., [1992]. *Phys. Rev.*, **B5**, 11067.

Stoner, B.R., Kao, C-t, Malta, D.M., and Glass, R.C., [1993]. *Appl. P hys. Lett.*, **62**, 2347.

Suzuki, K., Sawabe, A., Yasuda, H. and Inuzuka, T., [1987]. *Appl. Phys. Lett.*, **50**, 728.

Tessmer, A.J., Plano, L.S. and Dreifus, D.L., [1993]. *IEEE Electron Device Lett.*, **14**, 66.

Tsai, W., Delfino, M., Hodul, D., Riaziat, M., Ching, L.Y., Reynolds, G. and Cooper, III, C.B., [1991]. *IEEE Electron Device Lett.*, **12** , 157.

Vishnevskii, A.S., Gontar, A.G., Torishnii, V.I. and Shul'zhenko, A.A., [1981]. *Sov. Phys. Semicond.*, **15**, 659.

Visser, E.P., Bauhuis, G.J., Janssen, G., Vollenberg, W., van Enckevort, W.J.P. and Giling, L.J., [1992]. *J. Phys.:Condens. Matter*, **4**, 7365.

von Windheim, J.A., Venkatesan, V., Malta, D.M. and Das, K., [1993a]. *J. Electronic Mater.*, **22**, 391.

von Windheim, J.A., Venkatesan, V., Malta, D.M. and Das, K., [1993b]. *Diamond & Relat. Mater.*, **2**, 841.

Werner, M., Dorsch, O., Baerwind, H.U., Obermeier, E., Haase, L., Seifert, W., Ringhandt, A., Johnston, C., Romani, S., Bishop, H. and Chalker, P.R., [1994]. *Appl. Phys. Lett.*, **64**, 595.

Wild, C., Kohl, R., Herres, N., Muller-Sebert, W. and Koidl, P., [1994]. *Diamond & Relat. Mater.*, **3**, 373.

Wilks, J., Wilks, E., [1991]. *Properties and Applications of Diamond*, (Butterworth-Heinemann), Oxford, UK.

Williams, A.W.S., Lightowlers, E.C. and Collins, A.T., [1970]. *J. Phys. C: Solid St. Phys.*, **3**, 1727.

Wolter, S.D., Stoner, B.R., Glass, J.T., Ellis, P.J., Buhaenko, D.S., Jenkins, C.E. and Southworth, P., [1993]. *Appl. Phys. Lett.*, **62**, 1215.

Zhu, W., Stoner, B.R., Williams, B.E. and Glass, J.T., [1991]. *Proc. IEEE*, **79**, 621.

4: EXPERIMENTAL METHODS: CHARACTERISATION, PROCESSING AND DEVICE FABRICATION

4.1 INTRODUCTION

The following characterisation techniques have been employed at various points throughout the course of this study. Details of device fabrication techniques and the laser processing system are also described.

4.2 BULK CHARACTERISATION

4.2.1 Scanning electron microscopy

In an electron microscope, an incident electron beam is used to provide a magnified image of the surface of the sample, similar to the principal of an optical microscope. However the use of electrons as the probe instead of visible light means that the resolution of a scanning electron microscope (SEM) may be significantly higher, though ultimately the resolution is determined by the focused beam size on the sample. The image in an SEM is produced by scanning this focused electron beam over the sample surface and sensing the scattered electrons. All of these signals may then be detected and amplified to control the brightness of a cathode ray tube (CRT); typically, magnifications in the range 50-40k and resolutions of 2.5-10 nm are possible with SEMs [Schroder, 1990; Zhu, 1993].

SEM has proven to be the most widely used technique to characterise the surface morphology of deposited diamond films and, when used in conjunction with Raman spectroscopy, the quality of the deposit may be qualitatively judged in a quick and efficient manner [Zhu, 1993]. A Hitachi S-800 SEM has been employed in the studies carried out here; resolution = 20nm on secondary electron emission with magnification = 20-300k.

4.2.2 Raman scattering spectroscopy

Raman spectroscopy is a vibrational spectroscopic technique which explores the energy levels of molecules by examining the light scattered by them. It is thus free from charging effects which may occur for electron or ion based methods in the characterisation of insulating materials. The incident monochromatic beam is passed through a non-absorbing medium with some of the incident photons colliding with molecules of the sample; this scattered light is then found to contain a mixture of different wavelengths, the main component of which consists of the wavelength of the incident light (Rayleigh scattering). A very low proportion is found to be shifted in wavelength due to the interaction of the photons with the lattice vibrations in the material (phonons); interaction with optical phonons is called Raman scattering whilst that with acoustic phonons Brillouin scattering [Schroder, 1990]. The higher energy of the optical phonons means that Raman scattering is easier to detect. In Raman scattering, a number of the incident photons give up a proportion of their energy to excite the lattice phonons and hence emerge with a lower energy; such photons contribute to the lower frequencies of the emergent beam and are termed Stokes lines, being the usual mode that is monitored. Other photons may gain energy from the molecules by annihilation of existing thermally excited vibrations in the sample and these contribute to the higher frequencies in the emergent beam, the anti-Stokes lines. The vibrational modes are dependent on the atomic bonding of the material under test and this is used as the phenomenon for characterisation [Zhu, 1993].

A Raman scattering system consists of the following main parts: (i) laser excitation source; (ii) optical system for illuminating the sample and collecting the scattered radiation; (iii) monochromator; (iv) detector and recording device [Baranska, 1987]. A commercial Renishaw System 2000 Raman spectrometer with He-Ne (632.8 nm) red-light excitation was used for investigation of diamond films in the course of this study. The probing radiation was directed onto the sample and scattered radiation collected via a commercial microscope, *i.e.* the Raman system being in a microprobe configuration. Typical spot sizes used were in the region of 100 μm. Figure 4.1 shows a schematic of the system where the sample scattered excitation laser light is collected through the microscope and analysed by the Raman spectrometer which consists of a fore-monochromator (range selector) and a spectrograph. The output of the spectrograph is passed into a multichannel detector to give a plot of the optical intensity at each component frequency.

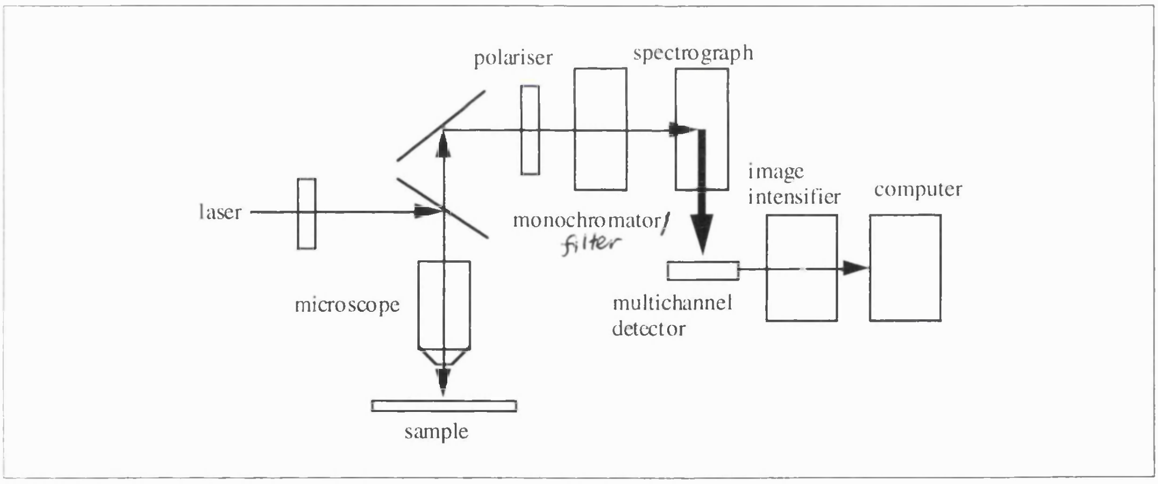

Figure 4.1 Schematic diagram of Raman microprobe system [redrawn from Huong, 1991].
Raman spectra was obtained in the monochromator mode in the course of this study.

In the case of carbon, and diamond films in particular, Raman spectroscopy has proved to be one of the most popular techniques for characterisation due to its inherent simplicity in operation including no vacuum requirements, minimal sample preparations and non-destructive nature. At room temperature, the first order Raman spectrum of natural diamond has been demonstrated to consist of an unambiguous single, intense line at 1332 cm^{-1}, differing significantly from that of other known carbonaceous material. Solin and Ramdas [1970] have excited this peak using 632.8 nm radiation at a range of temperatures from 300 K to 15 K; a change in the line position and full-width-half-maximum (FWHM) was observed from 1332.5 cm^{-1}, 1.65 cm^{-1} to 1333.3 cm^{-1}, 1.48 cm^{-1} respectively.

Furthermore, the Raman scattering efficiency of graphite (1580 cm^{-1}) with 514.5 nm (Ar ion) laser excitation has been found to be 50 times greater than that of diamond [Wada, 1981] at room temperature. The use of He-Ne laser irradiation has been reported to resonantly enhance the Raman bands of non-diamond carbons and thus has been suggested as a more sensitive tool in the evaluation of diamond films [Sails, 1995]; Figure 4.2 illustrates the differences which may arise from the utilisation of different excitation radiation. The combination of these properties lead to a technique which may be extremely sensitive to certain non-diamond components in thin film diamond deposits. The peak position and width of the diamond Raman line has been seen to depend on film preparation conditions and have been related to the structural order or crystallinity, temperature, defect density, and the distribution of internal or external stresses [Bachmann, 1994].

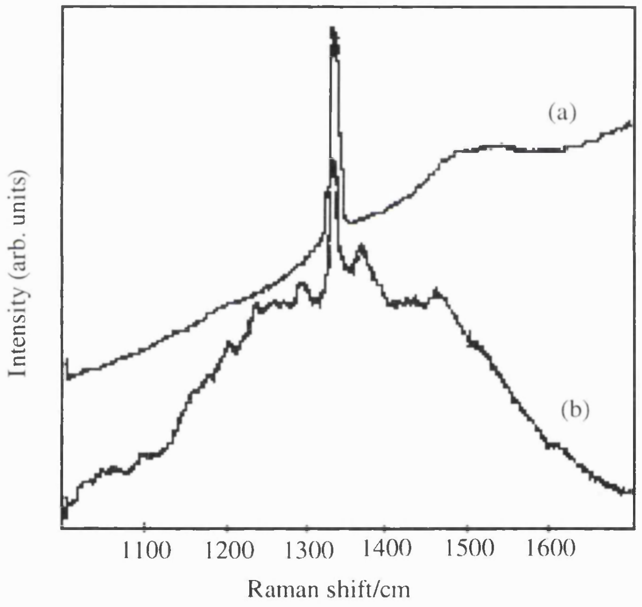

Figure 4.2 Raman spectra of a single CVD diamond film taken with (a) 514.5 nm and (b) 632.8 nm laser excitation [Williams, 1993].

Depth analysis by means of Raman spectroscopy is limited by the penetration depth of the laser light into the medium under test which depends both on the wavelength of excitation and on the extinction coefficient of the material under investigation; the characteristic depth to which the exciting radiation reaches 1/e of its initial intensity is given by [*e.g.* Tsai, 1987]:

$$\delta = \frac{\lambda}{4\pi k} \tag{4.1}$$

; where λ is the wavelength of excitation and k is the extinction coefficient of the medium at the wavelength of interest. The high value of extinction coefficient in opaque carbon materials (*e.g.* for amorphous carbon materials and graphite at an excitation wavelength of 632.8 nm $k \sim 10^{-1}$-10^{0} [Tsai, 1987]) limits the Raman signal to a region within tens of nanometers of the surface. Hence Raman spectroscopy may be considered as effectively a surface probing technique in the case of non-diamond carbon but a bulk characterisation technique in the case of diamond (at 632.8 nm, $k \sim 10^{-6}$ for diamond [Edwards, 1985]).

Raman scattering was carried out in the course of this study at the Defence Research Agency (Malvern, UK) employing a commercial Renishaw 2000 system with 632.8 nm He-Ne laser radiation.

4.2.3 Secondary ion mass spectroscopy

Secondary ion mass spectroscopy (SIMS) is an ion beam assisted analytical technique for the characterisation of foreign dopants in semiconductors. The element specific nature and the ability to detect isotopes and molecular species together with detection limits in the range 10^{14}-10^{15} cm^{-3} makes it a powerful and versatile method for semiconductor characterisation. It is a technique which is based on the destructive removal of material from a sample by sputtering and subsequent analysis of the ejected material by mass spectrometry. However, this process of ion bombardment leads not only to sputtering but also to ion implantation and lattice damage. The sputtered yield (number of sputtered atoms per incident primary ion) depends on the sample, crystallographic orientation, sample nature, ion energy and incidence angle of the primary beam [Schroder, 1990]. The sputtered population contains about 1% which is ejected as positive or negative ions; it is this which is detected in SIMS. The yield of ions may also be influenced by the type of primary ions; electronegative oxygen (O_2^+) is used for the detection of electropositive elements, whereas electropositive caesium (Cs^+) is used for electronegative elements. SIMS may be utilised in two configurations; at a low sputtering rate (~0.1 nm/h) *static* SIMS provides surface analysis, whereas at a higher primary ion energy (~10 μm/h) *dynamic* SIMS may be used to monitor specific elements as a function of depth. In order to obtain a quantitative profile, a selected mass (secondary ion yield) is plotted as a function of sputtering time; the absolute concentration may then be calculated by comparing to a set standard such as an ion implanted control sample. The depth into the sample at one moment in time is elucidated by using the total sputter time with the final depth. In the calibration of quantitative data it is important to take into account of preferential sputtering in polycrystalline material since this may lead to the component with the lowest yield being enriched at the surface, as well as the possible effect of the chemical environment of the element to be detected. This latter phenomenon is known as the matrix effect.

SIMS of samples in the course of this study have been carried out by staff at AEA Technology (Harwell, UK) using a CAMECA IMS 3F system. The system has a field of view of up to 400 μm diameter with a spatial resolution of 1 μm. The primary ion beam, accelerated typically at 17.5 keV (depending on the depth resolution and time requirements), is focused into a probe of 50 μm diameter which is rastered over an area of 500 μm^2 to promote uniform sputtering [Bishop, 1987]. Calibration was carried out using boron implanted samples.

4.3 SURFACE CHARACTERISATION

Auger electron spectroscopy (AES) is an electron spectroscopic technique capable of characterising the chemical composition of the top few atomic layers of a surface to a resolution of ~1%. This technique relies upon the monitoring of the kinetic energy of secondary electrons emitted from surface atoms following the ionisation of a core atom. A vacancy in a core subshell can be produced by X-ray photoionisation or electron impact ionisation. Two modes of relaxation are likely to occur; the first involves an electronic transition from an outer level to the core vacancy and the excess kinetic energy is emitted as a quantum of characteristic X-ray radiation. In the alternative mode of relaxation, the excess energy from the electron which fills the core vacancy causes a second electron to be emitted with a characteristic energy in a radiationless manner, leaving the system doubly positive charged. The secondary electron emitted via the latter process is called an "Auger" electron after its discoverer Pierre Auger [see Woodruff, 1986]. Radiative decay and Auger transitions are competing processes; however the relaxation by Auger emission is favoured over that by X-ray fluorescence for relatively shallow core levels. In the typical energy range of Auger transitions, 20-1000 eV, the electron escape depth of the Auger electrons is of the order of 3 atomic layers. This gives rise to the surface sensitivity of this technique, and the presence of any elemental contamination (1%) may be deduced from their characteristic Auger electron emission energy [Feldman, 1986].

Auger transitions are classified on the basis of the energy levels involved in the process. The position of the core hole is quoted first, followed by the level of the relaxing electron and finally the level from which the Auger electron is excited. For example, the Auger transition depicted in Figure 4.3 is a core-core-core (CCC) transition and is named

$KL_1L_{2,3}$ ($1s2s2p_{1/2}$). When electrons are taking part in the Auger process originate from the valence band of the solid, they are indicated by "V" (*e.g.* KVV transition). The kinetic energy of the Auger electron will be related to the final state of the atom or molecule, which is governed by the positioning of the double-hole formation and the interaction of the remaining electrons. This may be calculated from a knowledge of the binding energies of the levels involved in the process; such values are well tabulated [*e.g.* Davis, 1976].

The most common source of excitation used in AES is an electron beam which may be focused onto the sample surface producing a high intensity probe for primary excitation. However, a prominent limitation of electron-excited AES may arise through electron stimulated desorption/dissociation of any surface adsorbates; furthermore, high-intensity electron beams may also degrade the sample surface. Nevertheless, electron-excitation AES has become a major technique for surface elemental analysis. In this work AES has been employed as a tool for the qualification of the diamond surface as well as for the investigation of possible surface contamination/adsorbates after various processing steps.

In the case of carbon, AES has proven to be useful in distinguishing the diamond phase from graphite and amorphous carbon provided the AES system has moderate resolution (~1 eV) [Zhu, 1993]. It has been demonstrated by Lurie and Wilson [1977] that the AES fine structure of the carbon KLL peak is sensitive to the three types of carbon phases; the change in the chemical environment caused by the difference in chemical binding, results in a variation of the lineshape of the Auger signal. This lineshape is not affected by sample charging which is often a problem of AES on insulating material [Lurie, 1977]. Figure 4.4 shows typical AES spectra of a diamond film around the C KLL main peak at 268 eV (KV_1V_1 transition) with an inset for natural diamond, graphite and amorphous carbon. Three other peak energies for the spectrum of diamond have been assigned and designated A_0, A_1 and A_2 by Lurie and Wilson [1977] and others including Pate [1986]; these have energies of 259.4 eV, 247.7 eV and 233.5 eV.

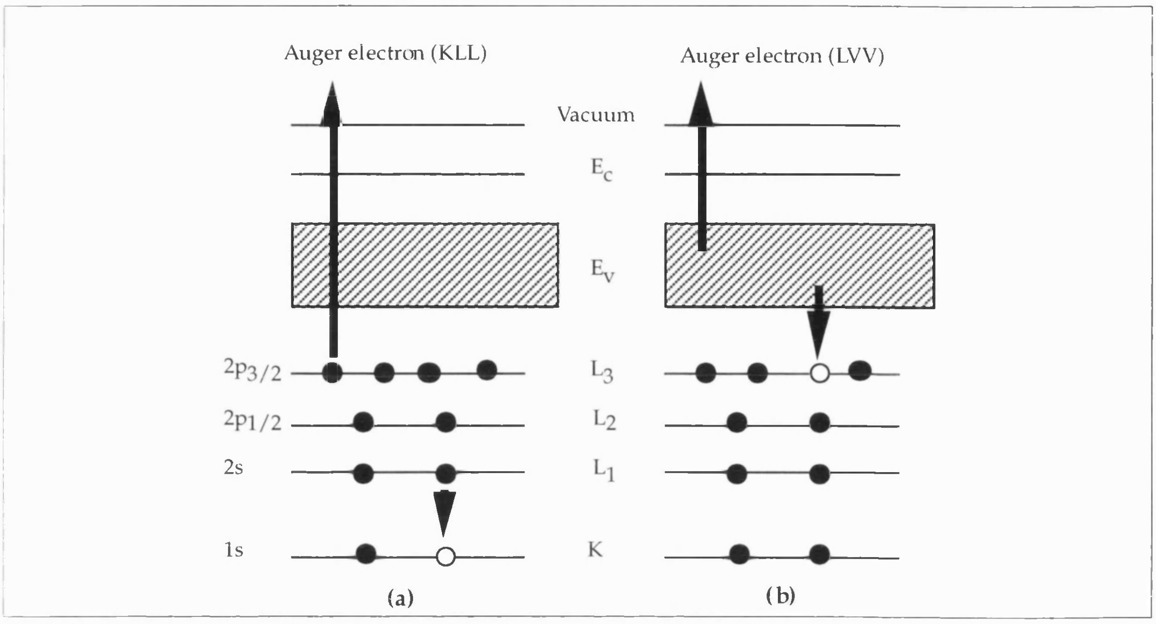

Figure 4.3 Schematic of (a) KLL and (b) LVV Auger de-excitation processes, where K, L and V are the X-ray notation equivalent of the spectroscopic notation 1s, 2p and the valence band. The first letter in the X-ray notation indicates the initial vacancy formed. [adapted from Feldman 1986].

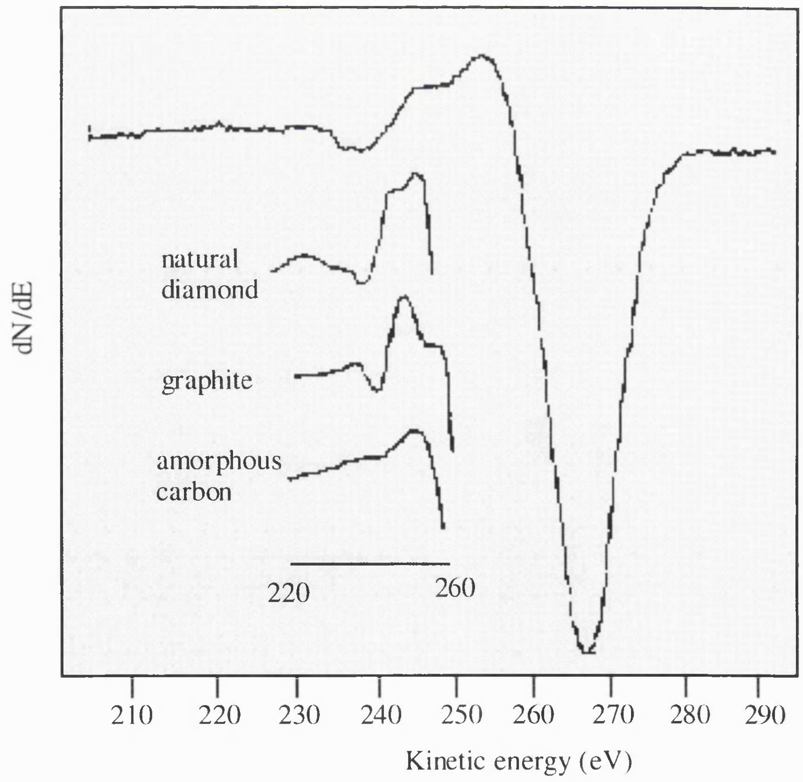

Figure 4.4 AES spectra of CVD diamond film with inset of spectra of natural diamond, graphite and amorphous carbon [redrawn from Zhu, 1993].

In the course of this study, AES was carried out in an ultra-high vacuum (UHV) chamber, which achieved base pressures < 5×10^{-10} torr following bake-out, equipped with a Varian 981-2707 cylindrical mirror analyser (CMA) for electron energy separation and a integrated electron gun. Figure 4.5 shows the experimental set-up used. The CMA consists of two cylindrical metal cylinders with the outer one connected to a negative voltage of V_{CMA}; electrons emitted during sample exposure to the electron gun are passed through annular slit A (with an acceptance angle of about 42°) and, depending on the repelling voltage V_{CMA}, will escape through slit B to be detected. Although an intensity/electron energy (N/E) plot can be obtained via this approach, the signal was differentiated (dN/dE) to provide a better signal to noise ratio of the Auger electrons in relation to the secondary and backscattered electrons [Woodruff, 1986]. Samples were mounted with tantalum foil in a resistively heatable configuration; K-type (Alumel-Chromel) thermocouples were spot welded onto tantalum foil and attached to the backside of the samples.

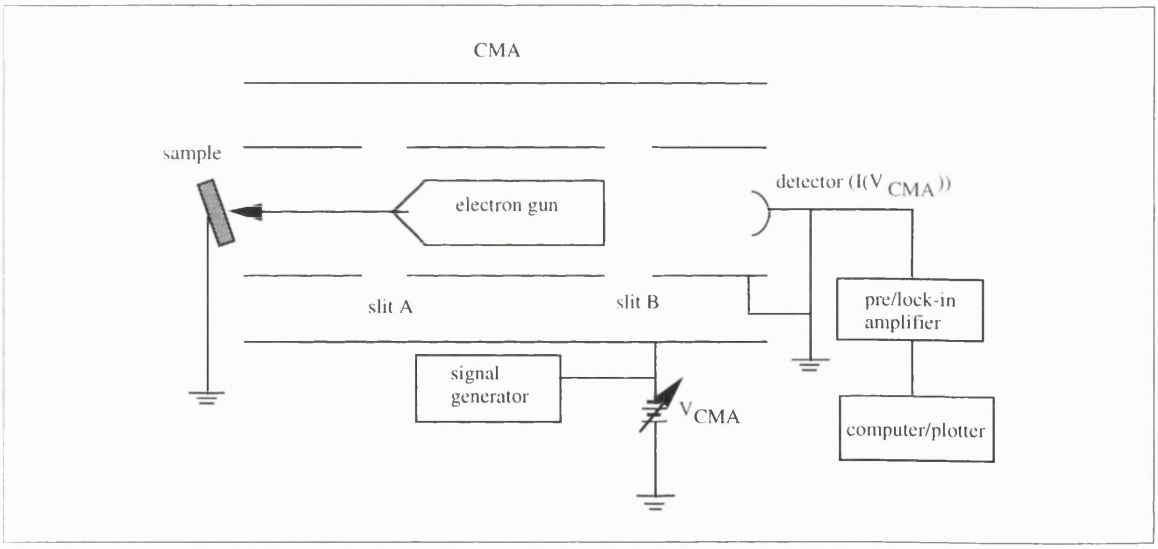

Figure 4.5 Experimental system used for Auger electron spectroscopy.

4.4 SURFACE PREPARATION AND DEVICE FABRICATION

Sample preparation and device fabrication was carried out in a clean room of Class 1000 in the open areas and Class 100 under the laminar flow hoods. The details of the processes employed are addressed in the appropriate chapters, and also in Appendix B (surface preparation) and Appendix C (device fabrication).

4.5 ELECTRICAL CHARACTERISATION

4.5.1 Current-voltage measurements

Electrical characterisation by two probe I-V has been carried out using the commercial Hewlett Packard HP4061A system which includes the HP4140B picoammeter/DC voltage source. The HP4140B unit is capable of providing an output voltage level of +/-100 V and has an measurement accuracy of 0.5% over a current range of +/-0.001 x 10^{-12} A to +/-1.999 x 10^{-2} A. The samples were placed on a Signatone heatable platform capable of reaching temperature levels ~450 °C in air. Measurements were obtained either via two tungsten probes in a planar device configuration, or else via one probe and the stage for vertical, "through" device measurements. Figure 4.6 shows a schematic of the I-V testing set-up.

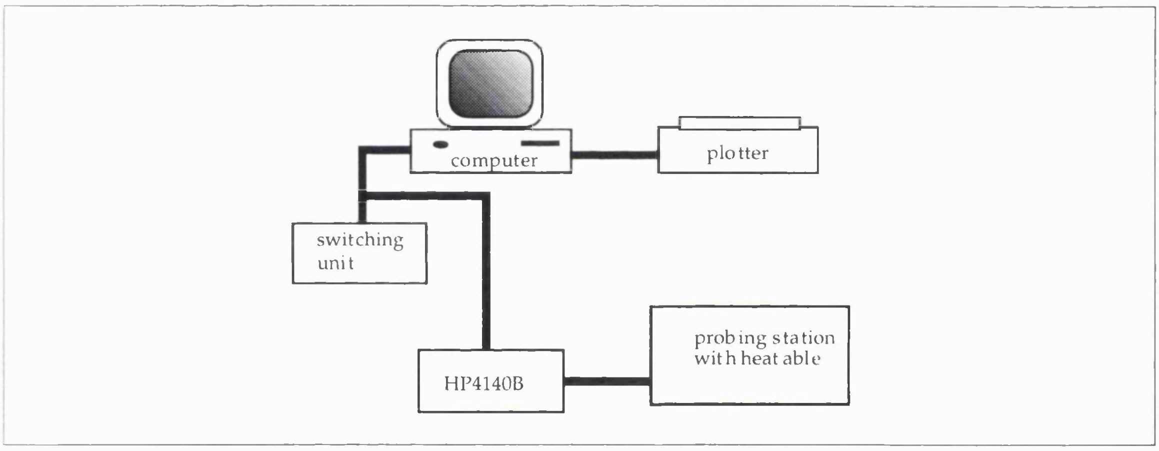

Figure 4.6 Schematic diagram of I-V electrical characterisation set-up.

4.5.2 Hall-effect measurements

The Hall effect measurement technique has found wide application in the electronic characterisation of semiconducting materials by providing information on the resistivity, the type of charge carrier, the carrier concentration and mobility of materials. This technique, which was discovered by E.H. Hall in 1879, relies on the fact that when a magnetic field is applied to a current carrying material in a direction perpendicular to the direction of the current flow an electric field is observed to develop. This Hall field, E_H, is perpendicular to both the current flow and the applied magnetic field (see Figure 4.7) [Smith, 1978].

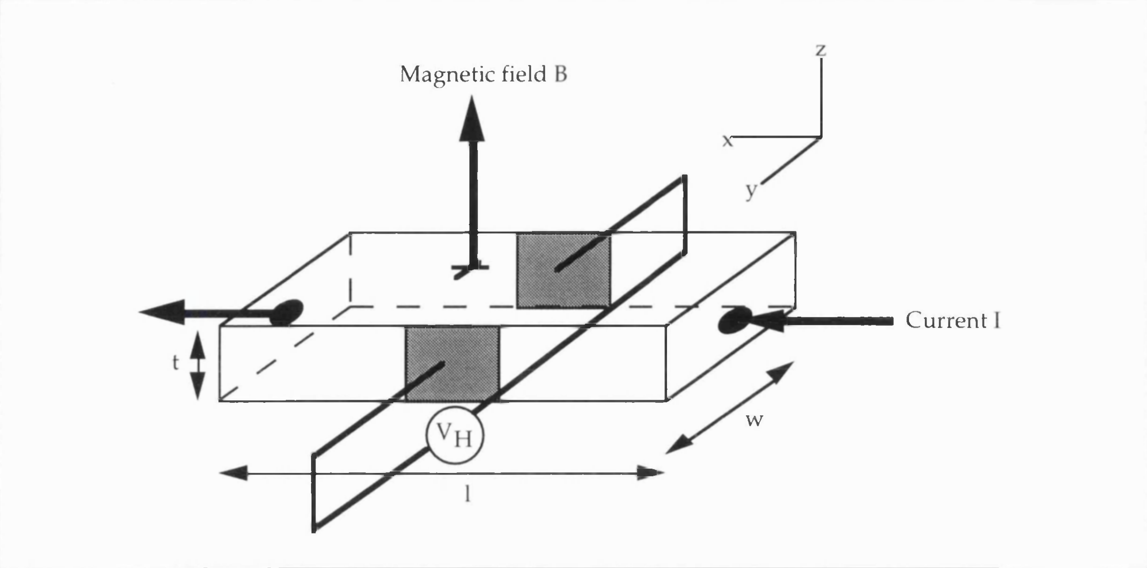

Figure 4.7 Hall effect in a p-type sample where, if the current (direction of holes) is in the x-direction and the applied magnetic field is in the z-direction, then the Hall voltage is developed in the y-direction.

In a p-type sample, the current density may be taken as:

$$j = \sigma E_x = pe\mu_p E_x = pev_p \qquad (4.2(a))$$

The force exerted by the magnetic field on the holes is given by the Lorentz force $f_{Lorentz} = ev_p \times B$ which leads To the Hall field of:

$$E_H = v_p B_z \qquad (4.2(b))$$

; where σ is the material conductivity, E_x the applied electric field in the x-direction, p the hole concentration, e the electronic charge, μ_p the hole mobility, v_p the average drift velocity of the hole carriers and B_z the applied magnetic field in the z-direction.

Equating Equations 4.2(a) and 4.2(b) results in a Hall voltage V_H of:

$$V_H = \frac{R_H B_z I}{t} \qquad (4.3(a))$$

where

$$R_H = \frac{1}{pe} \qquad (4.3(b))$$

$$\mu_H = \frac{R_H}{\rho}. \qquad (4.3(c))$$

Since all the parameters in Equation 4.3(a) may be experimentally determined, the hole carrier concentration may then be obtained from R_H which is the Hall constant (or Hall coefficient), and the carrier mobility derived if the resistivity of the material, ρ is known. However, Equation 4.3(b) only holds if the scattering mechanisms are energy independent; in the limit of a weak magnetic-field or low mobility material the Hall constant has to be modified by a Hall scattering factor, r_H which has a value dependent on the dominant scattering mechanism. The Hall mobility value μ_H is thus subsequently modified by this factor to obtain the drift mobility via:

$$\mu_{Hp} = r_H \mu_p \tag{4.4}$$

; where μ_{Hp} is the Hall mobility of majority hole carriers and μ_p is the conductivity mobility. The Hall scattering factor for holes in diamond has been investigated by Reggiani *et al.* [1983] using a range of valence band parameters from the literature; when compared with experimental values of drift and Hall mobilities, a value of $r_H = 0.6$ (300 K) was found to provide the optimum fit.

In order to realise the measurement of carrier mobility parameter from Equation 4.3(c), the four-point probe method is often used for resistivity measurements of ρ; in this case it is common for four probes to be arranged in-line equidistantly with the voltage drop being measured between the two inner probes while a small current is passed through the outer two electrodes [Schroder, 1990]. The sheet resistance (expressed in Ω/square) is the voltage to current ratio multiplied by a correction factor which takes into account of various geometry considerations including the effect of probe spacing, sample shape and dimensions. However it is desirable for a single sample preparation which would allow for the acquisition of the resistivity, carrier concentration and carrier mobility of a material. Although the preferred implementation for this may be the Hall "bar" or the bridge-type sample [Schroder, 1990], these prevent characterisation of thin films of material which may be difficult to process into the required configuration. A more general configuration was developed by van der Pauw [1958a; 1958b] which allows for the Hall effect evaluation of flat samples of arbitrary shape provided that the following conditions are fulfilled:

(i) the contacts are at the circumference of the sample;
(ii) the contacts are sufficiently small;
(iii) the sample is uniform in thickness; and
(iv) the surface of the sample is singly connected, *i.e.* no isolated holes.

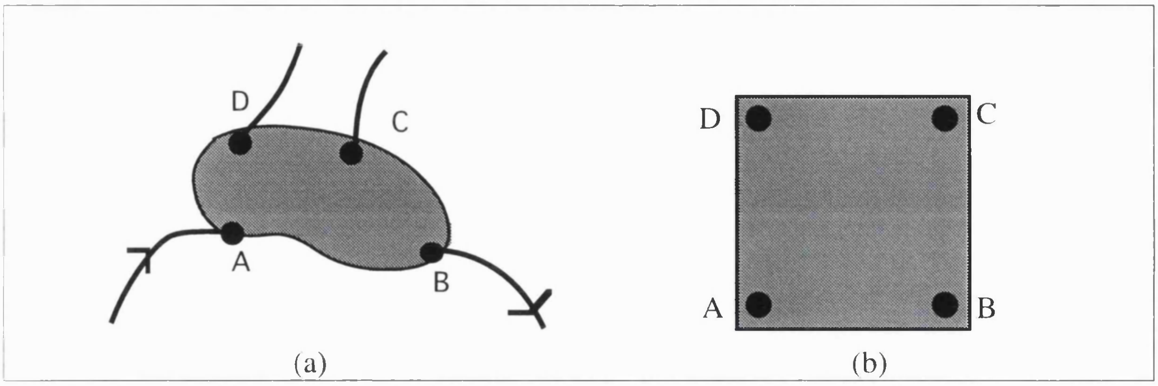

(a) (b)

Figure 4.8 (a)An arbitrary shaped lamella-type sample conforming to the conditions as specified by van der Pauw [1958a; 1958b] for Hall effect measurements. (b)Plan view of typical Hall sample in the square van der Pauw configuration with electrical contacts at the corner of the sample indicated by dark circles.

These conditions are satisfied by the samples shown in Figure 4.8 [Schroder, 1990]. Then, according to the theory developed by van der Pauw, the resistivity of the sample may be expressed as

$$\rho = \frac{\pi t}{\ln 2} \frac{(R_{AB,CD} + R_{BC,DA})}{2} f \qquad (4.5)$$

;where t is the sample thickness and $R_{wx,yz}$ is the resistance as derived from the voltage across contacts w and x, for a current flow between contacts y and z. The function f is found to vary with $R_{wx,yz}$ only, and is a measurement of the deviation from the symmetric situation; circular or square samples have $f = 1$ [see van Der Pauw, 1958a for the full correction curve]. If the sample is subjected to a magnetic field B in a perpendicular direction as specified, then Hall effect measurements can be performed and the Hall constant determined by from such sample configurations by [van Der Pauw, 1958a]:

$$R_H = \frac{t \Delta V_{AC}}{2 B I_{BD}} \qquad (4.6)$$

; where $\Delta V_{AC}/2$ is the average potential difference between contacts A and C when the sample is subjected to a positive then negative magnetic field. The carrier concentration and Hall mobility then follows from as Equation 4.3(a) and 4.3(b).

Hall effect measurements have been carried out using the commercial BIORAD HL5200 system at Imperial College (University of London, London, UK) which caters for data acquisition at room temperature and at 77 K (liquid nitrogen). Due to the inherent inert nature of diamond to wet chemical etching and also to the mechanical fragility of the thin diamond films (on silicon substrates), test samples were prepared in the square van der Pauw configuration with ohmic contacts deposited by standard photolithographic techniques.

4.6 EXCIMER LASER PROCESSING

The increasing desire for smaller linewidths (<0.25 μm) within the semiconductor industry has led to the logical development of deep-UV wavelengths for the fabrication of electronic components. Principally, excimer lasers operating at 308 nm (XeCl), 248 nm (KrF) and more recently at 193 nm (ArF) have been developed as solutions to this technological problem; complete excimer laser wafer steppers have been commercially available since 1986 [Goodall, 1992; Endert, 1995]. Ashby [1991] has discussed the general approaches to pattern formation utilising laser processing technology: (i) proximity masking; (ii) projection patterning; and (iii) direct writing. Proximity masking involves a stencil mask which is in direct contact with the substrate, giving a mask-to-feature ratio of ~1:1; the resolution, w is limited by Fresnel diffraction in the following manner:

$$w^2 = \frac{\lambda z}{2} \tag{4.7}$$

where z is the mask to substrate separation, and λ the wavelength of the radiation.

In addition to stringent controls required with mask fabrication as feature sizes decrease, proximity masking does not allow for ease of transfer towards laser chemical processing if gaseous or aqueous ambients are desired; if the mask is situated remotely from the substrate surface, then projection optics may be employed to de magnify the mask image giving the desired pattern at the surface of the substrate. The resolution of this system is then defined in a first order by:

$$w = \frac{\lambda}{2(NA)} \tag{4.8(a)}$$

with the numerical aperture, NA of the lens being;

$$NA = \frac{optical\ element\ diameter}{2\,x\ focal\ length} \tag{4.8(b)}$$

The depth of field of the projected image, *i.e.* the distance within which the image remains in focus is also dependent on the numerical aperture of the projection lens; the compromise which must then be made between the resolution and the depth of field has been addressed by Goodall [1992].

$$DOF = \frac{\lambda}{(NA)^2} \tag{4.9}$$

If a specific area is desired to be processed on a wafer, then the output beam may be focused directly onto the substrate in order that "direct-writing" may be achieved by translating the substrate in relation to the laser spot.

The advantages of excimer laser patterning, and projection patterning in particular over more established etching technologies such as that involving plasmas has been well discussed within the literature [*e.g.* Brannon, 1989; Ehrlich, 1989]. The intensity of the laser beam has been well demonstrated to ablate and etch a number of materials directly [Ashby, 1991], and, taken with the ability with which the laser beam may be patterned simply by the insertion of a standard Cr mask in the beam path, the overall process is effectively "maskless". This translates to the removal of at least three fabrication steps (deposition, patterning and removal) as compared to techniques requiring masking technology. In contrast to focused beam techniques, projection patterning is a parallel mode of processing in that complete mask patterns may be reproduced in a single exposure sequence.

Laser projection patterning of diamond films was carried out at the Excimer Laser Laboratory, Rutherford Appleton Laboratory (Chilton, Didcot) with the system shown schematically in Figure 4.9. A Lambda Physik LPX 305i excimer laser operating at 193 nm (ArF) provided a total output beam area of 3.5 cm x 1.5 cm; the beam energy density at the output of the laser was ~1.5 Jcm^{-2} at 193 nm. The pulse repetition rate of the laser was up to 50 Hz with pulsewidths of 15 ns (full width at half maximum). The output beam was directed onto a chrome on quartz mask which provided patterning of the laser radiation by reflecting/absorbing undesired parts of the beam with the chrome areas. This patterned beam is then directed through the quartz window of the processing chamber onto the sample via projection lenses designed for each particular wavelength; the projection lens has been designed with a NA of 0.05 (resolution ~3.5μm), depth-of-field of ~70 μm and a reduction factor of x10. The processing chamber has the capabilities to be evacuated to base pressures of ~10^{-3} mbar and is equipped with pirani and capacitive manometer pressure gauges to monitor the pressure ranges 10^{-2}-10^{0} mbar and 10-10^{3} mbar respectively. Gas inlets controlled by mass flow controllers into the processing chamber allows for the control of the chemical ambient during laser processing. The xyz sample stage is microprocessor controlled with a micrometer resolution allowing for precision step and repeat functions.

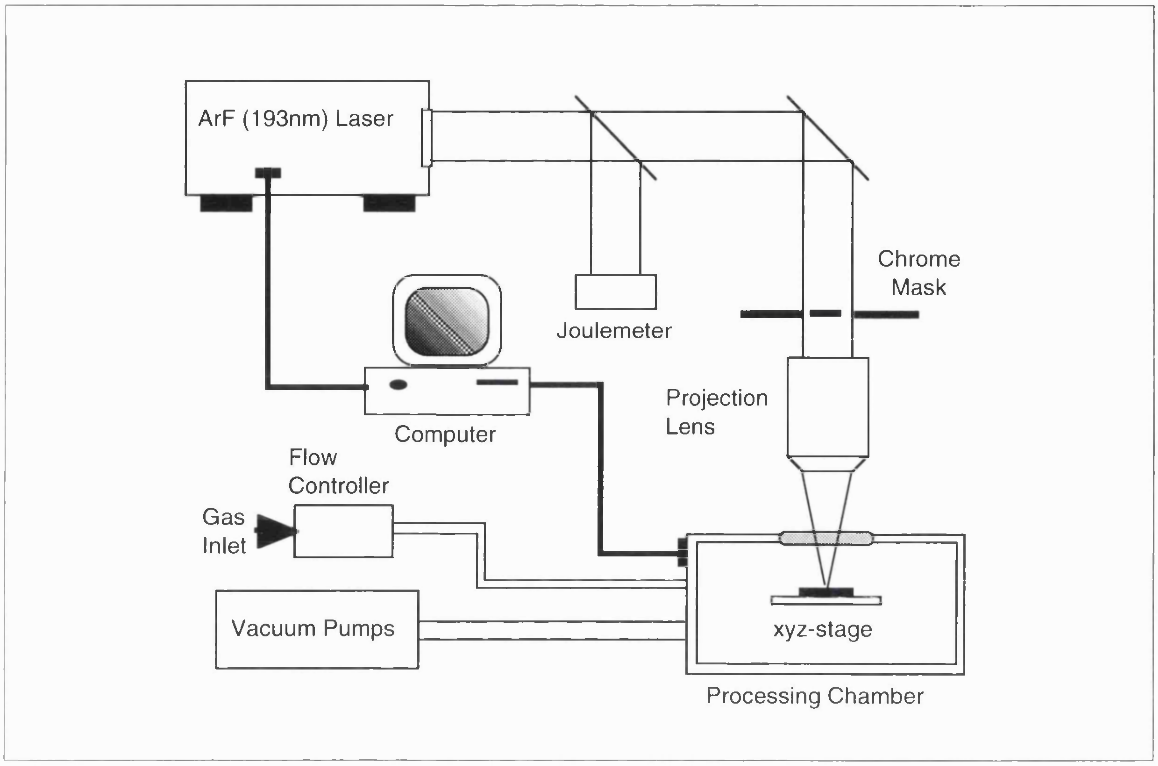

Figure 4.9 Schematic diagram of laser processing system.

REFERENCES

Ashby, C.I.H., [1991]. in *Thin Film Processes II,* ed. J.L. Vossen and W. Kern (Academic Press), San Diego, USA.

Bachmann, P.K., Bausen, H.D., Lade, H., Leers, D., Wiechert, D.U., Herres, N., Kohl, R. and Koidl, P., [1994]. *Diamond Relat. Mater.,* **3**, 1308.

Baranska, H., Labudzinska, A and Terpinski, J., [1987]. *Laser Raman spectroscopy: Analytical applications,* (Ellis Horwood), West Sussex, UK.

Bishop, H.E., Chalker, P.R. and Smart, D.W., [1987]. UKAEA, Harwell report on *Dynamic SIMS analysis of nickel sequentially oxidised in $^{16}O_2$ and $^{18}O_2$ a tmospheres,* Her Majesty's Stationery Office, London, UK.

Brannon, J.H., [1989]. *J. Vac. Sci. Technol.,* **B7**, 1064.

Davis, L.E., MacDonald, L.C., Palmberg, P.W., Riach, G.E. and Weber, R.E., [1976]. *Handbook of Auger Electron Spectroscopy*, Physical Electronics Industries, Inc., Eden Prairie, USA.

Edwards, D.F. and Philipp, H.R., [1985]. in *Handbook of Optical Constants of Solids,* ed. E.D. Palik, (Academic Press, Inc.), New York, USA.

Ehrlich, D.J. and Tsao, J.T. (eds.), [1989]. *Laser Microfabrication: Thin Film Processes and Lithography*, (Academic Press), San Diego, USA.

Endert, H., Patzel, R., Rebhan, U., Powell, M. and Basting, D., [1995]. *Jpn. J. Appl. Phys.,* **34**, 4050.

Feldman, L.C., and Mayer, J.W., [1986]. *Fundamentals of Surface and Thin Film Analysis*, (Elsevier Science), New York, USA.

Goodall, F.N., [1992]. in *Photochemical Processing of Electronic Materials,* ed. I.W. Boyd and R.B. Jackman, (Academic Press), London, UK.

Huoung, P.V., [1991]. in *Analysis of Microelectronic Materials and devices,* ed. M. Grasserbauer and H.W. Werner, (John Wiley), New York, USA.

Knight, D.S. and White, W.B., [1989]. *J. Mater. Res.,* **4**, 385.

Lurie, P.G. and Wilson, J.M., [1977]. *Surface Science,* **65**, 476.

Pate, B.B., [1986]. *Surf. Sci.*, **165**, 83.

Reggiani, L., Waechter, D. and Zukotynski, S., [1983]. *Phys Rev.,* **B28**, 3550.

Sails, S.R., Gardiner, D.J., Bowden, M., Savage, J. and Rodway, D., [1995]. presented at *Diamond Films '95, 6th Europen Conference on Diamond, Diamond-Like and Related Materials*, Barcelona, 10-15 September 1995.

Schroder, D.K., [1990]. *Semiconductor Material and Device Characterization,* (John Wiley & Sons), Inc., New York, UK.

Shur, M., [1990]. *Physics of Semiconductor Devices,* (Prentice Hall), New Jersey, USA.

Smith, R.A., [1978]. *Semiconductors*, 2nd edition, (Cambridge University Press), Cambridge, UK.

Solin, S.A. and Ramdas, A.K., [1970]. *Phys. Rev.,* **1**, 1687.

Tsai, H.-c. and Bogy, D.B., [1987]. *J.Vac. Sci. Technol.,* **A5**, 3287.

van der Pauw, L.J., [1958a]. *Philips Res. Rep.*, **13**, 1.

van der Pauw, L.J., [1958b]. *Philips Tech. Rev.,* **20**, 220.

Wada, N. and Solin S.A., [1981]. *Physica B,* **105**, 353.

Williams, K.P.J., Pitt, G.D., Smith, B.J.E., Whitley, A., Batchelder, D.N. and Hayward, I.P., [1993]. *J. Raman Spectros.,* **25**, 131.

Woodruff, D.P. and Delchar, T.A., [1986]. *Modern techniques of Surface Science*, (Cambridge University Press), Cambridge, UK.

Zhu, W., Kong, H.-S. and Glass, J.T., [1993]. in *Diamond Films and Coatings,* ed. by R.F. Davis., (Noyes Publications), New Jersey, USA.

5: SURFACE PREPARATION AND CHARACTERISATION OF THIN FILM DIAMOND

5.1 INTRODUCTION

The realisation of thin films of semiconducting diamond on non-diamond substrates by the incorporation of extrinsic dopant impurities over areas amenable to current integrated circuit fabrication methods allows for a more involved investigation into proposed electronic applications. Hence, evaluation of thin film diamond for device applications such as radiation detectors, rectifying contacts and field-effect transistors has been carried within the field [*e.g.* Gildenblat, 1991]. However, although devices have been demonstrated, it is critical that the diamond substrate material be suitably treated in order that reliable device operation may be obtained. This is of particular importance considering the wide range of techniques and deposition conditions available to synthesise thin-film diamond; growth of diamond on foreign substrates by these many techniques invariably results in material which is polycrystalline in nature and contain low levels of non-diamond carbon [Grot, 1990; Plano, 1994]. As-deposited diamond films whether intentionally doped or nominally intrinsic, often display significant electrical conductivity despite the insulating nature observed in natural diamond [Mori, 1992]. This aspect of as-deposited films, has also been attributed to the possible role of hydrogen in the passivation of traps [Landstrass, 1989a; 1989b]. In this latter report, the conductivity of as-deposited diamond was reduced by up to 6 orders of magnitude on heating to temperatures as low as 100 °C in an air or nitrogen ambient; the electrical conductivity was demonstrated to return to the as-deposited level by re-treating in a hydrogen plasma.

Diamond films deposited by microwave plasma CVD have also been demonstrated to be critically dependent on the ambient atmosphere during the end of the deposition sequence after the plasma is extinguished. Mori *et al.* [1992] observed the phenomenon that cooling either single- or poly-crystalline films in an oxygen containing ambient resulted in highly resistive material whereas *in-vacuo*, hydrogen or nitrogen ambients resulted in films with ~6 orders higher conductivity. This was attributed to the existence of a surface conductive layer which was considered to be removable in the oxygen ambient during the cooling of the deposited films; $\sim 10^{15}$ atoms.cm^{-2} of oxygen was seen to be present on the surface (Rutherford back scattering) but no oxygen peak was detected in the Auger spectrum. The resultant conductivity of non-oxygen cooled films was believed to arise from a combination of defects present in the surface region (as deduced by electron spin resonance), together with an amorphous carbon phase (from electron energy loss spectroscopy) which was judged not to be a complete overlayer by transmission electron microscopy [Mori, 1993].

Hence, in addition to the issue of reducing the surface roughness of as-deposited diamond films which may introduce difficulties during photolithography [Plano, 1995], electronic device fabrication on diamond films has to take into account the following preparatory considerations:

(i) the possible role of hydrogen in the overall electrical conductivity of the film both at room temperature, and its stability particularly at elevated temperatures; and
(ii) the possible presence of non-diamond carbonaceous layers on the surface of as-deposited diamond films and their contribution towards electrical conductivity.

In order to alleviate such issues, stabilisation of the diamond films have been achieved by heating the substrates prior to device fabrication; Harper and co-workers [1991] have demonstrated temperature-stable electrical characteristics after heating their films to 350 °C for 1 h. Methods aimed at removing surface graphitic/conducting layers are also commonly employed within the field; these have typically involved 'wet' methods wherein heated mixtures of sulphuric acid with strongly oxidising agents such as chromic acid [Geis, 1987] or ammonium persulphate [Grot, 1990] are deployed. In such cases, significant differences have been observed in device characteristics between material which have been treated by these methods; in a study conducted by Grot *et al.* [1990], sheet resistance measurements did not reflect the expected trend of the level of doping in the bulk material until chemical cleaning was carried out. Chemical cleaning has also been demonstrated to alter the characteristics from ohmic to rectifying of various metals contact metallisations on semiconducting diamond [Mori, 1991].

It is thus of interest to compare these various treatments which have been widely practised within the community in a systematic manner in order to assess both their roles and relative merits in the preparation of diamond films for electronic applications. This chapter presents a study employing the surface sensitive technique of Auger electron spectroscopy (AES) for the characterisation of as-deposited thin films of diamond with those after various post-deposition treatments.

5.2 EXPERIMENTAL DETAILS

Polycrystalline, silicon supported thin film diamond of thickness 5 μm grown by microwave plasma CVD was used in this investigation; Figure 5.1 shows a scanning electron micrograph and the corresponding Raman spectrum of the material which consists of a continuous film consisting of coalesced grains of average size 1-2 μm. Samples of approximately 8 mm by 8 mm were cut from the middle section of a ~10 cm wafer and subjected to various treatments as summarised in Table 5.1 using the procedure described in Appendix B. Characterisation of the effect of these treatments have been carried out employing the Auger electron spectroscopy system described in Chapter 4 with an electron beam energy of 3 kV resulting in a beam current of 1 μA to minimise electron induced changes within the surface region.

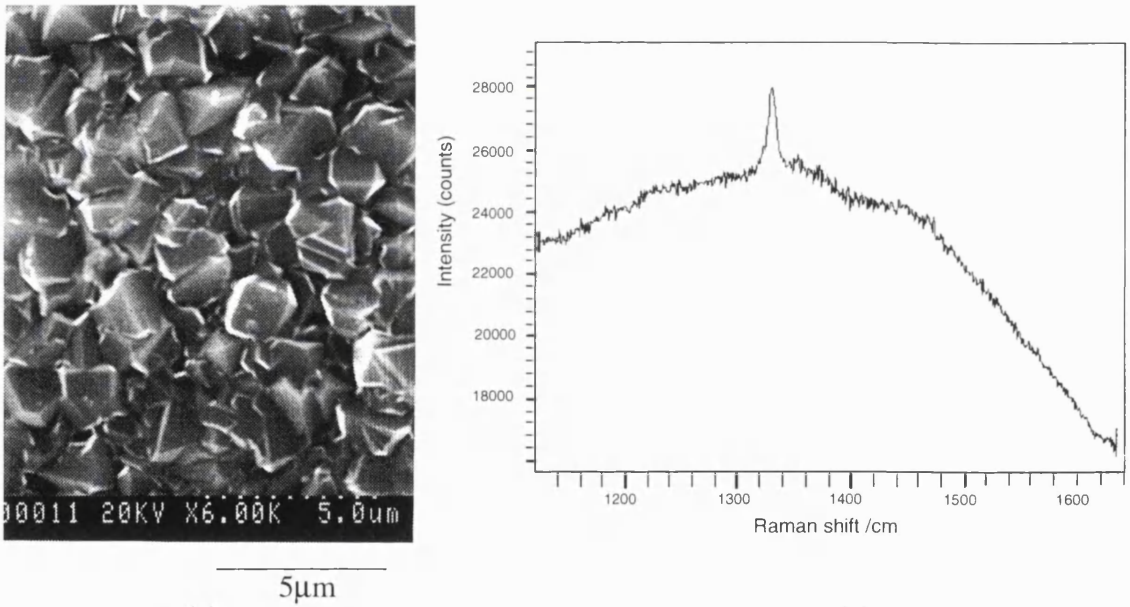

(a) (b)

Figure 5.1 (a) Scanning electron micrograph of thin film diamond with (b) associated Raman spectrograph of polycrystalline diamond used in the AES study on the effect of post-deposition surface treatments.

Treatment	Technique	Main components
A	De-grease	Trichloroethane, acetone, iso-propyl alcohol, de-ionised water
B	Hydrogen plasma	700 °C, 15 min, 20 Torr
C	Acid treatment (ammonium persulphate)	H_2SO_4: $(NH_4)_2S_2O_8$ (30 min, 200°C) (1:1) H_2O_2: NH_4OH (15 min, boiling)
D	Acid treatment (chromic acid)	H_2SO_4: CrO_3 (10 min, 170°C) (1:1) H_2O_2: NH_4OH (15 min, boiling)

Table 5.1 Summary of post-deposition treatments of diamond employed in this study.

5.3 RESULTS

Auger electron differential spectra recorded in the energy range 150-600 eV following various treatments are shown in Figure 5.2. All the spectra have been calibrated by reference to the main carbon (diamond) KVV peak energy which is located at 268 eV [Lurie, 1977]. It is apparent that in addition to the feature attributable to carbon (268 eV), other features are present in the wide scan spectra under some of the conditions employed. From a standard handbook on Auger spectroscopy, [Davis, 1976], these peaks may be associated with sulphur (expected around 152 eV) and oxygen (~510 eV). With 'as inserted' samples, *e.g.* spectrum (i), then a significant peak at 514 eV is obtained which suggests the presence of oxygen or chromium components. Since these samples have not been subjected to chromium containing treatments, this feature is most likely associated with oxygen. However, a small shift (~4 eV) from the energy more typically associated with oxygen on surfaces is apparent. A sample which was heated to ~600 °C prior to exposure to the Auger probe electron beam (treatment B, spectrum (ii)) does not show a peak at this energy; this indicates that residual contamination from exposure of the sample to the air leads to adsorbed oxygen or water which is readily lost upon heating *in-vacuo.* Spectra (iii) and (iv) relate to 'as inserted' samples following treatments C and D, respectively, whilst spectra (v) and (vi) represent samples that have also received these treatments, followed by heat cleaning *in-vacuo* prior to investigation by AES. It is of interest to note that both the 'as inserted' samples reveal a peak around 150 eV which may be attributed to sulphur, although this is stronger in the case of treatment D; this feature is not apparent on the heat cleaned samples. In all cases where the samples have been subjected to treatments C and D, a peak attributable to oxygen is apparent; the fact that heat cleaning has not led to the removal of this feature indicates the origin of this oxygen peak is not simply residual contamination, but that it is associated with the treatments used.

Figure 5.3 shows higher resolution spectra recorded in the energy range 220-300 eV (at a modulation of 2V) for the various samples following heat cleaning *in-vacuo* prior to AES investigation. Spectra taken on samples prior to heating were qualitatively similar. Significant variation in the structure of the peak, attributable to carbon, can be seen. In the case of the simple de-grease (treatment A, spectrum (i)) a peak minimum occurs at 268 eV with little other structure being evident. In contrast, treatment B (spectrum (ii)) leads to two peak maxima on the low energy side of the primary peak minimum, which again occurs at 268 eV. Similar structure is visible following treatment C (spectrum (iii)), but the higher energy of the two maxima is slightly strengthened in intensity. Treatment D (spectrum (iv)) gives rise to a spectrum where the two maxima are still discernible but the minimum between them has almost disappeared.

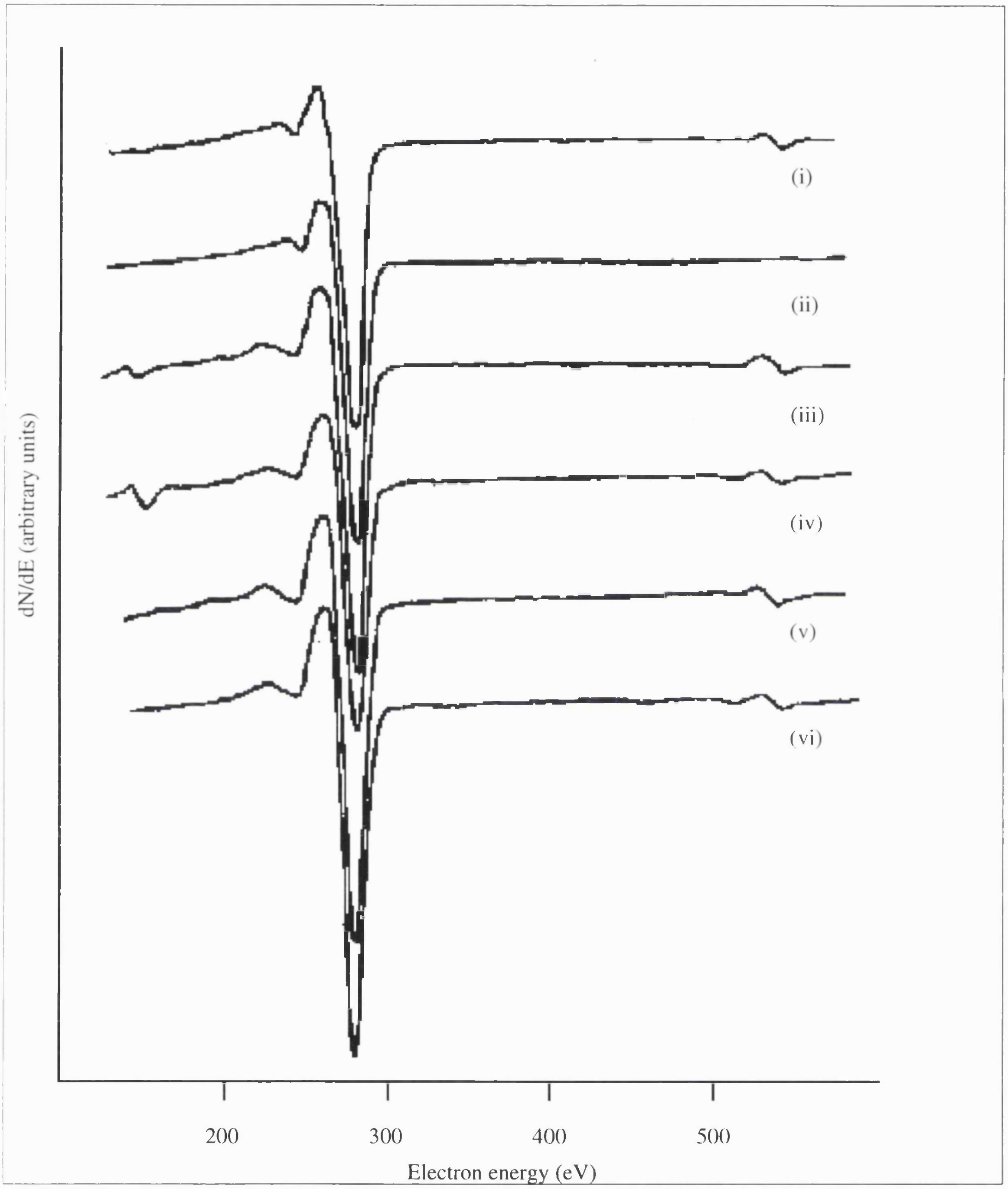

Figure 5.2 Wide energy scan Auger electron spectra (beam energy = 3 kV, beam current = 1 μA, modulation = 5 V) for CVD thin film diamond following: (i) treatment B; (ii) treatment B plus *in-vacuo* heating to 600 °C; (iii) treatment C; (iv) treatment D; (v) treatment C plus *in-vacuo* heating; and (vi) treatment D plus *in-vacuo* heating. The nature of each treatment is described in the text.

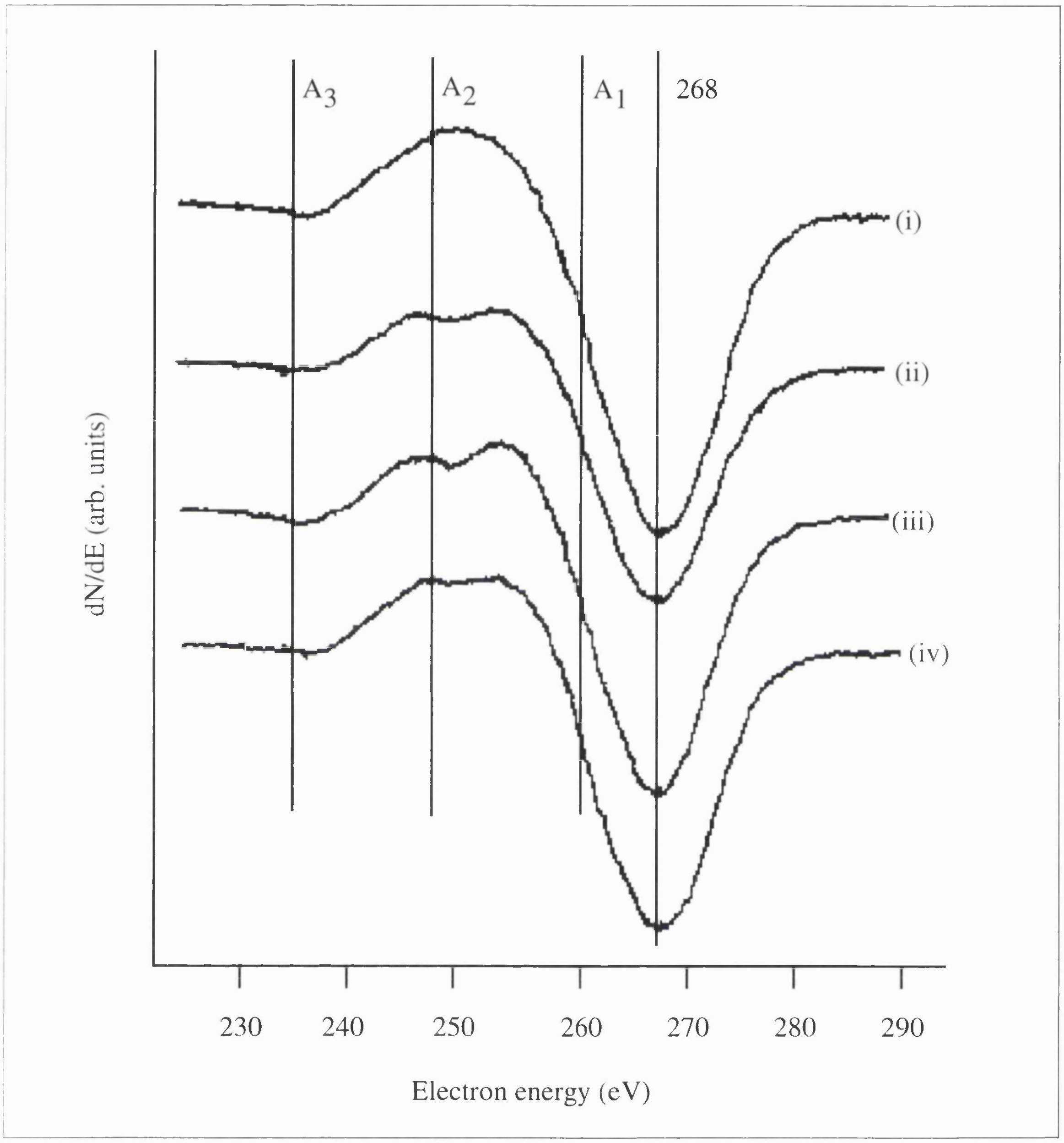

Figure 5.3 High resolution Auger electron spectra (beam energy = 3 kV, beam current = 1 μA, modulation = 2 V) of carbon KVV energy region of CVD thin film diamond samples following heating *in-vacuo* for: (i) treatment A; (ii) treatment B; (iii) treatment C; and (iv) treatment D. The nature of each treatment is described in the text, with peaks P_0 (=268 eV), A_1, A_2 and A_3 being referred to later.

5.4 DISCUSSION

Diamond surfaces have been studied with Auger electron spectroscopy by a number of other workers including Lurie and Wilson [1977] and Pate [1986]; representative spectra of diamond and graphite are presented in Figure 4.4. The main carbon peak arises from a KVV Auger process; in addition to this primary peak minima at 268 eV (P_0), Lurie and Wilson [1977] identified three further peak minima in the Auger spectra of single crystal diamond (A_1, A_2, A_3). From a band structure model, the density of states in the valance band structure of diamond shows 3 maxima (V_1, V_2, V_3) which may give rise to a number of Auger processes with slightly differing energies. Lurie and Wilson [1977] attributed the two highest energy of the four observed peaks in the Auger spectra of diamond to KV_1V_1 and KV_2V_2 transitions respectively. The remaining peaks were considered to arise from surface and bulk plasmon losses from the Auger electrons from the primary (KV_1V_1) transition. These peak energies are summarised in Table 5.2 including similar assignments made by Pate [1986], where P_0 refers to the lowest energy point in the differentiated Auger spectrum and A_1, A_2 and A_3 refer to points which correspond to peaks in the non-differentiated spectrum.

Diamond	P_0	A_1	A_2	A_3
Peak position	268	256	240	230
Band structure	269 (KV_1V_1)	256 (KV_2V_2)	245 (268 - sp)	235 (268 - bp)
Pate [1986]	267.7	259.4	247.7	233.5
Graphite				
Peak position	268	255	241	-
Pate [1986]	268	259.4	246.8	234.4
Amorphous carbon				
Peak position	268		243	

Table 5.2 Peak positions (eV) and identification of the structure in the carbon KLL spectra from diamond, graphite and amorphous carbon. The peak positions have been corrected for analyser work function surface charging. 'sp' and 'bp' refer to surface and bulk plasmon energies. 'Band structure' refers to predicted energies for the Auger peaks [adapted from Lurie, 1977; Pate, 1986].

The energy of the four peaks observed by Pate [1986] (268, 259.4, 247.7 and 233.5 eV), are marked in Figure 5.3. Close agreement is evident between the positions of these Auger peaks obtained for curves (ii)-(iv) in Figure 5.3. All three of the post-deposition treated CVD thin film diamond surfaces represented by these traces thus comprise good quality diamond over the probe depth of the AES technique (3-4 atomic layers). The relative peak intensities of A_1 to A_2 do, however, vary between these spectra. Curve (iii) shows the most pronounced A_1 feature followed by curve (ii) and curve (iv) respectively. Bugaets *et al.* [1994] observed a change in this region of the monocrystalline diamond (111) Auger electron spectra when the probe beam energy was changed from 3 keV to 6 keV; the point of maximum intensity in the differentiated spectra corresponding to A_2 was seen to reduce in intensity with respect to the peak of A_1. By consideration of the undifferentiated signal with the theoretical valence band density of states, this change in the relative intensities of the two peaks was attributed to electron beam induced changes to the valence band electron states rather than true graphitisation. Pepper [1981] has also suggested that using a primary electron beam energy of 2 keV, modification of the surface of type IIa diamond by the Auger probe takes place; a difference in the Auger spectral region around the A_1 and A_2 "peaks" was observed between samples which were stationary during the analysis and those which were moving at 7 μm.s^{-1} with respect to the electron beam. If the height between the maxima A_1 and the trough (situated between the two maxima A_1 and A_2) is taken as S_1, and that between the trough and the maxima at A_2 as S_2, then the factor S_1/S_2 was found by Pepper [1981] to be 3 for the spectra obtained for stationary diamond type IIa samples and 5 for moving samples (unmodified by the electron beam). This was suggested as a useful indicator for the diamondlike state of the carbon under investigation. For the spectra obtained in Figure 5.3, this factor may be approximated for the various samples to obtain: 1.1 for treatment B; 2 for treatment C; and 1 for treatment D.

The wide energy scan spectra (Figure 5.2) indicate that both sulphur (~152 eV) and oxygen (~510 eV) can contaminate diamond surfaces following some of the treatments used. Samples not treated with oxidising solutions (*e.g.* treatments A and B), measured prior to heat cleaning *in-vacuo* (spectrum (i)), show an oxygen to carbon peak ratio of approximately 0.05; using standard Auger sensitivity factors [Davis, 1976] and as given by Pate [1986], the coverage of oxygen may be estimated, if it is assumed that this component is adsorbed on the top of the diamond surface as opposed to a bulk phase, from:

$$\zeta = \frac{N_V}{N_S}\frac{I_O / S_O}{I_C / S_C}\lambda.\cos 43^0 \qquad (5.1)$$

;where N_V and N_S are the volume and surface densities of C in diamond respectively, I_O and I_C the respective intensities of the oxygen and carbon peaks, S_O and S_C the Auger sensitivity factors for oxygen and carbon respectively, λ the electron escape depth (= 7.5 Å at 262 eV [Pate, 1986] and 43° refers to the acceptance angle of the cylindrical mirror analyser (CMA).

It can then be estimated that oxygen comprises around 8% of a monolayer if it is resident on the diamond surface rather than as a disperse phase. The loss of this peak following heating to 600 °C is consistent with the observations of Thomas *et al.* [1992] investigating oxygenated diamond (100) surfaces by thermal desorption studies; CO desorption was detected at 600°C. Such an oxygen component arising from an adsorbed contamination layer by exposure to air was similarly concluded by Chia *et al.* [1994] in their Auger electron spectroscopic study of CVD diamond layers; removal in this case was achieved by sputtering with Ar ions (energy unspecified) for 5 s. Treatments C and D (oxidising solutions) lead to an oxygen peak which is *stable* to *in-vacuo* heating to temperatures of at least 600 °C. The oxygen to diamond peak ratios following heat cleaning indicate that around 8% of a monolayer of oxygen is present following treatment C, with a figure of 6% arising from treatment D. Prior to heat cleaning, both treatments C and D give rise to a sulphur peak with a S:C ratio of 0.036 and 0.0875 respectively. Assuming that both the oxygen and sulphur are distributed evenly on the surface of the diamond and again using tabulated Auger sensitivity factors [Davis, 1976] it can be estimated that sulphur constitutes around 1.9 % and 4.6 % of the surface region in each case. The subsequent loss of this phase upon heating indicates that sulphur is mobile within the diamond or within the grain boundaries in the CVD diamond film.

It is evident that whilst a sample that has only received a de-grease (treatment A) shows a spectra attributable to amorphous carbon, hydrogen plasma cleaning (treatment B) is capable of producing a qualitatively good diamond surface as judged by AES. The use of the wet etching methods studied here (C and D) introduces low concentrations of oxygen and sulphur contamination to the surface region, presumably as a result of the strongly oxidising conditions and the sulphur containing reagents used. Whilst the sulphur appears to be mobile and can be thermally driven into the bulk, the oxygen appears to be present as a stable oxide phase to about 8% of a monolayer. However, the fine structure within the high resolution carbon spectra recorded for treatment C, where this oxide phase is present, is the most well defined of all of the surfaces studied. This change could arise due to a reduction in the concentration of some form of non-diamond carbon, or due to the presence of the oxide phase; the similarity between the changes observed here and those of Bugaets *et al.* [1994] in addition to the potency of the oxidising solutions for non-carbon removal favour the latter conclusion. This suggests the oxygen is modifying the electronic structure of the surface such that the valence band of the diamond more closely resembles that reported for single crystal material. A change in surface reconstruction seems unlikely to be the cause of this difference on the polycrystalline diamond surfaces studied here given the low concentration of oxygen detected; more likely, oxygen is modifying the nature of defects within the surface region of the film. Indeed, Mori *et al.* [1993] suggested that in as-deposited CVD films, a surface layer, consisting of an incomplete amorphous carbon overlayer together with a large amount of defects within the surface, may exist as a result of plasma irradiation during growth conditions. This defective layer was identified by electron spin resonance measurements (ESR) and was suggested to be responsible for observed conductivity of as-deposited films. The fact that treatment leading to an oxygen component on the surface together with a subsequent reduction in conductivity also suggests that oxygen may lead to a modification of these defects within the surface layer [Mori, 1992]. Modifications to the chemical environment of the surface has been reported by Haas *et al.* [1972] to alter AES spectra including the possibility of changes in the relative intensity of Auger lines in various groups, and changes in the shape of a group of overlapping Auger lines. The use of such a chemical acid treatment may modify the electronic characteristics of device interfaces formed on diamond. Some evidence for this exists in the work of Mori *et al.* [1991] who found that oxidised diamond surfaces, which revealed a sub-monolayer oxide phase as judged by XPS measurements, dictated the electrical characteristics of a wide range of metallisation schemes. Treatment D, although also used as an oxidising agent, does not lead to this enhanced fine structure; slightly less oxygen is apparent on the surface following this treatment and either this or the possibility that some very low concentration of non-diamond carbon remains is presumably responsible for this. In addition, this treatment gives rise to higher levels of sulphur contamination suggesting it is less useful for the cleaning of CVD diamond films for device purposes; there is no evidence from the spectra recorded here that metallic contamination (such as Cr) occurs.

5.5 SUMMARY

Exposing a CVD grown polycrystalline diamond thin film to a hydrogen plasma at the termination of the growth run or the use of strongly oxidising solutions are both capable of removing non-diamond carbon from the surface, as judged by AES spectra of as-deposited film (treatment A) and after the various treatments. However, the oxidising solutions considered here (sulphuric acid -ammonium persulphate and sulphuric acid-chromic acid) both give rise to low concentrations of sulphur within the surface region and produce some form of oxide phase. Whilst these effects may be considered a disadvantage of this approach, AES indicates that the ammonium persulphate based etchant solution gives rise to a carbon KVV spectrum with a closer resemblance to natural single crystal diamond; it can be speculated that the low concentration of oxygen that is present is reducing the effects of defects within the material on the valence band structure of the diamond thin film surface.

REFERENCES

Bugaets, O.P., Smekhnov, A.A. and Kuzenkov, S.P., [1994]. *J. Electron Spectros. & Relat. Phenom.*, **68**, 713.

Chia, Q.S., Younes, C.M., Partridge, P.G., Allen, G.C., May, P.M. and Rego, C.A., [1994]. *J. Mater. Sci.*, **29**, 6397.

Davis, L.E., MacDonald, N.C., Palmberg, P.W., Riach, G.E. and Weber, R.E., [1976]. *Handbook of Auger spectroscopy,* Physical Electronics Industries, Edan Prairie, MN, USA.

Geis, M.W., Rathman, D.D., Ehrlich, D.J., Murphy, R.A. and Lindley, W.T., [1987]. *IEEE Electron Device Lett.,* **8**, 341.

Gildenblat, G.Sh., Grot, S.A. and Badzian, A. [1991]. *Proc. IEEE,* **79**, 647.

Grot, S.A., Gildenblat, G.Sh., Hatfield, C.W., Wronski, C.R., Badzian, A.R., Badzian, T. and Messier, R., [1990]. *IEEE Electron Device Lett.*, **11**, 100.

Haas, T.W., Grant, J.T. and Dooley, III, G.J., [1971]. *J. Appl. Phys.,* **43**, 1853.

Harper, R.E., Johnston, C., Blamires, N.G., Chalker, P.R. and Buckley-Golder I.M., [1991]. *Surface Coatings Technol.,* **47**, 344.

Landstrass, M.I. and Ravi, K.V., [1989a]. *Appl. Phys. Lett.,* **55**, 975.

Landstrass, M.I. and Ravi, K.V., [1989b]. *Appl. Phys. Lett.,* **55**, 1391.

Lurie, P.G. and Wilson, J.M., [1977]. *Surf. Sci.*, **65**, 476.

Mori, Y., Kawarada, H. and Hiraki, A., [1991]. *Appl. Phys. Lett.,***58**, 940.

Mori, Y., Eimori, N., Hatta, A., Ito, T. and Hiraki, A., [1992]. *Jpn. J. Appl. Phys.*, **31**, L1718.

Mori, Y., Show, Y., Deguchi, M., Yagi, H., Yagu, H., Eimori, N., Okada, T., Hatta, A., Nishimura, K., Kitabatake, M., Ito, T., Hirao, T., Izumi, T., Sasaki, T. and Hiraki, A., [1993]. *Jpn. J. Appl., Phys., **32**, L987.*

Pate, B.B., [1986]. *Surf. Sci.*, **165**, 83.

Pepper, S.V. [1981]. *Appl. Phys. Lett.,* **38**, 344.

Plano, M.A., Zhao, S., Gardinier, C.F., Landstrass, M.I., Kania, D.R., Kagan, H., Gan, K.K., Kass, R., Pan, L.S., Han, S., Schnetzer, S. and Stone, R., [1994]. *Appl. Phys. Lett.*, **64**, 193.

Plano, M.A., [1995]. in *Diamond: Electronic Properties and Applications,* ed. Pan, L.S. and Kania, D.R. (Kluwer, Academic Press) Massachusetts, USA.

Thomas, R.E., Rudder, R.A. and Markunas, R.J., [1992]. *J. Vac. Sci. Technol.*, **A10**, 2451.

6: ELECTRICAL CHARACTERISATION OF SEMICONDUCTING THIN FILM DIAMOND

6.1 INTRODUCTION

If the properties of pure single crystal diamond can be reproduced in commercially accessible thin film material then the realisation of high performance electronic devices from this material would appear possible [Geis, 1987; Gildenblat, 1991; Grot, 1995]. Microwave plasma enhanced chemical vapour deposition (CVD) has become the pre-eminent technique for the growth of thin film diamond due to the comparatively high quality films which emerge; boron can be incorporated during the growth process leading to p-type film characteristics as reviewed in chapters 2 and 3. When deposited on economically-viable non-diamond substrates however, the material is polycrystalline in nature, typically consisting of randomly aligned crystallites and containing low concentrations of nondiamond carbon [Plano, 1994]. The presence of contaminants and grain boundaries within the film leads to both carrier trapping and scattering: carrier mobilities of around 33 $cm^2V^{-1}s^{-1}$ in p-type material with a active carrier concentration of 3 x 10^{14} cm^{-3} have been recorded for boron doped polycrystalline material [Malta, 1993]. The recent demonstration of quasi-heteroepitaxial growth (*i.e.* oriented crystallites) of highly oriented (100) faceted polycrystalline films on Si(100) [Stoner, 1993] represents a significant advance in the field. Fox and co-workers [1994] have shown that carrier mobility values can be a factor of three higher in such types of film with an observed value of 135 $cm^2V^{-1}s^{-1}$ (2.4 x 10^{14} cm^{-3} carriers) compared to a value of 47.8 $cm^2V^{-1}s^{-1}$ (6.8 x 10^{14} cm^{-3} carriers) from a film comprised of randomly aligned crystallites; the presence of small angle grain boundaries (< 8°) was considered to be the primary origin of this improvement with an estimated 50% reduction in the density of interfacial traps within the grain boundary of the highly oriented material. However, in order to consider the influence of grain boundary angle on the electrical properties of films in more detail it is necessary to use material with similar grain sizes and textures to minimise the possible influence of defects incorporated within the diamond grains themselves; the fact that Fox *et al.* [1994] employed films with 4 μm and 7 μm grain sizes in their randomly and highly oriented films respectively, suggests that this may be a major contributing factor within their estimation of interfacial trap densities. Two types of materials have been studied here which have similar crystallite sizes and dominant crystal plane but differ primarily in the level to which the crystals are aligned with respect to each other. The transport characteristics have been considered in terms of resistivity levels within the active regions. The dependence of carrier mobility with doping levels in this state of the art material has not been previously addressed within the literature to the author's knowledge and so samples of various doping densities have thus been investigated.

6.2 EXPERIMENTAL DETAILS

The electrical characterisation was carried out on textured-randomly oriented (*T&R*), and textured-oriented (*T&O*) diamond thin films representing state of the art material; these films were produced by AEA Technology (Harwell) by the technique of microwave plasma enhanced CVD. The *T&R* films display predominantly (100) crystallite facets at the surface without respective crystallite orientation, whilst the *T&O* films also display predominant (100) faceting but with crystallite orientation. The *T&O* films followed the three stage process consisting of: (i) precarburisation; (ii) bias enhanced nucleation; and (iii) high rate oriented growth, whilst the *T&R* films resulted by the variation of the methane concentration during the precarburisation step [P.R. Chalker (AEA), 1995; private communications]. Both *T&R*, and *T&O* undoped diamond layers were deposited to a of thickness 50 μm onto silicon substrates which were subsequently removed. One sample of each type of film was then introduced into a separate growth chamber where, by the controlled introduction of trimethyl boron ($B(CH_3)_3$) into the diamond precursor gas mixture, p-type layers were simultaneously deposited onto the two types of undoped diamond layers. In this manner, a number of directly comparable samples of varying doping concentration were produced to enable an investigation between the two types of diamond. Dynamic secondary ion mass spectrometry (SIMS) revealed the depth of the doped layer thicknesses to be 5 µm +/- 10%. Prior to any electrical characterisation, the samples were subjected to a stabilisation pre-anneal at 430 °C (1h, air ambient) [Harper, 1991] followed by an acid treatment involving a saturated solution of H_2SO_4: $(NH_4)_2S_2O_5$ and (1:1) H_2O_2: NH_4OH to remove any surface conductive layer (chapter 5). Circular Ti (10 nm)/Au (400 nm) metallic contacts of diameter 200 µm were photolithographically defined and deposited in the square van der Pauw configuration; annealing of these contacts was carried out in air at 430 °C for 1 h.

6.3 RESULTS

Figure 6.1 shows the micro-Raman spectra recorded for each type of film (623.8 nm radiation, 100 μm spot size); the two types of films both demonstrate intense 1332 cm^{-1} peaks characteristic of diamond situated on top of luminescence bands with non-diamond peaks at 1380 cm^{-1} (iv: DLC) and 1500 cm^{-1} (v: unknown origins; see Table 10.3). The spectra clearly indicate that the properties are similar in both types of films within the sensitivity of this technique. Figure 6.2 shows representative scanning electron micrographs of *T&O* and *T&R* films; (a) shows a predominant composition of (100) textured crystallites which demonstrate a high percentage of crystallite orientation as judged by SEM in contrast to the textured-only films which display a non-orientation of crystallites (Fig 6.2(b)). However, it is apparent that the two types of films show similar grain sizes of up to 16 μm. X-ray texture analysis has indicated that > 98% of the growth surface in both types of films is (100)-textured [P.R. Chalker (AEA), 1995; private communications].

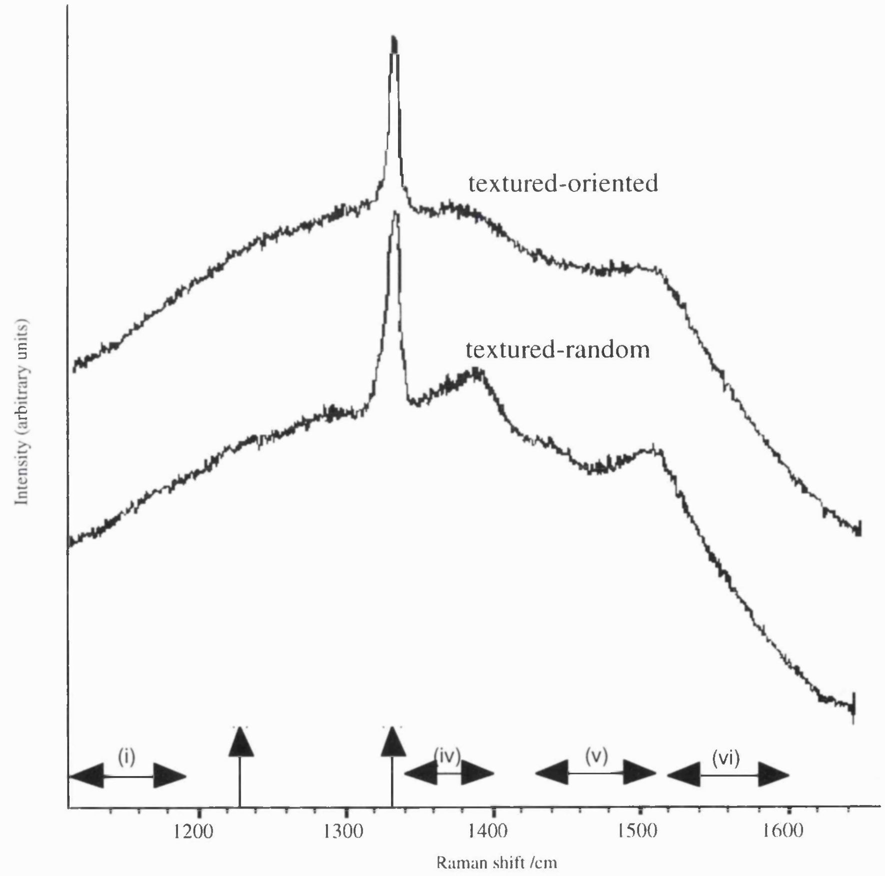

Figure 6.1 Raman spectrograph of *T&O* and *T&R* diamond films as depicted in Figure 6.2.

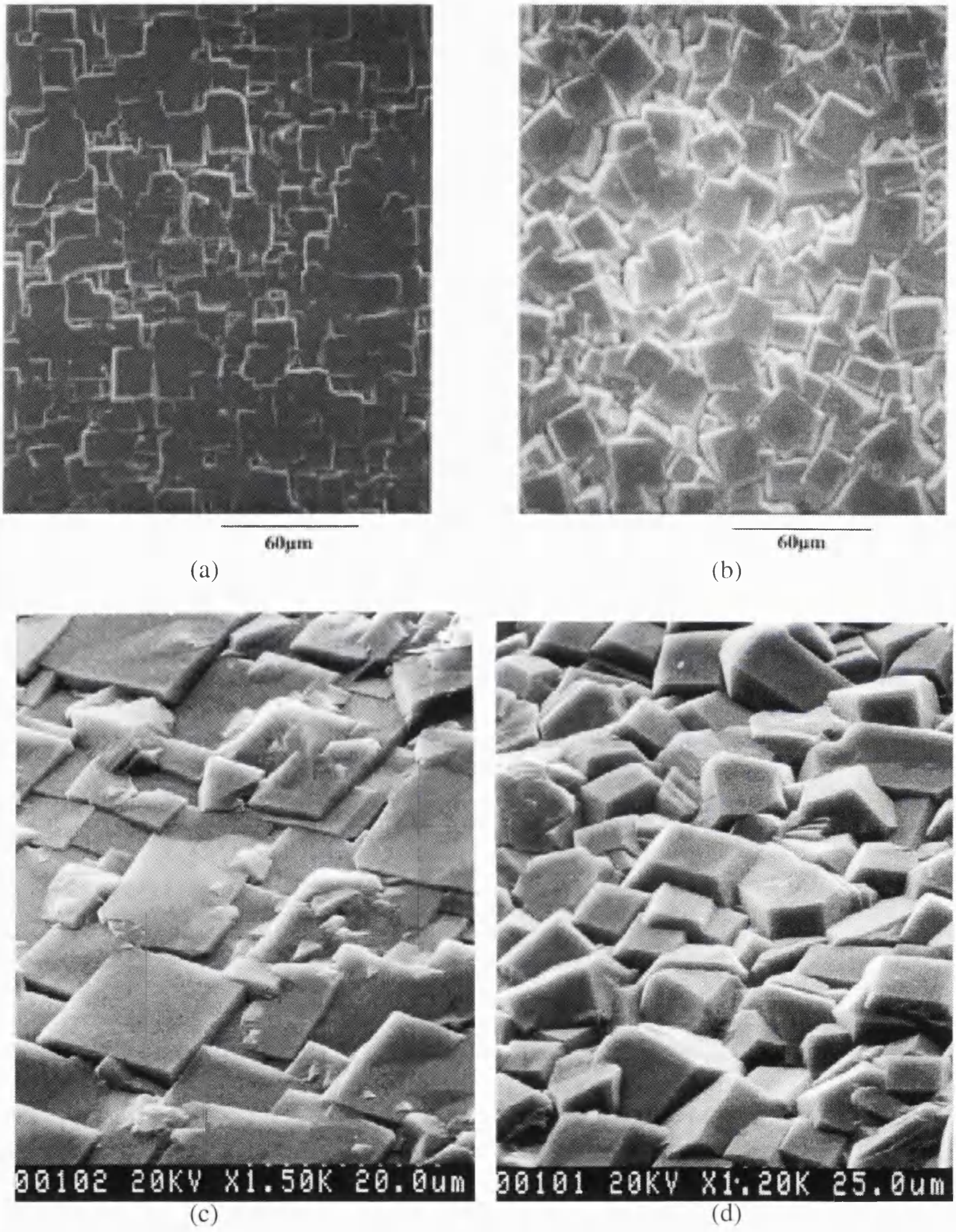

Figure 6.2 Scanning electron micrograph of chemically vapour deposited diamond of nature: (a) (100) textured-oriented (*T&O*), and (b) (100) textured-randomly oriented (*T&R*). Grain sizes in both types of films range up to 16 µm in width at the top surface. (c) which shows evidence of secondary nucleation, and (d) are SEMs (tilted sample) of (a) and (b) respectively.

Eight diamond films were prepared for Hall effect measurements, with four textured-randomly oriented samples of varying dopant concentrations (*T&R*-S1, *T&R*-S2, *T&R*-S3, *T&R*-S4) and four textured-oriented (*T&O*-S1, *T&O*-S2, *T&O*-S3, *T&O*-S4) samples. Samples *T&R-S1* and *T&O-S1 etc.* were doped simultaneously within the same chamber. Sheet resistivity, Hall mobility and carrier concentration data derived from Hall effect measurements at room temperature are shown in Table 6.1 along with the boron concentration as estimated by secondary ion mass spectroscopy (SIMS). Negligible effects on the measurements were detected when the ambient lighting condition was altered from a standard desk lamp and darkness for all the samples tested.

Sample	ρ_{sheet} (kΩ/sq)	f	R (m^2/C)	Dev (%)	μ_H	Carrier conc. (cm^{-3})	Boron conc. (cm^{-3})
T&R-S1	49.2	0.98	161	0	33	7.7×10^{15}	2.18×10^{18}
T&R-S2	23.6	0.87	83.5	1	35	1.5×10^{16}	3.36×10^{18}
T&R-S3	7.03	0.96	21.9	3	31	5.7×10^{16}	4.79×10^{18}
T&R-S4	7.44	0.93	9.94	9	13	1.3×10^{17}	5.56×10^{18}
T&O-S1	49.1	0.97	494	1	101	2.5×10^{15}	5.69×10^{17}
T&O-S2	30.4	0.95	286	4	94	4.4×10^{15}	2.49×10^{18}
T&O-S3	12.8	0.90	80.1	28	63	1.6×10^{16}	3.00×10^{18}
T&O-S4	12.2	0.93	40.3	1	33	3.1×10^{16}	-

Table 6.2 Room temperature sheet resistivity (ρ_{sheet}) corrected by the van der Pauw factor *f*, and Hall effect measurement data (*R* is the sheet Hall coefficient) for *T&R* and *T&O* diamond films of varying dopant concentrations. The deviation (Dev) is a measure of the Hall voltage values obtained by reversing the polarity of the magnetic field. Hall mobility μ_H is given in cm^{2}V^{-1}s^{-1}. The bulk carrier concentrations are derived from the sheet carrier concentrations and an estimation of the doped layer thickness; the B concentration values are from SIMS measurements.

The error attributed to the sheet resistivity measurement is related to the *f* factor arising from the non-ideal sample structure according to van der Pauw (Equation 4.5); the values obtained have been corrected by this value. The Hall voltage~~s~~, obtained by reversing the polarity of the magnetic field and the set of measuring contacts, is characterised by a deviation value (*Dev*). In order to conform to the American Society for Testing and Materials (ASTM Standard F-76-68) [de la Houssaye, 92] this value has to be less than 10%; it is evident apart from datum point *T&O-S3* that this is satisfied. The error in the carrier mobility is then a combination of the *f* factor and the *Dev* value. The bulk carrier concentration, derived from the Hall coefficient *R* and the doped layer thickness, yields an additional error of +/-10%. The Hall scattering factor r_H is assumed to be unity. Errors arising from non-ideal contact size have been studied by Chwang and co-workers [1974];

triangular contacts placed at the corners of a square van Der Pauw sample and of width 10% of the total sample width resulted in an error of ~8%. Since the contacts employed here were 200 μm in diameter, and samples were not less than 4 mm x 4 mm, the systematic error arising is not expected to exceed this figure.

It is of interest to study the effect of increasing carrier concentration on the resistivity of the deposited films in order to consider the overall effect of the introduction of dopants. Figure 6.6 depicts the sheet resistivity of the two types of films as a function of the activated carrier concentration as determined by Hall measurement. A general trend of decreasing sheet resistivity with increasing carrier concentration is observed for both types of films; however it is apparent that up to a carrier concentration of approximately 3 x 10^{16} cm^{-3}, lower values of sheet resistivity are obtained in textured-oriented films. Both types of films demonstrate a possible limiting value of sheet resistivity of around 10 kΩ/square for increasing carrier concentrations.

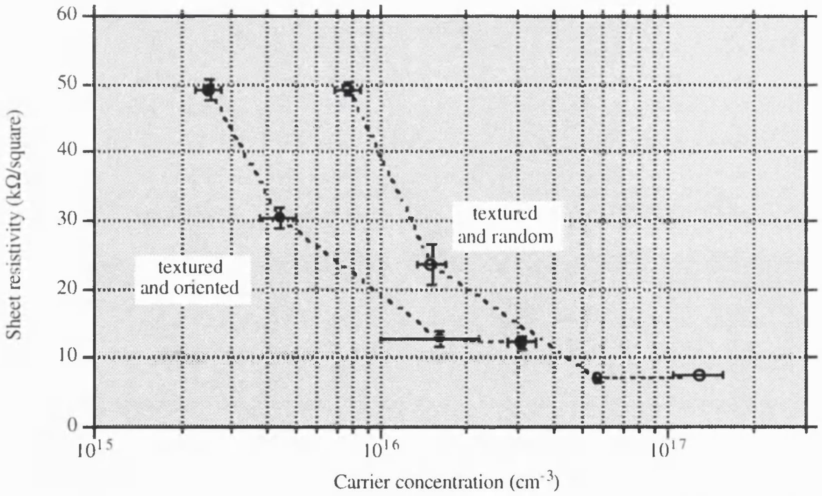

Figure 6.6 Plot of room temperature sheet resistivity versus active carrier concentration as determined by Hall measurements for *T&R* (open circles) and *T&O* (shaded circles) diamond films where, for corresponding samples, doping was carried out simultaneously in the same chamber. The dotted lines are drawn as a guide.

To consider the efficiency of the carrier activation, Figure 6.7 plots the active carrier concentration as a function of the boron dopant atoms. Since pairs of samples from both types of films are doped at the same time and within the same chamber, it is interesting to note that the level of incorporated boron atoms is less for the textured-oriented films. Considering the lowest doped*T&R* film, it is apparent that less that 0.5% of the boron is activated if it is assumed that no compensation of the acceptor states occur; with the highest doped *T&R* sample, a 2% activation of the boron atoms is observed. A similar effect for the *T&O* films exists. Within the accuracy of the measurements, a comparative level of active carriers are present within the two types of films for similar boron levels.

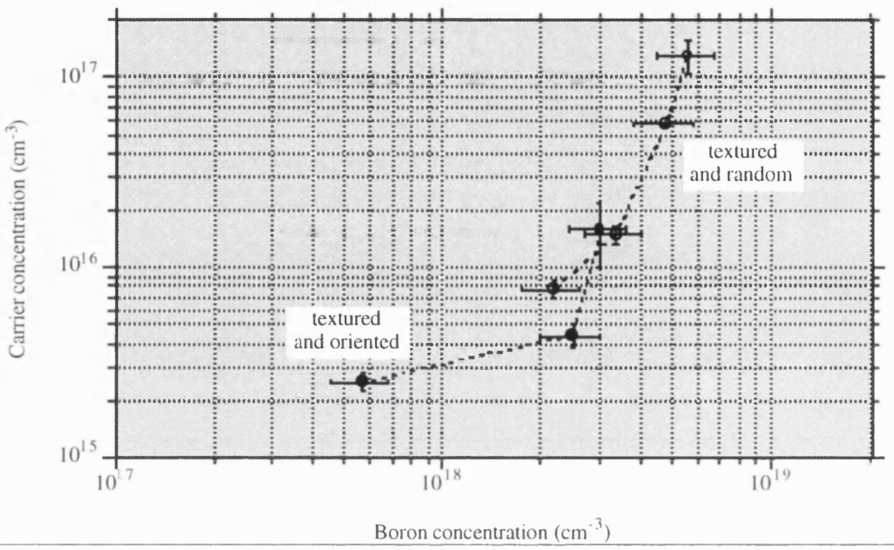

Figure 6.7 Plot of carrier concentration versus boron concentration as determined by Hall and SIMS analysis, respectively, for *T&R* (open circles) and *T&O* (shaded circles) films doped simultaneously in the same chamber. The dotted lines are drawn as a guide.

Figure 6.8 is a plot of the Hall mobility as a function of the active carrier concentration (indicated by solid lines connecting solid circles). Various values obtained by other workers for randomly oriented polycrystalline films, textured and oriented, and homoepitaxial films are also included within the figure as a comparison of the results obtained here.

The room temperature hole mobility value of 2100 cm^{2}V^{-1}s^{-1} obtained by Reggiani *et al.* [1981] for a natural diamond crystal was limited by the acoustic mode of lattice scattering with a $T^{-1.5}$ mobility-temperature dependence observed. Since this value for hole mobility is currently around the maximum reported, it has been included in Figure 6.8 as a limiting value for the films under investigation. To consider the trends observed here in more detail, theoretical predictions for the carrier mobility which may be expected from diamond have been calculated. Ionised impurity scattering models have been summarised by Smith [1978]; the Conwell-Weisskopf model [Conwell, 1950] which assumes the coulombic field of an ionised impurity to be an effective scattering centre up to half the average separation between the impurities results in the following ionised impurity limited mobility:

$$\mu_{ii} = \frac{e\langle \tau_{ii} \rangle}{m_h *} = \frac{64\pi^{1/2}\varepsilon^2 (2k_B T)^{3/2}}{N_{ii} Z^2 e^3 m_h *^{1/2}} \left[\ln\left\{ 1 + \left(\frac{12\pi\varepsilon k_B T}{Z e^2 N_{ii}^{1/3}} \right)^2 \right\} \right]^{-1} \tag{6.1}$$

where e is the electronic charge, m_h* is the effective mass of hole, $\langle \tau_{ii} \rangle$ is the average momentum relaxation time due to ionised impurities, ε the dielectric constant, k_B Boltzmanns constant, T the absolute temperature (300 K), N_{ii} the density of ionised impurities, and Z is the impurity charge (= 1 for hydrogenic impurities). The mobility values predicted by this model is shown in Figure 6.8. An effective mass value of $0.75m_o$ [Collins, 1979] has been used; however, as seen in Table 2.4, reported values vary and so a range of values have also been included.

In the case of boron acceptors in diamond where a low degree of ionisation may occur, scattering of charge carriers by neutral impurity centres must also be considered. Erginsoy [1950] the following expression for neutral impurity limited carrier mobility μ_{ni} based on electron collisions with neutral hydrogen atoms:

$$\mu_{ni} = \frac{e\langle \tau_{ni} \rangle}{m_h *} = \frac{e^3 m_h *}{80\pi\varepsilon\hbar^3 N_{ni}} \tag{6.2}$$

where N_{ni} is the density of neutral impurities with the other terms being defined in equation 6.1. Calculated neutral impurity limited mobilities have been included in Figure 6.8 employing the SIMS determined *boron concentrations* which directly correspond to the carrier concentrations for the samples investigated; since boron activation at these levels has been found to be at most 2%, such an assumption is not expected to introduce any significant errors in the calculated values though compensation of acceptor centres will lead to mobility limitations by this mechanism being overestimated. A curve fit has been applied to the calculated data: it should be noted that extension towards higher carrier concentrations will be increasingly error prone due to the lowering of the boron activation energy in more heavily doped films as reviewed in Chapter 3. As for the ionised impurity case, curves employing the effective mass values of 0.75 m_o, 0.25 m_o and 2.1 m_o have been included to account for the wide range of values reported in the literature.

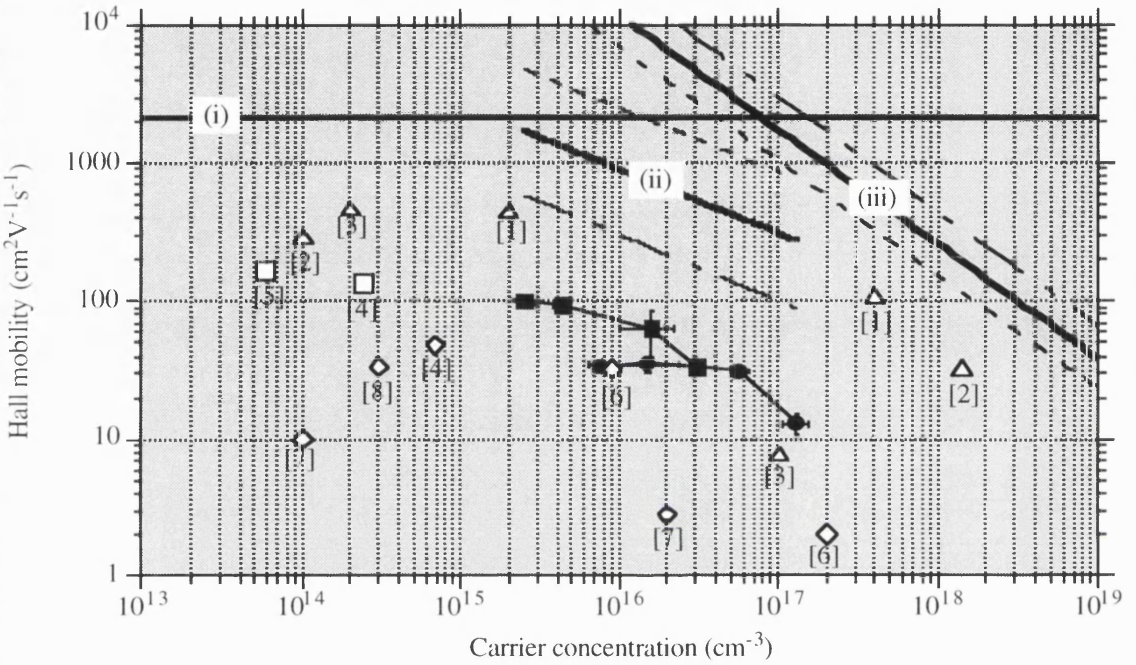

Figure 6.8 Hall mobility versus carrier concentration for *T&R* (●)and *T&O* (■)diamond films, where solid lines have been drawn as a guide. The effect of (i) lattice scattering, (ii) neutral impurity scattering, and (iii) ionised impurity scattering on carrier mobility from theoretical predictions are shown for various effective mass approximations; for (ii) and (iii), effective mass= $0.25m_0$ (--- - ---), $0.75m_0$ (____) and $2.1m_0$ (- - -). Hall mobility values from other workers for homoepitaxial (Δ), textured-oriented (□), and polycrystalline randomly aligned films (◊) are also shown; [1; Mori, 1993], [2; Grot, 1991], [3; Fujimori, 1990], [4; Fox, 1994], [5; Stoner, 1993b], [6; Masood, 1992], [7; vonWindheim, 1993], [8; Malta, 1993].

6.4 DISCUSSION

In order to make a valid comparison of the electrical properties between state of the art (100) textured-oriented CVD diamond films and previous standards, it is preferable to make a systematic study incorporating similar conditions during the deposition of the electrically active layer. To this aim, undoped diamond films displaying textured-randomly oriented, and textured-oriented crystallites were used as substrates for the subsequent deposition of the boron doped p-type layers. The decrease in the sheet resistivity of the two different types of films with increasing carrier concentration as shown in Figure 6.6 demonstrates that doping is effectual in controlling the electrical characteristics of the CVD material. The fact that the Raman signatures did not show significant increases in the non-diamond peaks strongly suggests that this decrease in resistivity is a result of the increased boron concentration. It is significant to note that for the same carrier concentration levels in the two different levels, the textured-oriented films possess higher conductivity levels than the textured non-oriented films. To elucidate the origin of this observation, the determining factors behind the resistivity of a material have to be considered; these are the charge carrier density and the charge carrier mobility.

As shown in Figure 6.7, boron incorporation for simultaneously doped *T&R* and *T&O* films is greater for the former case; this suggests the possibility of higher incorporation occurring within the grain boundaries or within the individual crystallites. However, the fact that for the same boron concentration similar active carrier concentrations are obtained in the two films, implies domination by the former possibility. The apparent rapid rise in active carriers with incorporated boron atoms has previously been observed by Nishimura *et al.* [1991] and vonWindheim *et al.* [1993] in polycrystalline randomly-oriented material over boron ranges of 6×10^{19}-2×10^{20} cm^{-3} and 2×10^{18}-2×10^{20} cm^{-3}, respectively. To account for this phenomenon, vonWindheim suggested the possibility of grain boundary or defect compensation (*e.g.* formed as a result of radiation damage from plasma) leading to depletion of carriers; alternatively it was suggested that impurity band conduction, where a lower activation energy would lead to greater levels of active carriers at the higher doping levels, may also play a significant role . Although activation analysis *e.g.* temperature varied Hall measurements is required in order to evaluate the probability of impurity band conduction within the films studied here, comparison of the carrier concentrations with Figure 3.8 reveals a possible activation energy in the region of 0.35 eV, thus suggesting a dominance of valence band conduction.

The variation of the carrier mobility with active carrier concentration is shown in Figure 6.8; both types of films are characterised by a decrease in the value of carrier mobility with increasing carrier concentration. It is apparent that greater mobility values may be obtained in the textured-oriented films. However, it is interesting to note that the drop off in mobility value with increasing carrier concentrations for the oriented films is more rapid such that similar mobility values are evident in both types of film for concentrations greater than $\sim 3 \times 10^{16}$ cm^{-3}. The mobility values representing the best reported by other groups for the various forms of diamond also appear to display this overall characteristic as shown in Figure 6.8. It may be seen that the values obtained for the randomly oriented polycrystalline films are consistently lower than those for oriented or homoepitaxial films for similar carrier concentrations. For carrier concentrations $\sim 10^{16}$ cm^{-3}, the best reported mobility value for films of randomly oriented crystallites by Masood *et al.* [1992] is very similar to the value obtained here for the textured non-oriented films. Indeed, if the trend observed here is extended to lower carrier concentrations then literature data for randomly-oriented, non-textured films [*e.g.* Fox, 1994; Malta, 1993] may also be incorporated. In a similar manner, the limited data available for textured-oriented films by Stoner *et al.* [1993] and Fox *et al.* [1994] for carrier concentrations of 6×10^{13} cm^{-3} and 3×10^{14} cm^{-3} respectively may be seen to fit the trend evident in the data recorded during this study for higher concentration values.

It is apparent from the mobility values predicted by the Erginsoy and Conwell-Weisskopf models that both neutral and ionised impurity scattering centres may be influential. ~~From~~ Assuming an average effective mass of 0.75 m_o, three regimes may be identified from the theoretical predictions:

(i) $<10^{15}$ cm^{-3}: lattice scattering limited;
(ii) 10^{15}- mid-10^{16} cm^{-3}: neutral impurity scattering limited; and
(iii) $>$ mid-10^{17} cm^{-3}: ionised impurity limited.

However, as is evident from Figure 6.8, the results observed here for both the oriented and non-oriented films reveal that, on the basis of the theoretical models applied, scattering induced by boron centres alone do not account for the transport characteristics. This suggests the existence of other underlying physical mechanisms being responsible for the reduced levels of measured mobility; two factors are of prime concern in the consideration of carrier transport within such types of films:

(i) the polycrystalline nature (grain boundaries between neighbouring grains); and
(ii) the intra-granular crystalline quality.

Seto [1975] developed a model for the effect of grain boundaries on the electronic transport within polycrystalline silicon; this model suggested grain boundaries contain a high density of traps which capture charge carriers leading to the formation of depletion regions around individual grains and an overall reduction in free carriers. The formation of potential barriers at the grain boundaries then reduce the mobility of free carriers across these regions. However, Seto's model was reported by Malta *et al.* [1995] not to completely describe the behaviour of polycrystalline diamond films. Firstly, no significant free carrier depletion was observed when similarly doped homoepitaxial and polycrystalline films were compared, and in temperature studies on their samples, no exponential increase in mobility as dictated by the grain boundary potential barrier was observed. However, as noted by Malta *et al.*, if similar grain boundary trap densities existed as for polycrystalline silicon, then the carrier concentrations would lead to a carrier depletion of only ~1% in all but the lowest doped sample (10%). Nevertheless, the effect of grain boundaries on carrier transport have been concluded to play a major role in the low mobility of apolycrystalline randomly-oriented film (33 $cm^2V^{-1}s^{-1}$) when compared with a simultaneously doped homoepitaxial film (514 $cm^2V^{-1}s^{-1}$), both films being of similar carrier concentration (~$2x10^{14}$ cm^{-3}) [Malta, 1993].

The two studies which have previously investigated the transport behaviour of state-of-the-art textured-oriented films have been those by Stoner and co-workers [1993] and Fox and co-workers [1994]. However in both these reports, the grain sizes of the materials were either not specified or non-similar; in addition the carrier mobility was not investigated as a function of carrier densities. In this most comprehensive study to date of the mobility variation with carrier concentration for textured-oriented material, it is demonstrated that for similar carrier concentrations and grain sizes, the oriented material provides superior properties only over a limited regime. The benefits of the oriented material is available only up to active carrier concentrations of ~10^{16} cm^{-3}. Lower angle grain boundaries arising from the orientation of crystallites approach within the *T&O* films may result in lower densities of grain boundary defects, as well as less stress (or associated defects) within the crystal network of neighbouring grains; further material characterisation is required in order to elucidate the primary cause. On the other hand, the process of texturing only, *i.e.* without orientation of individual grains does not appear to reduce the nature of this limitation to transport characteristics if the result of Masood *et al.* [1992] involving standard non-textured randomly-oriented material is compared with the observations here. However, as the density of dopants is increased, then the introduction of other defects within the films must account for the removal of the benefits accrued via the orientation of crystallites approach. It is interesting to note that in a study on homoepitaxial films of differing quality (as induced by varying CH_4 in the feed gas, and as judged by SEM), Yasu *et al.* [1994] also found a rapid decrease in the higher mobility values of the nominally higher quality material such that by a doping concentration of mid-10^{15} cm^{-3} all films displayed similar behaviour; an unidentified scattering centre was suggested. Furthermore, Fujimori and co-workers [1990] measured carrier mobility in (100) and (110) homoepitaxial diamond films and, although the mobility in the (100) films were an order of magnitude superior at low doping levels, by ~10^{17} cm^{-3} active carriers, similar values were obtained in both types of films. Such reports on single-crystalline material suggests that intra-granular crystalline quality may vary dramatically with dopant concentrations without conforming to standard impurity models; the fact that this decrease in carrier mobility in Fujimori's films occurs in a similar doping region to the observations here may be significant. A report by Graham and co-workers [1994] utilising a cathodoluminescence (CL) approach in a transmission electron microscope (TEM) on highly textured-oriented material demonstrated that although the boron dopant (gas phase concentration of 44 ppm) was uniformly distributed within the material, a dislocation related defect at 2.87 eV in the CL spectrum was believed to be to have been introduced by the act of doping. It is thus likely that both an additional scattering mechanism, and ionised impurity scattering is operating within the films studied here such that at the higher doping levels carrier mobility is more severely limited.

6.5 SUMMARY

State-of-the-art quasi-heteroepitaxial polycrystalline diamond films have been investigated in terms of their electrical and transport characteristics as a function of dopant concentrations; this is the first investigation involving a consistent set of measurements on this type of material over a wide doping concentration range. Although higher degrees of boron atoms are incorporated within textured-randomly oriented films when compared with simultaneously doped textured-oriented films, active carrier concentrations are near equivalent for films possessing similar levels of incorporated boron. The higher conductivity levels of the textured-oriented films is thus a primary consequence of the improvement in the mobility of the charge carriers. This superiority in the transport characteristics over non-oriented films is in agreement with the two previous reports on similar material for lower doping densities; the low angle grain boundaries is envisaged to lead to either lower densities of grain boundary defects, or the possibility of lower stress levels (or related defects) between neighbouring grains. However, it has been demonstrated here that such improvements are only valid over a selected region of the dopant parameter space; at carrier concentration values of mid-10^{16} cm^{-3}, the transport characteristics between the oriented and non-oriented films are effectively similar. Theoretical models are not sufficient to predict this, and since a similar effect has been observed in homoepitaxial films of varying quality, intra-granular crystalline quality as modified by the presence of increased dopant impurities is the most likely cause.

REFERENCES

Borst, T.H. and Weis, O., [1995]. *Diamond Relat. Mater.,* **4**, 948.

Chwang, R, Smith, B.J. and Crowell, C.R., [1974]. *Solid State Comm.*, **17**, 1217.

Collins, A.T. and Lightowlers, E.C., [1979]. in *The Properties of Diamond,* ed. J.E. Field (Academic Press) London, UK.

Conwell, E. and Weisskopf, V.F., [1950]. *Phys. Rev.,* **77**, 388.

delaHoussaye, P.R., Penchina, C.M., Hewett, C.A., Zeidler, J.R. and Wilson R.G., [1992]. *J. Appl. Phys.,* **71**, 3220.

Erginsoy, C., [1950]. *Phys. Rev.,* **79**, 1013.

Fox, B.A., Stoner, B.R., Malta, D.M., Ellis, P.J., Glass, R.C. and Sivazlian, F.R., [1994]. *Diamond Relat. Mater.*, **3**, 382.

Fox, B.A., Hartsell, M.L., Malta, D.M., Wynands, H.A., Kao, C.T., Plano, L.S., Tessmer, G.J., Henard, R.B., Holmes, J.S., Tessmer, A.J. and Dreifus, D.L., [1995]. *Diamond & Relat. Mater.*, 4, 422.

Fujimori, N., Nakahata, H. and Imai, T., [1990]. *Jpn. J. Appl. Phys.*, **29**, 824.

Geis, M.W., Rathman, D.D., Ehrlich, D.J., Murphy, R.A. and Lindley, W.T., [1987]. *IEEE Electron Device Lett.*, **8**, 341.

Gildenblat, G.Sh., Grot, S.A. and Badzian, T., [1991]. *Proc. IEEE,* **79**, 647.

Graham, R.J., Shaapur, F., Kato, K. and Stoner, B.R., [1994]. *Appl. Phys. Lett.,* **65**, 292.

Grot, S.A., Gildenblat, G.Sh., Hatfield, C.W., Wronski, C.R., Badzian, A.R., Badzian, T. and Messier, R., [1990]. *IEEE Electron Device Lett.*, **11**, 100.

Grot, S.A., Hatfield, C.W., Gildenblat, G.Sh., Badzian, A.R. and Badzian, T. [1992]. *Appl. Phys. Lett.,* **58**, 1542.

Grot, S.A., [1995]. in *Diamond: Electronic Proprties and Applications,* edited by L.S. Pan, D.R. Kania, (Kluwer Academic Press), Boston, USA.

Harper, R.E., Johnston, C., Blamires, N.G., Chalker, P.R. and Buckley-Golder I.M., [1991]. *Surface Coatings Technol.,* **47**, 344.

Malta, D.M., vonWindheim J.A. and Fox, B.A., [1993]. *Appl. Phys. Lett.*, **62**, 2926.

Malta, D.M., von Windheim, J.A., Wynands, H.A. and Fox, B.A., [1995]. *J. Appl. Phys.,* **77**, 1536.

Masood, A., Aslam, M., Tamor, M.A. and Potter, T.J., [1992]. *Appl. Phys. Lett.*, **61**, 1832.

Mori, Y., Kawarada, H. and Hiraki, A., [1991]. *Appl. Phys. Lett.,***58**, 940.

Mori, Y., Eimori, N., Hatta, A., Ito, T. and Hiraki, A., [1992]. *Jpn. J. Appl. Phys.*, **31**, L1718.

Mori, Y., Show, Y., Deguchi, M., Yagi, H., Yagu, H., Eimori, N., Okada, T., Hatta, A., Nishimura, K., Kitabatake, M., Ito, T., Hirao, T., Izumi, T., Sasaki, T. and Hiraki, A., [1993]. *Jpn. J. Appl., Phys., 32, L987.*

Mori, Y., Yagi, H., Deguchi, M., Sogi, T., Yokota, Y., Eimori, N., Yagyu, H., Ohnishi, H., Kitabatake, M., Nishimura, K., Hatta, A., Ito, T., Hira, T., Sasaki, T. and Hiraki, A., [1993]. *Jpn. J. Appl. Phys.*, **32**, 4661.

Nishimura, K., Das, K. and Glass, J.T., [1991]. *J. Appl. Phys.*, **69**, 3142.

Plano, M.A., Zhao, S., Gardinier, C.F., Landstrass, M.I., Kania, D.R., Kagan, H., Gan, K.K., Kass, R., Pan, L.S., Han, S., Schnetzer, S. and Stone, R., [1994]. *Appl. Phys. Lett.*, **64**, 193.

Reggiani, L., Bosi, S., Canali, C., Nava, F. and Kozlov, [1981]. *Phys. Rev.,* **B23**, 3050.

Reggiani, L., Waechter, D. and Zukotynski, S., [1983]. *Phys. Rev.,* **B28**, 3550.

Seto, J.Y.W., [1975]. *J. Appl. Phys.,* **46**, 5247

Smith, R.A., [1978]. *Semiconductors*, 2nd Edition,(Cambridge University Press), Cambridge, UK.

Steffan, H.F., Roux, C.D., Marton, D. and Rabalais, J.W., [1991]. *Phys. Rev.*, **B44**, 3981.

Stoner, B.R., Sahaida, S.R., Bade, J.P., Southworth P. and Ellis, P.J., [1993]. *J. Mater. Res.,* 8, 1334.

Stoner, B.R., Kao, C.-T., Malta, D.M. and Glass, R.C., [1993]. *Appl. Phys. Lett.*, **62**, 2347.

Sugino, T., Muto, Y., Shirafuji, J. and Kobashi, K., [1993]. *Diamond & Relat. Mater.*, **2**, 797.

Sze, S.M., [1981]. *Physics of Semiconductor Devices*, 2nd Edition, (John Wiley & Sons), New York, USA.

Visser, E.P., Bauhuis, G.J., Jansen, G., Vollenberg, W., van Enckevort, W.J.P. and Giling, L.J., [1992]. *J. Phys.: Condens. Matter*, **4**, 7365.

von Windheim, J.A., Venkatesan, V., Malta, D.M. and Das, K., [1993]. *J. Electronic. Mater.*, **22**, 391.

Williams, B.E. and Glass, J.T., [1989]. *J. Mater. Res.*, **4**, 373.

Wynands, H.A., Malta, D.M., Fox, B.A., von Windheim, J.A., Fleurial, J.P., Irvine, D. and Vandersande, J., [1994]. *Phys. Rev.,* **B49**, 5745.

Yasu, E., Ohashi, N., Ando, T., Tanaka, J., Kamo, M., Sato, Y. and Kiyota, H., [1994]. *Diamond Relat. Mater.,* **4**, 59.

7: NON-RECTIFYING Ti-BASED CONTACT METALLISATIONS TO THIN FILM DIAMOND

7.1 INTRODUCTION

The continued improvements in the electronic properties of chemically vapour deposited thin film diamond as described in the previous chapters has focused a need for an improved understanding in the formation of electrical contacts. For the development of electronic devices, contacts for connections to external circuits are required with characteristics which do not alter nor limit the intended device performance. Such "ohmic" contacts may be defined as that for which the resistance of the contact itself is insignificant in magnitude compared with the resistance of the associated device; this suggests that in some cases the electrical current-voltage (I-V) characteristic of the contact is not required to be linear [Rhoderick, 1988]. The formation of ohmic contacts is believed to generally take one of the following principles [Rhoderick, 1988]:

(i) appropriate matching of the metal work function to that of the semiconductor;

(ii) heavy doping of the semiconductor at the interface region so that, although the barrier height remains appreciably the same, the width of the barrier is reduced enough to allow quantum mechanical tunnelling of carriers; or

(iii) intentional damaging of the semiconductor surface to induce surface defects thus promoting the probability of recombination in the depletion region.

Theoretically, on a wide bandgap material such as diamond (5.5 eV), the realisation of low resistivity, non-rectifying electrical contact characteristics is expected to be problematic if work function considerations of the metal and the semiconducting diamond alone were taken. Nevertheless, ohmic contacts have been demonstrated on the various forms of diamond (natural, synthetic or CVD films).

In a review article by Seal [1969], it was suggested that from a wide variety of metals and alloys, the wetting of natural diamond may be optimally achieved by the use of the transition metals which were found to have a strong affinity for carbon. Apart from the transition metals, the possible carbide forming capabilities of Si and Al have allowed these elements to be considered. The most popular ohmic contact formulation has been the Ti-Au formulation where the Au capping layer is corrosion and oxidation resistant. Moazed et *al.* [1988] demonstrated the use of Ta and Ti of thickness 10 nm capped with a 150 nm thick Au layer as a non-rectifying contact on natural semiconducting diamond. The resistance of these samples were observed to decrease by seven orders of magnitude after annealing the contacts to 885 °C for 1 h in a hydrogen ambient; however it was suggested from secondary ion mass spectroscopy that shallow penetration of the Ta may have occurred into the diamond layer though no consequence of this was predicted. In a later report by Moazed *et al.* [1990], it was also suggested that an optimal time existed for annealing before a rise in resistance was observed. On homoepitaxial films of doping concentrations in the region of 10^{19} cm^{-3}, Ti-Au contacts annealed in hydrogen (950 °C, 2 min) have been found to result in specific contact resistance levels as low as 1.8×10^{-5} Ωcm^2 with carbide formation believed to have taken place [Hewett, 1991]. A transition from initially rectifying characteristics to linear behaviour was reported by Gildenblat *et al.* [1991] using Ti-Au contacts on homoepitaxial diamond with an annealing temperature of only 580 °C. On polycrystalline diamond films, the technique of ion implantation has been combined with the employment of the carbide forming abilities of Ti (Au capped) to result in specific contact resistance values in the region of 10^{-5} Ωcm^2 [Venkatesan, 1992a; 1992b; 1993]; the boron concentration was measured to be around 10^{20} atoms.cm^{-3} at the surface, and the contacts were annealed at 850° C *in-vacuo.* No degradation in the electrical characteristics of these contacts were observed under temperature cycling to 400 °C though the physical stability was of concern when investigated by SIMS. Das *et al.* [1994] demonstrated the electrical and physical stability of TiC (as-deposited)-Au ohmic contacts on ion implanted, polished diamond with a boron surface concentration of 10^{21} cm^{-3}; the contacts were annealed to 850 °C for 1 h *in-vacuo* to result in specific contact resistivities of 10^{-5} Ωcm^2. However TiC deposited on films of doping concentrations of $10^{18} cm^{-3}$ and annealed to 850 °C (30 min) have been found to be rectifying [Tachibana, 1993]. In a series of surface analysis on contact behaviour, Tachibana *et al.* [1992a; 1992b; 1992c] have proposed that carbide forming metals gives rise to a metal-diamond surface layer rich in electrically active defects that lowers the barrier height and increases the leakage current. Nevertheless, on polycrystalline samples, the leakage currents induced by this type of material have led to the observation that contact metallisations *e.g.* Au contacts of area greater than 1 mm^2 result in effectively ohmic behaviour [Gildenblat, 1990]. Nakanishi *et al.* [1994] have demonstrated that the specific contact resistance depends strongly on B concentration and that the best way to obtain low contact resistance values is to heavily dope the films; for Ti contacts, optimal performance was obtained by annealing at 400 °C for 4 min.

Other methods of contact formation on single crystalline diamond include the deposition of a thin silicon layer (500 Å) followed by the implantation of 240 eV Kr^+ ions to result in an Si-SiC-diamond graded structure after annealing at 1200°C in a hydrogen containing gas. A specific contact resistivity of 10^{-3} Ωcm^2 was obtained [Fang, 1989]. Surface modification of natural diamond by the use of excimer laser irradiation has been found to result in a diamond / graphitic layer which was both stable to 1800 °C and ohmic in nature [Geis, 1989].

Non-rectifying contacts have thus been successfully achieved on semiconducting diamond by a range of methods which are capable of achieving levels of specific contact resistivities lower than that believed to be required for general electronic devices operating at room temperature *i.e.* 10^{-4} Ωcm^2 [Tyagi, 1991]. These values have been most popularly achieved by the employment of carbide-forming metals ideally combined with ion implantation methods. However, although low resistivity contacts have been routinely reported, both the electrical and the mechanical stability of these contacts have to be considered to the extent required for operation under the extreme conditions predicted for diamond devices. In view of this, high temperature operation may be seen as an immediate aim considering the applications proposed. Hence, the formation of high performance ohmic contacts involving the carbide forming capabilities of Ti will be considered in this chapter with emphasis on a tri-layer metallisation scheme, Ti-Ag-Au, for its electrical performance and its physical stability. Moreover, the characteristics of the most commonly employed contact, the Ti-Au bilayer formulation will also be critically assessed in terms of these criteria and in light of more recent publications.

7.2 EXPERIMENTAL DETAILS

Boron-doped polycrystalline diamond films of thickness 0.3 μm grown by the technique of microwave plasma assisted chemical vapour chemical deposition were provided by AEA Technology (Harwell, UK). This doped layer was grown on a 3.2 μm thick layer of undoped diamond in order to eliminate undesired current paths via the underlying silicon substrate. Secondary ion mass spectroscopy (SIMS) analysis indicated a boron concentration in the doped layer of 5×10^{19} cm^{-3} [P.R. Chalker, private communications]. The films displayed an intense 1332 cm^{-1} Raman feature which is typical of diamond and similar to that of the Raman spectrum in Figure 5.1 and consisted of randomly aligned coalesced crystallites of 1-2 μm in size. Prior to device fabrication, all samples were annealed at 600-700 °C in a vacuum of 10^{-6} mbar in order to stabilise the film properties and then immersed in a saturated solution of H_2SO_4-$NH_4(SO_4)_2$ and rinsed in a boiling 1:1 solution of H_2O_2-NH_4OH; this treatment have been demonstrated to reduce non-diamond components which may be present on the as-deposited material surface as shown in Chapter 5. Standard photolithographic techniques (Appendix C) were used to form 100 μm circular contacts within a 300 μm circular space in a metal overlayer on the diamond as shown schematically in Figure 7.1. Samples, typically of size 8 mm x 8 mm, contained an array of such test structures and were shadow masked in order to prevent metallisation over the edges of the samples to connect with the underlying Si substrates (~~intrinsically~~ n-doped). The bi- and tri-layered metal formulations were resistively deposited at base pressures below 1×10^{-6} mbar to thicknesses of Ti (50 nm)-Au (200 nm) and Ti (50 nm)-Ag (150 nm)-Au (200 nm) respectively as judged by an *in-situ* crystal monitor (the convention of labelling the films such that the metal deposited on the substrate is written first has been employed here). Typical deposition rates were 2 $nm.s^{-1}$ for Ti and 20 $nm.s^{-1}$ for the Ag and Au layers. High temperature annealing (700 °C, 15 min) was performed either in a vacuum ($< 5 \times 10^{-6}$ mbar) or in a hydrogen ambient (15 Torr). Heating to 400 °C was performed in air. Characterisation by current-voltage (I-V) and scanning electron microscopy (SEM) were carried out employing the systems detailed in Chapter 4 with secondary ion mass spectroscopy by AEA Technology (Harwell, UK).

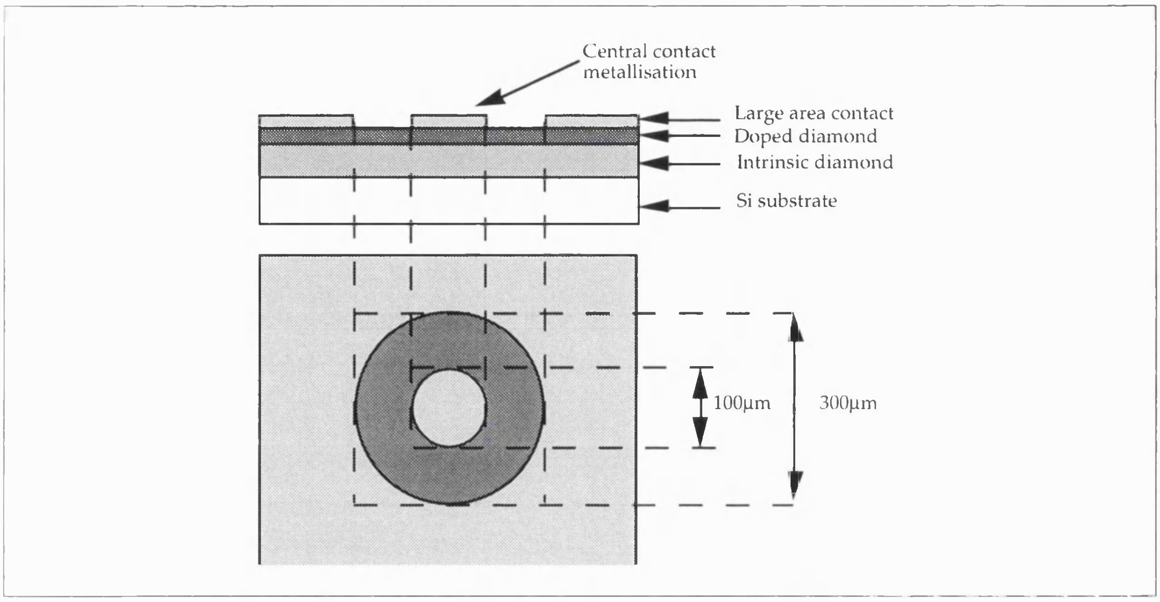

Figure 7.1 Schematic diagram of a single contact metallisation test structure.

7.3 RESULTS

7.3.1 Current-voltage characteristics

The I-V characteristics for Ti-Au contacts (both the large area contact and the central contact are of the same composition) are shown in Figure 7.2 for the case of 'as-deposited' (Figure 7.2(a)) and that following high temperature (700 °C) annealing in a hydrogen ambient (Figure 7.2(b)). The contacts were tested by probing the central contact and the large area contact, both in the as-deposited state and also as a function of increasing exposure to high temperature treatment (400 °C) in an air ambient. All curves appear to display a reasonably linear and symmetric response, indicating non-rectifying characteristics over the range of testing. Figure 7.2(a) shows a reduction in conductivity for the contacts as the duration of the heat treatment is increased. Figure 7.2(b) shows that a higher level of conductivity initially occurs for the hydrogen pre-annealed contacts; however, this advantage is rapidly lost upon heating to 400 °C in air, with the contact displaying similar characteristics to the un-annealed sample (Figure 7.2(a)) after a brief period at this temperature. A temperature stable ohmic response could not be achieved for the Ti-Au samples in both the 'as-deposited' and the hydrogen post-annealed cases over the tests periods used in this study.

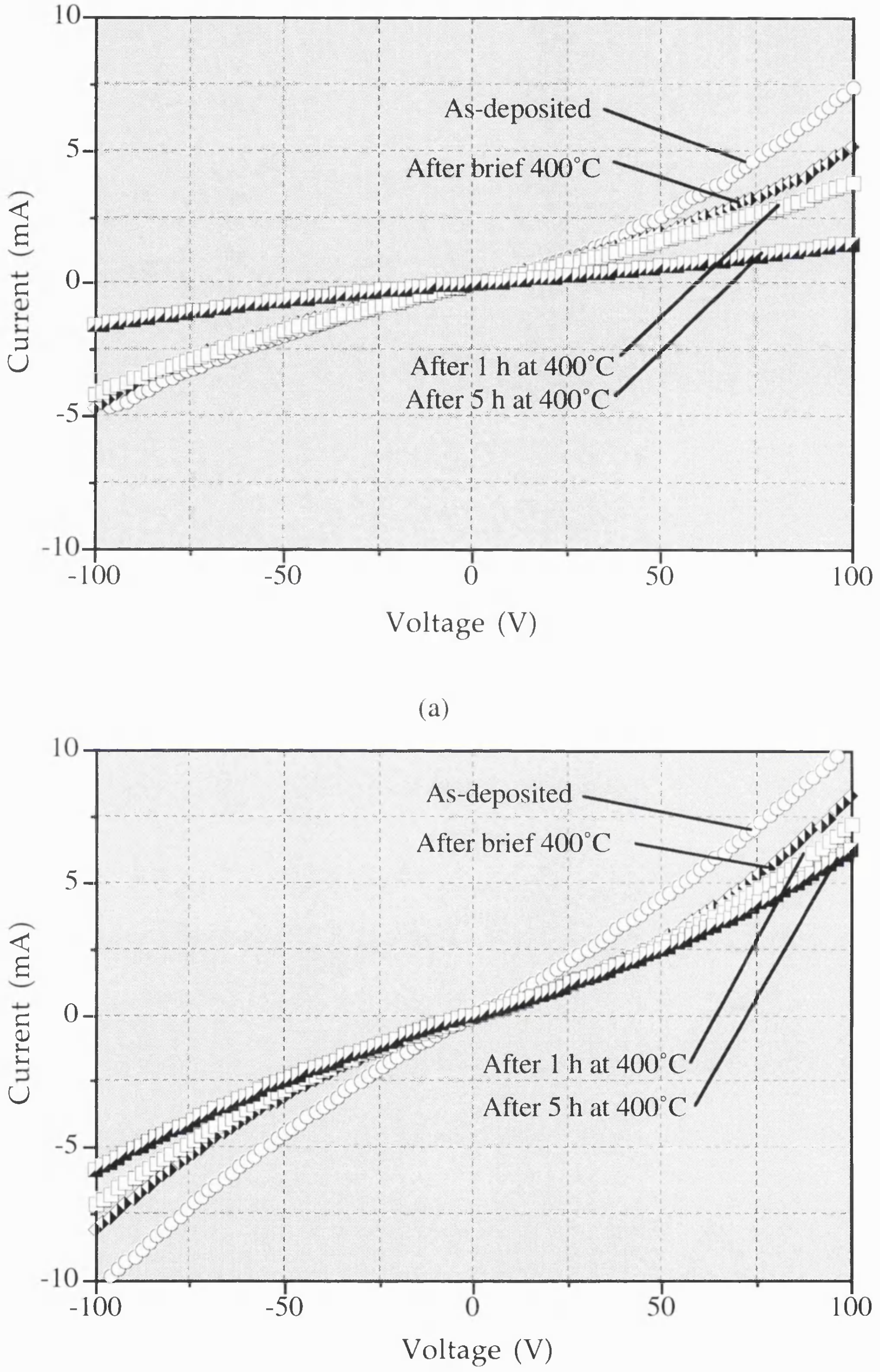

(a)

(b)

Figure 7.2 Room temperature current-voltage characteristics of Ti-Au contact metallisations to CVD diamond as a function of increasing time exposure to 400 °C in an air ambient for the case of: (a) as-deposited; and (b) hydrogen annealed at 700 °C.

Data measured for the Ti-Ag-Au contacts are revealed in Figure 7.3(a) ('as-deposited') and 7.3(b) (after 700 °C hydrogen anneal). All curves are again reasonably linear and show a decrease in conductivity upon initial heating. It is apparent that the highest conductivity is again achieved from contacts that have been high temperature annealed in hydrogen without further heating in air (Figure 7.3(b)); this effect is, however, lost as in the Ti-Au contact case, when the contacts are heated to 400 °C. Significantly, the value to which the conductivity of these Ti-Ag-Au contacts falls is both higher than the comparably treated Ti-Au contacts, and identical to the characteristics observed for the 'as-deposited' Ti-Ag-Au contacts that have undergone prolonged 400°C heating in air (Figure 7.3(a)). Moreover, the I-V characteristics appear to have fully stabilised after around 1 h at 400 °C.

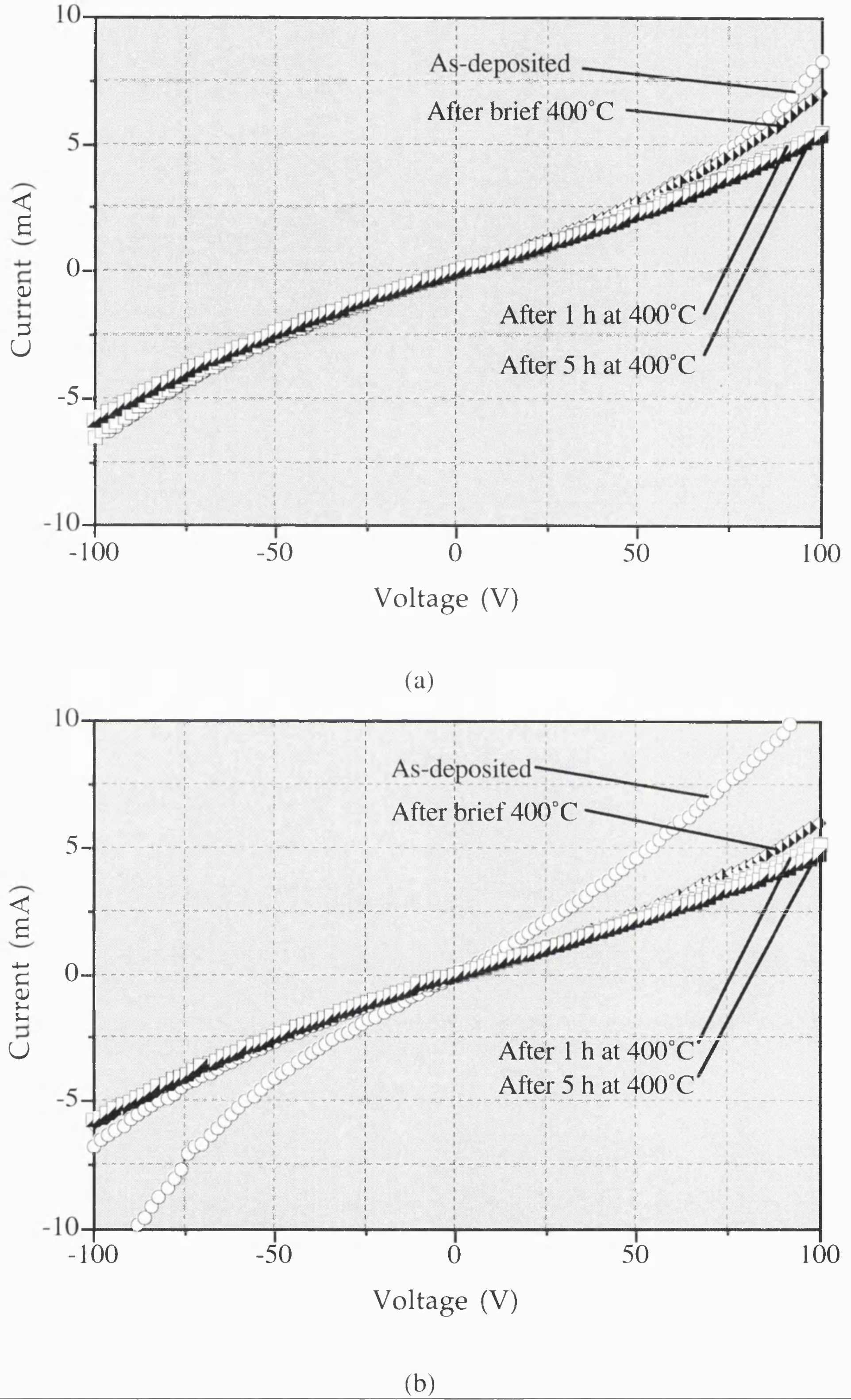

Figure 7.3 Room temperature current-voltage characteristics of Ti-Ag-Au contact metallisations to CVD diamond as a function of increasing time exposure to 400 °C in an air ambient for the case of: (a) as-deposited; and (b) hydrogen annealed at 700 °C.

Figure 7.4 shows the I-V characteristics of the Ti-Ag-Au contacts as a function of temperature; a dramatic increase in current levels is apparent as the temperature increases at all test voltages.

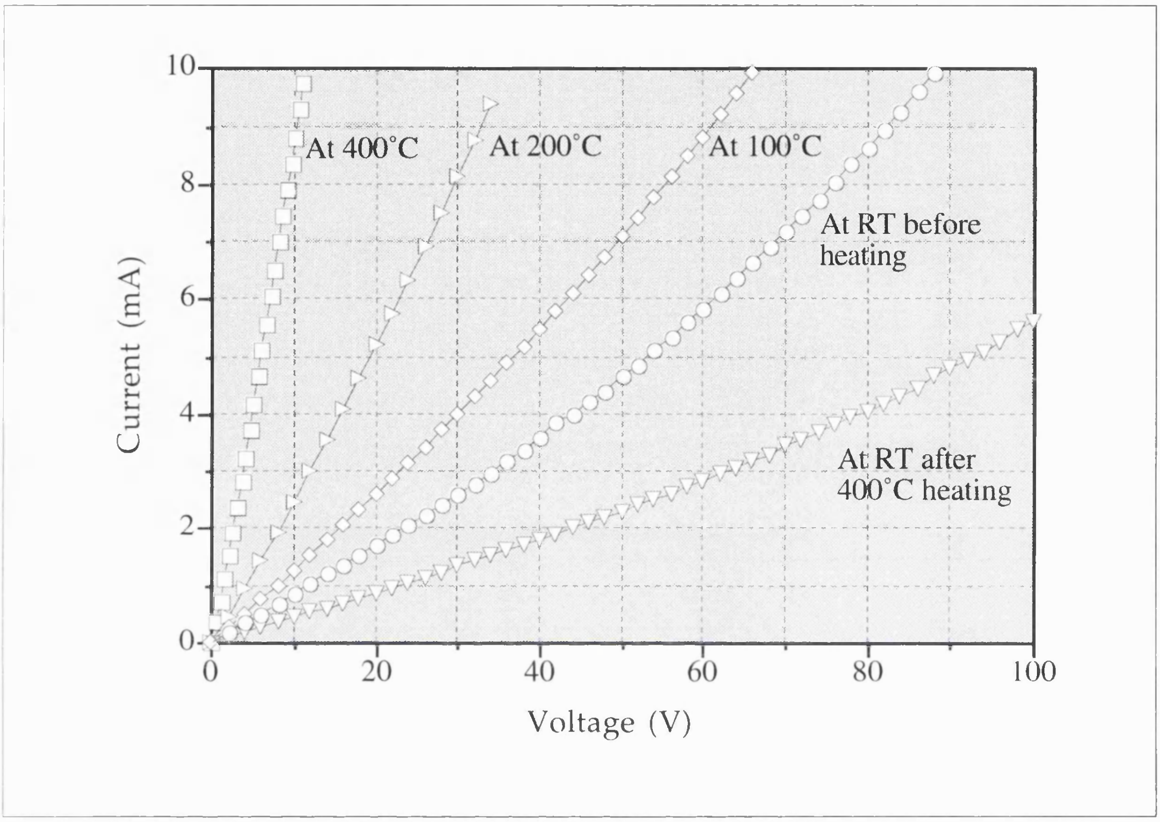

Figure 7.4 Current-voltage characteristics of Ti-Ag-Au contact metallisations to CVD diamond for a range of operating temperatures.

7.3.2 Secondary ion mass spectroscopy (SIMS)

Dynamic SIMS analyses for the Ti-Au contacts are shown in Figure 7.5, uncorrected for the differing cross sections for sputter removal of each element. Figure 7.5(a) reveals the nature of the 'as-deposited' contact, whilst Figures 7.5(b) and 7.5(c) relate to contacts following heating at 400 °C for 5 h and annealing at 700 °C in a hydrogen ambient for 15 min, respectively. In each profile the signals pertaining to the diamond layer (C), the boron dopant (B), and those of the metallic layers (Au, Ti) have been monitored. It is clear from Figure 7.5(a), that the diamond interface is reached after around 4 min of sputtering, as the C signal is seen to reach its peak at this point. It is interesting to note that the boron signal shows a peak at this point with a slight reduction in signal intensity as sputtering continues. The Au signal reaches a peak close to the surface of the contact as judged by a sputter time of only 2 min; a peak in the Ti concentration follows at around 3 min. Whilst the Au signal reduces by almost two orders at the point where the carbon signal peaks (4 min), a similar decrease in the Ti signal is not apparent until almost 10 min sputtering has been carrier out. Marked changes to this situation occur upon heating; both 5 h 400 °C heat treatment in an air (Figure 7.5(b))and 15 min 700 °C treatment in hydrogen (Figure 7.5(c)), cause the Au and Ti signals to adopt broadly similar profiles during sputtering. The C signal is seen to increase earlier during the erosion process although the actual peak remains around the 4 min sputter region. In addition, the decay of the Ti and the Au signal into the C signal appears to occur at a lesser rate for the contacts which have been subjected to the 700 °C treatment.

Comparable SIMS traces are presented in Figure 7.6 for the Ti-Ag-Au contacts; Figure 7.6(a) being the 'as-deposited' metallisation with (b) and (c) being typical of contacts treated at 400 °C (5 h, air) and 700 °C (15 min, hydrogen), respectively. The un-heated contact shows profiles similar to the un-heated Ti-Au metallisation other than the presence of an intermediate Ag peak (at around 3 min), a splitting of the Au peak into two (at around 1 and 4 min) and an increase in the sputter time needed to reveal the peak in the C and B traces (to around 6 min). This latter effect arises from the increased thickness of the contact region. Upon heating to 400 °C in air (Figure 7.6(b)), the Au and Ag profiles shift and co-incide, whilst the Ti peak appears to change very little. Similarly, the C and B traces remain un-perturbed. The 700 °C treatment in hydrogen (Figure 7.6(c)) shows a similar effect, with the Au and Ag peaks being broader but still co-incident and displaying little penetration into the region of peak C response. The Ti signal appears split, with a peak near the surface in addition to the peak present before heating a the contact-diamond interface.

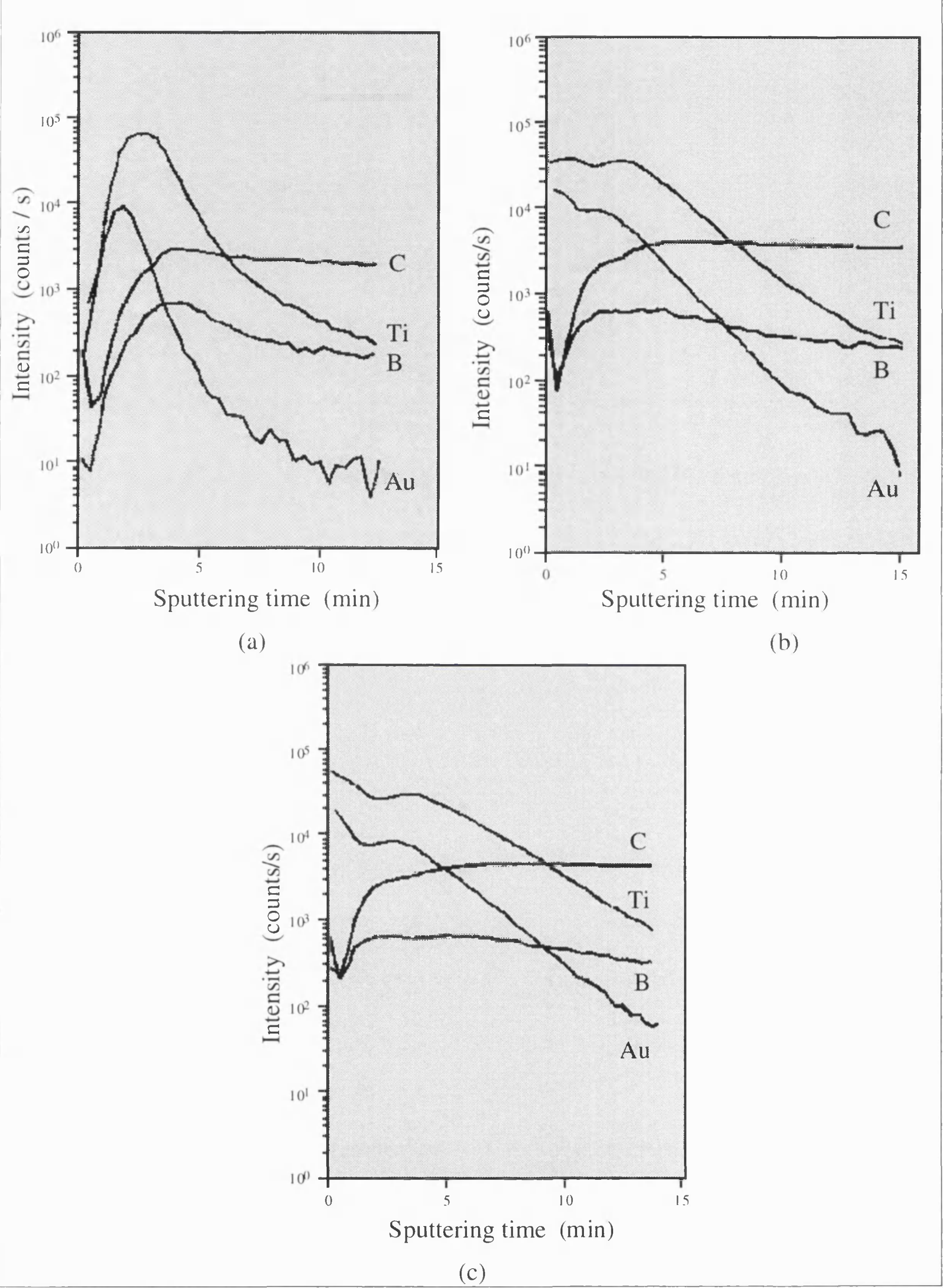

(a)

(b)

(c)

Figure 7.5 SIMS depth profile as a function of sputtering time of Ti-Au contact metallisations to CVD diamond for the case of: (a)as-deposited, (b)heat treated to 400 °C, (c)hydrogen annealed at 700 °C.

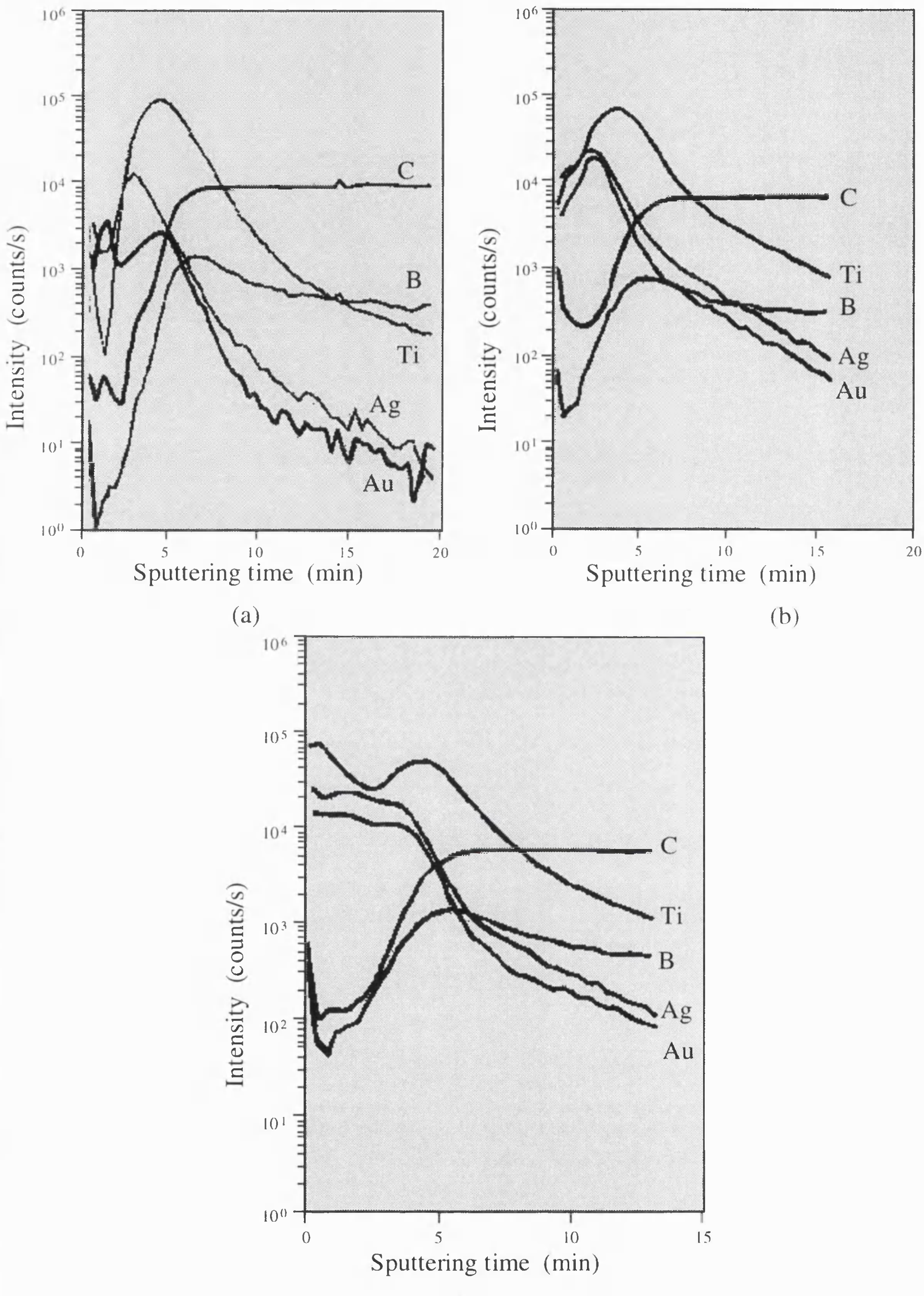

(a) (b) (c)

Figure 7.6 SIMS depth profile as a function of sputtering time of Ti-Ag-Au contact metallisations to CVD diamond for the case of: (a)as-deposited, (b)heat treated to 400 °C, (c)hydrogen annealed at 700 °C.

7.3.3 Scanning electron microscopy (SEM)

Visual observations after heating the various samples to either 400 °C or 700 °C indicated a change in the colour of the contact metallisations. In the case of the Ti-Au formulation, the characteristic bright gold colour had been altered in the course of the heat treatments to a bluish-green colour. SEM subsequently revealed a physical degradation in the Ti-Au contacts where a breaking up of the overlayer has occurred (Figure 7.7(a)). For the Ti-Ag-Au contacts, a whitish-gold colour following the heat treatments (400 °C or 700 °C) is assumed to be the result of the Ag and Au intermixing. However in this case, the macroscopic physical integrity of the contacts is seen to remain stable (Figure 7.7(b)).

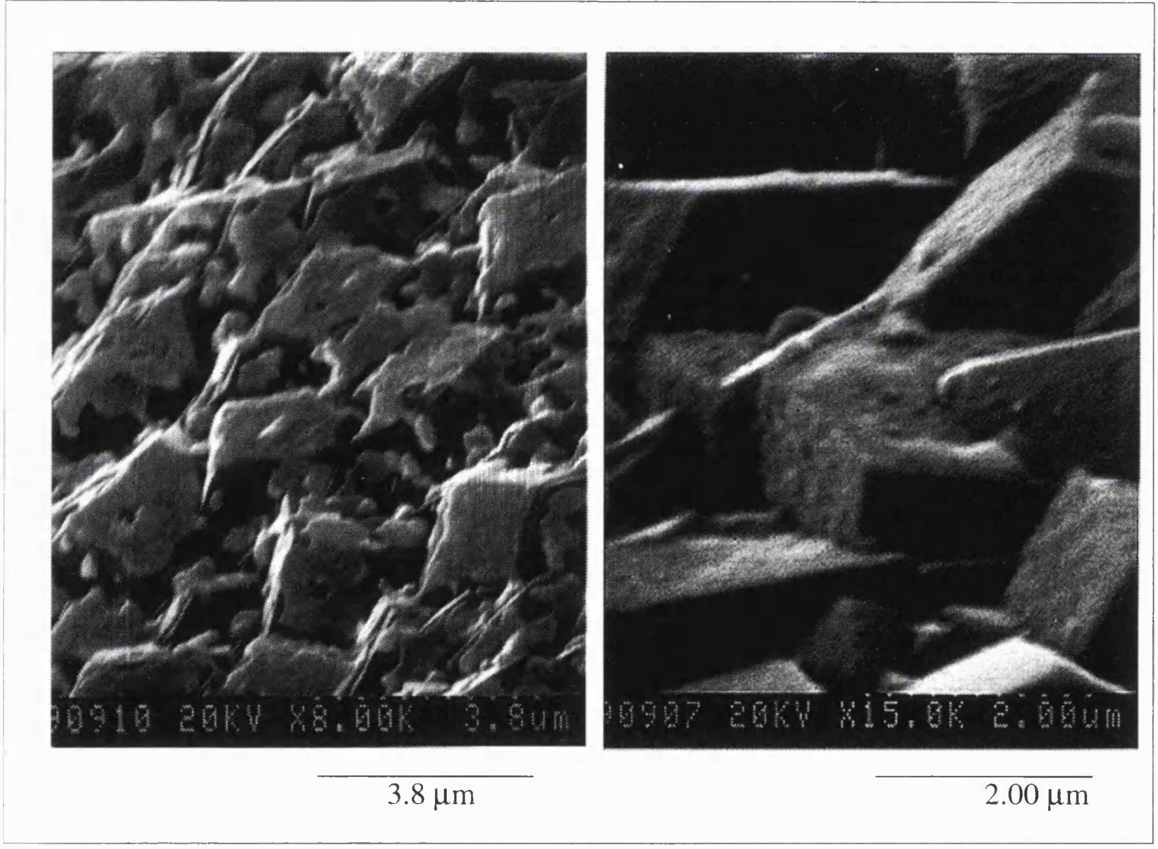

Figure 7.7 Scanning electron micrograph of: (a) Ti-Au; and (b) Ti-Ag-Au contact metallisations after > 5h exposure to a temperature of 400 °C in an air ambient.

7.4 DISCUSSION

The use of carbide-forming refractory metals such as Ti as a non-rectifying contact metallisation have been commonly employed within the field for the study of the electronic properties of diamond applications. Although from work function considerations alone the use of Ti would not be expected to lead to the formation of high quality ohmic contacts (theoretical barrier height = 1.2 eV), the observation by many workers of the existence of a carbide layer has led to suggestions concerning the nature of this layer on the electrical characteristics of the interface. Tachibana *et al.* [1992c] utilised the technique of x-ray photoelectron spectroscopy (XPS) to detect the formation of TiC after the deposition of Ti layers of thicknesses greater than 1.5 nm; the TiC peak was observed to continuously increase with the temperature of annealing which was studied from the as-deposited case up to 430 °C. By comparing the valence band edge by XPS, the effect of annealing was shown to reduce the barrier height from 1.3 eV to 0.8 eV. These authors attributed the ohmic nature of Ti on diamond to the introduction of defects at the interface due to the formation of the carbide layer; the result of this was suggested to either narrow the depletion region leading to a greater tunnelling current, or else effectively lowering the barrier height. Kawaguchi *et al.* [1994] employed transmission electron microscopy to observe a 2 nm thick layer of TiC after annealing a titanium layer on polycrystalline diamond at 400 °C for 5 min; annealing to 600 °C led to an additional 2 nm disordered layer at the TiC diamond interface with a corresponding 10% reduction in the contact resistance. The dependence of the specific contact resistivity as investigated by Nakanishi *et al.* [1994] showed an inverse relationship to the doping concentration when it was assumed that there was a 100% activation of the boron dopants at the metal-diamond interface. The fact that both of the contact formulations investigated here (*viz.* Ti-Au and Ti-Ag-Au) demonstrate specific contact resistivities [from a previous study, see Whitfield, 1994] which correlate well with the results of Nakanishi and co-workers [1994] over a range of doping levels suggests the active role of Ti.

It is apparent that heat treatment may modify both the electrical and physical characteristics. In both contact formulations, a reduction in current levels was observed with increasing exposure time to the heat treatments either at 400 °C or 700° C. In the case of Ti-Au contacts, physical instability has been reported by Harper *et al.* [1992] where annealing at 450 °C (30 min) in a N_2 ambient resulted in a Ti SIMS signal at the surface; this was suggested from x-ray diffraction analysis (XRD) to be TiO_2. No consequence of this observation on the electrical response was reported. X-ray photoelectron spectroscopy (XPS) was employed by Venkatesan *et al.* [1993] to show the formation of TiO_2 at the surface of a Ti (20 nm)/Au (100 nm) contact after annealing at 850 °C for 1 h *in-vacuo*; the contacts were found to be electrically stable after prolonged heating at 400 °C for 4 h in an air environment. In contrast, stable electrical response was not obtained here even after 5 h at 400 °C either for the as-deposited case, or after the 700 °C hydrogen anneal. Correlating the electrical characteristics with SIMS indicates a possible intermixing of the Ti and the Au metallic layers and a Ti signal at the surface of the contact. It is possible that the effect of greater surface roughness of the films used in this study as compared to Venkatesan's chemically machine polished material (no details given) might account for this difference. Indeed, a 200 nm thick Ti layer capped by a 150 nm thick layer of Au deposited on type IIb natural diamond demonstrated stable electrical characteristics when annealed at 450 °C for 20 min in a 90% N_2/10% H_2 forming gas; however Ti contacts capped with a 250 nm Au layer and treated to the higher temperature of 750 °C was not found to be stable [Viljoen, 1994]. Although the reported thicknesses of the metal layers vary, it has been reported that even with a 1µm thick Au capping layer on Ti contacts deposited on diamond films with surface roughness of less than 1 µm, a colour change and intermixing of the Au and Ti layers as detected by Auger analysis occurred when annealed to temperatures of 450 °C and greater in an N_2 ambient [Naseem, 1993]. In any event, the lack of electrical stability in the Ti-Au contact metallisations studied here may also be attributed to the formation of a Ti oxide phase, which, in this case arises directly from the loss of macroscopic physical structure as seen from SEM. The fact that break-up of the contact structure appears to occur preferentially at the edges of the crystallites suggests a possible factor in the differences observed here and in the literature concerning the electrical stability of such contacts.

Comparing the electrical characteristics between the as-deposited and 700 °C hydrogen annealed Ti-Ag-Au contacts reveals a greater degree of conductivity for the hydrogen treated case which eventually settles to similar values after extended 400 °C treatment. The possibility exists of hydrogenation of the films resulting in an increase in conductivity; the effect of hydrogen on the electrical properties of CVD diamond films has been reported by many authors *e.g.* Landstrass and Ravi [1989] have demonstrated that treatment in a hydrogen plasma at a substrate temperature of 400 °C decreases the resistivity of diamond films by up to six orders of magnitude. This change may subsequently be reversed by heating the sample at temperatures as low as 100 °C. The reduction in the current levels of the non-hydrogen treated contacts may arise from a combination of metallic intermixing, oxide of Ti formation and the possibility of optimum carbide formation. On this latter point, the degree of formation of the interfacial carbide layer has been demonstrated by Tachibana *et al.* [1992] by XPS where an increasing Ti-C signal was registered from the as-deposited case to temperature treatments of 430 °C; Moazed *et al.* [1990] for Mo (carbide former) contacts on type IIb diamond observed an increase in resistance measurements after annealing such contacts for >8 min. Nevertheless, the introduction of the Ag layer between Ti and Au has resulted in the attainment of contacts which display stable electrical characteristics after around 1 h of heating to 400 °C in an air ambient, and remain so for the duration of the testing period. In comparing the SIMS spectra for the 'as-deposited' case and after 400 °C treatment (Figure 7.6(a),(b)) there would appear to be little outdiffusion of the Ti signal to the surface of the contacts. Furthermore, although mixing of the Au and Ag layers appears to have occurred (Figure 7.6(b)) the level of penetration of the Ag and Au elements into the diamond (carbon) layer is seen to be minimal. In the case of 700 °C annealing, the SIMS data for the Ti-Ag-Au contact indicates outdiffusion of Ti to the outermost surface of the contact and some electrical degradation of the Ti-Ag-Au contacts may therefore be expected as a result of oxidation of the Ti elements on the surface.

7.5 SUMMARY

Although many reports within the literature have demonstrated the physical instability of Ti-Au contacts on various forms of diamond, the electrical behaviour has been reported to be stable by authors including Venkatesan and co-workers [1993]. In contrast, the formation of a temperature stable ohmic contact on polycrystalline diamond with a grain size of 1-2 μm could not be achieved with this contact formulation. The disparity between this and reports in the literature is suggested to arise as a result of the surface roughness of the films used; the employment of surface smoothening techniques prior to device fabrication may alleviate such concerns in Ti-Au contacts. However, a superior level of stability can be achieved from the Ti-Ag-Au tri-layer contact on diamond [first reported by McKeag, Chan and co-workers, 1995] which offers similar contact resistivities, but remains electrically unchanged, after an initial stabilising anneal, to temperatures of 700 °C. In addition to the stable electrical characteristics and minimal intermixing of the Ti/Ag/Au metallic layers to at least 400 °C, the macroscopic physical integrity of these contacts is demonstrated by SEM which reveal that smooth contact texture remain after the treatments carried out.

REFERENCES

Das, K., Venkatesan, V. and Humphreys, T.P., [1994]. *J. Appl. Phys.*, **76**, 2208.

Fang, F., Hewett, C.A., Fernandes, M.G. and Lau, S.S., [1989]. *IEEE Trans. Electron Device*, **36**, 1783.

Geis, M.W., Rothchild, M., Kunz, K.K., Aggarwall, R.L., Wall, K.F., Parker, C.D., McIntosh, K.A., Efremow, N.N., Zayhowski, J.J., Ehrlich, D.J. and Butler, J.E., [1989]. *Appl. Phys. Lett.*, **55**, 2295.

Gildenblat, G.Sh., Grot, S.A., Hatfield, C.W., Badzian, A.R. and Badzian, T., [1990]. *IEEE Electron Device Lett.*, **11**, 371.

Gildenblat, G.Sh., Grot, S.A. and Badzian, A., [1991]. *Proc. IEEE*, **79**, 647.

Harper, R.E., Johnston, C., Chalker, P.R., Totterdell, D., Buckley-Golder, I.M., Werner, M., Obermeier, E. and Van Rossum, M., [1992]. *Diamond Relat. Mater.*, **1**, 692.

Hewett, C.A., Zeidler, J.R., Taylor, M.J., Zeisse, C.R. and Moazed, K.L., [1991]. in "Proceedings of the 2nd International Conferenceon New Diamond Science and Technology", R. Messier, J.T. Glass, J.E. Butler, R. Roy, (eds.), Material Research Society, Pittsburgh, PA, USA, 1112.

Kawaguchi, G., Nakanishi, J., Otsuki, A., Oku, T. and Murakami, M., [1994]. *J. Appl. Phys.*, **75**, 5165.

Landstrass, M.I. and Ravi, K.V., [1989]. *Appl. Phys. Lett.,*, **55**, 975.

McKeag, R.D., Chan, S.S.M., Johnston, C., Chalker, P.R. and Jackman, R.B., [1995]. *Mater. Sci. Engineer.,* **B29**, 223.

Moazed, K.L., Nguyen, R., Zeidler and J.R., [1988]. *IEEE Electron Device Lett.*, **9**, 350.

Moazed, K.L., Zeidler, J.R. and Taylor, M.J., [1990]. *J. Appl. Phys.*, **68**, 2246.

Nakanishi, J., Otsuki, A., Oku, T., Ishiwata, O. and Murakami, M., [1994]. *J. Appl. Phys.*, **76**, 2293.

Naseem, H.A., Meyyappan, I., Prasad, C.S. and Brown, W.D., [1993]. *J. Microcircuits and Electron. Packaging,* **16**, 257.

Poate, J.M., Turner, P.A. and DeBonte, W.J., [1975]. *J. Appl. Phys.,* **46**, 4275.

Rhoderick, E.H., Williams, R.H., [1988]. *Metal-Semiconductor Contacts.* (Clarendon Press), Oxford, UK.

Seal, M., [1969]. *Industrial Diamond Rev.*, **29**, 408.

Tachibana, T. and Glass, J.T., [1992a]. *J. Appl. Phys.*, **72**, 5912.

Tachibana, T., Williams, B.E. and Glass, J.T., [1992b]. *Phys. Rev.,* **B45**, 11968.

Tachibana, T., Williams, B.E. and Glass, J.T., [1992c]. *Phys. Rev.,* **B45**, 11975.

Tachibana, T., Glass, J.T. and Thompson, D.G., [1993]. *Diamond Relat. Mater.*, **2**, 37.

Tyagi, MS, [1991]. *Introduction to semiconductor materials and devices* (John Wiley) New York, USA.

Venkatesan, V., Malta, D.M. and Das, K., [1992a]. Proc. Mater. Res. Soc. Symp., **270**, Material Research Society, Pittsburgh, USA.

Venkatesan, V. andDas, K., [1992b]. *IEEE Electron Device Lett.*, **13**, 126.

Venkatesan, V., Malta, D.M., Das, K. and Belu, A.M., [1993]. *J. Appl. Phys.*, **74**, 1179.

Viljoen, P.E., Lambers, E.S. and Holloway, P.H., [1994]. *J. Vac. Sci. Technol.,* **B12**, 2997.

Werner, M., Dorsch, O., Baerwind, H.U., Obermeier, E., Johnston, C., Chalker, P.R., and Romani, S., [1995]. *IEEE Trans. Electron Dev.,* **42**, 1344.

Whitfield, M.D., [1993]. *MSc. Thesis Report*, University College London, University of London, UK.

8: RECTIFYING CONTACT METALLISATIONS TO OXIDISED THIN FILM DIAMOND

8.1 INTRODUCTION

Although much progress has been made over the past few years in terms of the quality of the synthesised material, further advances must be made before successful implementation of certain classes of diamond electronic devices may be achieved. Foremost amongst these is the continuing desire for single-crystalline heteroepitaxial growth over areas amenable to present-day device fabrication techniques together with the realisation of efficient n-type doping. Diamond films with increasingly larger crystallite size of a textured and oriented nature are the present state of art for non-diamond substrates; however attempts at n-type doping has resulted only in films of a highly resistive nature [Popovici, 1995]. Thus, in the aim of active diamond devices, research has also concentrated on the development of rectifying metal-semiconductor junctions as an alternative to p-n junctions. Based on unipolar concepts, device structures such as metal-semiconductor field effect transistor structures (MESFETs) and photo-diode detectors may be designed.

In an ideal case of a metal in intimate contact with a p-type semiconductor, the potential barrier height, $q\phi_B$ (eV), presented to charge carriers crossing the interface between the two material systems at thermal equilibrium is given as:

$$q\phi_B = E_g - q(\phi_m - \chi_s) \tag{8.1}$$

where E_g is the energy bandgap of the semiconductor, q the electronic charge, ϕ_m the metal work function, and χ_s the electron affinity of the semiconductor measured from the bottom of the conduction band to the vacuum level [Sze, 1981]. Considering the wide bandgap nature of diamond (5.5 eV) with that of the work functions of typical metals (Table 8.1) suggests that rectifying behaviour may be obtained from many combinations. This is provided that other factors such as chemical reactivity (*e.g.* solid state reactivity of Ti) are not present.

Metal	Pt	Ni	Au	Cu	Ti	Al	Ag	In	Cs
ϕ_M(eV)	5.65	5.15	5.10	4.65	4.33	4.28	4.16	4.12	2.14

Table 8.1 Work functions values for some metals [adapted from Rhoderick, 1988].

In a low to moderately doped semiconductor where the depletion region is sufficiently thick to prevent quantum-mechanical tunnelling, the predominant current transport mechanism is thermionic emission; in the thermionic emission model developed by H.A. Bethe for carrier transport over the potential barrier in metal-semiconductor junctions, the electrical characteristics may be expressed as [Sze, 1981]:

$$J = J_s\left[\exp\left(\frac{qV}{nk_BT}\right) - 1\right] \tag{8.2a}$$

where $$J_s = A^* T^2 \exp\left(-\frac{q\phi_B}{k_BT}\right);\quad A^* = \frac{4\pi q m^* k_B{}^2}{h^3};\quad \frac{1}{n} \equiv \frac{k_BT}{q}\frac{\partial(\ln I)}{\partial V}; \tag{8.2b;c;d}$$

J= current density; J_S= saturation current density; V= applied voltage; n= ideality factor; A^*= effective Richardson constant; ϕ_B= barrier height; m^*= effective mass of charge carrier; and the other symbols have the standard definition.

If the dopant concentration within the semiconductor is increased, then quantum mechanical tunnelling of carriers may occur through the increasingly thin depletion region which extends into the material. In order to consider this possibility, the E_{oo} characteristic energy parameter is often determined from material properties to arrive at a guide to the dominant current conduction process as shown in Equation 8.3 [Rhoderick, 1988]. Current conduction then takes place as a combination of emission of carriers over the potential barrier together with quantum mechanical tunnelling through the barrier; the reverse current component may be approximated by the expressions given in Appendix D.

$$\frac{qE_{00}}{kT}\begin{cases} \ll 1; & \textit{thermionic emission} \\ \approx 1; & \textit{thermionic}-\textit{field emission} \\ \gg 1; & \textit{field emission} \end{cases} \qquad \text{where } E_{00}=\frac{h}{4\pi}\left[\frac{N_A}{m^{*}\varepsilon_s}\right]^{1/2}; \qquad (8.3a;b)$$

N_A is the acceptor concentration and ε_s the dielectric permittivity.

Such idealised behaviour on diamond has generally not been observed in practice: many factors may lead to deviation from the theoretically predicted behaviour including semiconductor surface states which leads to limited control of the barrier height by the selection of metal work functions. The possibility also exists of a heterogeneous state present on the semiconductor surface; this factor may be of particular significance for as-deposited thin film diamond. Barrier heights have been measured on both single- and poly-crystalline material and these has been summarised by Das [1992] (Table 8.2). This shows a variation existing between values measured for Au and Al; the lack of dependence of the barrier height on the metal work function has been attributed to Fermi level pinning at the diamond surface [Hicks, 1989; Beetz, 1990; Tachibana, 1995].

Metal	Barrier height (eV)	Material	Method	Reference
Au	1.7 +/-1.1	(100)- natural	C-V	[Glover, 1973]
Au	1.7 - 2.0	natural	C-V, I-V, IPS	[Mead, 1976]
Al	1.9 - 2.0			
Au	1.3	(111)- natural	photoelectron	[Himpsel, 1980]
Al	1.5		spectroscopy	
Au	1.13	polycrystalline	IPS	[Hicks, 1989]
Al	1.13			
Au	1.15	polycrystalline	IPS	[Grot, 1990]

Table 8.2 Summary of barrier height measurements of selected metal-diamond contacts. (C-V= capacitance-voltage, I-V= current-voltage, IPS= internal photoelectron spectroscopy).

The preparation of the diamond surface prior to contact metallisation has been shown to have a significant effect on contact behaviour. Grot and co-workers [1990] have demonstrated that Au contacts on as-deposited homoepitaxial films were ohmic regardless of the boron concentration in their films; when treated to an acid treatment consisting of CrO_3 and H_2SO_4, such contacts displayed rectifying characteristics. Mori *et al.* [1991] reported of contact behaviour varying between ohmic and rectifying depending on the electronegativity of the metal for contacts on as-deposited polycrystalline diamond of unspecified doping level. This dependence was lost when the initial films were treated to an oxidising treatment consisting either of CrO_3 or an oxygen plasma, whereupon rectifying character was observed.

To date, contact metallisations most closely conforming to theoretical predictions have been obtained on single-crystalline diamond employing a variety of metals such as Au [*e.g.* Shiomi, 1989; Gildenblat, 1990], W [*e.g.* Geis, 1987; Shiomi, 1989], Ni [*e.g* Humphreys, 1991] and Al [*e.g.* Hartsell, 1994; Kiyota, 1995]. Al contacts on natural diamond of doping level $2x10^{16}$ cm^{-3} have demonstrated pico-ampere reverse leakage currents at room temperature (bias voltage of 5 V) and 6 orders of rectification [Hartsell, 1994]. On oxygenated diamond surfaces, *i.e.* surfaces treated in an oxidising solution (CrO_3) rectifying junctions involving Al or Au were reported by Kiyota *et al.* [1995] to give rise to sub-pico-ampere room temperature leakage currents (7 orders of magnitude rectification at 2 V bias); the concentration of acceptor centres was estimated to be in the region 10^{16}-10^{17} cm^{-3}. The diode ideality factor, *n*, which is a measure of the forward current transport characteristics when thermionic emission applies [Sze, 1981], has been found in all cases to be greater than the theoretical value of 1; values of 2.4 [Humphreys, 1991], 1.67 [Venkatesan, 1992] and 1.24 [Kiyota, 1995] have been obtained. Geis and co-workers [1993] reported that the ideality factor of Hg contacts on natural type IIb diamond (doping unspecified) may be reduced from ~20 to 1.3-2.0 by prior annealing of the material in air at 660 °C; this was believed to remove a layer of impurities or defects acting as a compensation layer to the boron acceptors.

In the case of polycrystalline material, reported ideality factors have ranged from 64.8 [Gomez-Yanez, 1992] for Au contacts, to values of 1.85 [Al: Jeng, 1990] and 2 [Ag: Zhao, 1992] contacts (unspecified material doping concentrations). In these cases, investigations involved vertical structures with the ohmic contact placed on the back of the Si substrate. On planar structures, a value of 2.5 was obtained by Tachibana *et al.* [1993] for TiC contacts directly deposited by radio frequency sputtering rather than by solid state reaction of Ti; the rectification was two orders with a leakage current at 5 V bias of 0.4 μA (atomic boron concentration by SIMS was $3x10^{-18}$ cm^{-3}).

High temperature operation is of interest in the considered applications of diamond electronics; rectifying junctions at elevated temperatures have essentially involved single-crystalline material. Geis and co-workers [1987] reported operation on natural diamond at temperatures greater than 580 °C with W contacts. Homoepitaxial films chemically treated with CrO_3 were employed by Gildenblat *et al.* [1990] to demonstrate the rectifying properties of Au contacts to 580°C; the acceptor level present in their films was not specified. Reverse leakage currents as low as 4 nA at 20 V and temperatures of 400 °C have been obtained by the use of heteroepitaxially deposited nickel dots on natural semiconducting diamond of resistivity 10^4 Ωcm [Humphreys, 1991]; the leakage levels at room temperature was measured at 2 nA. On polycrystalline material, little evidence is present within the literature to suggest satisfactory operation; Zhao *et al.* [1992] have reported of non-symmetric I-V characteristics with Ag contacts on chemically cleaned (CrO_3) material of unspecified doping with approximately one order of magnitude rectification at 250 °C (10 V bias).

The various reports summarised here demonstrate the potential for the formation of rectifying junctions with acceptable levels of leakage currents if natural or epitaxial material is employed. Furthermore, reports of operation at temperatures in excess of 580 °C experimentally demonstrates the promise of high temperature electronic devices. However, on polycrystalline material, diode device performance has not achieved the level attained on single-crystalline material; typically, rectification levels of only 2 orders are achieved [Tachibana, 1993; Venkatesan, 1992]. This low ratio may arise from the low levels of forward conduction as suggested by the high ideality factors observed, and/or the high reverse current levels. Of the factors which may contribute to high reverse lcurrents, sp^2 bonded amorphous carbon type material existing on the surface of as-deposited diamond films may be reduced by acid treatments involving oxidising agents. Indeed, Kiyota and co-workers [1995] reported of Al and Au rectifying contacts on oxidised surfaces of single-crystalline diamond (doping level unspecified) possessing sub-pico-ampere leakage currents at 2 V bias; this shows the suitability of such a treatment. However, the temperature stability of the contacts on the oxidised surface was not investigated. Furthermore, the effect of bulk properties (dopant concentrations) have not been studied in conjunction with rectifying contacts and oxidised surfaces. It is thus the purpose of this study to look into the possibility of conditioning the surface of thin film polycrystalline diamond for the investigation of doping concentration on the junction characteristics. In addition the stability of these contact metallisations at elevated conditions have been tested.

8.2 EXPERIMENTAL DETAILS

Polycrystalline diamond films of varying doping concentrations were grown by the technique of microwave plasma assisted chemical vapour deposition on a 10 μm thick wafer of nominally undoped diamond in order to eliminate undesired current paths via the underlying silicon substrate (provided by AEA Technology, Harwell, UK). Dopant levels within subsequently deposited conductive layers were controlled by altering the boron containing precursor gas flow rate to result in three films labelled HIGH, MED and LOW corresponding to high, medium and low dopant gas flow rates, respectively. The films consisted of randomly aligned coalesced crystallites of 1-2 μm in size (Figure 5.1). The samples were annealed at 430 °C for 1 h in an air environment in order to stabilise films properties [Harper, 1991], and then subjected to the oxidising surface treatment as described in Appendix B to reduce any non-diamond components which may be present on as-deposited diamond films. Photolithography (Appendix C) was used to form 100 μm circular contacts within a 300 μm circular opening in a metal overlayer on the diamond (Figure 7.11). The edges of the samples, typically of size 8 mm x 8 mm, were shadow masked in order to prevent metallisation in this region. The metal overlayer was deposited as the ohmic contact employing the tri-layered Ti (10nm)-Ag (150 nm)-Au (200 nm) formulation which has been shown to be both electrically and physically stable to temperatures of at least 400 °C (Chapter 7). The central contact employed Al or Ni metallisations resistively evaporated at base pressures $< 10^{-6}$ mbar to study their contact behaviour at room temperature and up to 430 °C. Material characterisation was carried out by Raman spectroscopy, Hall effect measurements and secondary ion mass spectroscopy (SIMS). The electrical properties of the contacts were investigated by current-voltage (I-V) measurements with scanning electron microscopy (SEM) employed to study the macroscopic properties of the contacts after elevated temperature operation.

8.3 RESULTS

8.3.1 Material characterisation

Raman spectra of the three differently doped layers deposited on a common intrinsic diamond layer after treatment in the oxidising acid solution were found to be essentially similar to that presented in Figure 5.1. SEM showed similar average grain sizes being present in the three films.

Hall effect measurements carried out on the three films (HIGH, MED and LOW) revealed sheet resistance, carrier concentration and Hall carrier mobility data as presented in Table 8.3. The carrier concentration is calculated from the sheet carrier concentration as measured by the Hall effect, together with the thickness of the doped layers which were 0.5 µm +/-10%. It is evident that as the gas phase boron concentration is increased, the resistance of the films fall; the corresponding increase in the carrier concentrations as detected by the Hall measurements suggests that the increased electrical conductivity is due to activated boron acceptor centres. Comparing the carrier concentration results with those of the atomic boron concentration as determined by SIMS (+/-20%), the dopant activation assuming no carrier compensation at room temperature for the HIGH doped film is ~55%, with the corresponding factor of ~8% for the MED film; such a decrease in the activation energy with increasing carrier concentration has been reported by Nishimura and co-workers [1991] (Figure 3.10). Furthermore, the increasing boron concentrations within the three films reveals the trend that as the doping is increased, the charge carrier mobility decreases. Relating these data points with Figure 6.8 suggests that carrier mobility in these films are predominantly limited by ionised impurity scattering. At the lower measurement temperature of 77 K, a lower degree of boron acceptor centre activation results in the higher carrier mobilities observed.

Sample	HIGH	MED	LOW
Dopant gas flow rate	highest	intermediate	lowest
Sheet resistance (Ω/square)	185 (507)	1273 (8374)	>1273
Hall mobility (cm^{2}V^{-1}s^{-1})	15 (26)	28 (374)	-
Carrier conc. (cm^{-3})	4.5x10^{19} (9.4 x 10^{18})	3.48x10^{18} (3.8 x10^{16})	-
Boron concentration (cm^{-3})	8.13 x 10^{19}	4.13 x 10^{19}	6.47 x 10^{18}

Table 8.3 Room temperature resistivity and Hall effect measurements for polycrystalline, randomly-oriented diamond films of varying doping concentrations. Measurements at 77 K are shown in brackets. Boron concentrations have been determined by SIMS.

8.3.2 Electrical characterisation of contacts

The electrical I-V behaviour of Al contacts incorporated in the test structure as shown schematically in Figure 7.1 and fabricated on the three films is shown in Figure 8.1(a); the I-V characteristics of corresponding structures employing Ni metallisations are revealed in Figure 8.1(b). It is apparent that the electrical behaviour of the Al contact is critically dependent on the doping concentration of the diamond film; at the highest dopant concentration investigated, symmetrical and linear I-V characteristics are achieved over the limits of the testing equipment (10 mA). However, as the dopant level is decreased, a degree of non-linearity is introduced (MED) which, at the lowest level of doping in this set of samples (LOW), non-symmetrical characteristics are observed and rectification is achieved over the range of testing (+/-10 V). Forward current conduction is considered to be in the third quadrant in the convention of electron current being positive *i.e.* hole majority charge carriers are dominant in the semiconducting diamond films. In the case of the Ni contacts (Figure 8.1(b)), similar behaviour is evident.

The temperature stability of the Al and Ni rectifying contacts has been tested to 400 °C in an air environment. Since it is crucial that the contacts be investigated in conjunction with temperature stable ohmics, Ti-Ag-Au contacts have been employed. Figure 8.2(a) shows the electrical operation of the Al contacts on the LOW doped material as a function of ambient temperature where each set of I-V data was sampled after approximately 5 min at the indicated condition. At 100 °C rectification is still evident but at temperatures greater than this, a steady increase in the reverse characteristics is apparent until at 400 °C the electrical behaviour is effectively linear and symmetric. Similar characteristics were observed for the Ni contacts (Figure 8.2(b)).

After this first series of electrical measurements at temperatures of up to 400 °C, the samples were kept at this temperature in an air ambient for a total time of 5 h. Subsequent I-V characterisation at room temperature revealed that the electrical behaviour of the Al contact metallisation remained electrically stable to this treatment as shown in Figure 8.3(a). However, although initial measurements for Ni contacts demonstrated similar trends as observed for Al (Figure 8.2), further testing at room temperature after a comparable 5 h treatment at 400 °C indicated a drastic deterioration in the electrical properties of this metallisation (Figure 8.3(b)). Figure 8.4 reveals room temperature electrical testing of Ni contacts treated to intermediate temperatures prior to exposure to extended heating at 400 °C; a gradual degradation of electrical properties is evident after all the temperature treatments. Testing of the contacts on wafers of HIGH and MED doping demonstrated similar degradation.

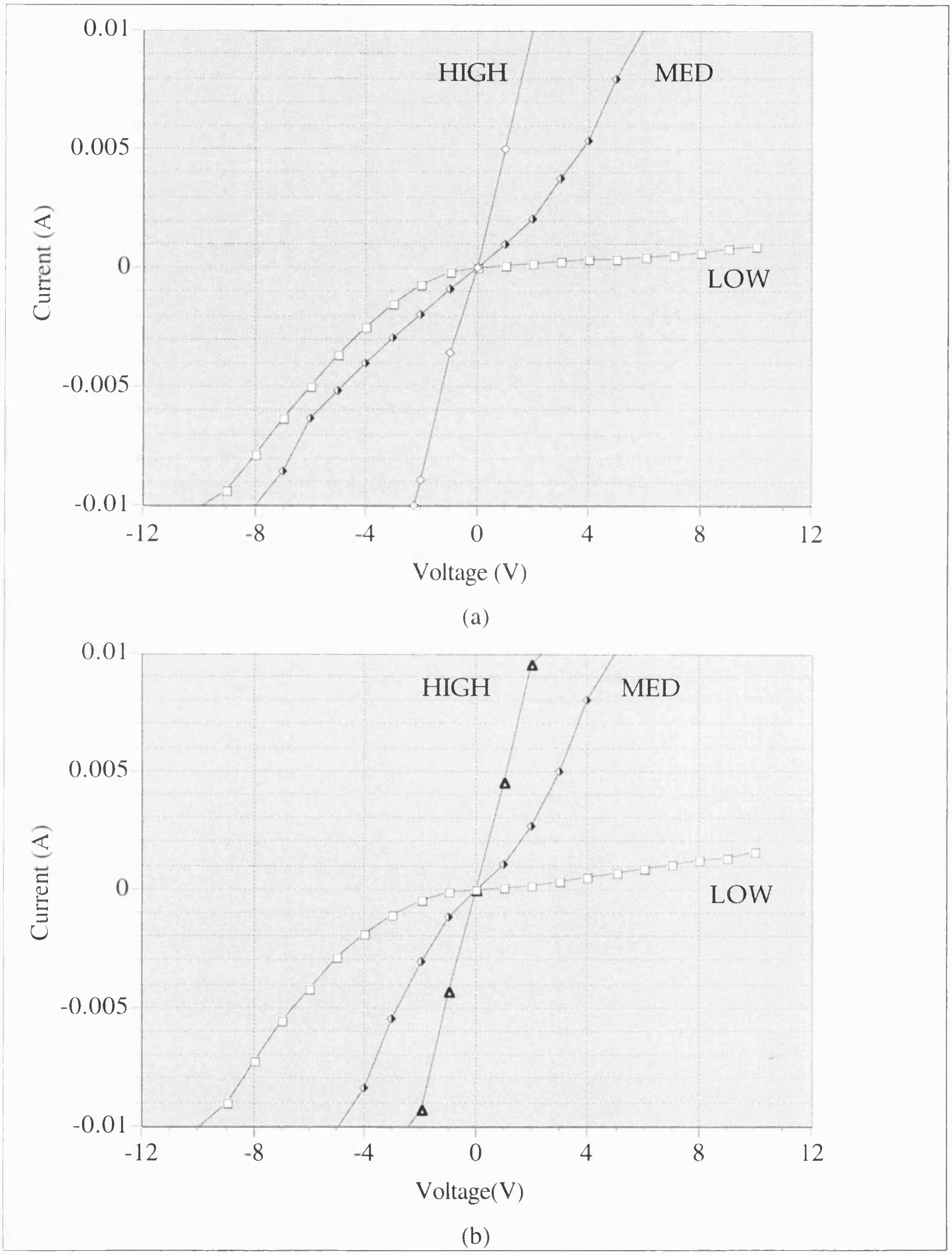

Figure 8.1 Room temperature current-voltage characteristics of as-deposited (a) Al; and (b) Ni contact metallisations to polycrystalline diamond films of doping concentrations as detailed in Table 8.3.

The ohmic contact is positively biased with respect to the central (rectifying) contact.

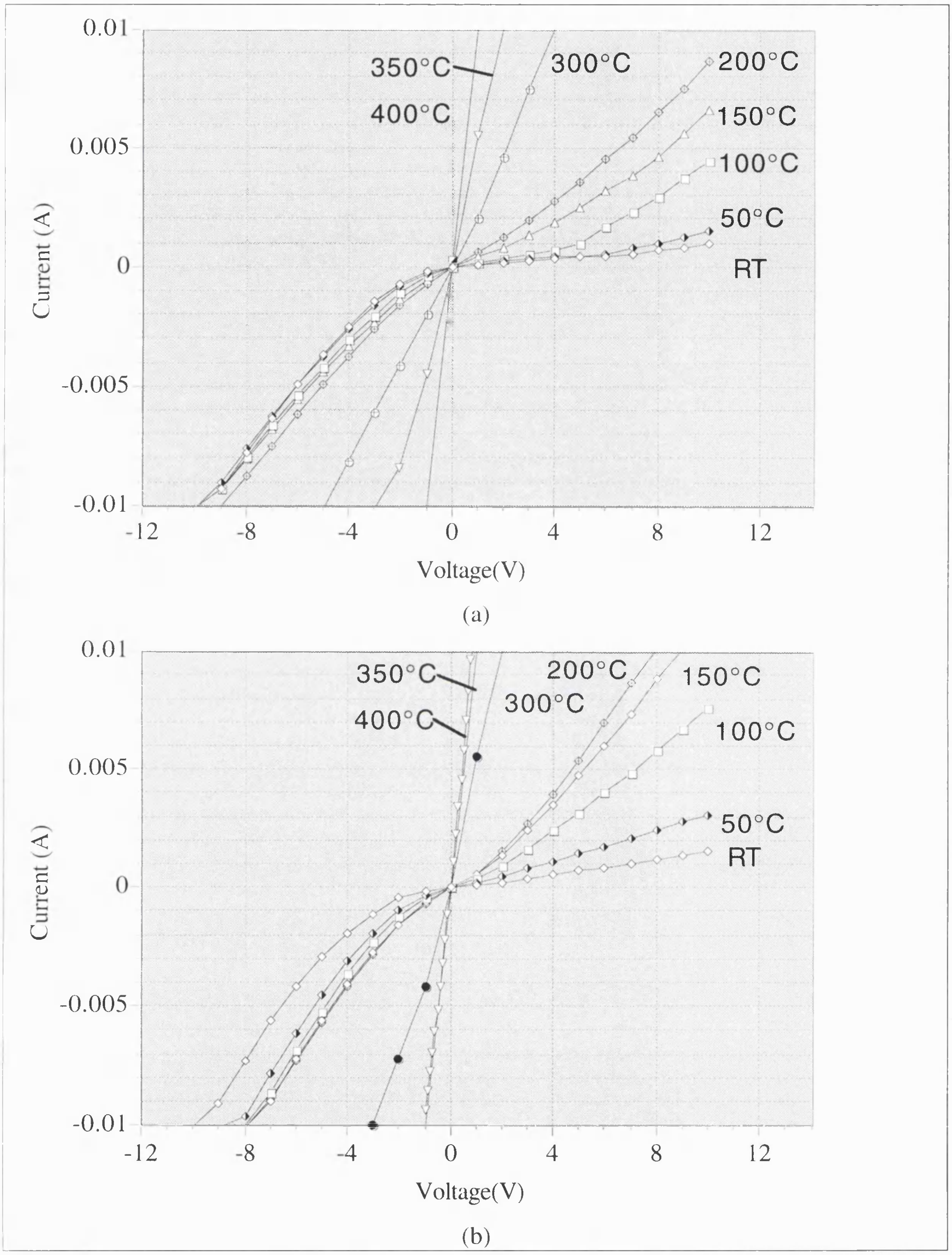

(a)

(b)

Figure 8.2 First series of elevated temperature measurements of (a) Al; and (b) Ni contact metallisations to polycrystalline diamond of LOW doping concentration.

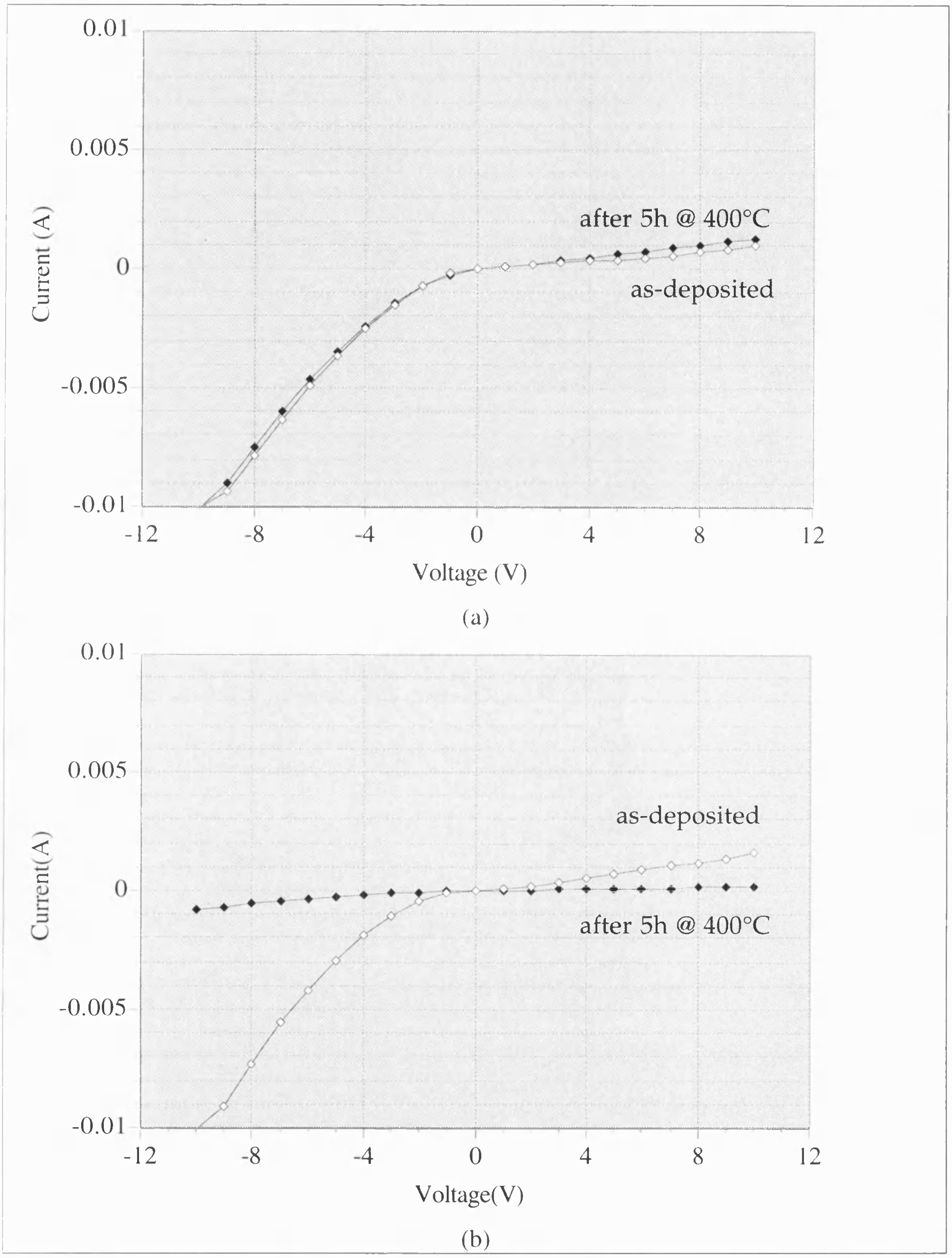

Figure 8.3 Room temperature current-voltage characteristics of (a) Al; and (b) Ni contact metallisations to polycrystalline diamond films of LOW doping concentration as detailed in Table 8.3 for the as-deposited case and that after heat treatment in an air ambient at 400 °C for 5 h.

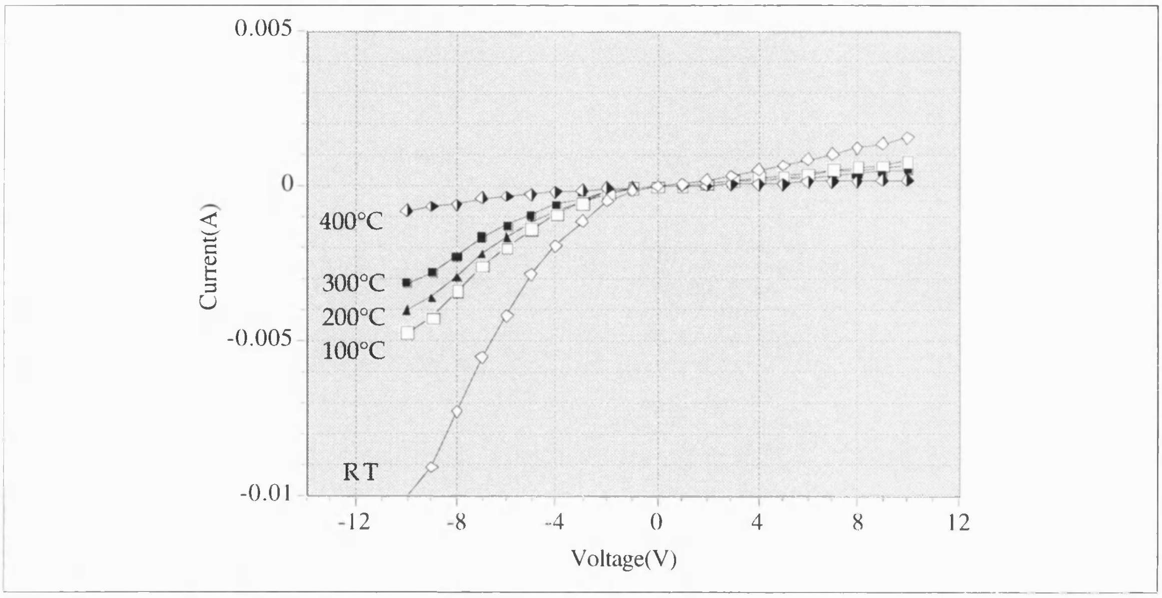

Figure 8.4 Room temperature current-voltage characteristics of Ni contact metallisations to polycrystalline diamond films of LOW doping concentration as detailed in Table 8.3 following 5 min heat treatments at the indicated temperatures.

8.3.3 Analysis of electrical characteristics

In order to characterise the forward characteristics of the rectifying contacts on the LOW doped material, Equation 8.3(d) is employed to extract the ideality factor *n*. Figure 8.5 shows curve fittings applied to two bias regions of the I-V characteristics as a result of the variation of the ideality factor with bias voltage; values of $n = 4.8$ ($0.1<V< 0.2$) and $n = 10.6$ ($0.3 < V < 0.45$) are obtained.

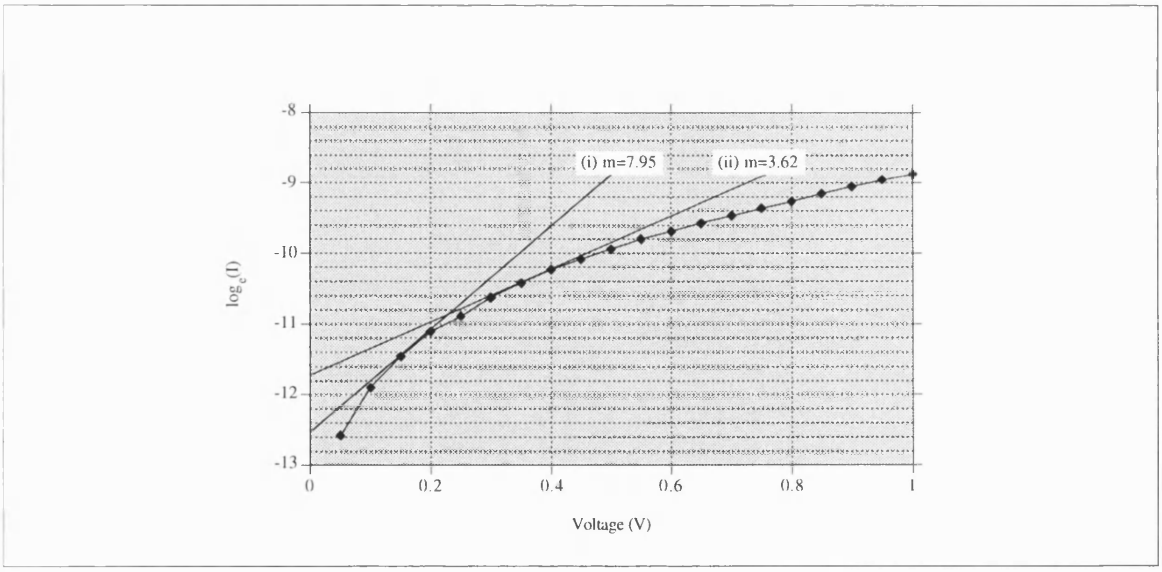

Figure 8.5 Plot of I-V characteristics of Al rectifying contact on LOW doped material for the extraction of diode ideality factor fitted over the voltage range (i) 0.1-0.2 V (correlation coefficient of 0.998); and (ii) 0.3-0.45 V (correlation coefficient of 0.997) where m is the gradient.

In terms of the reverse characteristics, Figure 8.6 shows the current density obtained at a reverse bias of 2 V for Al contacts on the three films; it is evident that the current levels increase with dopant concentrations. Limited reports presently exist describing the leakage currents of rectifying contacts on polycrystalline diamond which explicitly state the dopant levels within the diamond layer; nevertheless consideration of these reports emphasise this trend [Zhao, 1992; Tachibana, 1992; 1993; Whitfield, 1996]. Of these reports, that by Whitfield, Jackman and the present author [1996] employed the identical preparation techniques used in this study, whilst Tachibana and co-workers [1992; 1993] employed a treatment of H_2SO_4:HNO_3;$HClO_4$ (3:4:1), and Zhao and co-workers [1992] an oxidising treatment involving CrO_3. Since the impurity concentration in this latter report was given in terms of the B/C gas phase ratio, a value for the diamond bulk density of 1.76×10^{23} atoms/cm^3 [Borst, 1995] has been used together with the assumption that the gas phase concentration is reproduced within the bulk material.

However, assuming a potential barrier height at the Al-diamond interface of 1.13 eV [Hicks, 1989] and an effective hole mass of $0.75m_o$ [Collins, 1979], it follows from Equation 8.2 that a saturation current of $\sim 10^{-16}$ A is predicted from thermionic emission theory. The observed reverse characterictics clearly show a deviation from the ideal thermionic emission model. Consideration of the characteristic energy parameter E_{00}, and the dominant current conduction process according to Equation 8.3 for the three films results in the values presented in Table 8.4 (assuming an effective mass of $0.75m_o$):

Film / qE_{00}/kT	LOW	MED	HIGH
Carrier conc.	-	0.65	2.35
Boron conc.	0.89	2.27	3.16

Table 8.4 Characteristic energy parameter E_{00} according to Equation 8.3 for both the carrier and the boron concentration as the input parameter.

From the condition given in Equation 8.3 that $qE_{00}/k_BT \approx 1$ is suggestive of thermionic-field emission, then the HIGH and, depending on whether the carrier or boron concentration is used, the MED film will be within this regime. Figure 8.6 includes a prediction of the conduction current (2 V bias) as a function of the dopant density following Appendix D regarding thermionic-field emission. It is evident that as the dopant concentration within the semiconductor is increased, an increasingly greater contribution to the conduction current is via the thermionic-field mechanism.

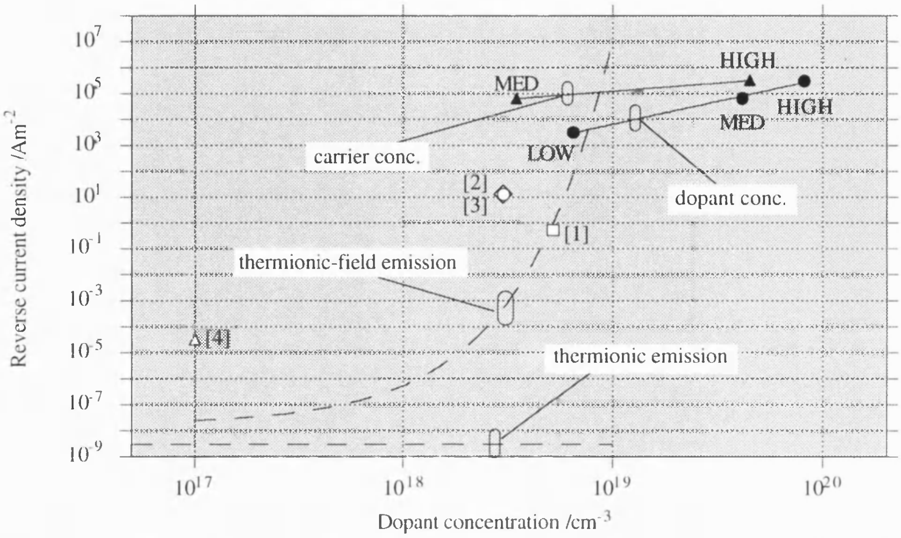

Figure 8.6 Current levels at reverse bias levels of 2 V plotted both as a function of the carrier, and the atomic boron dopant concentrations for LOW, MED and HIGH doped films. The predicted current level (2 V bias) in the thermionic-field regime is shown as a function of the doping concentration (broken line). Dopant concentrations in literature reports included are: [1] [Zhao, 1992] (Ag); [2] [Tachibana, 1992] (Al); [3] [Tachibana, 1993] (TiC); [4] [Whitfield, 1996] (Au).

8.3.4 Scanning electron microscopy (SEM)

SEM characterisation of the metallic layers were carried out after the prolonged heat treatment (5 h) at 400 °C in order to investigate the macroscopic physical integrity of the contacts. Figure 8.7 shows scanning electron micrographs of edges of Al and Ni contacts. The similar morphology and crystallite size are evident for the two differently doped films; the Al and Ni contacts have been deposited on the LOW and MED doped materials, respectively. The other combinations of contact metallisation and material were observed to be qualitatively similar. It is also evident that both metallisations follow the morphology of the underlying film and that the macroscopic physical structure does not appear to have degraded as a result of the testing treatment to which the structures have been subjected .

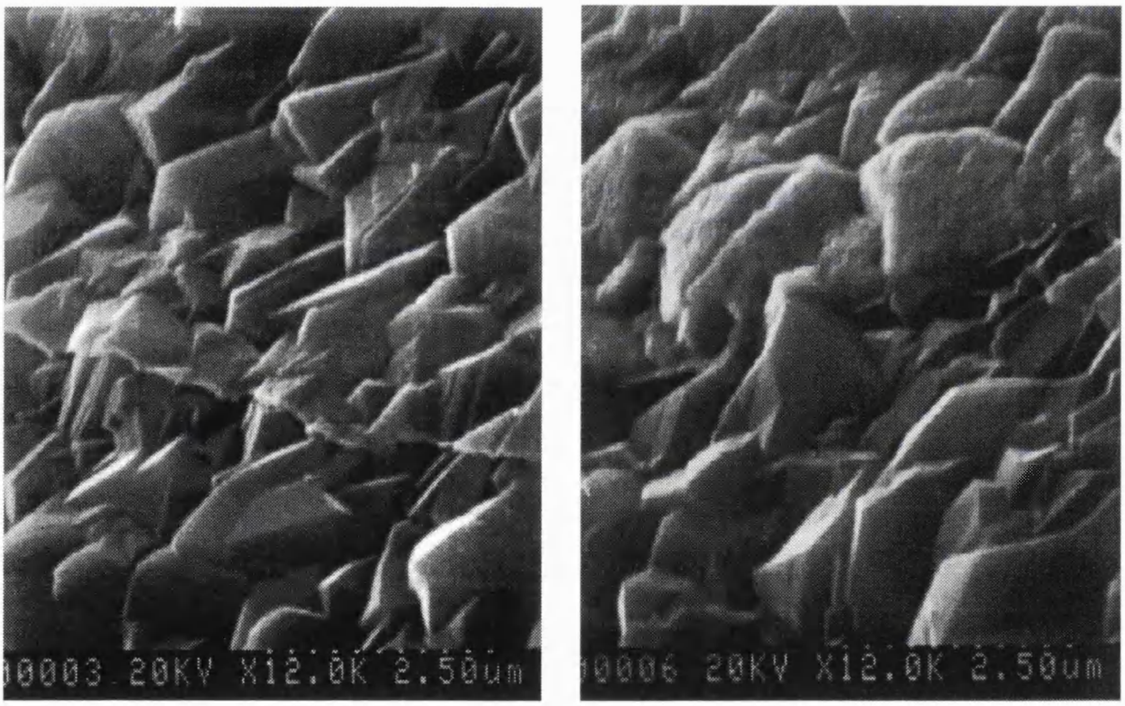

Figure 8.7 Scanning electron micrographs of (a) Al; and (b) Ni contact metallisations on polycrystalline thin film diamond of random crystalline orientation after a heat treatment of 5 h at 400 °C.

8.4 DISCUSSION

Hall-effect characterisation together with SIMS of the polycrystalline diamond films show that control of bulk parameters may be obtained by varying the dopant gas concentration in the gas phase during diamond deposition. As judged by SEM and Raman spectroscopy, material quality does not vary significantly; indeed, the similar crystallite size and morphology of the films prevent the device testing structures being preferentially dominated in a single material by extraneous effects such as grain boundaries.

The variation in the electrical characteristics of the metal-diamond contacts demonstrate that p-type dopant levels within the films play a determining role in device behaviour. Previous reports investigating material dopant concentrations on contact behaviour have been made by Kobayashi *et al.* [1993] and Iwasaki *at al.* [1993] where rectifying characteristics were observed on their lower doped as-deposited films. However, Harper *et al.* [1992] did not obtain rectifying behaviour with Al or Au contacts on doped films (10^2-10^{11} Ω/square) which were treated in a saturated solution containing potassium permanganate. Similarly, Venkatesan *et al.* [1992] reported near-ohmic characteristics of Al contacts on their lowest doped material (gas phase B/C ratio of 0.8 ppm, leading to B concentrations of ~10^{17} cm^{-3} if 100% B incorporation is assumed); rectifying behaviour became evident for *increasing* gas phase B/C ratios (up to 20 ppm B). The films in this case were subjected to an RCA clean (primarily involving hydrogen peroxide) followed by a 950 °C anneal in an unspecified ambient. These reports clearly demonstrate the possibility of large variations in the electrical behaviour of devices if post-deposition treatments are not controlled; the lack of rectifying behaviour/ expected trend in the films employed by Harper *et al.* and Venkatesan *et al.* may suggest the presence of a non-diamond conductive surface layer. In chapter 5 it was shown as-deposited films may have an Auger signature typical of amorphous carbon and that acid treatments produce surfaces more similar to that of high quality single-crystalline diamond; however, these treatments leave an oxidised surface. Mori *et al.* [1991] have shown that oxidised diamond surfaces lead to metal contacts (14 different metals investigated) displaying rectifying behaviour even if ohmic characterictics were previously demonstrated on the non-oxidised surface. The results here however, show that this oxidised state does not interfere with the domination of bulk properties on the electrical behaviour of contacts as the dopant level is increased. In considering the forward characteristics of the contacts on the LOW doped material (Figure 8.5), high ideality factors have been obtained; this is consistent with reports by others on similar material and has been speculated to arise as a result of defects at the interface leading to deep-level traps [Tachibana, 1993]. However alternative current transport mechanisms may also lead to high n values; Rhoderick and Williams [1988; Figure 3.10] show that $n>4$ is obtained for contacts on GaAs for doping concentrations

$>10^{18}$ cm^{-3}. The high reverse leakage currents observed in the rectifying contacts on the LOW doped material do not saturate at the values predicted by simple diode theory (Equation 8.2); various factors may contribute to this effect including surface conduction, increased fields at the asperities of the individual crystallites or defects acting as traps within the bandgap. However tunnelling is also a cause for the "soft" breakdown observed [Rhoderick, 1988]; this is suggested by the high n values obtained for the forward characteristics. From calculation of the characteristic energy parameter E_{oo} (Equations 8.3), the high "reverse" leakage currents observed in the HIGH and possibly the MED doped samples are suggested to arise from the increasing contribution of carrier tunnelling to the conduction process. For the MED film to be in better agreement with thermionic-emission theory, then the atomic boron rather than active carrier concentration has to be plotted on the abscissa. If this is the case then the possibility exists of either a greater degree of acceptor ionisation occuring in the vicinity of the junction, or else of an accumulation of acceptor centres within this region. Nakanishi *et al.* [1994] found a better theoretical fit to Ti ohmic contacts when 100% activation was assumed in their films (B= $3\text{x}10^{18}$-10^{20} cm^{-3}). However, from C-V measurements with Al rectifying contacts, Kobayashi *et al.* [1993] suggested a depletion of acceptor states at the interface. In contrast, Kiyota *et al.* [1995] measured an accumulation of acceptor states near the interface region by C-V techniques; these states were suggested to be non-boron related.

The deterioration in the rectifying performance of the contacts observed on the lowest doped films at elevated temperatures is attributed to the phenomenon of incomplete activation of the relatively deep-lying boron acceptor centres (possibly only those far from the interface) at room temperature. This increased carrier density may then result in the system being driven further into the thermionic-field emission regime; such a factor is of prime consideration in the design of future high temperature diamond devices. Al contact metallisations have been shown to be stable to temperatures of at least 400°C; the corresponding state of the oxidised surface is therefore stable to this temperature as suggested by chapter 5 where the oxidised surface was stable to a 600 °C *in-vacuo* anneal. In the case of Ni contacts however, drastic failure was observed following exposure at elevated temperatures; reaction with the oxide component or perhaps more probably the fact that Ni acts as a solvent for diamond at elevated temperatures [Lurie, 1977] may account for this.

8.5 SUMMARY

In addition to the possibility of conduction involving hydrogen as suggested by Landstrass and Ravi [1989], surface conductive layers present on as-deposited films may influence the electrical response of devices. The prolonged heating of the bulk material to temperatures greater than that used in the testing sequence together with oxidising acid treament have been employed in this study to reduce the influence arising from these phemonena. Following this preparation, Al and Ni contacts on polycrystalline diamond films have been found to be critically dependent on the material doping. Sheet resistance levels in the region of 1200 Ω/square and below prevent rectification being obtained; thermionic field emission is suggested as the mechanism by which linear and symmetrical characteristics are obtained in the higher doped films. The metallisations have been studied in a planar configuration in the context of a stable ohmic formulation and Al rectifying contacts have been found to be physically stable to heat treatments up to 400 °C.

REFERENCES

Beetz, C.P., Jr., Lincoln, B.A. and Winn, D.R., [1990]. in A.Feldman and S. Holly (eds.), Diamond Optics III, *Proc. SPIE* , **1325**, 241.

Borst, T.H. and Weis, O., [1995]. *Diamond Relat. Mater.,* **4**, 948.

Collins, A.T. and Lightowlers, E.C., [1979]. in *The Properties of Diamond,* ed. J.E. Field (Academic Press) London, UK.

Das, K., Venkatesan, V., Miyata, K., Dreifus, D.L. and Glass, J.T., [1992]. *Thin Solid Films,* **212**, 19.

Geis, M.W., Rathman, D.D., Ehrlich, D.J., Murphy, R.A. and Lindley, W.T., [1987]. *IEEE Electron Device Lett.*, **8**, 341.

Geis, M.W., Efremow, N.N. and von Windheim, J.A., [1993]. *Appl. Phys. Lett.*, **63**, 952.

Gildenblat, G.Sh., Grot, S.A., Wronski, C.R., Badzian, A.R., Badzian, T. and R. Messier, [1988]. *Appl. Phys. Lett.*, **53**, 586.

Gildenblat, G.Sh., Grot, S.A., Hatfield, C.W., Badzian, A.R. and Badzian, T., [1990]. *IEEE Electron Device Lett.*, **11**, 371.

Gomez-Yanez, C. and Alam, M., [1992]. *J. Appl. Phys.,* **71**, 2303.

Grot, S.A., Gildenblat, G.Sh., Hatfield, C.W., Wronski, C.R., Badzian, A.R., Badzian, T. and Messier, R., [1990]. *IEEE Electron Device Lett.,*, **11**, 100.

Harper, R.E., Johnston, C., Chalker, P.R., Totterdell, D., Buckley-Golder, I.M., Werner, M., Obermeier, E. and Van Rossum, M., [1992]. *Diamond Relat. Mater.*, **1**, 692.

Harper, R.E., Johnston, C., Blamires, N.G., Chalker, P.R., Buckley-Golder, I.M., [1991]. *Surface Coatings Technol.*, **47**, 344.

Hartsell, M.L., Wynands, H.A. and Fox, B.A., [1994]. *Appl. Phys. Lett.,* **65**, 430.

Hicks, M.C., Wronski, C.R., Grot, S.A., Gildenblat, G.Sh., Badzian, A.R., Badzian, T. and Messier, R., [1989]. *J. Appl. Phys.*, **1989**, 2139.

Iwasaki, T., Okano, K., Matsumae, Y., Matsushima, E., Maekawa, H., Kiyota, H., Kurosu, T. and Iida, M., [1993]. *Diamond Relat. Mater.,* **3**, 30

Humphreys, T.P., LaBrasca, J.V., Nemanich, R.J., Das, K. and Posthill, J.B., [1991]. *Jpn. J . Appl. Phys.*, **30**, L1409.

Jeng, D.G., Tuan, H.S., Salat, R.F. and Fricano, G.L., [1990]. J. Appl. Phys. **68**, 5902.

Kiyota, H., Matsushima, E., Sato, K., Okushi, H, Ando, T., Kamo, M., Sato, Y. and Iida, M., [1995]. *Appl. Phys. Lett.,* **67**, 3596.

Kobayashi, T., Hou, G.R., Maki, T. and Shikama, S., [1993]. *Jpn. J. Appl. Phys.*, **32**, L1588.

Lurie, P.G. and Wilson, J.M., [1977]. *Surf. Sci.,* **65**, 465.

Mori, Y., Kawarada, H. and Hiraki, A., [1991]. *Appl. Phys. Lett.,* **58**, 940.

Popovici, G., Prelas, M.A., Sung, T., Khasawinah, S., Melnikov, A.A., Varichenko, V.S., Zaitsev, A.M., Denisenko, A.V. and Fahrner, W.R., [1995]. *Diamond Relat. Mater.,* **4**, 877.

Rhoderick, E.H. and Williams, R.H., [1988]. *Metal-semiconductor contacts*, 2nd edition, Oxford University Press, Oxford, UK.

Shiomi, H., Nakahata, H., Imai, T., Nishibayashi, Y. and Fujimori, N., [1989]. *Jpn. J. Appl. Phys.*, **28**, 758.

Sze, S.M., [1981]. *Physics of semiconductor devices*, 2nd edition, Wiley, New York, USA.

Tachibana, T. and Glass, J.T., [1992]. *J. Appl. Phys.*, **72**, 5912.

Tachibana, T., Glass, J.T. and Thompson, D.G., [1993]. *Diamond Relat. Mater.*, **2**, 37.

Venkatesan, V., Thompson, D.G. and Das, K., [1992]. Mater. Res. Soc. Symp. Proc., **270**, Material Research Society, Pittsburgh, USA, 419.

Whitfield, M.W., Chan, S.S.M. and Jackman, R.B., [1996]. *Appl. Phys. Lett.,* **68**, 290.

Zhao, G., Stacy, T., Charlson, E.J., Charlson, E.M., Chao, C.H., Hajsaid, M., Meese, M., Popovici, G. and Prelas, M., [1992]. *Appl. Phys. Lett.*, **61**, 1119.

9: PATTERNING OF DIAMOND FILMS BY EXCIMER LASER PROJECTION

9.1 INTRODUCTION

Traditional wet etching methods employed to remove undesired material, whether for providing pathways to underlying layers in multilayer structures or for the purpose of delineating patterns on the substrate for particular device structures or connections, are commonly used in present day semiconductor processing [Sze, 1988]. Such techniques though, are not readily amenable to the purpose of material removal in the case of diamond. Diamond has been found to be resistant to all known acids and bases, and is only etched by oxidising agents at high temperatures [Field, 1992; p673]. In view of these difficulties, selective patterning and dry etching techniques have been developed. Selective patterning was originally reported by Hirabayashi *et al.* [1988] where selective growth was observed on regions of a diamond powder pre-scratched Si substrate modified by an Ar^+ ion beam. This relied on the fact that nucleation may be enhanced by controlled "seeding" of the growth substrate which, by necessity, has to be non-diamond in nature. Alternatively, the small degree of nucleation on materials such as SiO_2 [Davidson, 1990] and amorphous-Si [Inoue, 1990] has allowed these materials to be employed as masks in the deposition process. Heterogeneous masking technology permits greater flexibility including the ability to selectively pattern diamond substrates. By this technique, Davidson and co-workers [1990] have demonstrated micro-mechanical structures such as cantilevers and bridges (typical dimensions 3000 μm by 300 μm). However, it has been shown by Inoue *et al.* [1990] that growth parameters and mask thicknesses have to be strictly controlled in order to prevent lateral outgrowth *i.e.* growth in the plane of the substrate to maintain the desired dimensions. Maki and co-workers [1993] observed morphological changes at the edges of selectively grown diamond structures when a yttria-stabilised zirconia thin film mask, which demonstrated the lowest nucleation density amongst a range of materials including SiO_2, was employed. This was attributed to the possible migration of growth species into the mask during deposition of the diamond layer.

In terms of post-deposition processing, dry etching has been approached by ion beam and plasma-based systems. Whetten and co-workers [1984] demonstrated the greater etch yield of a 500 eV beam of oxygen ions compared with an argon ion beam; this was attributed to the chemical reactivity of oxygen on the diamond surface. Inert 2 keV Xe^{2+} ions have been used in conjunction with a reactive gas flux of NO_2 to obtain etch rates of 150 $nm.min^{-1}$ for the delineation of 17 μm deep grating patterns with 18 μm pitch in monocrystalline diamond [Efremow, 1985]. Trenches were formed at the edges of the etched structures and contamination of the substrate during etching led to the appearance of spikes in the etched areas. The utilisation of ion beams for the processing of polycrystalline material has been reported by Hirata and co-workers [1992] where Ar and O_2 ion beams (1.5 keV) at 80° incidence reduced surface roughness from 3 μm (peak-valley) to 0.5 μm. However, it was found that after irradiation at normal incidence, the surface of CVD films grown by plasma jet method contained gaps where grain boundaries previously existed. A columnar and roughened nature in the etched regions was also observed in the reactive ion etching (RIE) of polycrystalline films in an O_2 plasma [30 $nm.min^{-1}$: Dorsch, 1992] and in a CF_4 plasma [2 $nm.min^{-1}$: Kobayashi, 1991]. This latter author was able to demonstrate smoothening of diamond films of a polycrystalline nature in an inert Ar plasma [Kobayashi, 1990]. In order to reduce the ion energies to below the threshold for ion bombardment damage of diamond [~150 eV: Marsh, 1964], microwave electron cyclotron resonance (ECR) excited plasmas have been explored by Pearton and co-workers [1992] to obtain etch rates of up to 400 $nm.min^{-1}$ on polycrystalline material. In this case, a 400 W O_2 discharge was used in conjunction with Au/photoresist masks and a -80 VDC substrate bias to obtain anisotropic features. On homoepitaxial material, Grot *et al.* [1992] employed this technique to obtain 1μm resolution patterning with an etch rate of 8.6 nm.min^{-1} (1kW RF power); Ar was added in the discharge to improve the reproducibility of the etch rate.

An alternative approach is to remove material with pulses of laser radiation, which may be a purely physical process (ablation) or a light assisted chemical process; the potential superiority demonstrated by Bhushan *et al.* [1994] of laser-based polishing techniques in terms of speed and quality of finish when compared to traditional mechanical polishers such as the thermochemical based method [Yoshikawa, 1990] suggests that advantages may be gained in the development of laser processing of diamond. Laser processing of diamond has been investigated at a variety of wavelengths including 10.8 μm (CO_2) [Ageev, 1988], 1.064 μm (YAG) [Yoshikawa, 1990], 510 nm (Cu) [Obratzsov, 1994] and 457-514 nm (Ar^+) [Ral'chenko, 1995]. Apart from the CO_2 laser where no appreciable etching effect was observed with energy densities of up to 30 Jcm^{-2} (sample in an evacuated environment), the scanning of single focused spots of laser radiation from YAG, Cu and Ar^+ sources demonstrates the feasibility of patterning diamond substrates using this approach. However, excimer lasers have also been employed, offering the advantage of a broad beam and shorter wavelength ultra-violet (UV) radiation with the possibility of higher optical absorption within diamond: 308 nm (XeCl) [Ageev, 1988; Tokarev, 1995], 248 nm (KrF) [*e.g.* Pimenov, 1993; Konov, 1993; George, 1993] and 193 nm (ArF) [*e.g.* Rothschild, 1986; Bogli, 1992; Johnston, 1993; Bhushan, 1994]. Photons of energy greater than the 5.45 eV bandgap (equivalent to 228 nm radiation) will induce electronic transitions between the valence and conduction bands, *i.e.* fundamental bandgap absorption leading to an efficient mode of energy transfer; for the case of sub-bandgap radiation, optical absorption takes place via far less efficient means such as lattice vibration, impurity, multiphoton and intraband absorption mechanisms [Smith, 1978; Boyd, 1992]. Excimer laser patterning of diamond employing radiation of energy sufficient to excite interband electronic transitions was first reported by Rothschild and co-workers [1986] employing 193 nm (ArF source) excimer lasers. Etch rates involving type IIa monocrystalline diamond of around 50 nm per 15 ns pulse of radiation were achieved at a laser fluence of 10 Jcm^{-2}, increasing to 160 nm per pulse at 30 Jcm^{-2}. Processing of thin film polycrystalline diamond in air has been studied by Johnston *et al.* [1993] revealing 2-4.5 nm per pulse for a 193 nm laser fluence of 2.5 Jcm^{-2}; the higher etch rates were achieved for films with the most non-diamond content.

The feasibility of excimer laser patterning of diamond suggests that it may be developed into a process for the fabrication of diamond devices and systems. However, in order for the potential of UV lithography, and particularly the maskless mode of projection patterning (as described in Chapter 4) to be realised in diamond, both the quality and the nature of the etching process have to be further investigated and characterised. The aim of this chapter concerns the quality of the etch product and how various process parameters may affect this. With the interest in the application of diamond to micro-electromechanical systems (MEMS) [Roppel, 1992; Bryzrk, 1994; Hunn, 1994], the performance of projection patterning in the creation of free-standing microstructure components has been considered. The chemical nature of ArF excimer irradiated surfaces will be examined in the following chapter.

9.2 EXPERIMENTAL DETAILS

The investigation of excimer laser projection patterning of diamond films was carried out using the system described in Chapter 4; the excimer laser was operated with 193 nm (ArF) radiation with an average pulse duration of 20 ns and, unless specified otherwise, at a repetition rate of 20 Hz. All the experiments in this chapter have been carried out in an air ambient. The diamond films used have been categorised as follows: (a) silicon-supported THIN films; and (b) free standing THICK films,. The main consequence of the difference in thickness is the average size of the individual grains at the top surface of the films. The film properties are summarised in Table 9.1, with Figure 9.1 presenting an optical and a scanning electron micrograph of the THICK films.

Sample	Thickness (μm)	Grain size (μm)	Doping (cm^{-3})	Substrate	SEM
THIN	5-6	1-2	10^{20}	Si	5.1
THICK	80 and 135	20-30	undoped	free-standing	9.1

Table 9.1 Details of samples used within this study. Scanning electron micrographs (SEM) have been presented in Figures elsewhere as indicated.

Prior to laser processing the wafers were subjected to an acid treatment (Appendix B); this reduces the effect of surface layers which may interfere with subsequent analysis as presented in the following chapter. Physical characterisation of the patterned samples were carried out using a Hitachi S800 scanning electron microscope (SEM) and a Tencor Instrument profilometer.

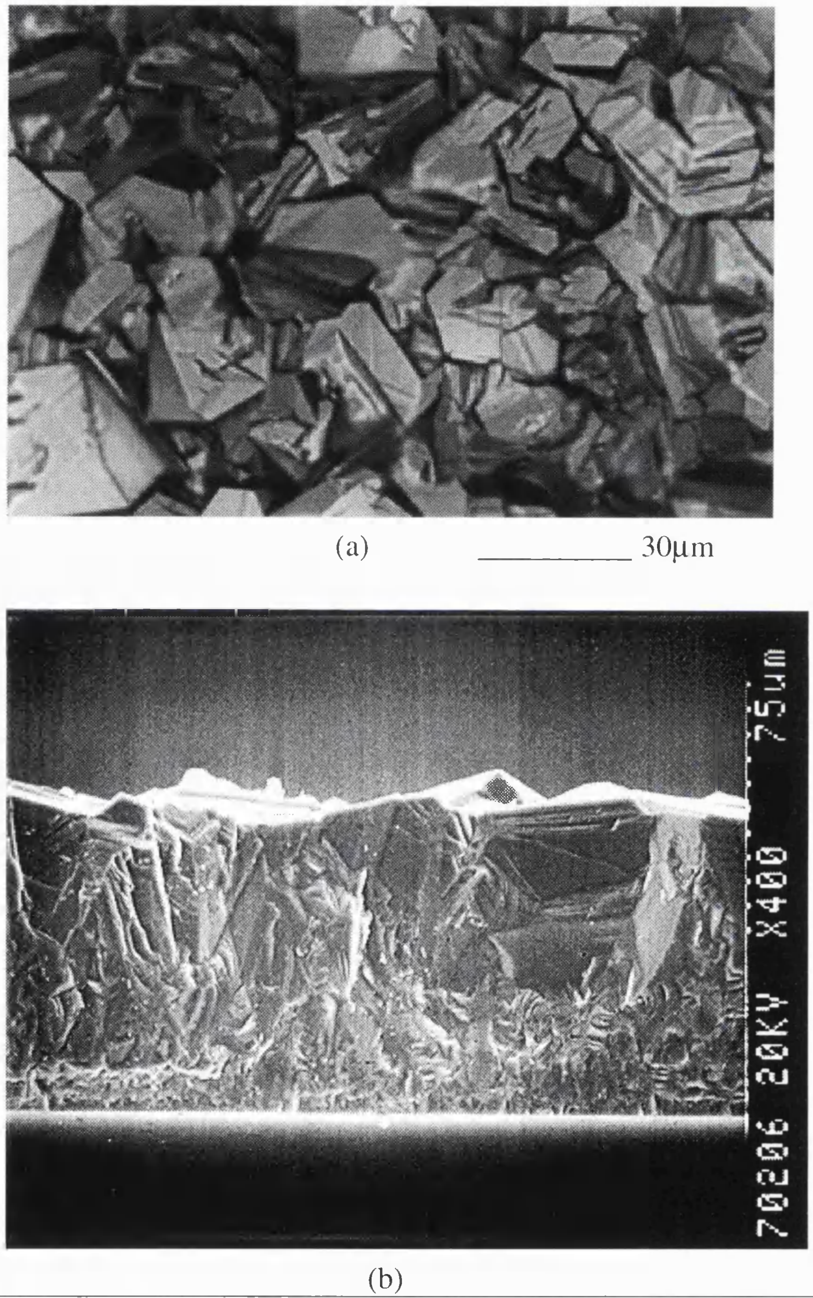

Figure 9.1 Free standing polycrystalline material of thickness 80 μm demonstrating a random crystal orientation of average grain size 30 μm at the top surface. (a) optical micrograph of plan view; and (b) scanning electron micrograph of cross-section.

9.3 RESULTS

9.3.1 THIN diamond films

Uniform laser fluence levels of up to 2 Jcm^{-2} over a 2 mm by 1 mm area (derived from the 20 mm x 10 mm laser beam) were directed onto the surface of the THIN samples; patterned masks placed in the path of the laser beam were chosen such that surface patterning over a range of feature sizes could be investigated. Line patterns generated on the surface of the diamond films using a single exposure sequence with a laser fluence of 1.5 Jcm^{-2} and 1000 shots are shown in the SEM images in Figure 9.2: (a) shows a large area view of the line pattern which indicates an even reproduction of the mask at least over the area of the image. However, it was evident at the extreme edges of the overall exposure (not shown here) that a fall off in the intensity of the laser beam results in a lesser extent of material removed; this is estimated to be approximately 10-15% of the total area of the exposure though a beam homogenising system will alleviate this [Liu, 1989]. Figure 9.2(b) is an SEM image, again taken with sample tilt, of a selected region of this pattern showing a depth of material removed in the region of 2 μm. Figure 9.2(c) shows the resolution of the process which may routinely be achieved by the projection patterning technique using the system optics employed here; patterns generated by a mask in the path of the laser beam such as 3 μm lines separated by varying distances may be reproduced over a sample area of 2 mm by 1 mm.

In order to assess the rate of material removal with laser fluence (0.5 Jcm^{-2} to 2 Jcm^{-2}) and the response of increasing laser shots (10 to 1000 pulses) at each fluence, a series of squares (100 μm x 100 μm) were imaged on the sample plane. For laser fluence levels < 0.5 Jcm^{-2}, surface modification of the diamond surface by the incident laser beam was not observed; laser fluence levels greater than this threshold resulted in the processed areas displaying an increase in specular reflection. Depth profiling of the irradiated squares indicated a process dependent on both the number of shots and the laser fluence in the manner as depicted in Figure 9.3. It is apparent that a linear rate of material removal with increasing laser shots exists for all the laser fluence levels investigated; least squares fit to the data resulted in correlation coefficients of 0.7903 (0.5 Jcm^{-2}), 0.9673 (1.0 Jcm^{-2}), 0.9949 (1.5 Jcm^{-2}), and 0.9947 (2 Jcm^{-2}). At the highest laser energy used here (2 Jcm^{-2}) an average of 2.5 nm per pulse is achieved and, at a laser operating frequency of 20 Hz, results in a process rate of 3 μm per min.

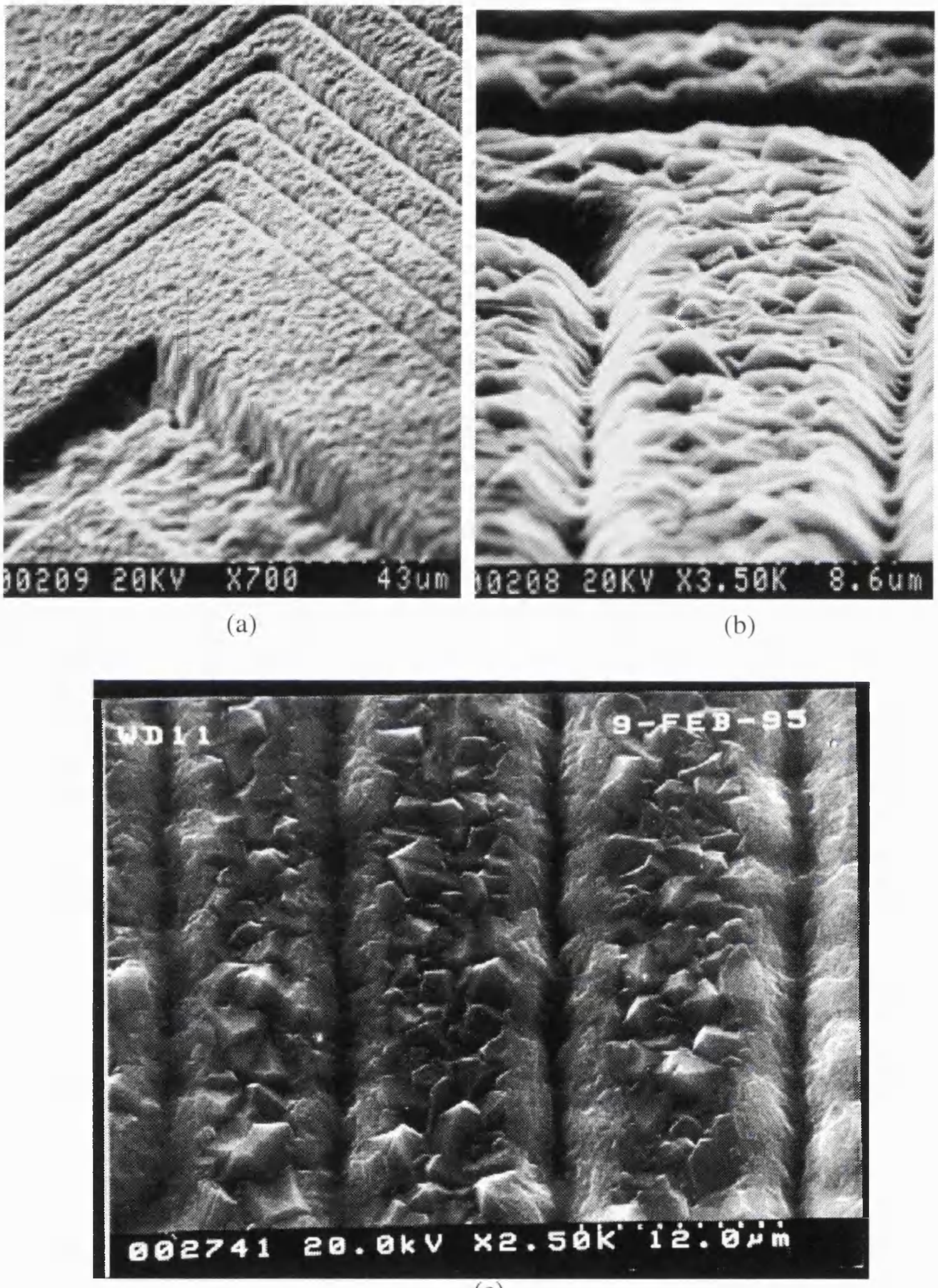

(a) (b)

(c)

Figure 9.2 Scanning electron micrographs of ArF excimer laser projection patterned thin film diamond: (a) surface patterned lines; (b) close up of (a); and (c) 3 µm wide line patterns.

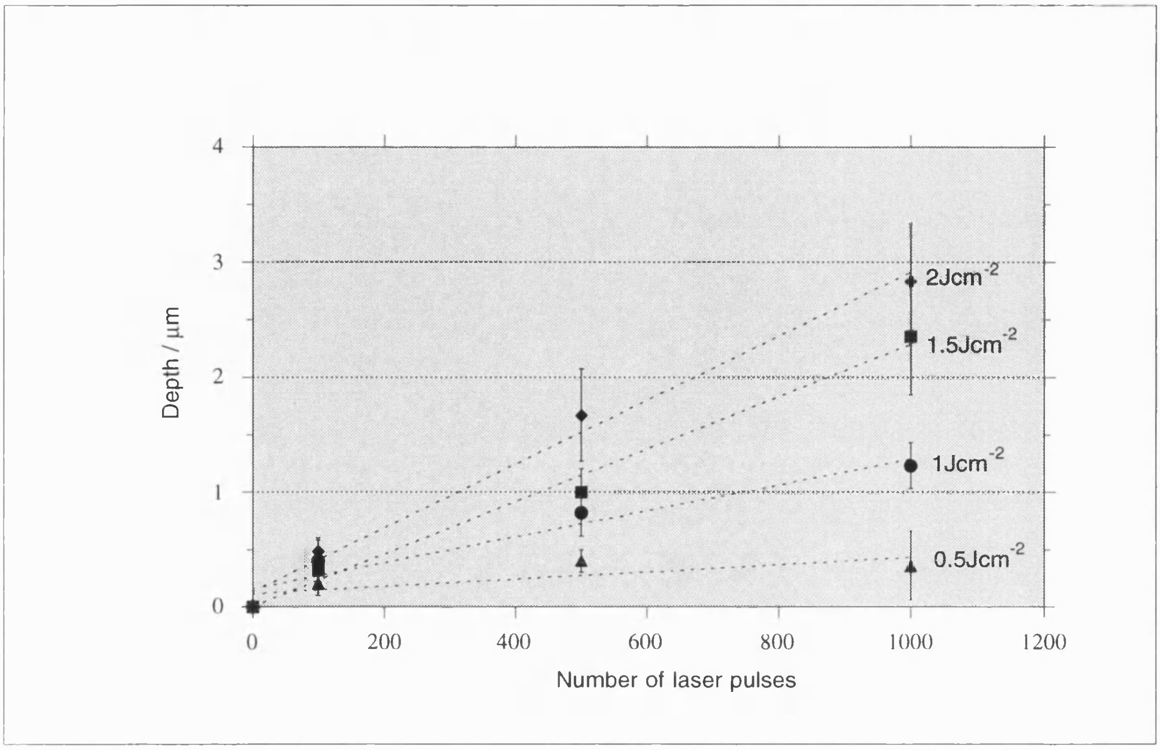

Figure 9.3 Plot of depth of material removed as a function of the number of laser shots for laser fluence levels of 0.5-2 Jcm^{-2} in the processing of thin film CVD diamond with ArF (193 nm) excimer laser irradiation. The dashed lines are least squares fit to the data as described in the text.

Figure 9.4(a) shows an SEM image of surface patterns created on thin-film material using a fluence of 1.25 Jcm^{-2}. The features were formed by using up to 3000 shots; a single illumination created all of the visible images, but regions of the imaged mask were shadowed such that the number of shots each feature received were 500, 750, 1000 or 3000. Figure 9.4(b) shows the pattern created after 500 laser shots; it is evident that little surface debris is present after the process. However, the use of greater than 3000 laser shots at this laser fluence led to exposure of the underlying silicon substrate and the formation of features coated with silicon debris (Figure 9.4(c)). It was not possible to identify conditions at a fixed laser fluence that led only to the removal of the diamond film; this may be the result of a higher proportion of non-sp^3 carbon at the diamond-silicon interface which would result in an increased absorption of the laser radiation and a significant increase in etching rate per shot in this region.

Figure 9.5(a)-(d) shows one arm of microgear patterns after 500 to 3000 shots. It is apparent that laser processing results in a surface which does not display the morphology present in the as-deposited diamond film; this lack of feature may suggest a non-uniform material removal pattern with preferential removal of sharp features such as the tips of individual crystallites or may reflect the morphology of the actual film cross-section.

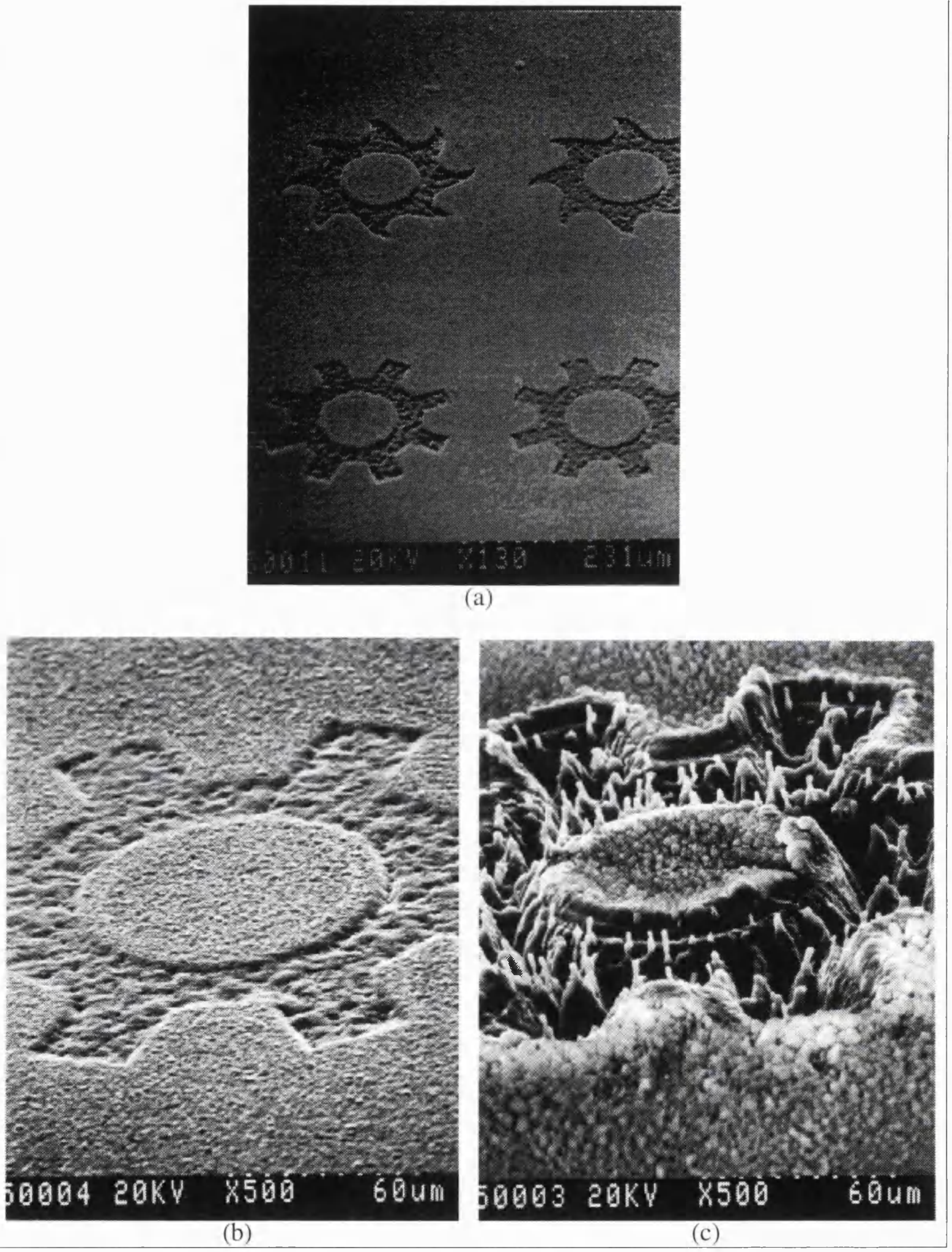

Figure 9.4 Scanning electron micrograph of patterns on thin-film diamond formed by projection patterning from a single mask. (a) The pattern shown in the top left position of this micrograph is formed by 3000 shots at a laser fluence of 1.25 Jcm^{-2}; the others, in a clockwise direction, by 750, 500 and 1000 shots. (b)500 pulses at 1.25 Jcm^{-2}; (c) 10k pulses at 1.25 Jcm^{-2} showing etching into Si substrate.

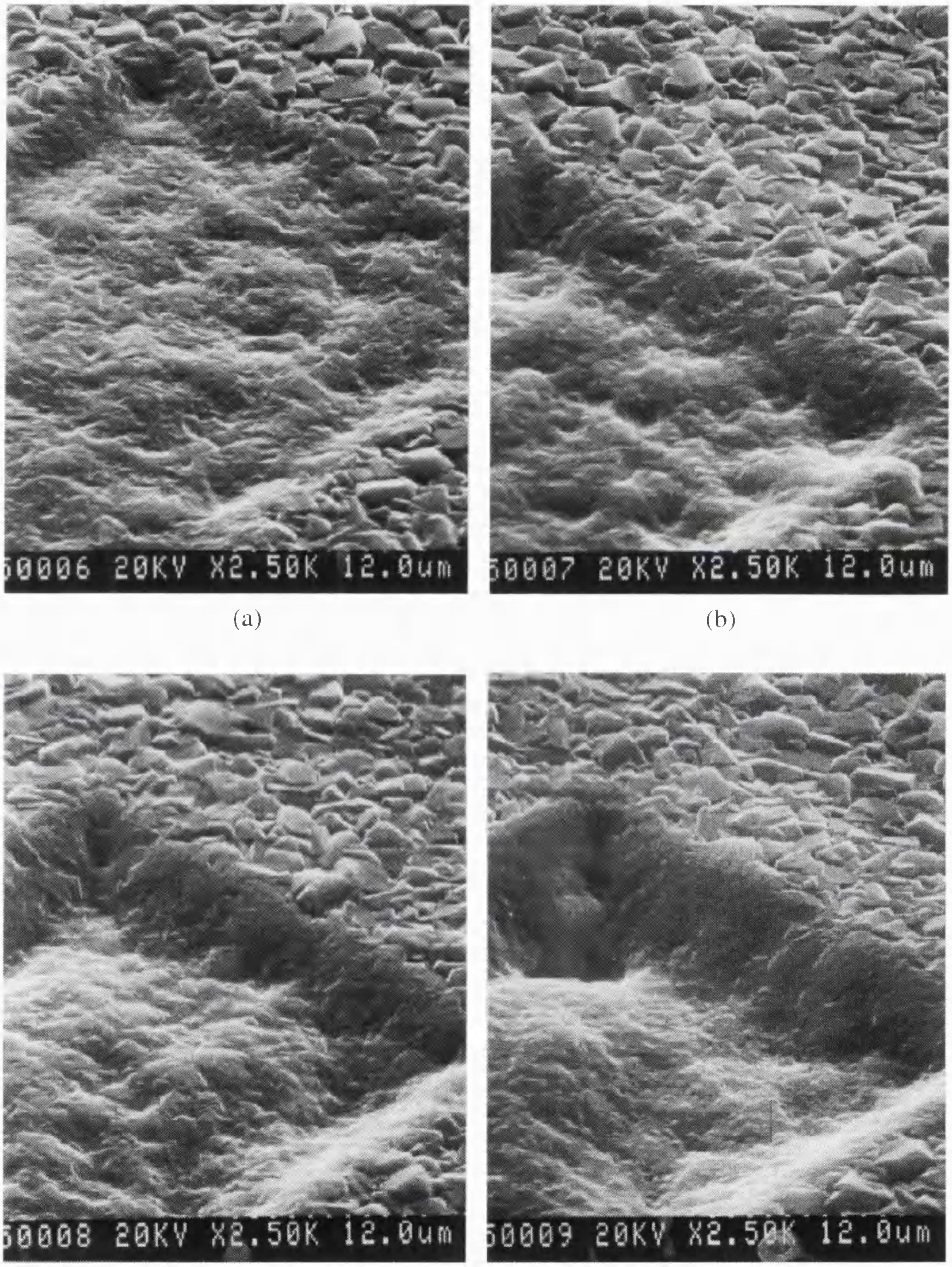

(a) (b)

(c) (d)

Figure 9.5 SEM images of 193 nm excimer laser processed regions in thin film diamond at 1.25 Jcm^{-2} for: (a) 500; (b) 750; (c) 1000; and (d) 3000 laser shots.

9.3.2 THICK diamond films

Free-standing THICK diamond films have been projection patterned using a mask consisting of lines of varying width separated by differing spacing in order to investigate the possible effects of linewidths. Figure 9.6(a) shows such surface patterning employing a laser fluence of 12 Jcm^{-2} and 1000 shots; decreasing linewidths of laser irradiation on the diamond surface may be seen from left to right of the SEM micrograph. Increasing the number of shots to 10k leads to a greater degree of material removal within the individual lines as shown in Figure 9.6(b). It is apparent in this latter image that the bottom-most section of the line pattern has a well-defined termination; this may be attributed to the top-most section of the pattern mask being placed outwith the high intensity area of the laser beam, *i.e.* away from the constant intensity central region. Similar investigations were also carried out on the underside (substrate) side of the THICK films. The effect of this may be seen from the SEM images presented in Figure 9.6 for (c) 1000 shots and (d) 10k shots, where increasing linewidths are from left to right. In these cases, better definition of the lines appears to be achievable as compared to processing on the growth (top) surface. However, higher magnification SEM images of the areas exposed to 10k shots on both the growth and substrate surfaces reveal that the surface roughness inherent in as-deposited films (~10-15 μm) would account for this observation (Figure 9.7); remnants of a grain maxima *e.g.* near the top right corner of Figure 9.7(a) may be envisaged to prevent a level etch pit, if a constant material removal rate is assumed. The pitting in Figure 9.7(b), which may be seen on the unexposed regions, exists prior to laser processing and is assumed to be a combination of the original non-uniform nucleation, together with the removal of non-diamond elements when the original substrate was detached.

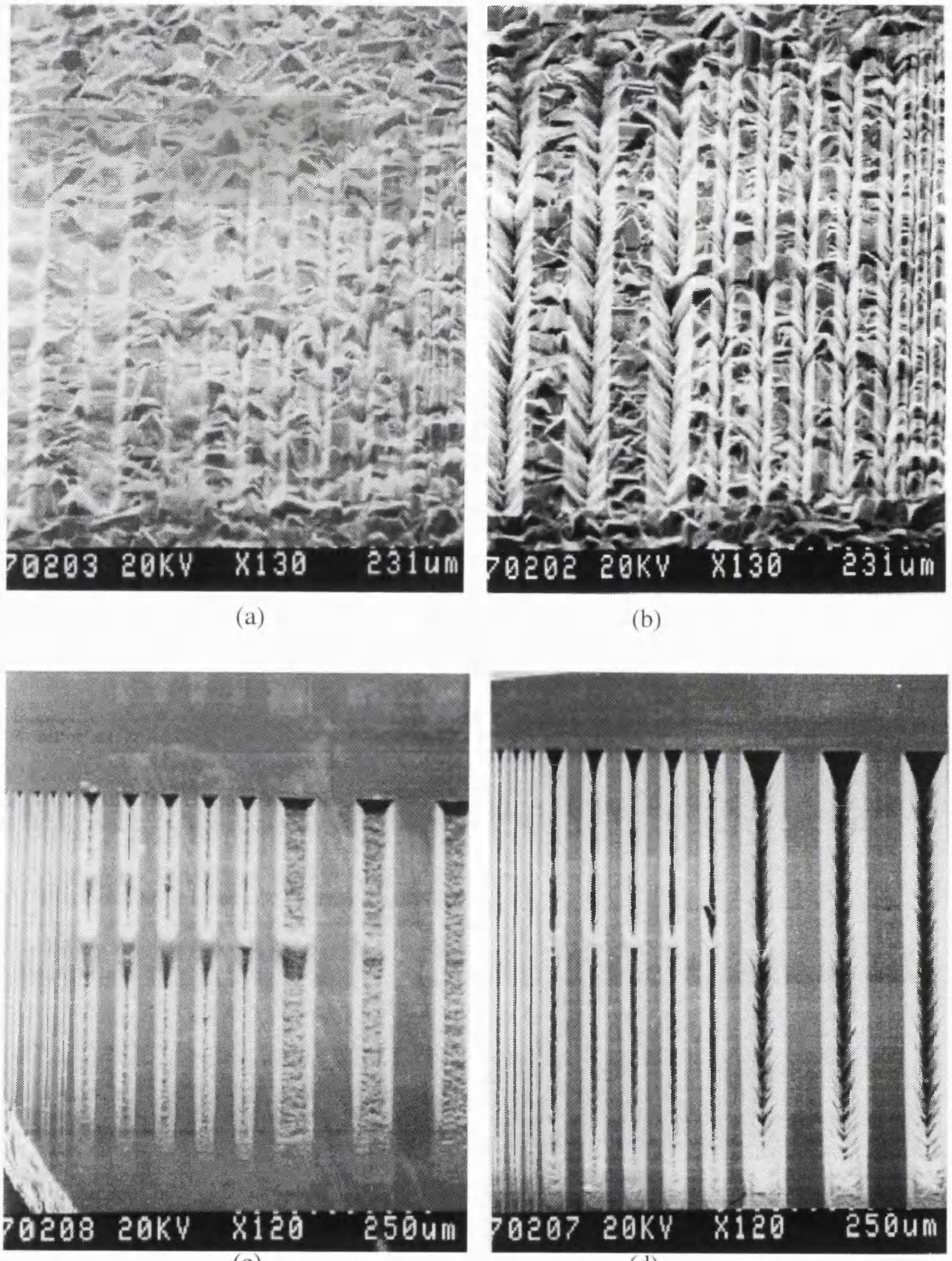

(a) (b)

(c) (d)

Figure 9.6 SEM micrographs of laser (193 nm, 12 Jcm^{-2}) processed line patterns on thick diamond films for (a) growth side, 1k shots; (b) growth side, 10k shots; (c) substrate side, 1k shots; and (d) substrate side, 10k shots. The line perpendicular to the overall line pattern is a result of a defect on the mask.

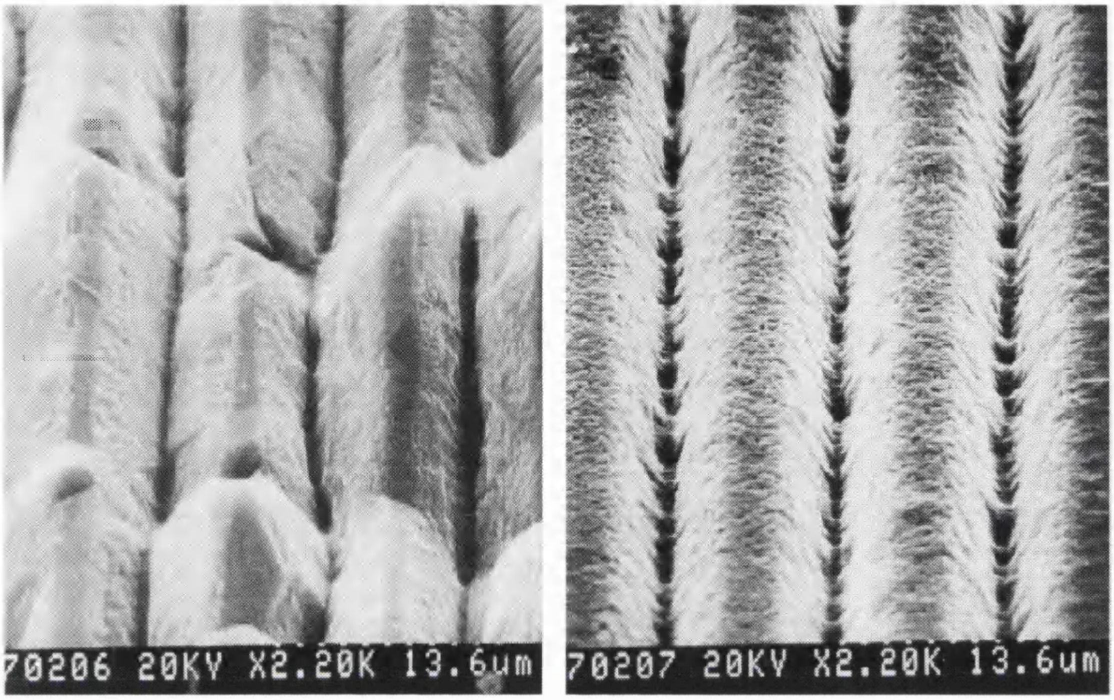

(a) (b)

Figure 9.7 SEM micrographs of laser (193 nm, 12 Jcm^{-2}, 10k shots) processed line patterns for (a) growth side; and (b) substrate side indicating the possible effect of surface roughness.

Sloping sidewalls present within the etched regions are discernible in the previous two figures; Figure 9.8 reveals single 50 μm wide lines (as determined by the patterned mask in line of the laser beam) for 1k and 10k shots at 12 Jcm^{-2}. Figure 9.8(a) and (b) presents the effects of 1k laser shots on the top and substrate surfaces, respectively; in both cases excellent reproduction of the lateral dimensions of the illuminating image is apparent, with the etched features displaying sloping sidewalls. As in the thin film case, debris free surfaces are achieved under processing at these conditions for both surfaces. In the case of processing from the top surface, the laser processed regions reveal a structure which may be attributed to the original rough and granular nature. By depth profiling, the depth of material removed was 31 μm for processing initiating from the substrate side, as compared with 22 μm from the top surface, corresponding to 31 and 22 nm per shot, respectively. The material removal rate suggests that exposure to 10k shots should etch through the 80 μm thick diamond film; it is clear that this has not occurred and that the sloping sidewalls have persisted to give rise to a "V" shape cut in the diamond as demonstrated in Figure 9.8(c) for the top surface and (d) for the substrate surface. It is also of interest to note that the width of the etched line at the top surface has increased to 53 μm and 56 μm for illumination of the top and substrate surfaces, respectively.

To investigate the possible dependence of the sloping wall angle on the intensity of the laser beam, squares of dimension 100 µm x 100 µm on the top-surface of the diamond films were exposed to 10k shots at fluence levels of 2, 4, 6, 8, 10 and 12 Jcm^{-2}. At 2 Jcm^{-2}, negligible effects were observed; SEM images of some of the samples showing an increase in the material removed at higher fluence levels are re-produced in Figure 9.9. Depth profilometry of the square etch pits revealed a wall angle dependence on laser fluence as shown in Figure 9.10, where the slope of the wall angle was calculated from regions of the profiles which were not influenced by the tip diameter (12.5 µm) *i.e.* away from the turning point (midpoint) of the profiles.

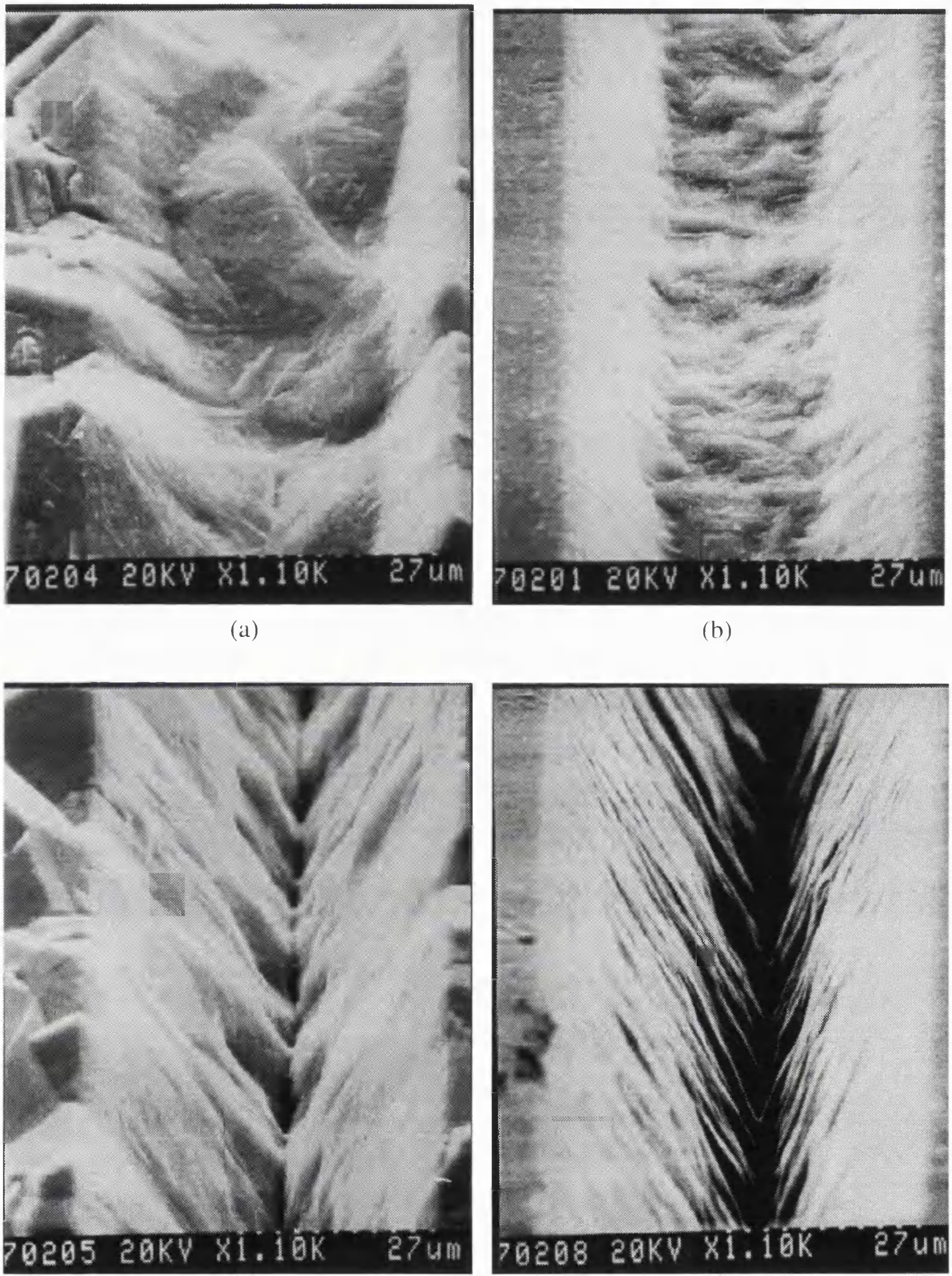

(a) (b)

(c) (d)

Figure 9.8 SEM images of laser (193 nm, 12 Jcm^{-2}) processed lines on THICK film diamond obtained via 50 μm wide line openings in a chrome on quartz mask in the path of the laser beam after (a) 1k shots, top surface; (b) 1k shots, substrate surface; (c) 10k shots, top surface; and (d) 10k shots, substrate surface.

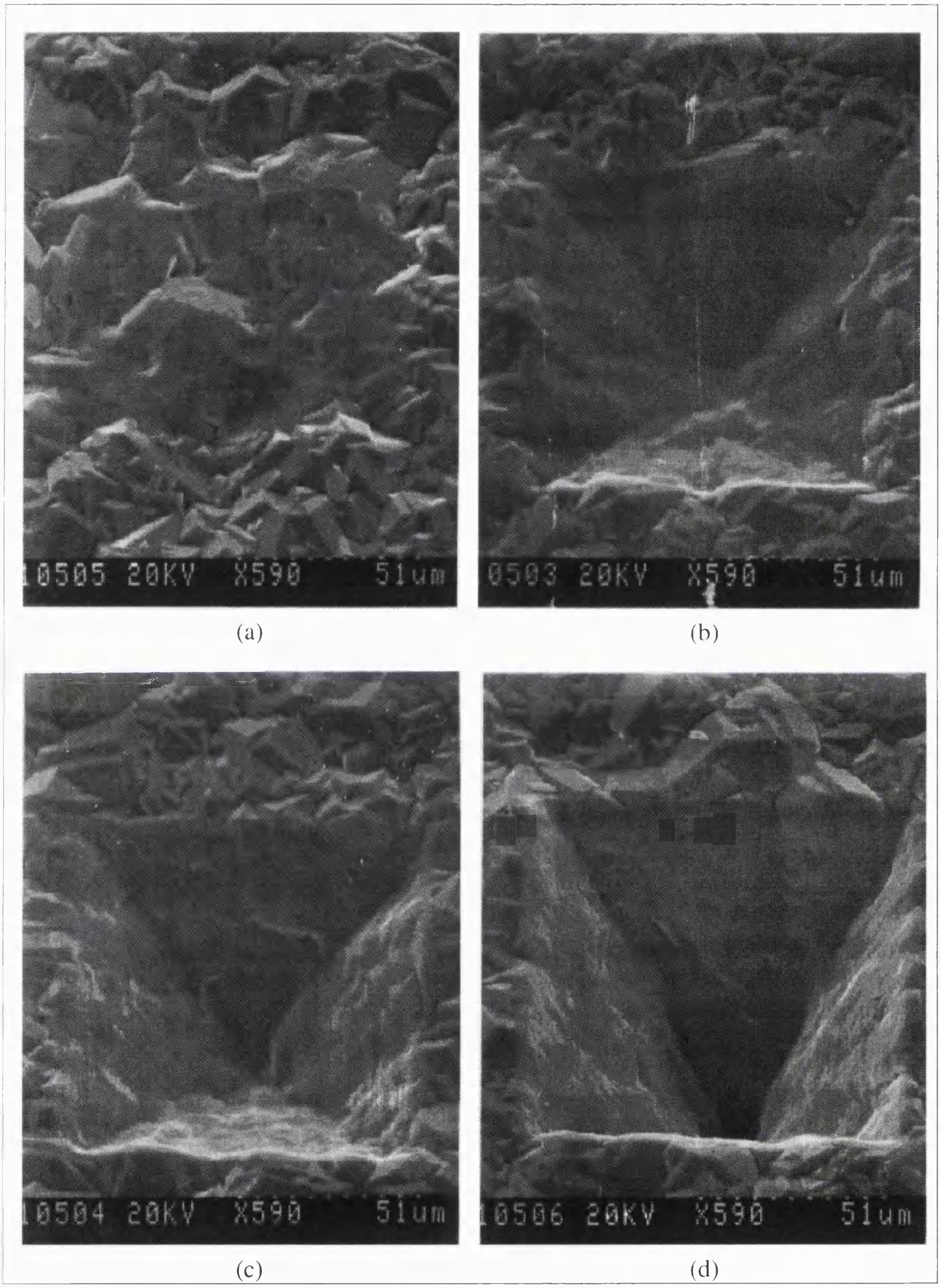

(a) (b)

(c) (d)

Figure 9.9 SEM (tilted samples) of square patterns created by exposure to 10k shots of ArF excimer laser irradiation at fluence levels of (a) 4 Jcm^{-2}; (b) 6 Jcm^{-2}; (c) 8 Jcm^{-2}; and (d) 10 Jcm^{-2}.

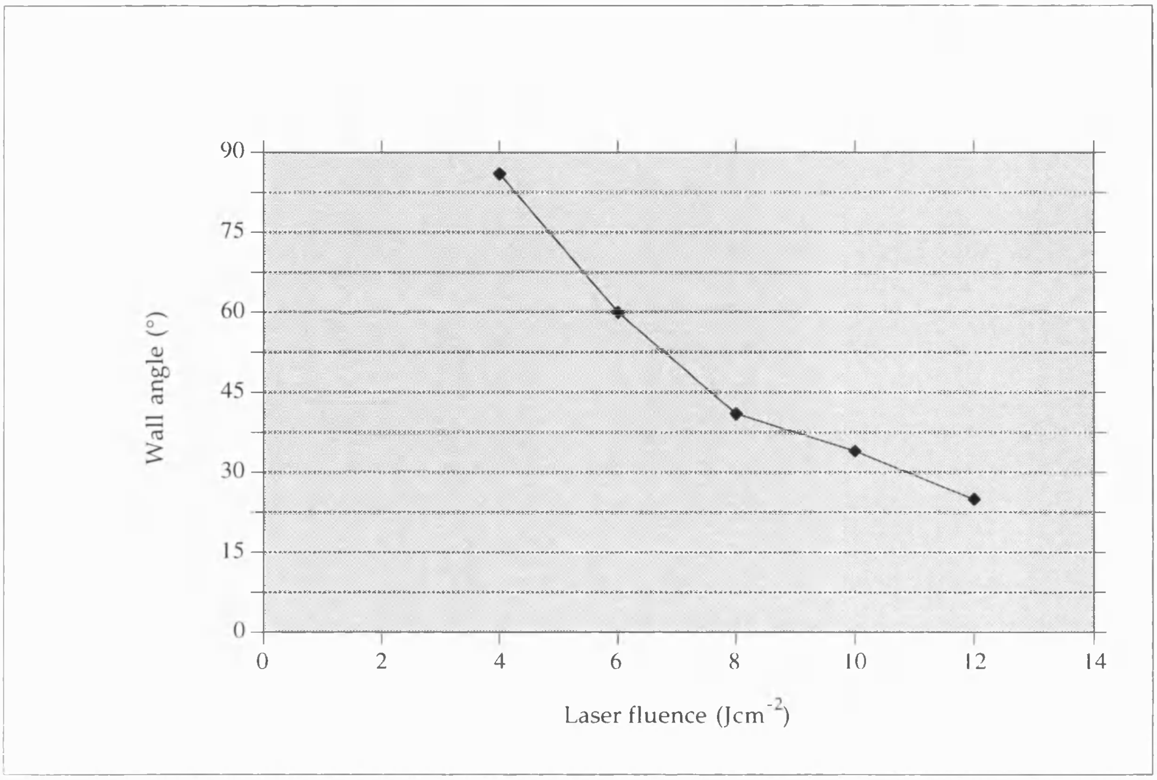

Figure 9.10 Wall angle (defined with respect to the vertical plane *i.e.* normal to the film surface) versus laser fluence (193 nm). The solid line is drawn only as a guide.

A mask which allowed a projection of 930 μm diameter micro-gear images onto the diamond surface was used to fabricate free-standing microstructures; sloping sidewalls were not expected to prevent the realisation of structures on this lateral scale. SEM micrographs of typical micro-gear structures formed following 50k shots (initiating from the substrate side) at 12 Jcm^{-2} are shown in Figure 9.11(a) and (b); four arms of an eight-armed structure are clearly visible along with the supporting diamond substrate in (a). It is apparent in Figure 9.11(b) that some surface debris may remain on the sample after processing which was not previously observed on the results presented above; however such surface debris may be removed by rinsing samples in acetone as demonstrated by the optical microscope image of the free-standing structure shown in Figure 9.11(c) which was formed under similar conditions but with exposure initiating from the growth side. The polycrystalline film, with an average grain size of around 30 μm, has not prevented the formation of a well defined structure; the dark regions apparent in the outline of the micro-gear structure in the optical micrograph may be attributed to the limited depth of field in the optical system together with the sloping walls of the structure.

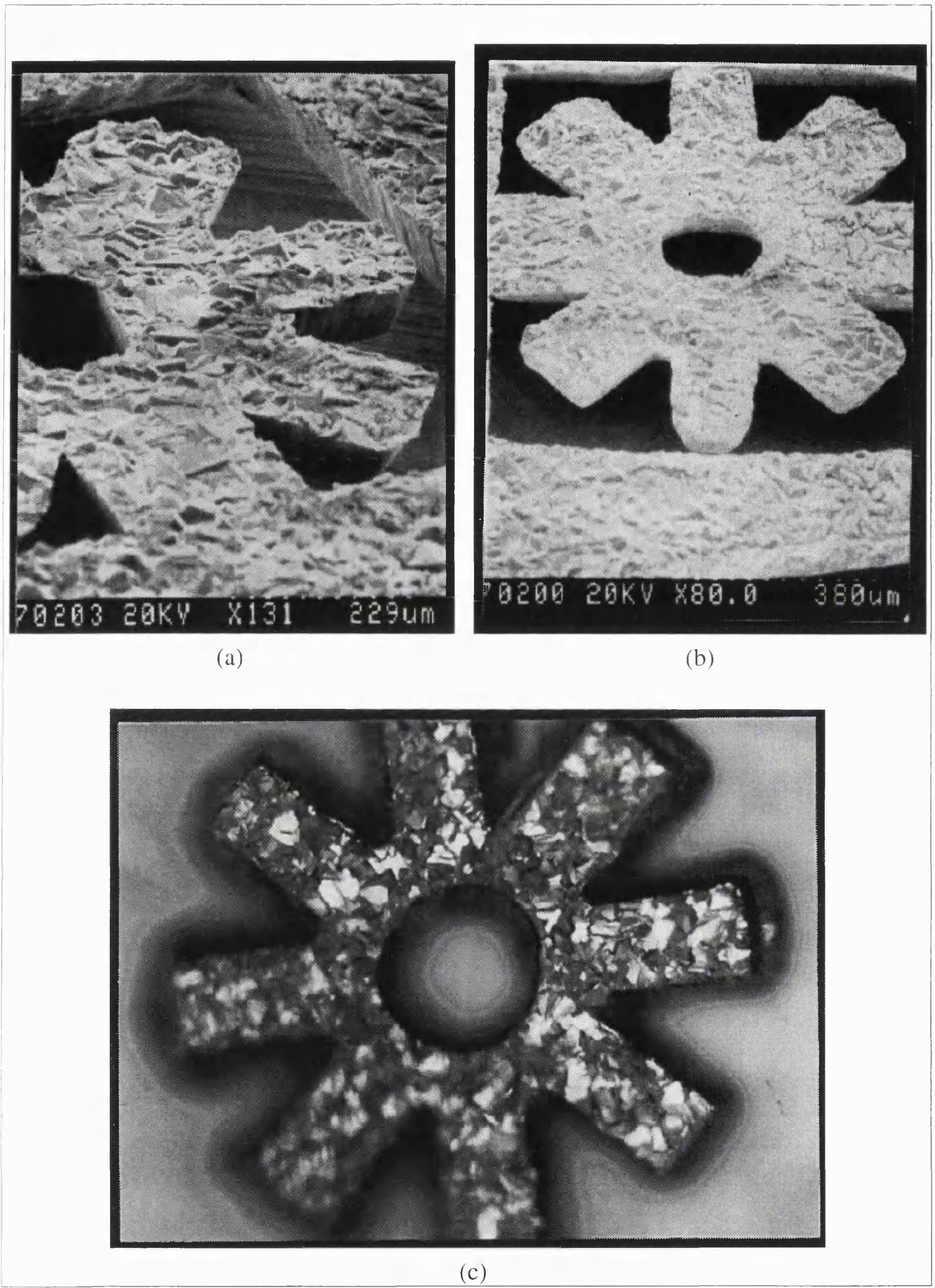

(a) (b)

(c)

Figure 9.11 (a) and (b) SEM micrograph of micro-gears formed by ArF laser projection patterning with a laser fluence of 12 Jcm^{-2} on THICK diamond; (c) optical micrograph of a free standing diamond micro-gear of thickness 80 μm and diameter 930 μm.

9.4 DISCUSSION

Patterning of polycrystalline diamond films with ArF excimer laser irradiation has resulted in the formation of features in the limit of the optical system used within this study (~3 μm). The projection patterning mode of UV laser processing, which is being developed for the next generation of optical lithography as a result of its ability to reproduce a complete mask pattern in a single exposure run, has been demonstrated to be a feasible method for the patterning of diamond by Rothschild *et al.* [1986]. However, for this technique to be employed in a reliable and routine manner for the patterning of diamond substrates, the quality of the etch product, surface debris, aspect ratio of features and process reproducibility have to be addressed. The work carried out here demonstrates that good reproduction of mask features may be made over an area on the sample plane which is dependent on the areal output of the laser beam and the magnification (reduction) of the projection lens. The magnification of the projection lens, which dictates the ultimate resolution, results in a uniform reproduction on the sample plane of over approximately 2 mm x 1 mm (as derived from the output beam of 3 mm x 1.5 mm); at a energy density of 2 Jcm^{-2} an etch rate of 2 nm per laser shot was obtained for the THIN diamond films, equating to an etch rate of 2.4 $\mu m.min^{-1}$ at a laser repetition rate of 20 Hz. Although such a rate compares favourably with that achieved with other techniques such as 150 $nm.min^{-1}$ by an ion beam approach [Efremow, 1985], 30 $nm.min^{-1}$ using RIE [Dorsch, 1992], and 400 $nm.min^{-1}$ using ECR plasma [Pearton, 1992], it should be noted that the high instantaneous process rate has to compromised by the factor required for step-and-repeating the relatively small active area that is processed. Nevertheless, the fact that laser projection patterning is a maskless process relieves at least three processing stages (deposition, patterning and subsequent removal of a heterogeneous mask) from the device fabrication procedure. Furthermore, the repetition rate of the laser may be increased to 50 Hz in the system used here with apparently little deterioration in the chemical nature of the exposed areas (see following chapter); more recent lasers may operate efficiently at repetition rates of at least 300 Hz [Endert, 1995].

Examination of the morphology of the etched regions within the THIN films reveals a surface that apparently has little resemblance to the original structure; however it is difficult to distinguish between the possibility of an actual physical process which results in this effect or else to the inherent cross-sectional variations that exists within the films. A consequence of this latter phenomenon results in the requirement of a more controlled process such as reducing the laser energy levels if the diamond layer is to be fully and cleanly removed from the underlying substrate. In the case of the higher quality THICK material which possesses average grain sizes in the region of 30 μm, energy densities of up to 12 Jcm^{-2} have been utilised to give higher rates of etching (31 nm per pulse) without cracking and flaking of the layer as was apparent in the THIN films; it is likely that the higher quality of the films together with removal of stress present between the diamond layer and the underlying Si substrate are responsible for this latter property. The consequence of a lowering of the quality also results in the difference in etch rates being observed between the higher quality growth surface and the substrate side in the THICK films; such a difference emphasises the need for strict characterisation if control of critical thickness is desired. Of further consideration is processing from the growth side of as-deposited polycrystalline diamond where the surface is intrinsically rough in nature; Figure 9.6(a) shows a good example where significant roughness remains in the etched regions. A possible effect of this on the delineation of features with smaller feature-sizes is shown in Figure 9.7(a) where apparent distortion is present in nominally straight features. Such a distortion is not obvious in the corresponding process on the smooth substrate side; this suggests a direct consequence of the rough nature of the starting material. Nevertheless, the promising development of polishing/ smoothening techniques involving excimer lasers [Bogli, 1992; Bhushan, 1994] suggests that by the integration of both polishing and etching techniques with equipment based on the same processing philosophy, such problems may be alleviated.

Investigation of the aspect ratio revealed the presence of features possessing non-vertical sidewalls; sidewall angles were found to vary with laser energy intensity in a manner as summarised in Figure 9.10. It is possible that non-vertical sidewalls may arise from a non-uniform illumination beam profile at the entrance of the imaging lens. However, the output beam profile is "top-hat" *i.e.* of uniform intensity across the x-axis [G. Arthur (Rutherford Appleton Lab.), private communications]; the fact that the square images formed in Figure 9.9 demonstrate similar wall-angles on all sides of each square suggests the presence of alternative mechanisms for the sloping side-walls. Kahlert and co-workers [1992] have investigated various system parameters in the excimer laser processing of polyimide. Using a fully homogenised beam (profile +/-5%), they reported a reducing wall angle (25° to -2°) as the laser energy density (0.5-20 Jcm^{-2}) and/or the numerical aperture of the lens (0.02-0.16) was increased. Further improvements in the optical system employed are therefore required to improve this issue on thin film diamond. Nevertheless, 80 μm thick free-standing micro-structures of a lateral dimension not limited by the wall angle have been obtained in diamond by projection patterning.

9.5 SUMMARY

Investigation of excimer laser processing of diamond films of varying quality has been carried out in detail and demonstrates the capability of at least micron-sized resolution patterning reproducible over an area of 2 mm x 1 mm when used in the maskless mode of projection patterning. Clean surfaces are achievable by the employment of this method. Various concerns, however, have been raised from the results of this study: firstly the nature of the rough surface intrinsic in as-deposited polycrystalline films may be reflected in the final etched surface depending on the quality of the material. This effect though, will be alleviated by the prior application of polishing techniques; such polishing will be required as the development of more complicated electronic device structures are encountered, and may be conveniently based on excimer lasers. In addition, the cross-sectional variation in material quality will demand strict control of laser parameters if either critical thicknesses, or the removal of diamond material to a heterogeneous substrate is required. The observation of non-vertical sidewalls is of immediate concern and prevents structures with high aspect ratios being developed for the application of diamond in micro-electromechanical systems. Although it has been demonstrated here for the first time that wall angles depend on the laser energy intensity, a value of 25° still exists in the structures delineated. Nevertheless, this study is the first report to the author's knowledge [Chan *et al.,* 1995] of the formation of free-standing diamond microstructures from a etching-based technique that may be superior in terms of throughput and quality of finish to more established etching approaches such as RIE which requires masking processes, and also to the "direct-writing" mode of focused laser beam scanning.

REFERENCES

Ageev, V.P., Builov, B.B., Konov, V.I., Kuzmichev, A.V., Pimenov, S.M., Prokhorov, A.A.M., Ral'chenko, V.G., Spitsyn, B.V. and Chapliev, B.I., [1988]. *Sov. Phys. Dokl.,* **33**, 840.

Bhushan, B., Subramaniam, V.V. and Gupta, B.K., [1994]. *Diamond Film Technol.,* **4**, 71.

Bogli, U., Blatter, A., Pimenov, S.M., Smolin, A.A. and Konov, V.I., [1992].*Diamond Relat. Mater.,* **2**, 782.

Bogli, U., Blatter, A., Bachli, A., Luthi, R. and Meyer, E., [1993]. *ibid,* **2**, 924.

Boyd, I.W., [1992]. in *Photochemical Processing of Electronic Materials,* ed. I.W. Boyd and R.B. Jackman, (Academic Press), London, UK.

Bryzrk, J., Petersen, K. and McCulley, W., [1994]. *IEEE Spectrum*, **May**, 20.

Chan, S.S.M., Jackman, R.B., Arthur, G., Goodall, F. and Lawes, R.A., [1995]. *Diamond Films Technol.,* **5**, 291.

Davidson, J.L., Ramesham, R. and Ellis, C., [1990]. *J. Electrochem. Soc.,* **137**, 3206.

Dorsch, O., Werner, M., Obermeier, E., Harper, R.E., Johnston, C. and Buckley-Golder, I.M., [1992]. *Diamond Relat. Mater.,* **1**, 277.

Efremow, N.N., Geis, M.W., Flanders, D.C., Lincoln, G.A. and Economu, N.P., [1985]. *J. Vac. Sci. Technol.,* **B3**, 416.

Endert, H., Patzel, R., Rebhan, U., Powell, M. and Basting, D., [1995]. *Jpn. J. Appl. Phys.,* **34**, 4050.

Field, J.E., (ed) [1992]. *Properties of Diamond*, Academic Press, London, UK.

Geis, M.W., Rothschild, M., Kunz, R.R., Aggarwal, R.L., Wall, K.F., Parker, C.D., McIntosh, K.A., Efremow, N.N., Zayhowski, J.J. and Ehrlich, D.J., [1989]. *Appl. Phys. Lett.,* **55**, 2295.

George, T., Foote, M.C., Vasquez, R.P., fortier, E.P. and Posthill, J.B., [1993]. *Appl. Phys. Lett.,* **62**, 2880.

Grot, S.A., Ditizio, R.A., Gildenblat, G.Sh., Badzian, A.R. and Fonash, S.J., [1992]. *Appl. Phys. Lett.,* **61**, 2326.

Hirabayashi, K., Taniguchi, Takamatsu, O., Ikeda, T., Ikoma, K. and Iwasaki-Kurihara, N., [1988]. *Appl. Phys. Lett.,* **53**, 1815.

Hirata, A., Tokura, H. and Yoshikawa, M., [1992]. *Thin Solid Films,* **212**, 43.

Hunn, J.D., Withrow, S.P., White, C.W., Clausing, R.E., Heatherly, L. and Christensen, C.P., [1994]. *Appl. Phys. Lett.,* **65**, 3072.

Inoue, T., Tachibana, H., Kumagai, K., Miyata, K., Nishimura, K., Kobashi, K. and Nakaue, A., [1990]. *J. Appl. Phys.,* **67**, 7329.

Kahlert, H.-J., Sarbach, U., Burghardt, B. and Klimt, K., [1992]. *SPIE Proc.,* **1835**, 110.

Johnston, C., Chalker, P.R., Buckley-Golder, I.M., Marsden, P.J. and Williams, S.W., [1993]. *Diamond Relat. Mater.,* **2**, 829.

Kobayashi, K., Yamamoto, K., Mutsukura, N. and Machi, Y., [1990]. *Thin Solid Films,* **185**, 71.

Kobayashi, K., Mutsukura, N. and Machi, Y., [1991]. *Thin Solid Films,* **200**, 139.

Konov, V.I., Ral'chenko, V.G., Pimenov, S.M., Smolin, A.A. and Kononenko, T.V., [1993]. *SPIE,* **2045**, 184.

Maki, T., Hou, G.L. and Kobayashi, T., [1993]. *Jpn. J. Appl. Phys.,* **32**, 3227.

Marsh, J.B. and Farnsworth, H.E., [1964]. *Surf. Sci.,* **1**, 3.

Obratzov, A.N. and Pirogov, V.G., [1994]. *Diamond Film Technol.,* **4**, 243.

Pearton, S.J., Katz, A., Ren, F. and Lothian, J.R., [1992]. *Electronics Lett.,* **28**, 822.

Pimenov, S.M., Smolin, A.A., Ralchenko, V.G., Konov, V.I., Likhanski, S.V., Veselovski, I.A., Sokolina, G.A., Bantsekov, S.V. and Spitsyn, B.V., [1993]. *Diamond Relat. Mater.,* **2**, 291.

Ral'chenko, V.G., Korotushenko, K.G., Smolin, A.A. and Loubnin, E.N., [1995]. *Diamond Relat. Mater.,* **4**, 893.

Roppel, T., Ramesham, R., Ellis, C. and Lee, S., [1992]. *Thin Solid Films,* **212**, 56.

Rothschild, M., Arnone, C. and Ehrlich, D.J., [1986]. *J. Vac. Sci. Technol.,* **B4**, 310.

Smith, R.A., [1978]. *Semiconductors*, 2nd Edition,(Cambridge University Press), Cambridge, UK.

Sze, S.M., [1981]. *Physics of Semiconductor Devices*, 2nd Edition, (John Wiley & Sons), New York, USA.

Tokarev, V.N., Wilson, J.I.B., Jubber, M.G., John, P. and Milne D.K., [1995]. *ibid,*. **4**, 169.

Whetten, T.J., Armstead, A.A., Grzybowski, T.A. and Ruoff, A.L., [1984]. *J. Vac. Sci. Technol.,* **A2**, 477.

Yoshikawa, M., [1990]. *SPIE*, **1325**, 210.

10: CHARACTERISATION OF EXCIMER LASER PROCESSED DIAMOND FILMS

10.1 INTRODUCTION

As demonstrated in the previous chapter, complex patterns may be delineated on the surface of diamond films by the dry etching technique of excimer laser processing at 193 nm. Such ability for material removal is of interest in a variety of applications including polishing films for optical components, controlling critical layer thicknesses of electronic device structures and for the creation of micro-mechanical structures. However, in order to assess the suitability of laser treated material for proposed applications, it is important to characterise the regions of the material exposed to the photon beam. Of the reports containing characterisation details of the irradiated regions, most authors have reported graphitisation of the diamond material resulting from material removal; for laser radiation of energy below the theoretical fundamental absorption edge of diamond *i.e.* $\lambda > 227$ nm, Raman scattering has been deployed to show the presence of amorphous carbon/graphite in polycrystalline diamond films processed by a Cu-vapour laser [Obratzsov, 1994], and also by an Ar ion laser [Ral'chenko, 1995]. Although in the case of YAG (1.06 μm) laser processing Yoshikawa [1990] has suggested that oxygen pressures >700 Torr prevent the formation of graphite formation within polycrystalline diamond films (no evidence provided), Miyazawa *et al.* [1994] have shown that irradiation of HPHT synthesised material at this wavelength in an air ambient leads to a complete loss of the diamond peak in the Raman spectrum. However, this latter author showed that processing in a thermochemical mode with laser heating of a stainless steel plate in a liquid ambient (H_2O or KOH) produced a graphite-free irradiated region. A rare-gas halide (or excimer) laser (KrF) operating at 248 nm has resulted in an irradiated region with an electron diffraction pattern characteristic of graphite [George, 1993].

The characterisation of diamond processed at energies greater than the bandgap transition has been discussed by a number of workers [Rothschild, 1986; Geis, 1989; Bogli, 1992; 1993; Johnston, 1993; Bhushan, 1994; Deshmukh, 1994] utilising laser fluence levels of 0.1-200 Jcm^{-2} focused onto the surface of natural and polycrystalline material These reports are summarised in Table 10.1. Graphitisation of natural single-crystalline diamond (type IIa), as implied by an optical transmission technique, was observed by Rothschild and co-workers [1986] to occur at energies greater than 60 $mJcm^{-2}$, with etching only occurring at energies greater than 3 Jcm^{-2}. On similar material, Geis *et al.* [1989] modified the diamond surface with 15 ns pulses of 193 radiation at an energy 0.5 Jcm^{-2} to obtain a chemically and thermally stable electrically conductive layer; it was observed from electron diffraction that, in addition to the diamond phase, unidentified carbon phases were present even after a helium-oxygen plasma/acid treatment. In this latter case, Raman spectroscopy detected a diamond phase only. On polycrystalline diamond films, irradiation of the surface with 193 nm light (2-3 Jcm^{-2}) has also led to the formation of an electrically conductive layer which was removable by heating in air at 500 °C [Bogli, 1992]. Raman scattering has also been used to characterise the purity of the irradiated material in terms of its diamond content; Johnston and co-workers [1993] demonstrated the formation of microcrystalline graphite after exposure of such films in an air ambient to pulses of energy 2.5 Jcm^{-2}. However it has also been shown by Bhushan and co-workers [1994] that an effectively unchanged Raman signal may be obtained; processing of polycrystalline diamond films was carried out in a 50 Torr pure oxygen environment at a laser power density of 50 $MWcm^{-2}$ (unspecified pulsewidth) on the sample surface. In this case, the absorption of 193 nm radiation by O_2 leading to multi-photon dissociation and the creation of O atoms and O_3 was proposed to be an important property.

Although characterisation of ArF irradiated films have been discussed by these authors as summarised in Table 10.1, various areas remain to be addressed and clarified before laser processing may be considered for its intended applications. Foremost amongst these is the quality of the regions exposed to laser irradiation, an issue which, as discussed above, remains unresolved within the literature. In order to address some of the central issues, characterisation of CVD diamond films has been undertaken as a function of a number of process controllable parameters including laser energy intensity and pulse repetition rate. These latter two parameters contribute directly to the overall rate of the process. The effect of the initial quality of the material and the processing ambient on the final quality of the irradiated areas have also been investigated.

Laser	Process condition	Characterisation
CO_2 (10.6 μm) [Ageev, 1989]	E>18 Jcm^{-2} A= 10^{-6} Torr	G at E=18 Jcm^{-2}.
YAG (1.06 μm) [Miyazawa, 1994]	P= $2.5x10^4$ Wcm^{-2} A= air, KOH, H_2O	Process in air leads to a-C, but in KOH or H_2O no change in Raman.
Cu (510 nm) [Obratzsov, 1994]	P= 0.5 W (p.width= 20ns) A= air	G at P> 20 $MWcm^{-2}$ (natural), P> 0.2 $MWcm^{-2}$ (CVD). Raman shows a-C only after process.
Ar^+ (457-514 nm) [Ral'chenko, 1995]	P= 2 W A= air, O_2, vacuum, Ar	No etching *in-vacuo* or Ar. In air or O_2 Raman shows G.
XeCl (308 nm) [Ageev, 1989]	E= 30 Jcm^{-2} (max) A= air, Xe, vacuum	G at E> 0.02 Jcm^{-2} (CVD). Etch rate same in air or *in-vacuo* but air gives cleaner etch.
KrF (248 nm) [George, 1993]	E= 20 Jcm^{-2} A= air	Electron diffraction shows G.
KrF (248 nm) [Pimenov, 1993]	E= 10 Jcm^{-2}(max) A= air	Electrically conductive layer forms, remove by oxidation (air, 450°C).
ArF (193 nm) [Rothschild, 1986]	E= 0.1-200 Jcm^{-2} A= Cl_2, NO_2, NH_3	G at E> 60 $mJcm^{-2}$. Etching only at E> 3 Jcm^{-2} but in Ar leads to graphitic buildup at edges.
ArF (193 nm) [Geis, 1989]	E= 0.5 Jcm^{-2} A= air	Stable conductive layer formed. Diffraction shows unknown phases. Raman shows diamond only.
ArF (193 nm) [Bogli,1992;1993]	E= 2-3 Jcm^{-2} A= air	Conductive layer removable (air, 500 °C); chemically, thermally stable layer remains.
ArF (193 nm) [Johnston, 1993]	E= 3.6 Jcm^{-2} (max) A= air	E= 2.5 Jcm^{-2}, severe G (Raman).
ArF (193 nm) [Bhushan, 1994]	P= 50 $MWcm^{-2}$ A= O_2 (50 Torr)	Raman shows no modification of the diamond film after processing.
ArF (193 nm) [Deshmukh, 1994]	E= 2 Jcm^{-2} A= air	G layer on ^{13}C-rich diamond but not on ^{12}C diamond.

Table 10.1 Summary of characterisation performed on laser irradiated diamond from a variety of laser sources. A= processing ambient; G= graphitisation; E, P = laser energy and power respectively.

10.2 EXPERIMENTAL DETAILS

The films employed in this study have been described in Table 9.1. Prior to laser irradiation, the films have been treated to an initial acid treatment consisting of ammonium persulphate (Appendix B) to reduce non-diamond components on the surface of the material; this has been labelled 'non-irradiated' in the following spectra. Acid treatment has also been employed in some instances after laser irradiation. Characterisation of the processed areas have been carried out using scanning electron microscopy (SEM), Raman spectroscopy, Auger electron spectroscopy (AES) and electrical current-voltage (I-V) testing.

10.3 RESULTS

10.3.1 THIN diamond films

(a) Raman spectroscopy

Raman scattering was performed with a laser spot size on the sample plane of 100 μm diameter to characterise ArF laser modified regions (400 μm by 400 μm) on THIN film diamond. Figure 10.1 reveals the Raman spectra for the non-irradiated diamond sample along with spectra for areas of the diamond exposed to 10, 100 and 500 shots of laser radiation at a fluence of 0.5 Jcm^{-2}. The depth into the diamond film after 500 pulses was determined by depth profilometry to be 0.3 μm. The Raman spectrum obtained for the non-irradiated diamond sample consists of a single prominent diamond peak at a wavenumber shift of 1332 cm^{-1} superimposed on a background of peaks at 1230 cm^{-1}, 1360 cm^{-1} and 1480 cm^{-1}. The full width at half maximum (FWHM) of the diamond signal is estimated to be around 10-15 cm^{-1} and is typical for diamond films of this nature [Ager III, 1991]. After exposure to 10 pulses of ArF laser radiation at an energy of 0.5 Jcm^{-2}, the diamond peak remains unchanged both in position and in linewidth. However, a relative reduction in the 1480 cm^{-1} feature is detectable together with an increase both in the 1230 cm^{-1} peak and the peak at 1580 cm^{-1}. As the number of laser pulses is increased to 100, peaks at 1355 cm^{-1} and 1580 cm^{-1} become more significant. When compared to the Raman spectrum of the non-irradiated sample, however, this emergence appears to be associated with a decrease in the intensity of the components at 1120 cm^{-1} - 1230 cm^{-1} and 1480 cm^{-1}. After 500 pulses the diamond signal at 1332 cm^{-1} is still detectable though the 1355 cm^{-1} peak relative to that at 1332 cm^{-1} has increased beyond that observed in the non-irradiated sample. In addition, although both the peaks at 1230 cm^{-1} and 1480 cm^{-1} have increased in intensity relative to the spectra obtained after 100 pulses, the intensity of these two peaks are only comparable to those in the non-irradiated sample.

The nature of laser modified regions was similarly analysed following exposure to 193 nm laser radiation at the higher fluence of 2 Jcm^{-2}. In this case, only regions exposed up to 100 laser pulses were analysed; this leads to only modest material removal (0.5 μm) and hence any changes in Raman spectra that may arise as a result of the film varying with depth from the surface are minimised. Figure 10.2 compares the Raman spectrum of the non-irradiated sample with those after exposure to 10 and 100 pulses. After 10 pulses the diamond peak present at 1332 cm^{-1} is superimposed on an intense band with a FWHM of approximately 180 cm^{-1} centred around 1330 cm^{-1}; a further peak is apparent at 1590 cm^{-1}. An increase in the number of laser pulses to 100, leads to the emergence of peaks at 1230 cm^{-1} and 1480 cm^{-1} in additional to the 1330 cm^{-1} and 1590 cm^{-1} bands. A peak at 1620 cm^{-1} is also present.

Fig. 10.3(a) displays a series of Raman spectra for diamond regions exposed to 10 pulses with ArF laser fluence levels of 0.5, 1, 1.5 and 2 Jcm^{-2}. It is apparent that a diamond content remains in the laser exposed regions for all the laser energies examined here, as indicated by the Raman peak at 1332 cm^{-1}. However as the energy of the laser is increased, this diamond peak becomes progressively less distinct as the broad peak centred around 1330 cm^{-1} increases in significance. Furthermore, apart from the 0.5 Jcm^{-2} case in which the Raman spectrum shows a change in the 1230 cm^{-1} and 1480 cm^{-1} bands, the spectra for laser energies of 1 Jcm^{-2} and greater display intense peaks at 1330 cm^{-1} and 1590 cm^{-1}. Raman spectra of the same sample but following acid treatment are displayed in Figure 10.3(b). It is not clear why the particular sample treated at a laser energy density of 0.5 Jcm^{-2} results in the spectra which displays a highly obscured diamond peak; it appears likely that an artefact may have been introduced in the process of the acid treatment. Nevertheless, for the regions exposed to laser energies of 1 Jcm^{-2} and greater, the effect of the acid treatment is clearly seen to reduce the relative intensity of the peaks at 1330 cm^{-1} and 1590 cm^{-1} with a corresponding increase in the relative intensity of the peaks at 1150 cm^{-1}, 1230 cm^{-1} and 1400-1500 cm^{-1}.

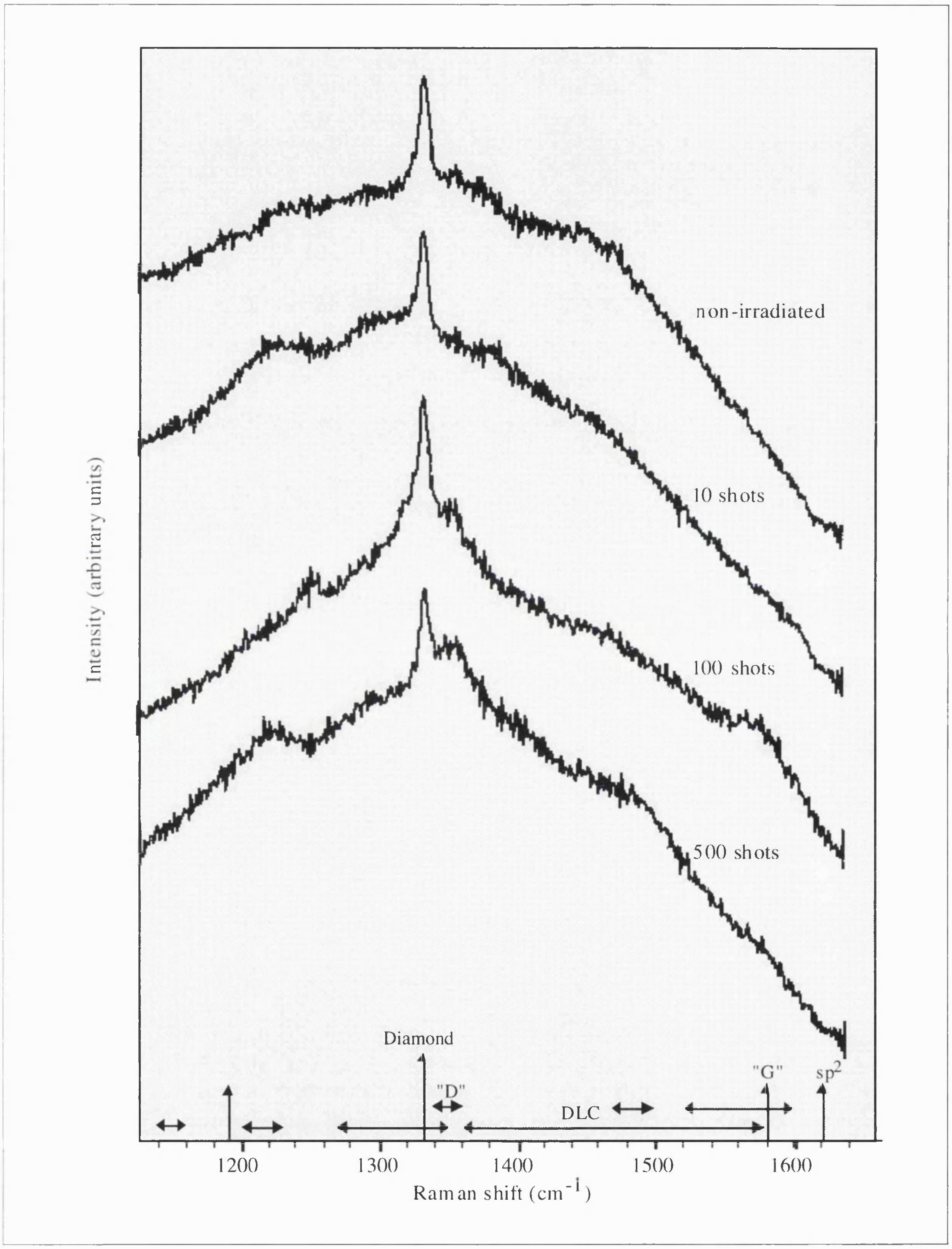

Figure 10.1 Raman spectrograph of diamond film modified by 193 nm laser radiation at a fluence of 0.5 Jcm^{-2} for a varying number of laser shots of 20 ns pulsewidth. Various assigned and observed Raman peaks are indicated.

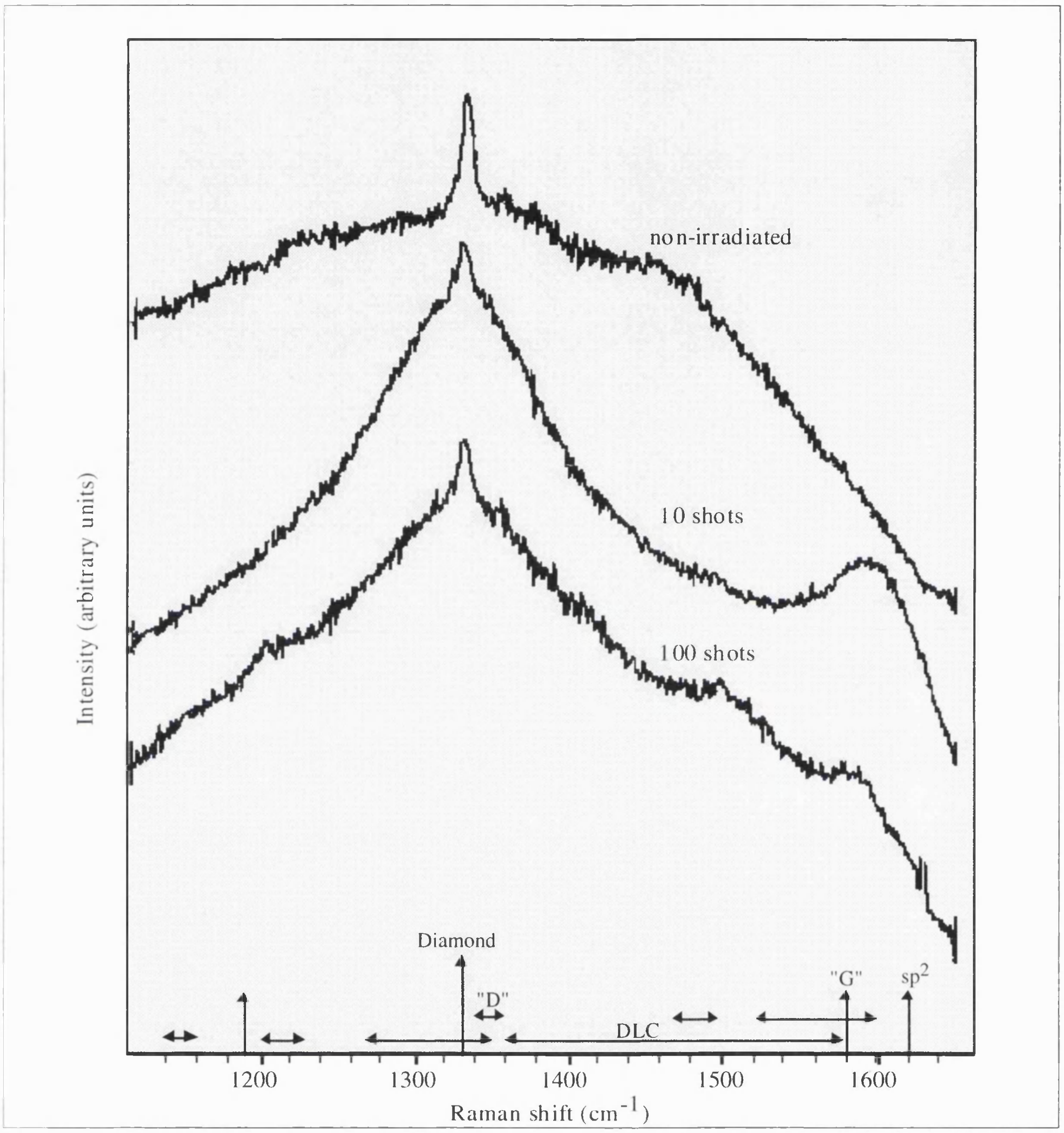

Figure 10.2 Raman spectrograph of diamond film modified by 193 nm laser radiation at a fluence of 2.0 Jcm^{-2} for a varying number of laser shots of 20 ns pulsewidth. Various assigned and observed Raman peaks are indicated.

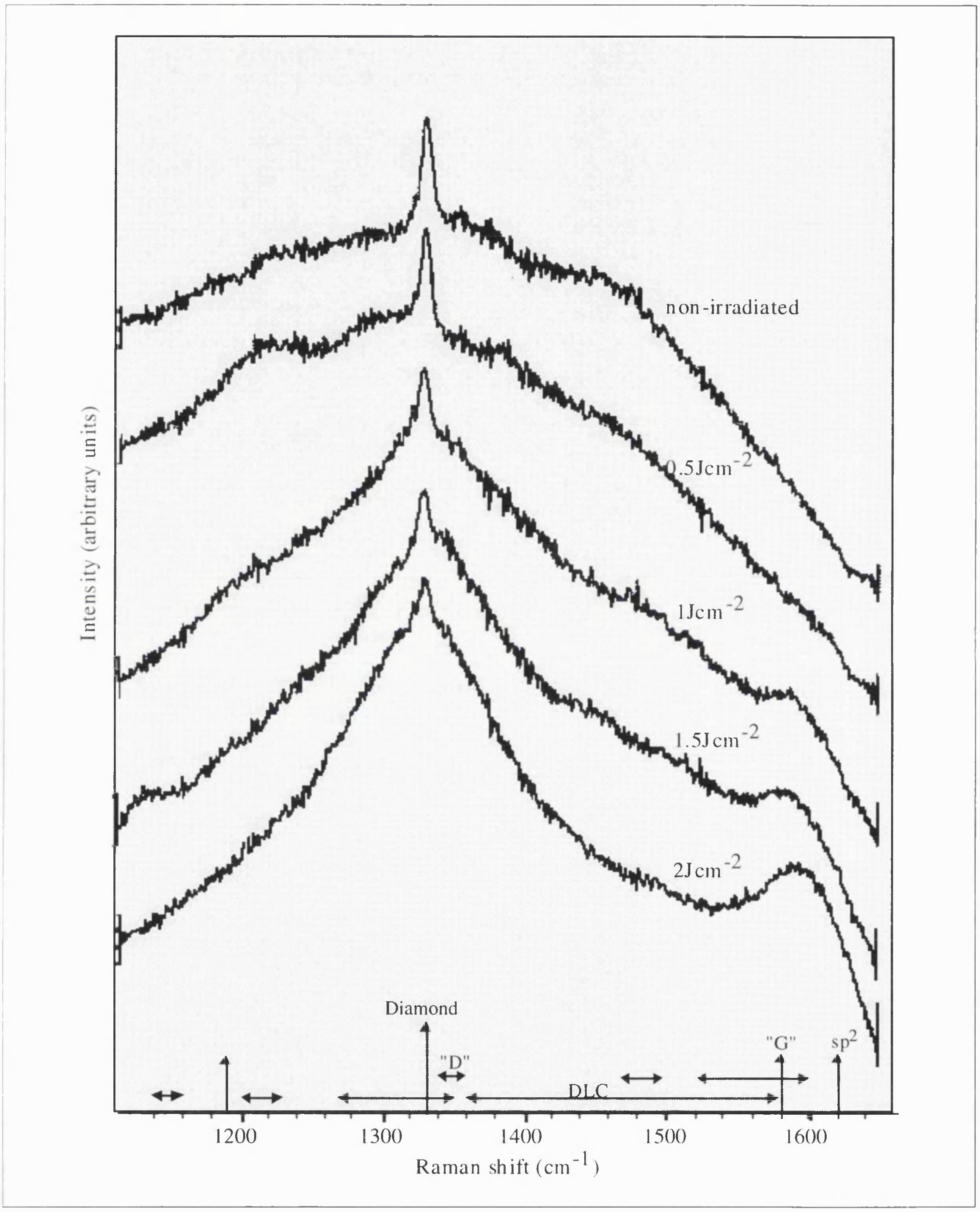

Figure 10.3(a) Raman spectrograph of diamond film modified by 10 shots (20 ns pulsewidth) of 193 nm laser radiation at varying fluence levels. Various assigned and observed Raman peaks are indicated.

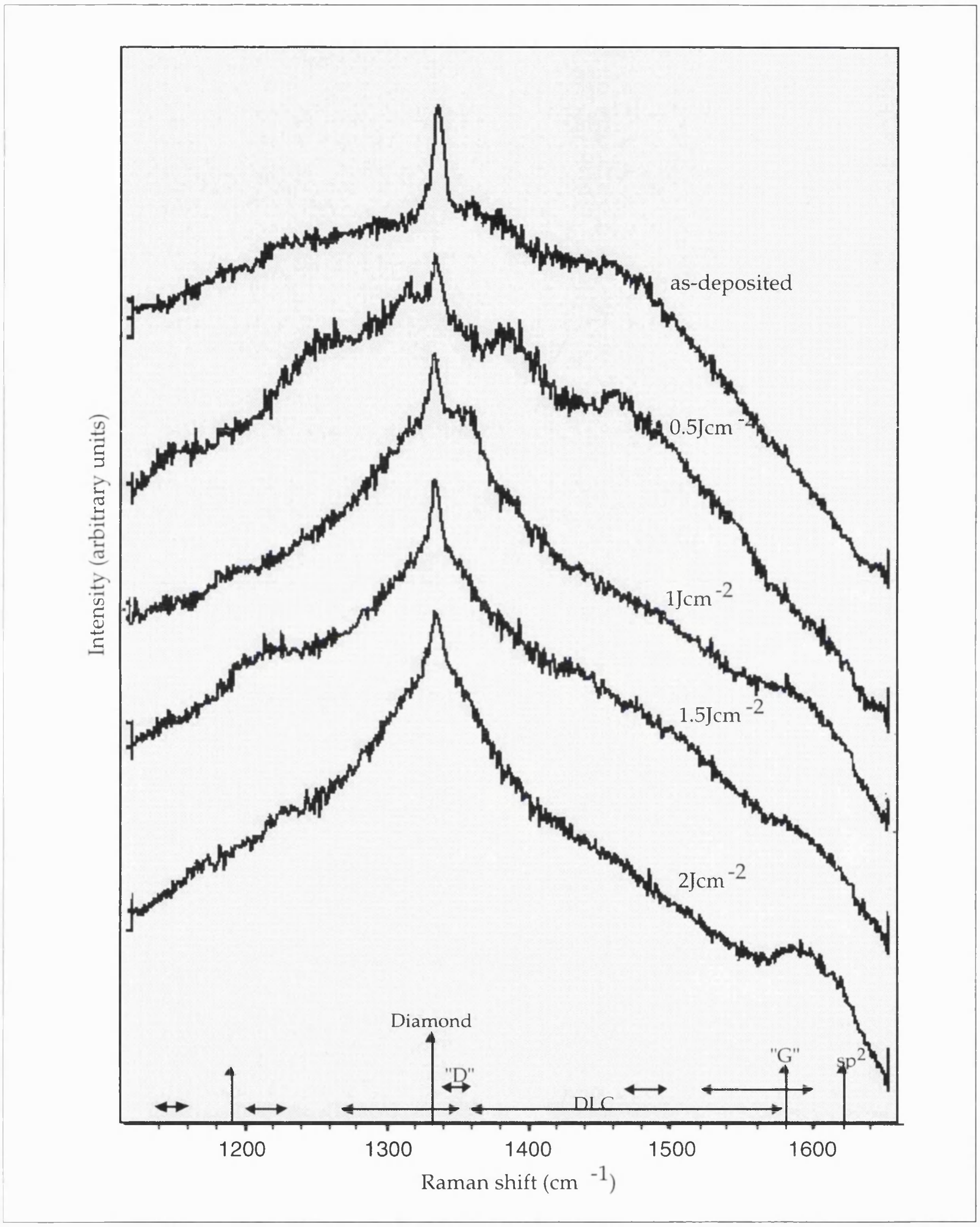

Figure 10.3(b) Raman spectrograph of acid-treated diamond film modified by 10 shots (20 ns pulsewidth) of 193 nm laser radiation at varying fluence levels. Various assigned and observed Raman peaks are indicated.

(b) Auger electron spectroscopy

AES was carried out on the as-deposited, acid treated, 193 nm laser modified (0.5 Jcm^{-2} and 1 Jcm^{-2} (100 pulses)) samples. Prior to exposure to the Auger probe beam, all apart from the 0.5 Jcm^{-2} modified sample, were heated *in-vacuo* to 600 °C for 5 min in order to remove residual (air) contamination. Differential spectra in the energy range 50-600 eV are shown in Figure 10.4(a) for the various samples taken at a modulation voltage of 5 V peak-to-peak. The dominant feature evident in the spectra is attributed to the carbon signal and has been set to 268 eV [Lurie, 1977] in order to correct for sample charging. In addition, it is apparent that both the oxidising acid treatment (re-presented from Figure 5.2) and the effect of laser processing at 1 Jcm^{-2} lead to the presence of an oxygen phase (~510 eV) which is stable to heating *in-vacuo* to 600 °C; the large O_2 signal in the 0.5 Jcm^{-2} laser sample is attributed to air/water contamination. From standard Auger sensitivity factors [Davis, 1976], it can be estimated that in the case of the 1 Jcm^{-2} laser sample, oxygen comprises around 8% of a monolayer if is assumed to be evenly distributed on the surface.

Figure 10.4(b) shows higher resolution spectra recorded in the energy range 220-300 eV (at a peak-to-peak modulation of 2V) for the various samples. It is apparent that for the non-irradiated, acid treated and 0.5 Jcm^{-2} laser processed samples the main peak minima coincide at the fixed value of 268 eV. Furthermore, for these samples, two peak maxima may be identified at the low energy side of the main peak minima. There is a close agreement between these differential mode peak positions and the N(E) peak positions as identified by Lurie and Wilson [1977] in their study of single crystal diamond; peaks at 268 eV, 259.4 eV (P_0), 247.7 eV (A_1) and 233.5 eV (A_2) have been attributed to the KV_1V_1 and KV_2V_2 transitions, surface and bulk plasmon losses, respectively. This indicates that the surface of these samples is composed of diamond which is comparable to that of single crystal material over the probe depth of the AES technique (around 3 atomic layers). However a change in the relative intensities of the P_0 to A_1 peaks is perceivable. It appears that after acid treatment a carbon signal with a greater P_0/A_1 ratio is obtained which more closely resembles that of single crystal material [Lurie, 1977]. After laser processing at 0.5 Jcm^{-2}, it is apparent that not only is this ratio reduced, but an additional feature at 290 eV is formed.

In the case of the higher energy laser processed sample (1 Jcm^{-2}), the primary peak minima is seen to shift by 3 eV to 271 eV, together with the change in the relative intensities of the P_0/A_1 peaks. Furthermore, a shoulder is observed at ~278 eV as well as 290 eV.

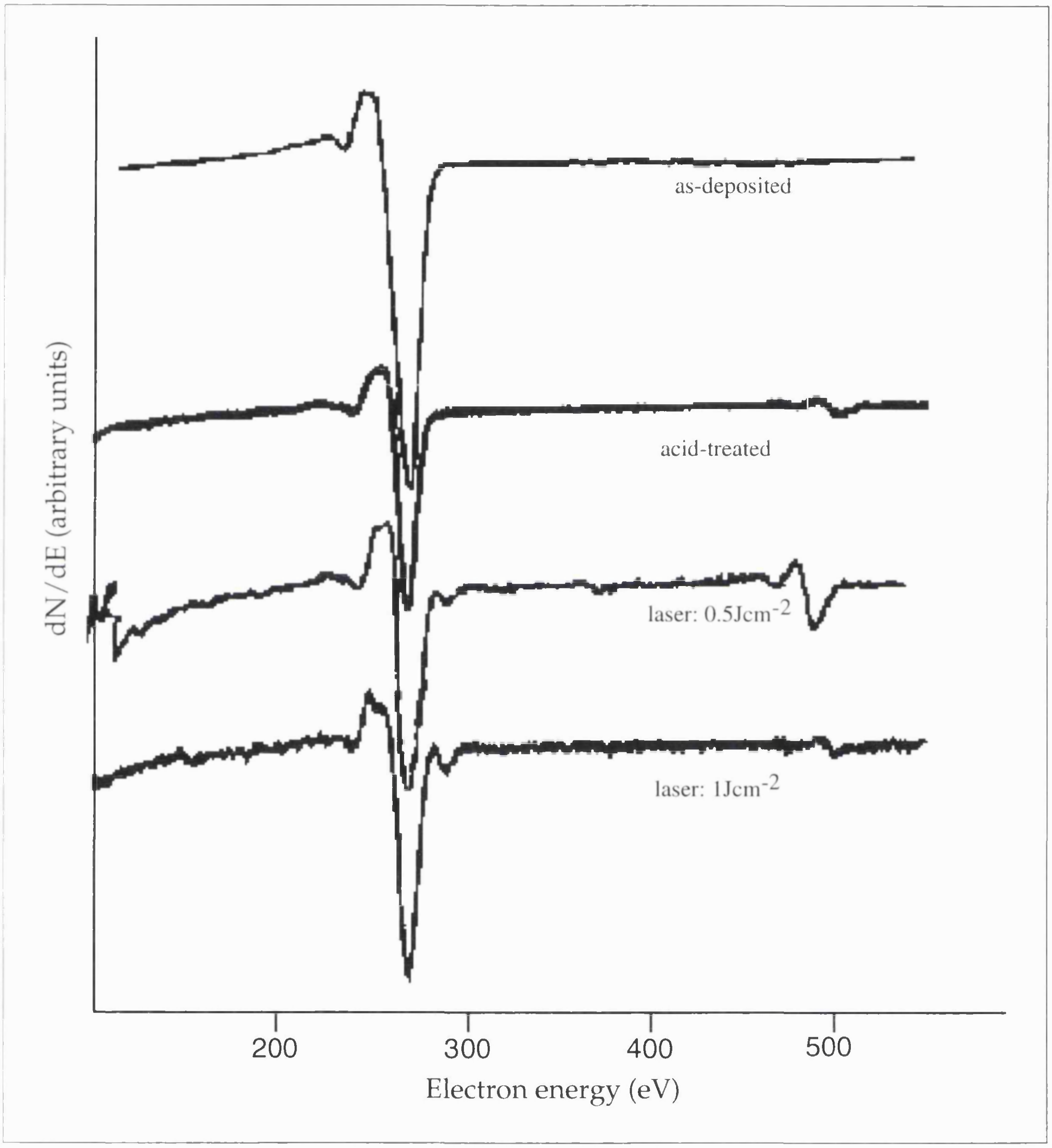

Figure 10.4(a) Wide scan Auger electron spectra (E_{beam}= 3 kV, I_{beam}= 1 μA, Modulation= 5 V) of carbon KVV energy region of CVD diamond after the treatments as described in the text.

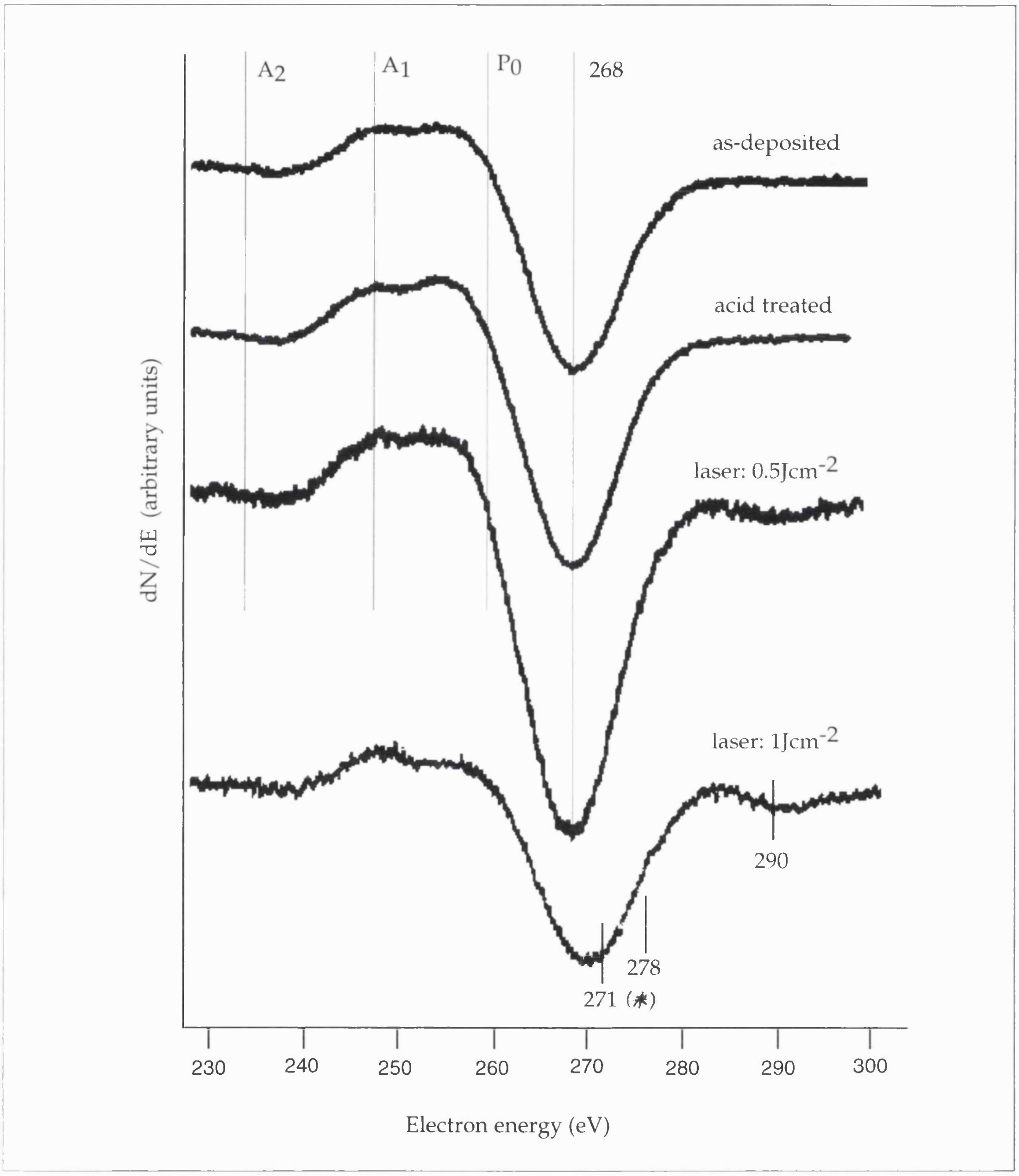

Figure 10.4(b) High resolution Auger electron spectra (E_{beam}= 3 kV, I_{beam}= 1 μA, Modulation= 2 V) of carbon KVV energy region of CVD diamond after the treatments as described in the text.

(*) Bottom trace should be shifted +1eV in electron energy with minima at 271eV.

(c) Electrical characterisation

To ascertain possible changes in the electrical behaviour of the metal-semiconductor interface arising from laser processing, selective areas of the doped THIN diamond films were treated to 800 shots of 193 nm laser radiation (pulsewidth of 20 ns, fluence of 0.5 Jcm^{-2}) at a repetition rate of 20 Hz in an air ambient. The depth into the diamond films was ~0.3 μm. In order to investigate the effect of the different reactivities of various metals on the laser processed surface, Au (200 nm), Al (200 nm) and a tri-layer metallisation of Ti(10 nm)/ Ag (150 nm)/ Au (200 nm) were selectively deposited onto the irradiated areas of the diamond films. Comparison of contact behaviour was made with similarly spaced contacts on non-irradiated material. These particular metals have been chosen with Au representing a non-carbide former, Al a possible carbide former [Tachibana, 1992] and Ti a strong carbide former. Measurements have been conducted by I-V testing between 2 contacts of similar nature at room temperature for pre- and post-annealing for 1h in air at 430 °C. The test structure is shown in Figure 10.5.

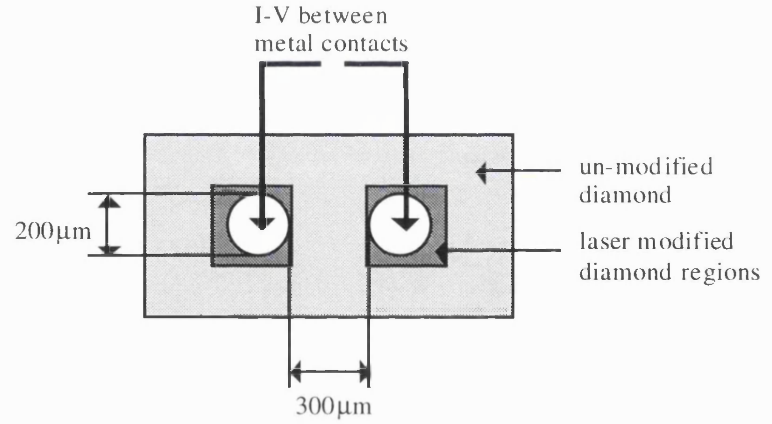

Figure 10.5 Test structure for the investigation of the electrical properties of the metal- laser modified diamond interface.

The electrical I-V characteristics for Au and Al metallisations on laser processed regions which have been subjected to the acid treatment prior to contact deposition are shown in Figure 10.6(a) and (b) respectively; corresponding characteristics for non-laser treated material are also included. Over the range of testing (5 V), it is apparent that linear and symmetric behaviour is obtained for both these contact metallisations on the laser modified and unmodified regions; the absence of non-linearity may be expected at the high doping levels present within this particular wafer. The behaviour of these metal-diamond junctions do not appear to be altered by the combined effect of laser processing and subsequent acid treatment prior to contact deposition. Furthermore, annealing the contacts at 430 °C for 1 h in an air ambient led to essentially similar characteristics.

Ti contacts were tested in a similar manner and, as shown in Figure 10.7 (a), metallisations on non-laser modified and laser-modified (+ subsequent acid treatment prior to contact deposition) regions of the sample again demonstrated similar electrical characteristics as observed with Au and Al. In contrast however, on annealing the contacts to 430 °C in order to promote carbide formation (Chapter 7), it was observed that whereas a increased conductivity was achieved with contacts on the non-modified regions, the contacts on the laser modified regions did not demonstrate such an alteration in characteristics. Investigations were also carried out on laser modified samples which were not subjected to a subsequent acid treatment; the results presented in Figure 10.7 (b) show a similar phenomenon occurring for the Ti contacts on laser modified material before and after annealing, whilst those on unmodified material improves on annealing. The higher resistivity for contacts on this sample is attributed to doping variations across the wafer leading to the possibility of lower doping levels present in this sample (which was taken nearer the edge of the wafer).

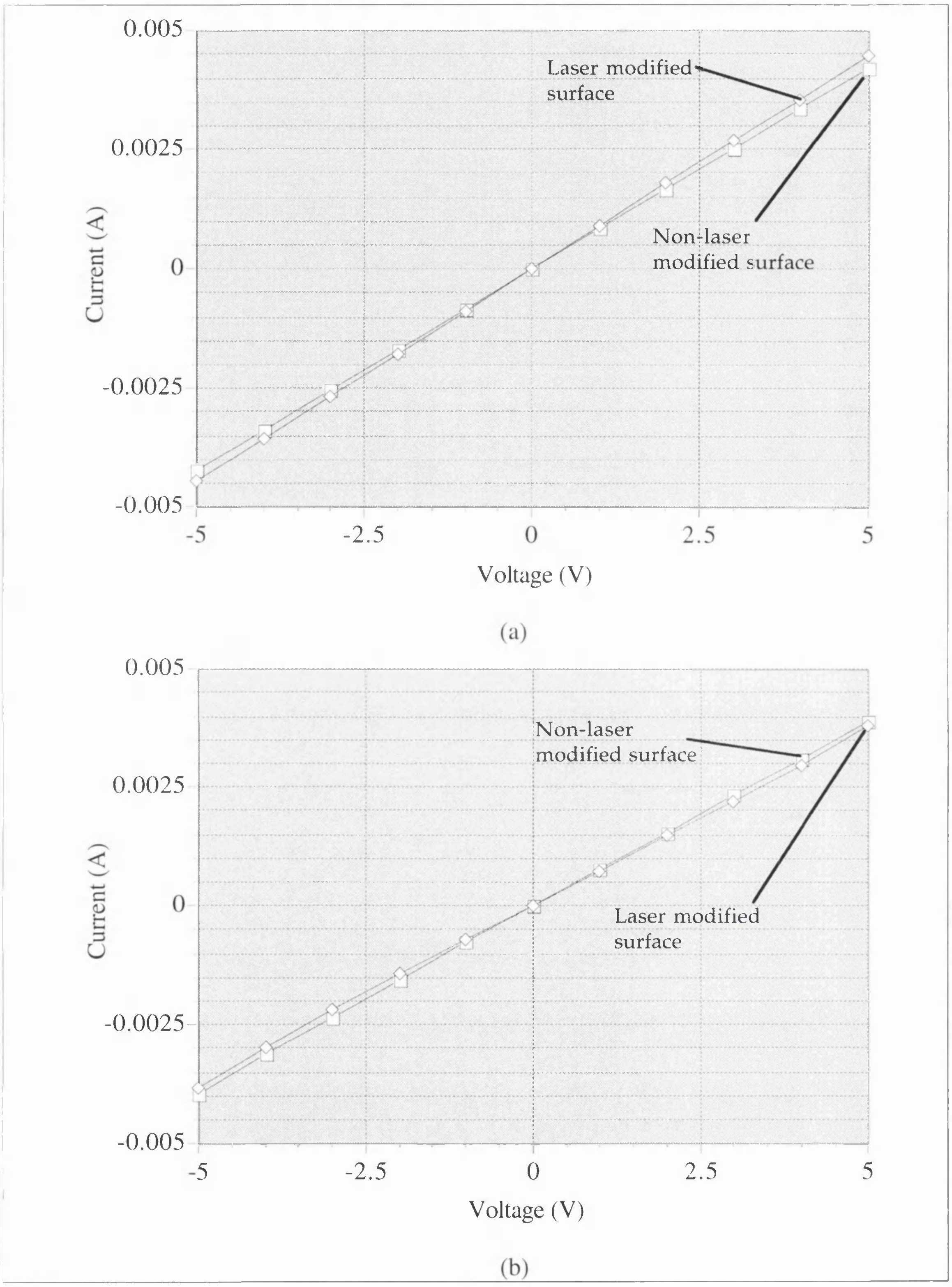

(a)

(b)

Figure 10.6 Current-voltage characteristics of (a)Au and (b) Al contact metallisations deposited on acid treated regions of 193nm laser irradiated diamond (fluence = 0.5 Jcm^{-2}) compared with similar contacts on non-laser modified material.

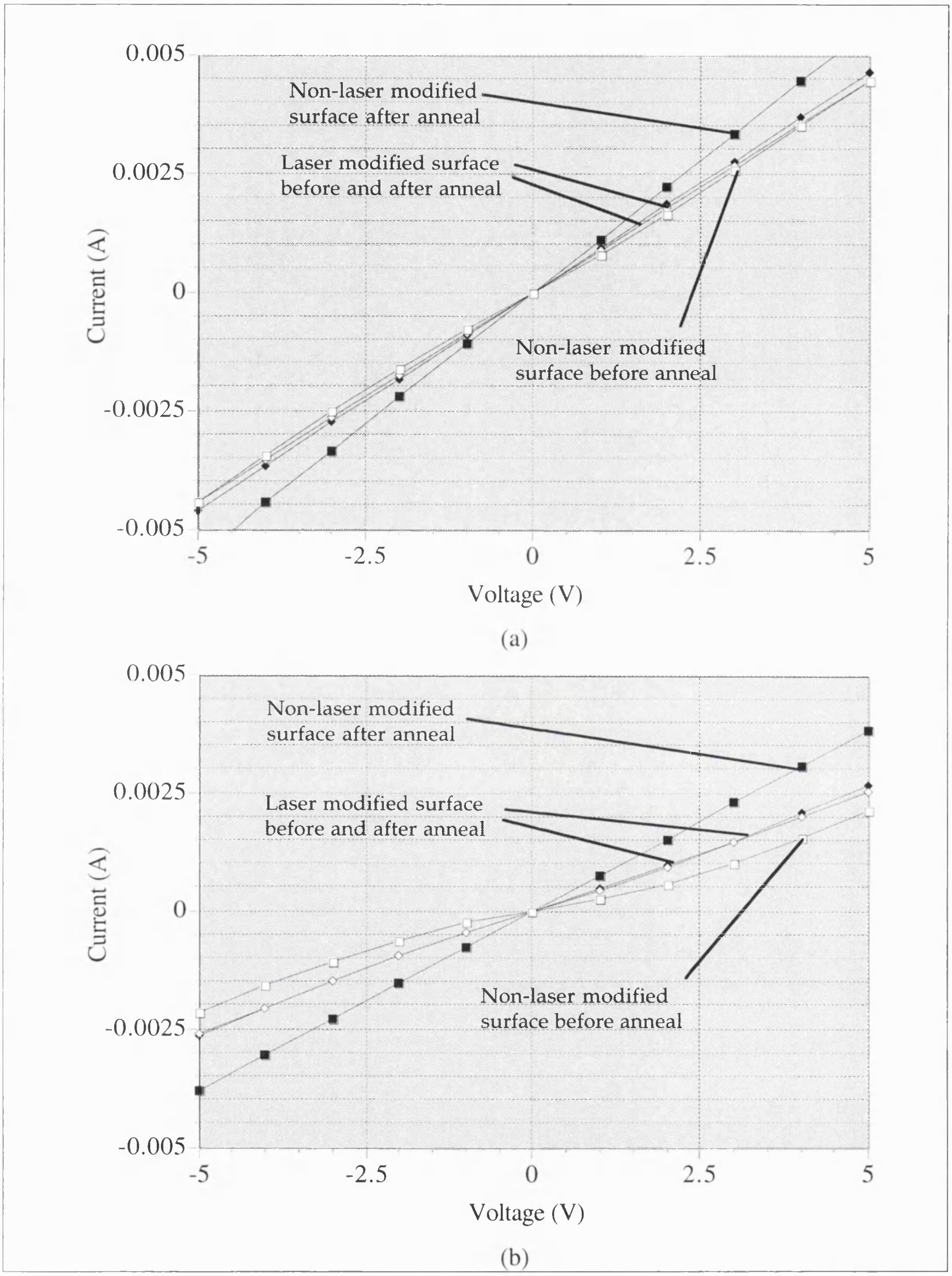

Figure 10.7 Current-voltage characteristics of Ti/Ag/Au contact metallisations (before and after a 1h air anneal) deposited on (a) laser modified + acid treated material, and (b) as-laser modified regions of 193nm laser irradiated diamond (fluence = fluence = 0.5 Jcm^{-2}). In both cases these are compared with similar contacts on non-laser modified material.

10.3.2 THICK diamond films

(a) Raman spectroscopy of surrounding material

It is of interest to consider the quality of the diamond film in the immediate vicinity of the laser processed regions; this is of particular significance in *e.g.* mechanical applications such as the microgear formed in the previous chapter (Figure 9.11). The Raman spectra shown in Figure 10.8 compares the quality of the material prior to laser processing with that at the immediate edge of one of the microgear arms. The intense peak apparent at 1332 cm^{-1} in both spectra indicates the presence of diamond; the narrow width of this peak (3 cm^{-1}), the absence of other peaks and the very low background indicate a pure diamond phase within the untreated material. Following laser irradiation (laser fluence of 12 cm^{-2}, 50k shots), this peak still dominates the spectrum but weak peaks centred around 1160 cm^{-1}, 1190 cm^{-1}, 1355 cm^{-1}, 1380 cm^{-1}, 1400 cm^{-1}, 1510 cm^{-1} and 1580 cm^{-1} are now visible.

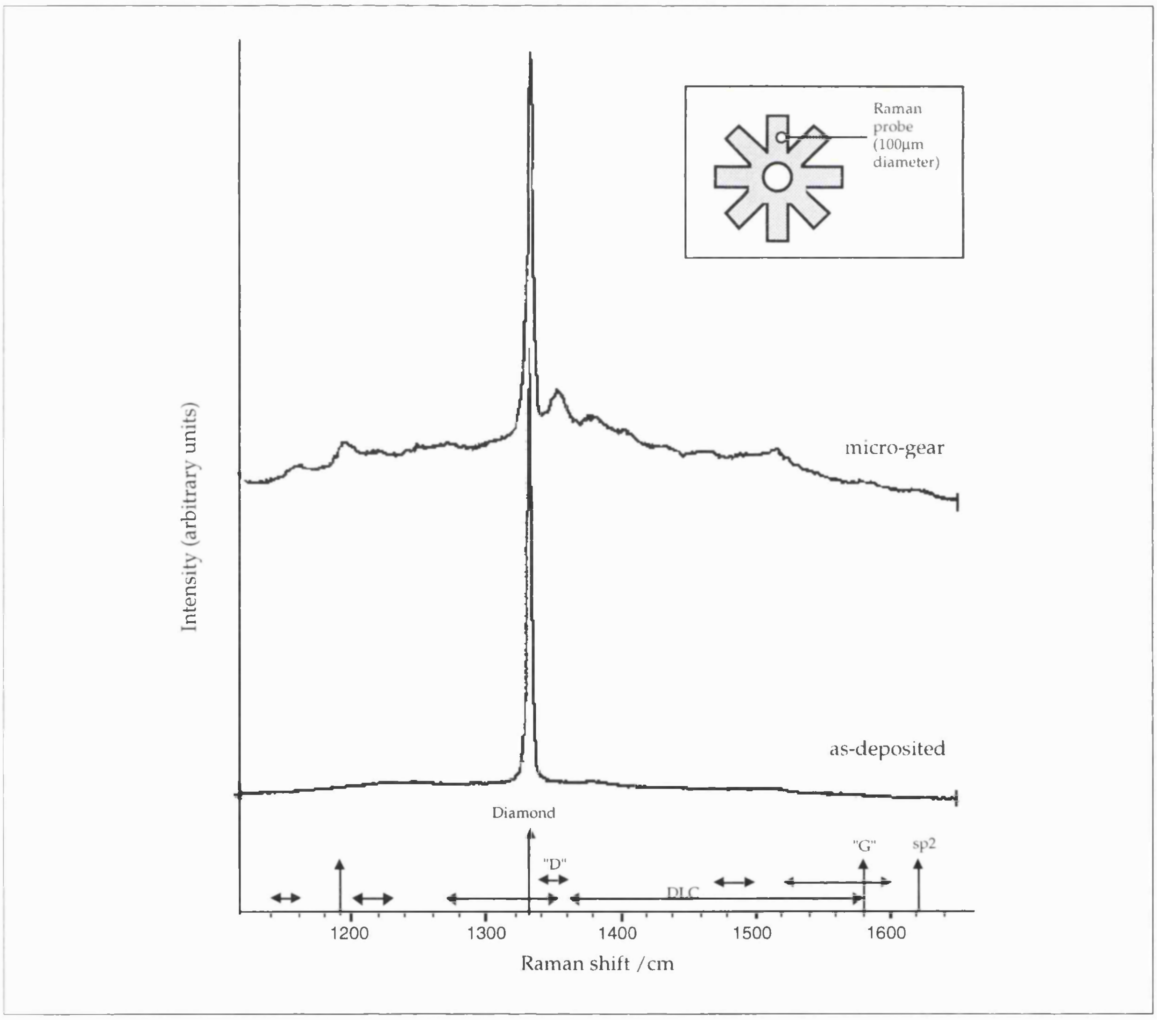

Figure 10.8 Raman spectra excited by 632.8 nm laser radiation of as-deposited diamond and of diamond in the immediate vicinity of a laser etched region as indicated by the inset.

(b) Effect of processing ambient

Raman scattering has also been deployed to investigate the quality of the diamond which remain in the regions after direct exposure to 193 nm laser radiation in an air environment; patterned squares of width 100 μm at a number of laser fluence levels were probed by a Raman beam of 100 μm diameter to reveal the spectra presented in Figure 10.9. As is evident from Figure 10.9(a), the intense Raman peak of FWHM 5 cm^{-1} situated at 1332 cm^{-1} together with the low background consisting of peaks at 1220 cm^{-1}, 1440 cm^{-1}, and 1500 cm^{-1} indicates a high quality diamond phase within the non-laser treated free-standing material. The corresponding spectrum for the substrate side of the film is shown in (b) and, although relatively stronger peaks at 1220 cm^{-1}, 1370 cm^{-1} and 1500 cm^{-1} are now present which reflects a poorer quality of the material when compared with the top surface, the strong diamond peak is again dominant. Processing of diamond with 30k laser shots proceeding from the top surface of the material results in the Raman spectra of Figure 10.9(c), (d), (e) and (f) for laser fluence levels of 4 Jcm^{-2}, 6 Jcm^{-2}, 8 Jcm^{-2} and 12 Jcm^{-2}, respectively. At the lower three fluence levels, little increase in the background is evident when compared with the signal of the non-laser treated material. Small peaks though arise; at an energy density of 4 Jcm^{-2} the 1370 cm^{-1} peak becomes more prominent and for the 6 Jcm^{-2} and 8 Jcm^{-2} conditions, the same is true for the 1340 cm^{-1} and 1580 cm^{-1} peaks. Nevertheless, examination of these spectra reveals that the 1332 cm^{-1} peak remains for all the processing conditions employed here which strongly suggests a dominating diamond phase in the processed regions. Furthermore, the diamond peaks do not display any widening of the FWHM.

Figure 10.10 displays Raman spectra for diamond modified in a similar manner to the above but in an evacuated ambient (~10^{-3} mbar); at a fluence level of 2 Jcm^{-2}, it is evident that peaks at 1330 cm^{-1}, 1580 cm^{-1} and 1620 cm^{-1} have been introduced within the Raman spectrum. These peaks are present up to a processing fluence of 8 Jcm^{-2}, but at 12 Jcm^{-2}, a significant increase in the intensity of these peaks obscure the sharp diamond peak at 1332 cm^{-1}.

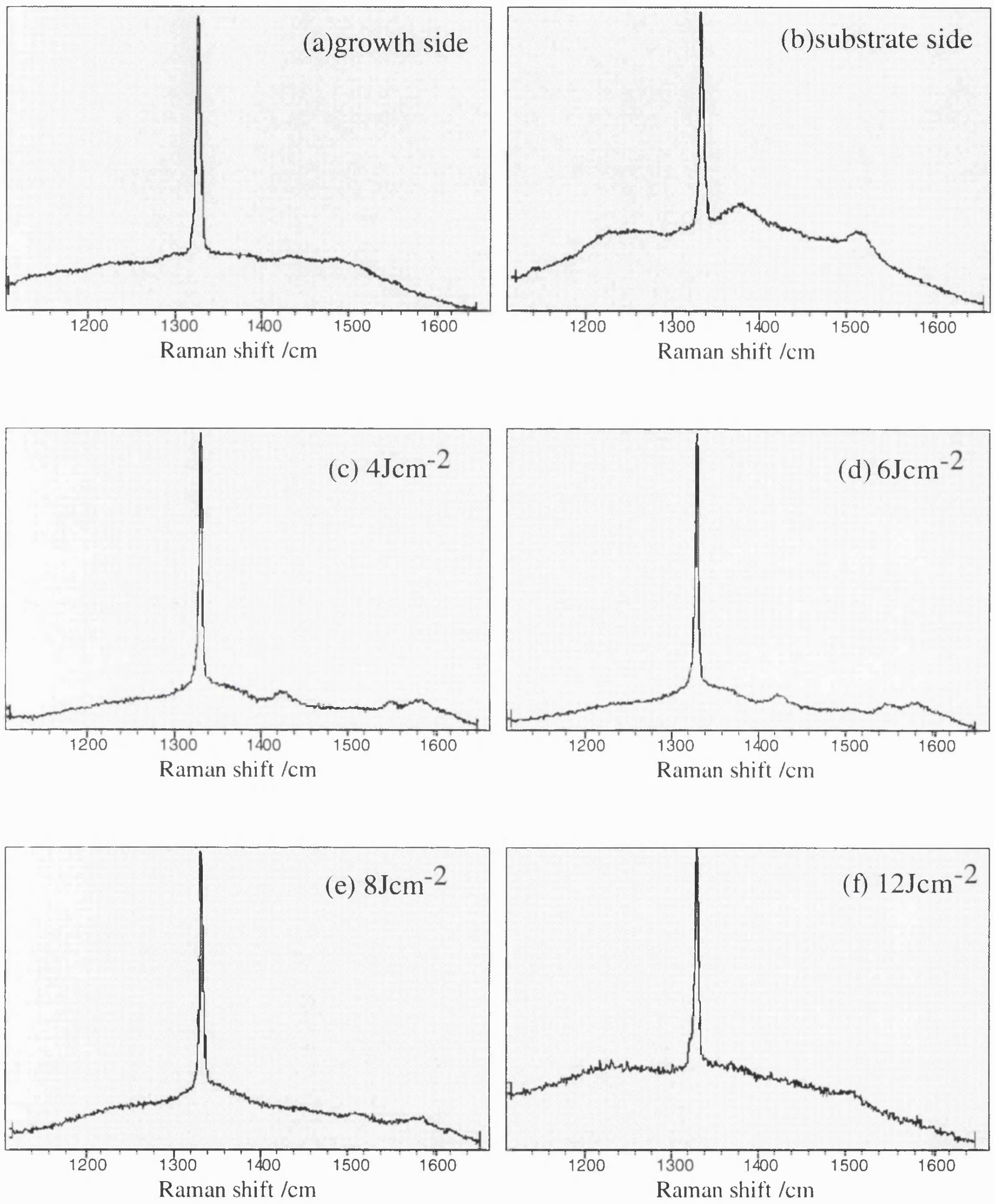

Figure 10.9 Raman scattering spectra (632.8 nm laser excitation, 100 μm diameter spot size) of non-laser exposed diamond on (a) top surface and (b) substrate surface. Corresponding spectra for 193nm laser irradiated diamond in an air ambient are also given for processing laser fluence levels of: (c) 4 Jcm^{-2}; (d) 6 Jcm^{-2}; (e) 8 Jcm^{-2} and (f) 12 Jcm^{-2}. A shot repetition rate of 20 Hz and 30k shots were used at each fluence condition.

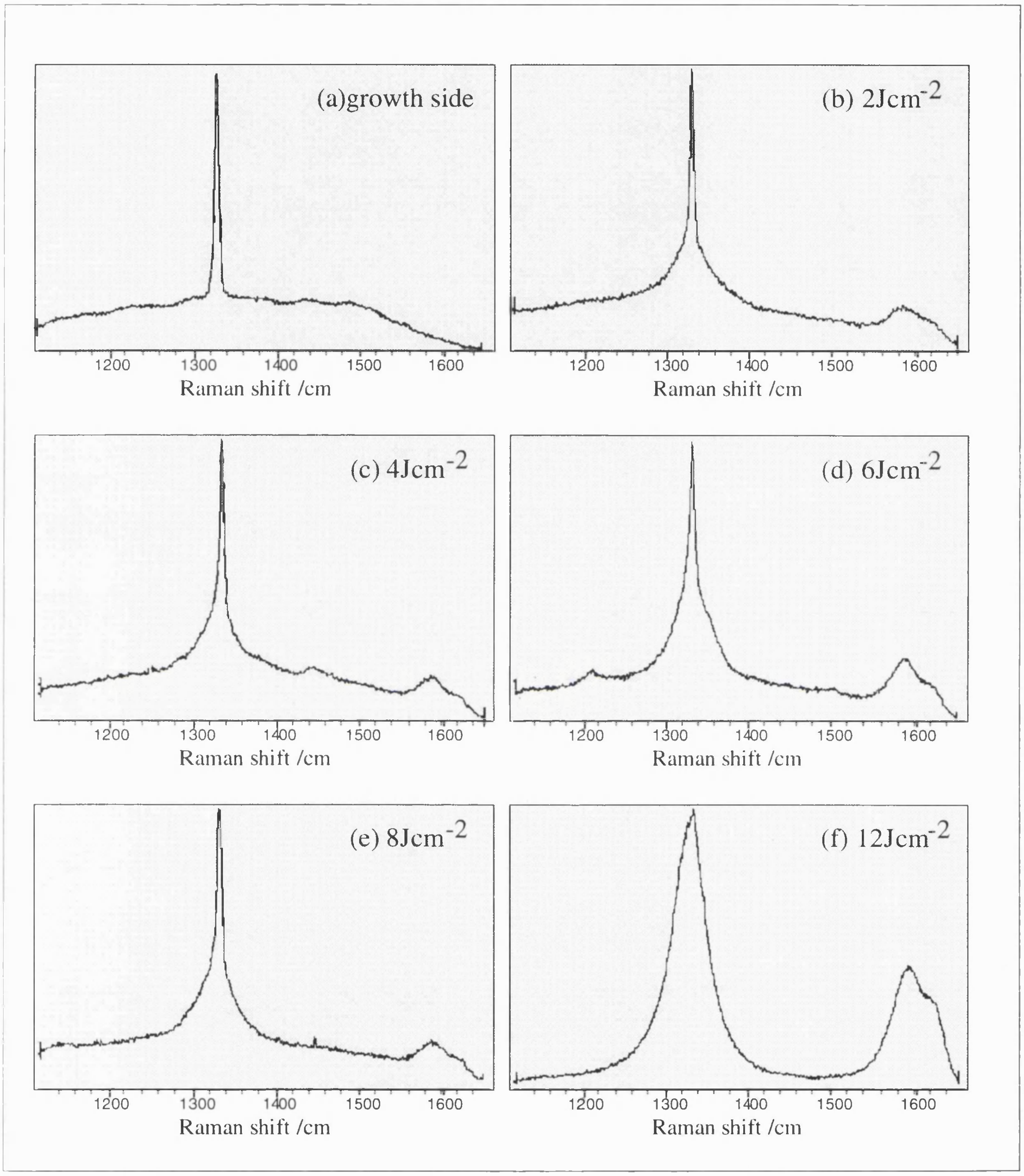

Figure 10.10 Raman scattering spectra (632.8 nm laser excitation, 100 μm diameter spot size) of non-laser exposed diamond on (a) top surface and corresponding spectra for 193nm laser irradiated diamond in an evacuated environment (10^{-3}mbar) are also given for processing laser fluence levels of: (b) 2 Jcm^{-2}; (c) 4 Jcm^{-2}; (d) 6 Jcm^{-2} (e) 8 Jcm^{-2} and (f) 12 Jcm^{-2}. A shot repetition rate of 20 Hz and 30k shots were used at each fluence.

Figure 10.11 shows a comparison of the material quality as determined by Raman spectroscopy which remains after direct exposure to 20k shots of 193 nm laser radiation at a fluence of 10 Jcm^{-2} in environments of air and electronic grade oxygen (supplied by Electra Si). Prior to processing in a pure oxygen environment, the vacuum chamber was evacuated to ~10^{-3} Torr; the chamber pressure of 20 mbar was controlled by throttling the pumping to the chamber with a 50 sccm flow of oxygen. It is evident that processing at this environment results in an increase in the background signal when compared with the non-irradiated material; the 1332 cm^{-1} diamond peak remains essentially unaltered. Processing in an air environment reveals a lower broad background intensity, but peaks at 1330 cm^{-1} and 1580 cm^{-1} are evident as previously demonstrated in Figure 10.9.

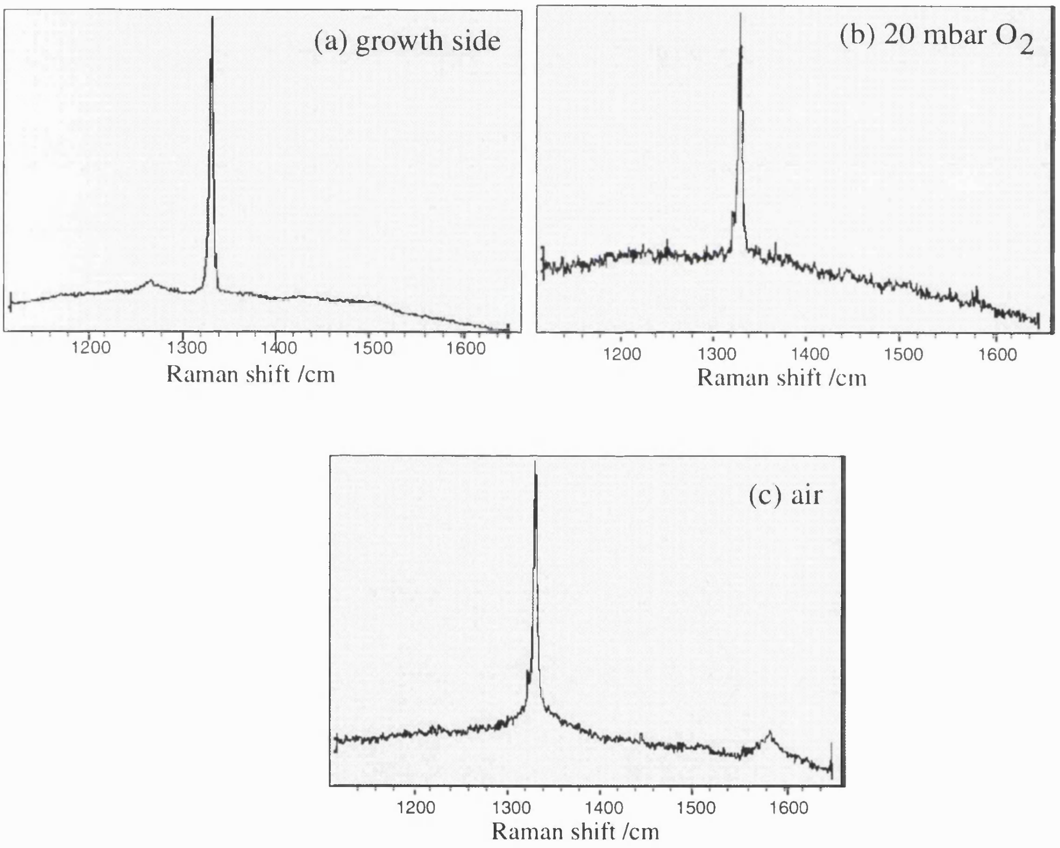

Figure 10.11 Raman scattering spectra (632.8 nm laser excitation, 100 µm diameter spot size) of (a) non-laser exposed diamond and corresponding spectra for 193nm laser irradiated diamond in: (b) 20 mbar O_2 and (c) air . 20k shots at a repetition rate of 20 Hz at a fluence of 10 Jcm^{-2} were used in each case.

(c) Effect of laser pulse repetition rate

Possible differences in material modification arising from the employment of higher laser shot repetition rates were investigated by exposing the THICK diamond to 100 μm by 100 μm patterned squares of 193 nm laser radiation at laser repetition rates of 20, 30, 40 and 50 Hz in an air ambient. At a laser fluence of 10 Jcm^{-2}, the total number of shots (pulsewidth of 20 ns) each patterned square received was 20k. Raman spectra recorded for each condition are presented in Figure 10.12; it is evident that apart from a relatively more prominent 1350 cm^{-1} peak within the 50 Hz processed film, the material remains effectively unchanged as the processing frequency is increased.

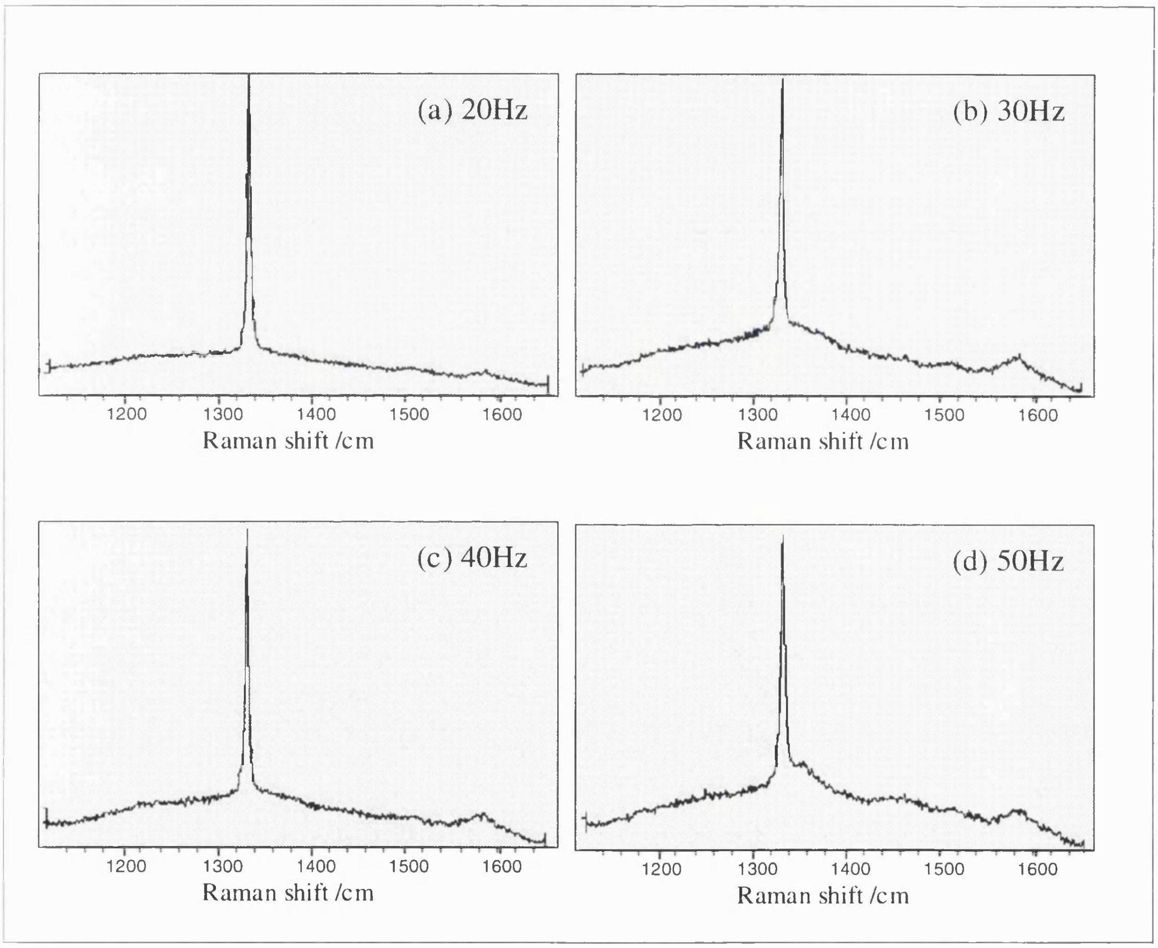

Figure 10.12 Raman spectra of diamond exposed to 193nm laser radiation of fluence 10 Jcm^{-2} at a laser repetition rate of: (a) 20Hz; (b) 30Hz; (c) 40Hz and (d) 50Hz.

10.4 DISCUSSION

Raman scattering spectroscopy has been employed to investigate the effects of laser irradiation on diamond films synthesised by chemical vapour deposition; literature reports of peaks within the Raman spectrum of diamond films arising not only from the main diamond component but also from a number of differing carbon phases are summarised in Table 10.3. At the excitation wavelength used here (632.8 nm), the probe depth of Raman scattering is a few tens of nanometers in graphitic material but is effectively a bulk characterisation technique in the case of diamond.

It is apparent that after exposure to 10 pulses of ArF laser radiation at an energy of 0.5 Jcm^{-2}, a significant diamond component still remains as demonstrated by the 1332 cm^{-1} feature (Figure 10.1). However a reduction in the DLC (diamond-like carbon) phase (peak ~1450 cm^{-1}) that was present in the diamond prior to laser processing is detectable together with an increase in the previously reported peak at 1230 cm^{-1} of ambiguous origins (amorphous diamond [Yoshikawa, 1988]; B-C bonds in doped diamond [Werner, 1994]), and also the unreported peak at 1290 cm^{-1}. This implies that the laser pulses at this energy create these latter phases primarily at the expense of DLC. As the number of laser pulses is increased to 100, the microcrystalline graphitic D (~1340 cm^{-1}) band strengthens in relative intensity (suggestions that the G band at ~1580 cm^{-1} may also increase) whilst those associated with the amorphous and nanocrystalline phases decrease; this again indicates that it is the non-crystalline diamond phases which are undergoing transformation. After 500 pulses, the D band has increased in relative intensity, being more pronounced than that in the non-irradiated material though the diamond peak is still evident. Although the nanocrystalline phases have increased in intensity relative to the spectrum obtained after 100 pulses, the relative intensity of these peaks are only comparable to those in the non-irradiated sample. The re-emergence of these features in this particular spectrum may either arise from a conversion of the diamond substrate, or else from the removal of a laser modified region leading to the exposure of the non-irradiated material to the Raman probe; the fact that there is a close correlation in the relative intensities of these particular bands with those in the non-irradiated sample supports the latter possibility. Thus, at this energy, the primary reaction driven by the laser appears to be:

diamond + nanocrystalline diamond forms ------> diamond + graphite (primarily D band) (10.1).

Raman peak position (cm^{-1})	Likely origin and previous observations
1133	Possible presence of carbon clusters containing double bonds e.g. polyacetylene(a.
1140 - 1150	Present in films with small amounts of diamond crystalline domains indicating the possible presence of nanocrystalline diamond or a precursor structure(b, c. A FWHM of 80 cm^{-1} has been quoted(d.
1190	Un-assigned band with FWHM of ~50 cm^{-1}(e.
1200 - 1230	Origins uncertain. Suggestions include amorphous diamond(f, or may be boron related(g. Also observed in annealed carbon films(h due to the breakdown of selection rules in the disordered material..
1274	Observed in low pressure acetylene flame grown diamond with FWHM of ~250 cm^{-1}(i.
1315 - 1320	Hexagonal diamond (Lonsdaleite)(a.
1332	Diamond peak(j.
1340 - 1360	"D" peak associated with microcrystalline graphite (grain size < 25 nm). Appears due to a breakdown of selection rules, and broadens with disorder(a, d, i.
1271 - 1353	Observed in carbon films. Annealing believed to increase the number or size of crystallites, as well as removing disorder; assigned to "D" peak(h.
1470 - 1500	Origins uncertain; suggestions include a diamond precursor (FWHM = 80 cm^{-1})[d], and amorphous carbon rich SiC material(b.
1357 - 1580	Diamond-like carbon material; Raman spectrum consists of several overlapping components within this band(a,f.
1580	"G" peak associated with single crystalline graphite which broadens with disorder within the carbon sheet(a.
1520 - 1600	Observed in carbon films. Annealing believed to increase the number or size of crystallites, as well as removing disorder; assigned to "G" peak(h.
1620	Disordered sp^2 carbons; present due to a breakdown of selection rules in fine crystalline material(a.

Table 10.3 Summary of Raman peak positions as observed in the literature; (a[Knight, 1989a], (b[Nemanich, 1988], (c[Obratzsov, 1994], (d[Bachmann, 1991], (e[Bachmann, 1994], (f[Yoshikawa, 1988], (g[Werner, 1994], (h[Dillon, 1984], (i[Knight, 1989b], (j[Solin, 1970].

At the higher laser intensity of 2 Jcm^{-2}, 10 pulses leads to a spectrum consisting of the diamond peak super-imposed on features primarily relating to crystalline graphite (both the D and G bands); by 100 pulses, peaks relating to nanocrystalline diamond have again emerged. This suggests that at this level of laser intensity, the amorphous/nanocrystalline phases present in the diamond film is converted or removed more efficiently whilst promoting the formation of crystalline graphite, *i.e.*

diamond + nanocrystalline diamond forms ------> diamond + graphite (D + G bands) (10.2).

Indeed, a comparison of Raman spectra for irradiated material as a function of laser intensity (Figure 10.3(a)) emphasises the significant effect of this laser parameter in the process; it is clear that as the laser intensity is increased, the crystalline graphitic form becomes increasingly dominant as the other non-diamond forms fade in relation to the non-irradiated material. After treating the non-irradiated sample to the acid treatment described in Chapter 5, a decrease in the DLC component is evident; however this appears to be associated with the appearance of stronger nanocrystalline/amorphous features at ~1200 cm^{-1}. More prominent though, is the effect of the acid-based solution on the graphitic elements present after irradiation; a strong reduction in both the crystalline graphitic D and G peaks is observed after this treatment. Hence the possibility exists for the acid treatment either to remove surface graphite to expose nanocrystalline features present in the non-irradiated films to the Raman probe, or else to convert the graphite to such forms.

The increased modification of the diamond material, and in particular the top 3 atomic layers, with increasing laser intensity is also well illustrated by Auger electron spectroscopy (Figure 10.4(b)); marked differences are observed in the fine line spectra of films exposed to 0.5 Jcm^{-2} and 1 Jcm^{-2} of 193 nm radiation. At 0.5 Jcm^{-2}, a deterioration in the quality of the diamond samples may be deduced from the reduced P_0/A_1 ratio, though the ability to identify the two maxima associated with the main Auger peak at 268 eV in the intensity ratio observed suggests that the surface of the material has not been completely converted to the amorphous or graphitic carbon forms. The new peak in the spectra with a minimum at 290 eV has been reported previously by Hoffman *et al.* [1994] for a type IIa natural diamond crystal but was not observed on CVD diamond films; no assignment was offered. However, Chia and co-workers [1994] show a weak peak at this energy on spectra derived from CVD diamond material. To originate from the carbon film, this peak must either be a high energy satellite peak caused by energy 'gain' from a plasmon, or from an Auger transition from a doubly ionised inner shell [Lurie, 1977].

However, the energy difference between the primary peak minima and this peak precludes the former explanation. Alternatively, calcium contamination (290 eV [Schrader, 1978]), either via handling or present in the bulk, may have occurred though this is considered unlikely due to the common observation of this peak on all the laser processed samples.

At the higher laser energy of 1 Jcm^{-2}, the Auger primary peak minima is seen to shift 3 eV to 271 eV. This shift and the change in the nature of the fine structure *i.e.* the change in the ratio of the P_0/A_1 parameter is consistent with the presence of a graphitic surface [Pate, 1986; Bugaets, 1994; Hoffman, 1994] and hence is in good agreement with the observations gathered from the Raman spectra. Furthermore, in addition to the peak at 290 eV which was observed in the samples processed at 0.5 Jcm^{-2}, a new feature at 278 eV has been introduced; neither of these features have been observed on well defined graphite surfaces. Hoffman *et al.* [1994] and Stefan *et al.* [1991] have reported the weak peak at 278 eV on argon ion irradiated carbon films and it was attributed to irradiation promoted point defects.

The results of the metal contacts on the highly doped THIN diamond samples demonstrate that for metals possessing little or no reactivity with the diamond surface, namely the metals Al and Au used here, the electrical behaviour of contacts on laser irradiated material, at least for low laser energy densities, remains effectively unchanged. In contrast, the observations made for the reactive Ti metallisation leads to the conclusion that modification of the diamond surface has indeed taken place at the energy density of 0.5 Jcm^{-2}. The change in behaviour which occurs during the annealing stage for the modified and unmodified material may arise from a differing degree of carburization, being affected by the disruption in material quality caused by laser exposure. Moazed *et al.* [1990] and Kawaguchi *et al.* [1994] have previously reported an optimum time for annealing, with this phenomenon suggested to be a result of the degree of carburization. Results of diamond modification induced by the same energy density used here (0.5 Jcm^{-2}) was presented by Geis and co-workers [1989] who suggested that this modified layer, which was approximately a few nanometers below the surface diamond layer as judged by transmission electron microscopy, was a combination of diamond together with graphite-like carbon phases (by electron diffraction). Furthermore, this layer which was found to be resistant to both an acid treatment consisting of CrO_3 and also He-O plasma, was not detectable by Raman spectroscopy. Bogli and co-workers [1992; 1993] have also examined the modified layer produced as a result of exposing polycrystalline diamond layers to 193 nm radiation at an energy density of 3 Jcm^{-2}; it was inferred from atomic force microscopy that a topmost graphitic layer of thickness 150-200 nm was present on top of an unidentified layer. In a similar manner, the metal contacts presented here display an unchanged behaviour both before and after an acid treatment thus suggesting a layer is present which is also resistant to such treatments. The fact that processing at 0.5 Jcm^{-2} leads to an unidentified 290 eV Auger peak may suggest that a connection exists between this peak and the unidentified layers of Geis *et al.* [1989] and Bogli *et al.* [1993] though this remains speculative without further investigation.

Johnston *et al.* [1993] have previously reported the difference in the rate of material removal with an ArF laser for three CVD films of varying quality as judged by Raman spectroscopy; the fact that the rate of material removal was the highest for the lowest quality film and *vice versa* suggests that the actual material quality is an important consideration. Indeed, when compared with the lower quality THIN films, the Raman scattering results of the irradiated THICK diamond films indicate that the *quality* of the irradiated material and not just the rate of material removal depends on the initial state of the films; at energy levels of at least up to 12 Jcm^{-2} (*c.f.* 2.5 Jcm^{-2} in the THIN film case), neither graphitisation of the films nor deterioration of the diamond component appears to have occurred to any significant extent. Indeed, any variation within the spectra may be related to that already present within the film if the quality of the irradiated material is compared with the substrate side of the free-standing films. Nevertheless, graphitisation of high quality material may also occur if the processing environment is not controlled. Several authors have commented on the relevance of the processing ambient [Rothschild, 1986; Yoshikawa, 1990; Bhushan, 1994; Ral'chenko, 1995] though conclusive evidence has not previously been presented. In a paper by Rothschild and co-workers [1986], ArF excimer laser etching was carried out on type IIa natural crystals in a number of different ambients; from profilometer traces of features processed *in-vacuo,* graphitic build-up was suggested which was reduced if the processing was carried out in NO_2, O_2 or Cl_2. Ral'chenko and co-workers [1995] have reported the lack of etching of fine-grained diamond films (< 1 μm) when Ar^+ laser processing was carried out *in-vacuo* instead of air or a pure O_2 atmosphere. The characterisation here of ArF irradiated regions of material of the same origin at corresponding laser energy densities in air and *in-vacuo* (Figures 10.9 and 10.10 respectively) reveal that graphitisation occurs only in the latter case. Indeed Raman spectroscopy suggests that the end-product of this modification is a sole conversion to microcrystalline graphite with classic peaks appearing at 1330-1340 cm^{-1}, 1580 cm^{-1} and 1620 cm^{-1} [Knight, 1989b]. The fact that processing in pure O_2 ambients (Figure 10.11) also leads to Raman spectra indicating little graphitisation strongly suggests that it is the role of oxygen in air which is significant in the etching of diamond. In addition, wide-scan Auger analysis of the THIN film diamond have shown that oxygen remains on the surface of the material after laser processing; the fact that this oxygen component is stable to a 600 °C heat treatment *in-vacuo* implies a chemical interaction with the diamond/carbon surface.

10.5 SUMMARY

The employment of ArF excimer laser irradiation for the processing of diamond films has been shown here to lead to material modification which may alter the electrical behaviour of metal-diamond interfaces. Graphitisation of the diamond surface by irradiation with ArF excimer lasers has been demonstrated by both Raman spectroscopy and, for the first time to the author~~'~~s' knowledge [Baral, Chan and Jackman, 1995], by Auger electron spectroscopy. However the degree and extent of this conversion has been demonstrated to vary not only as a function of laser intensity but also to critically depend on the initial quality of the films. Moreover, the chemical integrity of the exposed regions have been shown to be severely affected by the processing ambient. The fact that oxygen presence has been demonstrated to be of critical significance if the diamond component is to be maintained, together with the oxygen signal in Auger spectra implies that a photochemically assisted material removal mechanism is in operation and that this is in competition with the rate of graphitisation when the quality of the product is under consideration. Figure 10.13 summarises the quality of the remaining product after ArF laser processing encompassing these process controllable parameters.

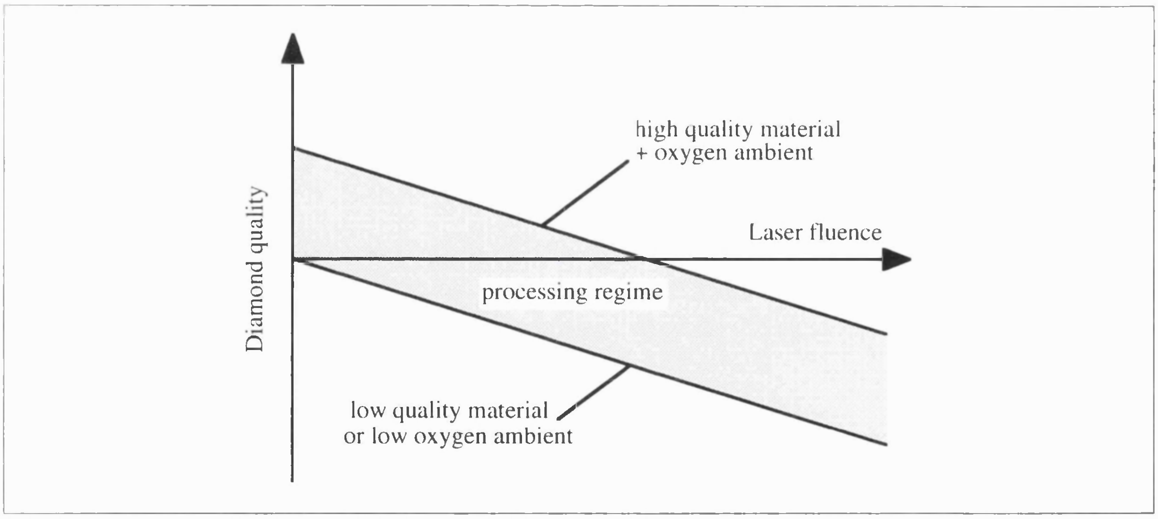

Figure 10.13 Summary of diamond quality after ArF excimer laser processing as a function of initial material quality and processing ambient (oxygen).

REFERENCES

Ageev, V.P., Builov, L.L., Konov, V.I., Kuzmichev, A.V., Pimenov, S.M., Prokhorov, A.A.M., Ral'chenko, V.G., Spitsyn, B.V. and Chapliev, B.I., [1989]. *Sov. Phys. Dokl.,* **33**, 840.

Ager III, J.W., Viers, D.K. and Rosenblatt, G.M., [1991]. *Phys. Rev.,* **B43**, 6491.

Bachmann, P.K. and Wiechert D.U., [1991] in "Diamond and Diamond Like Films and Coatings" (edited by R.E. Clausing *et al.*), Plenum Press, New York, USA.

Bachmann, P.K., Bausen, H.D., Lade, H., Leers, D., Wiechert, D.U., Herres, N., Kohl, R. and Koidl, P., [1994]. *Diamond Relat. Mater.*, **3**, 1308.

Baral, B., Chan, S.S.M. and Jackman, R.B., [1995]. *J. Vac. Sci. Technol.* (in press).

Bhushan, [1994]. *Diamond Films Technol.*, **4**, 71.

Bogli, U., Blatter, A., Pimenov, S.M., Smolin, A.A. and Konov, V.I., [1992]. *Diamond Relat. Mater.*, **1**, 782.

Bogli, U., Blatter, A., Bachli, A., Luthi, R. and Meyer, E., [1993]. *Diamond Relat. Mater.*, **2,** 924.

Bugaets, O.P., Smekhnov, A.A. and Kuzenkov, S.P., [1994]. *J. Electron Spectros. & Relat. Phenom.*, **68**, 713.

Chia, Q.S., Younes, C.M., Partridge, P.G., Allen, G.C., May, P.W. and Rego, C.A., [1994]. *J. Mater. Science*, **29**, 6397.

Davis, L.E., MacDonald, N.C., Palmberg, P.W., Riach, G.E. and Weber, R.E., [1976]. *Handbook of Auger spectroscopy,* Physical Electronics Industries, Edan Prairie, MN, USA.

Deshmukh, S., Hitchcock, L.M., Rothe, E.W. and Reck, G.P., [1994]. *Diamond Relat. Mater.,* **3**, 195.

Dillon, R.O., Woolam, J.A. and Katatanant, V., [1984]. *Phys. Rev.*, **B29**, 3482.

Geis, M.W., Rothschild, M., Kunz, R.R., Aggarwal, R.L., Wall, K.F., Parker, C.D., McIntosh, K.A., Efremow, N.N., Zayhowski, J.J. and Ehrlich, D.J., [1989]. *Appl. Phys. Lett.*, **55,** 2295.

George, T., Foote, M.C., Vasquez, R.P., Fortier, E.P. and Posthill, J.B., [1993]. *Appl. Phys. Lett.*, **62,** 2880.

Hoffman, A., [1994]. *Diamond Relat. Mater.,* **3**, 691.

Kawaguchi, G., Nakanishi, J., Otsuki, A., Oku, T. and Murakami, M., [1994]. *J. Appl. Phys.*, **75**, 5165.

Johnston, C., Chalker, P.R., Buckley-Golder, I.M., Marsden, P.J. and Williams, S.W., [1993]. *Diamond Relat. Mater.*, **2,** 829.

Knight, D.S. and White, W.B., [1989a]. *J. Mater. Res.*, **4**, 385.

Knight, D.S. and White, W.B., [1989b]. *Proc. SPIE,* **1055**, 144.

Konov, V.I., Kononenko, T.V., Pimenov, S.M., Smolin, A.A. and Chapliev, N.I., [1991]. *Sov. J .Quantum Electron.*, **21**, 1112.

Lurie, P.G. and Wilson, J.M., [1977]. *Surf. Sci.*, **65**, 476.

Miyazawa, H., Miyake, S., Watanabe, S., Murakawa, M. and Miyazaki, T., [1994]. *Appl. Phys. Lett.*, **46,** 387.

Moazed, K.L., Zeidler, J.R. and Taylor, M.J., [1990]. *J. Appl. Phys.*, **68**, 2246.

Nemanich, R.J. and Solin, S.A., [1979]. *Phys. Rev.*, **B20**, 392.

Nemanich, R.J., Glass, J.T., Lucovsky, G. and Shroder, R.E., [1988]. *J. Vac. Sci. Technol.*, **A6**, 1783.

Obratzsov, A.N. and Pirogov, V.G., [1994]. *Diamond Films Technol.*, **4**, 243.

Pate, B.B., [1986]. *Surf. Sci.*, **165**, 83.

Pimenov, S.M., Smolin, A.A., Ralchenko, V.G., Konov, V.I., Likhanski, S.V., Veselovski, I.A., Sokolina, G.A., Bantsekov, S.V. and Spitsyn, B.V., [1993]. *Diamond Relat. Mater.*, **2**, 291.

Ral'chenko, V.G., Korotushenko, K.G., Smolin, A.A. and Loubnin, E.N., [1995]. *Diamond Relat. Mater.*, **4**, 893.

Rothchild, M., Arnone, C. and Ehrlich, D.J., [1986]. *J. Vac. Sci. Technol.,* **B4**, 1986, 310.

Schrader, M.E., [1978]. *Surf. Sci.,* **78**, L227.

Solin, S.A. and Ramdas, A.K., [1970]. *Phys. Rev.*, **B1**, 1687.

Steffan, H.F., Roux, Marton, D. and Rabalais, J.W., [1991]. *Phys. Rev.,* **B44**, 3981.

Tachibana, T. and Glass, J.T., [1992]. *J. Appl. Phys.,* **72**, 5912.

Tsai, H. and Bogy, D.B., [1987]. *J. Vac. Sci. Technol.*, **A5**, 3295.

Werner, M., Dorsch, O. Baerwind, H.U., Obermeier, E., Harper, R.E., Johnston, C., Chalker, P.R. and Buckley-Golder, [1994]. *Appl. Phys. Lett.,* **64**, 595.

Vidano, R.P., Fischbach, D.B., Willis, L.J. and Loehr, T.M., [1984]. *Solid State Comms.*, **39**, 341.

Yoshikawa, M., Katagiri, G., Ishida, H., Ishitani, A. and Akamatsu, T., [1988]. *Solid State Comms.,* **66**, 1177.

Yoshikawa, M., [1990]. *Proc. SPIE*, **1325**, 210.

11: THIN FILM DIAMOND FIELD EFFECT TRANSISTOR

11.1 INTRODUCTION

Theoretical predictions suggest that electronic devices based on semiconducting diamond offer the prospect of superior characteristics in terms of high temperature operation. Experimental reports of diamond devices demonstrating transistor action have been provided by authors including Prins [1982] and Geis [1982] on natural and high pressure high temperature (HPHT) crystals, respectively. Both of these reports were of bipolar-type structures, and, although transistor action was demonstrated up to 510 °C [Geis, 1982], the difficulties in controlling the quality of the doped regions resulted in non-ideal transistor characteristics. The lack of a suitable n-type dopant for diamond suggests that diamond field-effect transistors [Sze, 1981] may provide better performance. Field-effect transistors (FETs) may be realised by two basic structures; the metal-semiconductor field-effect transistors (MESFETs) based on the depletion layer of a Schottky contact, and the metal-insulator semiconductor field-effect transistor (MISFET) with a capacitor-type gate. Zeisse *et al.* [1991] reported a MISFET with a 210 nm thick ion-implanted active layer in natural diamond with an insulating SiO_2 gate layer; current saturation and pinch-off were observed at room temperature though high temperature operation was not investigated. The economic costs and difficulties in the fabrication of complex device structures arising from the size and shape of natural or HPHT crystals are, however, prohibitive. Nevertheless, improvements in the quality of semiconducting thin film diamond layers has enabled active electronic devices to be investigated on this type of material. MESFETs [Shiomi, 1990] and MISFETs with SiO_2 gates [Gildenblat, 1991; Grot, 1992] have been demonstrated on homoepitaxial diamond films though neither complete current saturation nor channel pinch-off were observed in these reports. More ideal transistor characteristics have been reported by Fox and co-workers [1995] on homoepitaxial material; current saturation and channel pinch-off was evident at the elevated temperature of 773 K. On polycrystalline material, MISFETs employing SiO_2 insulating gate layers have been demonstrated by Kiyota *et al.* [1991] and Tessmer *et al.* [1992; 1993], with the latter report showing channel modulation at 285 °C. Nishimura and co-workers [1994] first demonstrated the use of intrinsic diamond as the insulating gate layer on polycrystalline material; performance at 398 K was degraded as a result of gate leakage.

This study aims to design and fabricate high temperature operational thin film polycrystalline diamond transistors based on the processing techniques developed in the preceding chapters. MISFET structures have been chosen for device implementation to achieve low leakage currents without the requirement of high performance Schottky contacts as in MESFETs. Since the quality of the SiO_2-diamond interface does not appear to have been fully characterised on polycrystalline material, an insulating diamond gate is preferred in the aim of reducing interfacial defects between the insulating and active layers; such defects degrade gate induced modulation of the channel.

11.2 EXPERIMENTAL DETAILS

(a) Device structure and implementation

The MISFET structure is shown schematically in Figure 11.1 with a gate length, width, and source to drain separation of 30 μm, 100 μm and 50 μm respectively. The rough surface nature of as-deposited diamond films reduces the alignment accuracy which may be achieved during device fabrication with standard photolithographic mask aligners; the critical device dimension in the design is +/-15 μm. As apparent in Figure 11.1, the device consists of an active p-layer channel on top of an intrinsic diamond layer, which minimises conduction via the underlying silicon substrate. Connection of the source and drain contacts to the channel is via boron ion implantation step through the depth of the insulating diamond gate layer. The fabrication sequence is presented in Appendix E (photomasks produced by the Rutherford Appleton Laboratory (Chilton, Didcot)).

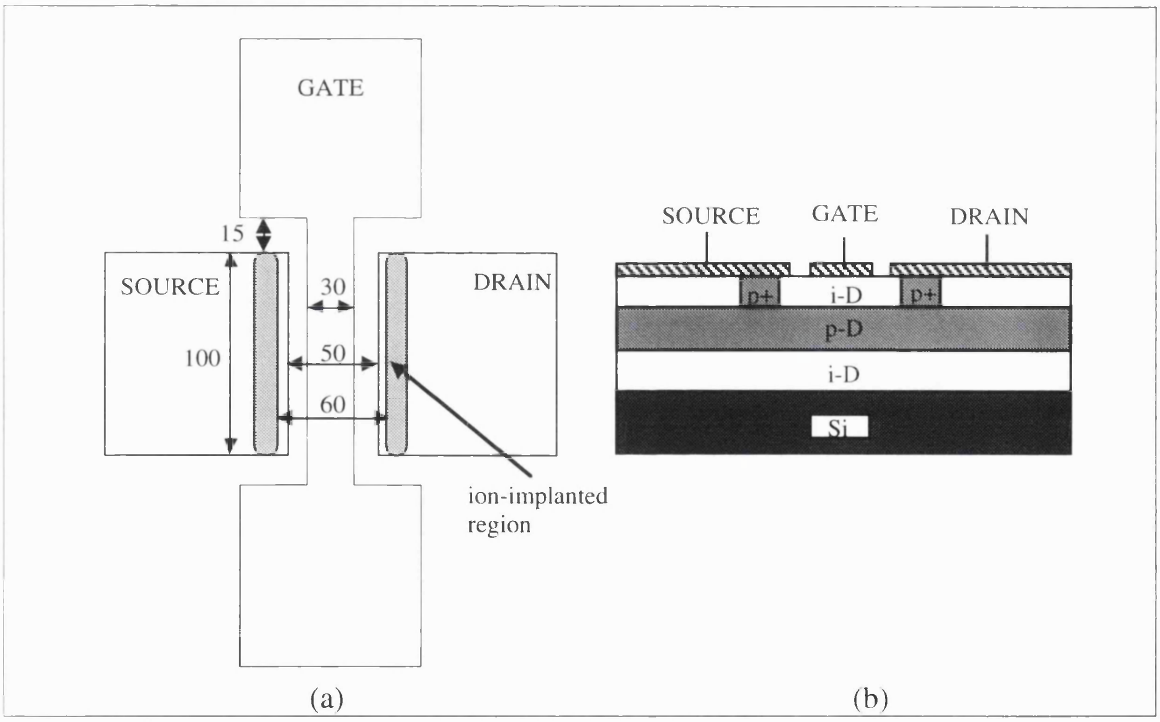

Figure 11.1 Diamond MISFET : schematic views of (a) plan; and (b) cross-section of device structure with dimensions in μm.

(b) Material preparation and device fabrication

An intrinsic diamond layer of thickness ~20 μm was deposited on a Si (100) substrate by the technique of microwave plasma assisted chemical vapour deposition. The diamond wafer consisted of randomly-aligned crystallites with a top surface grain size of ~5 μm; Raman scattering from the film demonstrated a sharp 1332 cm^{-1} diamond peak. Prior to device fabrication, the diamond wafer was annealed in air for 1 h at 430 °C, and subsequently chemically treated as described in Appendix B for the removal of non-diamond components. An optical photograph of the completed device structure is shown in Figure 11.2. Ion implantation of the source and drain regions with boron was carried out with a 120 keV implant followed by a 90 keV dose [P.R. Chalker (AEA Technology), private communications]) to form heavily doped p^+ regions for the creation of ohmic contacts. Metallisation of the implanted source and drain regions was done by thermally evaporating Ti-Ag-Au contacts as described in Chapter 7. A final metal layer of Au allowed the gate, source and drain regions to be probed and/or bonded. Finally, the devices were annealed in air for a further 1 h in air at 430 °C to stabilise the ohmic contact formulation.

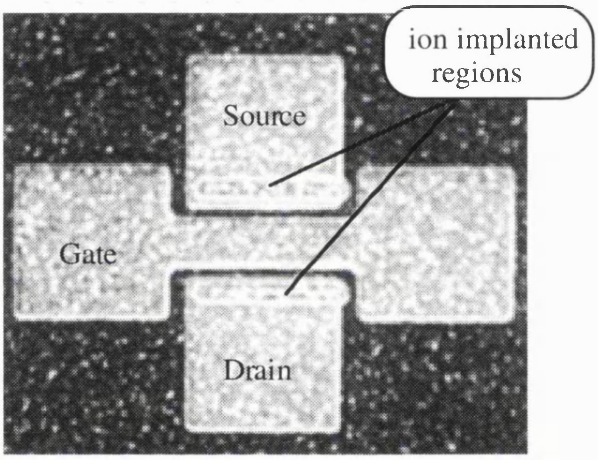

Figure 11.2 Optical micrograph of a completed MISFET device.

Secondary ion mass spectroscopy (SIMS) was used to determine the actual thickness and B concentration of the diamond layers; the boron implant through the source and drain regions gave peak B concentrations of 10^{20} cm^{-3} at 0.15 μm from the surface and 5 x 10^{19} cm^{-3} at 0.4 μm, remaining above 6 x 10^{17} cm^{-3} to a depth of 1.3 μm; the active channel was shown to be 0.7 μm thick with a B concentration of 2 x 10^{19} cm^{-3}. The SIMS profile also showed that the intrinsic diamond gate was 1.3 μm thick with a B level not detectable above the background signal in the SIMS instrument. Source to drain current-voltage (I_{ds}-V_{ds}) characteristics were measured using the Hewlett Packard 4061A parameter analyser as a function of applied gate bias and operating temperature.

11.3 RESULTS

Figure 11.3 shows the I_{ds}-V_{ds} characteristics for a typical device operated at 150 °C. At zero applied gate bias, increasing V_{ds} values can be seen to increase I_{ds}. As V_g is made increasingly positive, the current flow (I_{ds}) decreases to a value associated with leakage through the gate (nanoamperes), and hence, an applied positive gate bias can be used to "pinch-off" I_{ds}. Thus, gate promoted modulation of the channel current is occurring. At a negative bias of 10 V and a V_{ds} value of -100 , I_{ds} reaches a value of 0.7 μA, which indicates an enhancement of channel current. However the I_{ds}-V_{ds} characteristics shown in Figure 11.3 do not show current saturation occurring over the voltage range investigated.

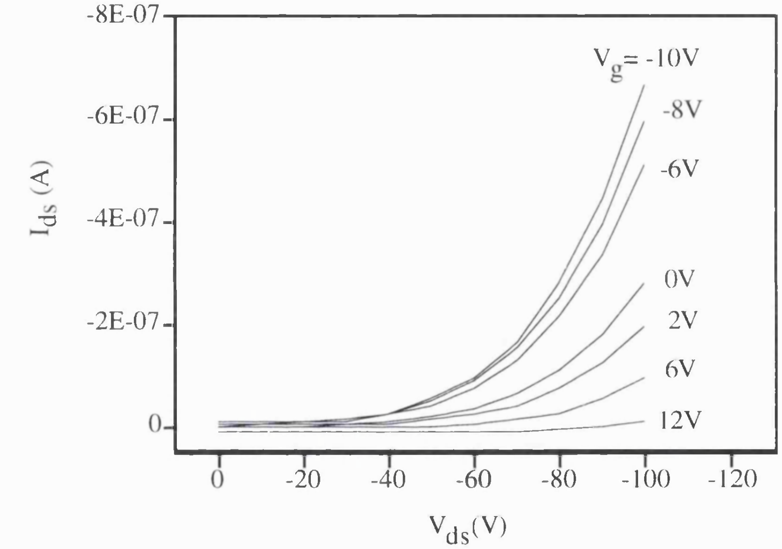

Figure 11.3 I_{ds}-V_{ds} characteristics of a MISFET operated at 150 °C.

I_{ds}-V_{ds} characteristics typical of the device operated at 300 °C are shown in Figure 11.4; current levels are significantly higher than those seen at 150 °C. High levels of gate promoted current modulation and pinch-off are revealed. The source to gate leakage current at this temperature was measured to be less than 10 nA. At a V_{ds} value of -100 V and zero gate bias, I_{ds} is around 0.2 μA; a V_g of +2 V gave an I_{ds} of -37nA. I_{ds} values as high as -17 μA can be promoted by application of negative V_g values. However, the 300 °C I-V characteristics do not show saturation over the V_{ds} values investigated.

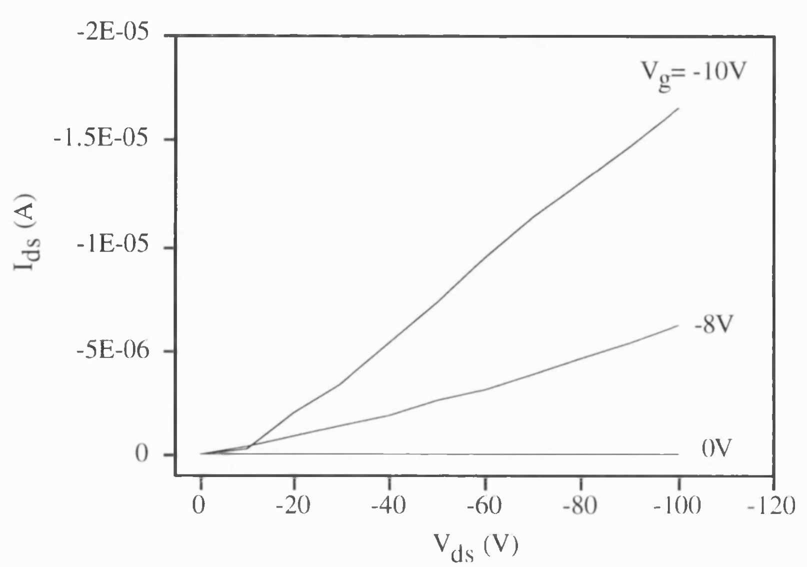

Figure 11.4 I_{ds}-V_{ds} characteristics of a MISFET operated at 300 °C.

11.4 DISCUSSION

Modulation and pinch-off of the channel current by application of a gate voltage have been observed at both 150 °C and 300 °C. Positive gate biases lead to depletion-mode characteristics while negative gate biases induce enhancement-mode characteristics. In a conventional transistor a linear increase in I_{ds} can be expected for increasing V_{ds} values (the 'linear' region) until V_{ds} is sufficiently high to pinch off the channel and cause current saturation (the 'saturation' region) [Sze, 1981]. This latter region is important for stable switching with FET structures. Neither of the temperatures investigated here revealed saturation; the most likely explanation lies in the fact that for the implantation parameters used, the channel region is sufficiently thick that higher V_{ds} values would be required to bring on saturation. At 300 °C the 'ohmic' region expected at lower V_{ds} values is clearly seen, but at 150 °C the channel current increases non-linearly. The low doping density within the regions connecting the source and drain implantations to the channel results in a highly-resistive/barrier layer at this region. At 300 °C the boron is sufficiently ionised to avoid this problem.

The transconductance, g_m of a FET is an important figure of merit describing control of the channel current by the gate bias; g_m values were determined from the I-V characteristics according to Equation 11.1 [Sze, 1981].

$$g_m = \left.\frac{\partial I_{ds}}{\partial V_g}\right|_{V_{ds}=const.} = \frac{Z}{L}\mu C_i V_{ds} \qquad (11.1)$$

where Z and L are the gate width and length, μ the channel mobility, and C_i the gate capacitance.

At the highest V_{ds} values investigated (-100 V), g_m is found to be 1.56 μS/mm at 150 °C (-6 V $<V_g<$ -2 V), and 174 μS/mm at 300 °C (-10 V $<V_g<$ -8 V); these are the highest transconductance values at these temperatures for polycrystalline diamond (PCD) MISFETs that have been reported. Tessmer *et al.* [1993] have fabricated PCD MISFETs (SiO_2 gate) with transconductance values of 65 nS/mm, 300 nS/mm, and 330 nS/mm at 150 °C, 250 °C, and 285 °C respectively; testing at temperatures greater than 285 °C led to SiO_2 breakdown. Indeed the results obtained here are superior to some homoepitaxially grown diamond FETs; typical g_m of 87 μS/mm (200 °C) and 60 μS/mm (350 °C) from homoepitaxial MISFETs have been reported by Grot *et al.* [1992]. The degraded performance at the higher temperature was attributed to gate leakage. Only a few FETs utilising a diamond gate have been fabricated, but they have not demonstrated superiority over SiO_2 gated FETs. Fujimori *et al.* [1992] have produced homoepitaxial MISFETs (i-D gate) with g_m = 0.5 μS/mm at room temperature, but were leaky at 300 °C. Nishimura *et al.* [1994] fabricated PCD MISFETs that showed a transconductance of 5 μS/mm at room temperature, but they also suffered from excessive leakages. The highest transconductance value to date for CVD diamond has been reported by Fox *et al.* [1995] from homoepitaxial MISFETs with g_m = 1.3 mS/mm at 500 °C, leakage currents <1 nA and breakdown at > 550 °C.

11.5 CONCLUSIONS

The first high temperature thin film polycrystalline CVD diamond p-channel depletion MISFET with an insulating diamond gate has been fabricated which displays low leakage currents, good gate promoted channel current modulation and pinch-off, and high transconductance values (being the highest for PCD FETs at elevated temperatures). The improved interface between the intrinsic diamond gate and the channel layer as compared with SiO_2 gates is believed to account for the superior channel modulation characteristics obtained here. Saturation characteristics were not obtained and improvements in the device structure have to be made. A reduction in the thickness of the channel and the gate insulating layer, together with optimisation of the source and drain implantation depths with respect to the channel layer will improve the characteristics of this device.

REFERENCES

Fox, B.A., Hartsell, M.L., Malta, D.M., Wynands, H.A., Kao, C.T., Plano, L.S., Tessmer, G.J., Henard, R.B., Holmes, J.S., Tessmer, A.J. and Dreifus, D.L., [1995]. *Diamond & Relat. Mater.*, 4, 422.

Fujimori, N. and Nishibayashi, Y., [1992]. *Diamond Relat. Mater.,* **1**, 665.

Geis, M.W., Rathman, D.D., Ehrlich, D.J., Murphy, R.A. and Lindley, W.T., [1982]. *IEEE Electron Device Lett.,* **8**, 341.

Gildenblat, G.Sh., Grot, S.A., Hatfield, C.W. and Badzian, A.R., [1991]. *IEEE Electron Device Lett.,* **12**, 37.

Grot, S.A.,Gildenblat, G.Sh.,Hatfield, C.W. and Badzian, A.R., [1992]. *IEEE Electron Device Lett.,* **13**, 462.

Kiyota, H., Okano, K., Iwasaki, T., Izumiya, H., Akiba, Y., Kurosu, T. and Iida, M., [1991]. *Jpn. J. Appl. Phys.,* **30**, L2015.

Nishimura, K., Kumagai, K.,Nakamura, R. and Kobashi, K., [1994]. *J. Appl. Phys.*, **76**, 8142.

Prins, J.F., [1982]. *Appl. Phys. Lett.,* **41**, 950.

Shiomi, H., Nishibayashi, Y. and Fujimori, N., [1990]. *Jpn. J. Appl. Phys.,* **28**, L2153.

Sze, S.M., [1981]. *Physics of semiconductor devices*, 2nd edition, John Wiley, USA.

Tessmer, A.J., Plano, L.S. and Dreifus, D.L., [1992]. *IEEE Trans. Electron Device,* **39**, 2666.

Tessmer, A.J., Plano, L.S. and Dreifus, D.L., [1993]. *IEEE Electron Device Lett.*, **14**, 66.

Zeisse, C. R., Hewett, C.A., Nguyen, R., Zeidler, J.R. and Wilson, R.G., [1992]. *IEEE Electron Device Lett.*, **12**, 602.

12: CONCLUDING REMARKS

Recent developments in the chemical vapour deposition technique for synthesising uniform films of semiconducting diamond over wide substrate areas have been a primary impetus in the realisation of electronic devices from this material. The many superior material properties as suggested from theory and measurements on natural crystals, promises the introduction of diamond as a superior wide energy bandgap semiconductor. As summarised in Chapter 2, the Johnson, Keyes and Baliga figures of merit predict the superiority of diamond for high power, high frequency and high temperature applications; it is the unique combination of extreme properties that makes diamond attractive. The realisation of high performance electronic devices may only be feasible if the properties of natural diamond are reproduced in the more commercially accessible, and indeed technologically more appropriate, thin film form of the material. At present, homoepitaxial synthesis is evidence that extension of the crystal network of single-crystalline diamond substrates by chemical vapour deposition is possible. However, such an approach is, in itself, certainly not sufficient for the commercial introduction of diamond into the many prospective areas of application. The irregular shapes and sizes of natural or high-pressure high-temperature synthetic material prevents this. Successful heteroepitaxial growth over large areas has at present not been achieved: films deposited on commercially viable substrates typically result in material of a polycrystalline nature, with the individual crystallites being randomly oriented with respect to neighbouring grains. The resulting effect on the transport characteristics have been shown both within this thesis and in the literature to be degraded by at least 1-2 orders of magnitude when compared to the best reports for natural crystals. Nevertheless, as reviewed in Chapter 3, significant progress has been achieved by the separate techniques of mosaic growth, and bias-enhanced nucleation combined with textured growth (BEN). Mosaic growth is currently envisaged as a method for producing high quality templates for the subsequent deposition of semiconducting layers. By the BEN approach, textured material, *i.e.* a predominant crystal faceting, together with crystallite orientation between neighbouring grains and also with the substrate represents current state-of-the-art material: free standing films of this nature is available to thicknesses and areal dimensions of greater than 1 mm and (5 mm x 5 mm), respectively. The top surface grain size is a significant parameter in the performance of diamond films and determines the density of grain boundary defects that charge carriers may encounter in a particular device structure; dimensions of up to 30 μm have been employed within this thesis. In terms of textured-oriented semiconducting diamond films, few reports of the electrical characteristics have existed prior to the study carried out here. The higher levels of conductivity of this material when compared with polycrystalline, textured non-oriented material of comparable grain size and dopant concentration is directly attributed to improvements in carrier mobility. The two previous reports within the literature involving textured-oriented material at lower doping concentrations appear to fit well with the trend observed here; superior carrier mobility is believed to be the result of lower angle grain boundaries. However, as demonstrated here, such benefits are lost when carrier concentrations within the films exceed mid-10^{16} cm^{-3}; this is suggested to arise from a degradation of intra-granular crystalline quality. Since a high activation energy is associated with boron dopants in the diamond lattice, this results in high resistivity material at room temperature unless high dopant levels are employed; the degradation in carrier transport in doped films thus requires further investigation. Basic material characterisation such as cathodoluminescence, transmission electron microscopy and temperature-dependent Hall analysis may aid in the gaining of insight into the nature of such defects and to their reduction. For high temperature applications, the greater population of activated carriers alleviates the need for high doping levels .

In developing diamond as a semiconducting device material, many building blocks in the device engineer's repertoire require significant effort in order to tailor standard fabrication techniques to a material with extreme physical properties. To take a standard electronic device such as the field-effect transistor (FET), fabrication steps typically involve material preparation, photolithography, substrate pattern delineation, insulating layer deposition, selective doping, and metallisation. Many of these areas have been addressed within the course of this thesis and operational devices have been fabricated based on these developments. In order to achieve reliable and reproducible device performance from a material which may vary significantly as a result of the large range of growth techniques and conditions, post-deposition material treatments are considered mandatory. From Auger analysis carried out, as-deposited films may display a surface quality typified by amorphous carbon; it is shown that this layer may be removed by a wet chemical treatment which restores the surface to one that closely resembles natural crystals. As opposed to as-deposited surfaces which are often hydrogen-terminated, this chemical treatment tends to oxidise the diamond surface; the oxidised surface is stable to at least 600 °C and is thus suitable for high temperature devices. For operation in these extreme conditions, contact metallisations on diamond have to be developed to a stage where limitations are not placed on the performance of the material. The ohmic contact formulation of Ti-Ag-Au developed in the course of this work performs reliably to temperatures of at least 400 °C, and perhaps 700 °C. The popularly employed Ti-Au bilayer metallisation is unstable at 400 °C and its stability reported by some in the literature may in part depend on the surface roughness of the diamond. Rectifying contacts on diamond may be considered to be a required development in order to partially compensate for the present lack of a dopant displaying n-type character. In contrast to some previous reports in the literature, bulk properties of the materials may dominate if careful preparation of the material is carried out prior to fabrication of device structures. At sheet resistance levels of > 1200 Ω/square, rectifying characteristics may be obtained, and at doping levels higher than this, then thermionic-field emission is responsible for symmetric electrical behaviour. Al based rectifying contacts have been demonstrated to be stable on oxidised diamond surfaces to temperatures of at least 400 °C, though at these elevated temperatures, the higher degree of activation of impurities lead to a degradation in device behaviour. Since pico-ampere leakage currents have been demonstrated on similar material (doped to $\sim 10^{17}$ cm^{-3}) using the procedures described within this thesis [Whitfield, 1996], a range of material covering the lower doping region of 10^{16}-10^{18} cm^{-3} is suggested for further investigation as such work is not present within the literature. From Figure 6.7, a sharp rise in the active carrier concentration with incorporated boron may lead to concerns regarding the accuracy of dopant control in material of polycrystalline form.

Laser patterning of diamond films using ArF excimer laser has been developed within this thesis to a point where complicated surface patterns may be delineated in a routine and reliable manner. The resultant product shows a good quality of finish with little evidence of surface debris. Instantaneous etch rates have been found to be dependent on the quality of the substrate, incident laser energy density, and the repetition rate of the pulsed source. When compared with literature reports, this rate is at least 1-2 orders of magnitude higher than other proposed dry etching techniques such as ion-beam assisted etching and reactive ion etching. The etch rate may realistically be increased by a factor of 2.5 by altering the repetition rate; at the higher rate of 50 Hz, no significant degradation in the chemical nature of the films was detected by Raman scattering (Chapter 10). A parameter found to alter the nature of the diamond is the laser energy density which, at a high enough level, leads to the formation of graphite as detected by Raman scattering and Auger spectroscopy. At the lowest energy densities found to etch diamond, well defined graphite is not formed but sufficient modification occurs such that electrical characteristics of Ti-based contacts may be altered. The laser energy densities required to induce these effects is found to be dependent on the initial quality of the diamond films. The processing ambient is also found to be critical towards maintaining the quality of the films; processing *in-vacuo* leads to the formation of graphite. Oxygen radical formation in a photochemical-based mode with subsequent formation of CO or CO_2 is the most likely candidate for preventing graphitic formation.

The fact that oxygen is a fundamental component in the excimer laser processing of diamond at 193 nm facilitates design of the overall system in that no demands are made for vacuum requirements as in the case of reactive-ion etching and ion-beam techniques. Improvements in the control of the laser beam, viewing optics for multi-level alignment, projection lens design, and accuracy of "stitching" patterns on the substrate are all system issues being addressed in the projection patterning type systems used in this thesis. The shorter wavelength of the radiation, the maskless approach for single step lithography, and areal selectivity are seen as strong advantages in what is a consistent development in the philosophy of optical lithographic techniques. The advance in excimer lasers such that repetition rates of 300 Hz may now be obtained industrially means that deep structures (*e.g.* >10μm) pertaining to three-dimensional microstructures for micro-electromechanical applications may be produced at a commercially viable rate. The fabrication of 80 μm thick free standing structures demonstrates the feasibility of laser patterning of diamond for these applications. However, non-vertical sidewalls have been revealed which responds to laser intensity; current efforts to overcome this phenomenon within other material systems suggests that this is a systems-related problem. Improvements in the current experimental set-up are required for further investigations. At the other extreme, surface patterns of 2-3 μm wide lines have been delineated on diamond corresponding to the limits of the projection lens employed. Improvements in lens design and optical materials at the operational wavelength of 193 nm suggests that future linewidth requirements of <0.2 μm will be met.

The principles of surface preparation, contact metallisations and device fabrication techniques presented in this thesis have been employed in several device implementations. Field-effect transistors based on the MISFET structure have been designed and fabricated on polycrystalline diamond. An intrinsic diamond gate has been employed as the insulating layer to demonstrate current modulation at operational temperatures of 150 °C and 300 °C. This device represents the first high temperature thin film polycrystalline diamond MISFET with an insulating diamond gate which displays low leakage currents, good gate promoted channel modulation and pinch-off, and high transconductance values. However, ideal electrical characteristics have not been observed and work is currently undergoing to obtain current saturation and lower current leakage levels. Thin film diamond photodetectors operating within the ultraviolet region of the spectrum in a "visible-blind" manner have also been demonstrated. With strict material preparation and design methodology such devices may be fabricated from current polycrystalline material; photoconductors fabricated in a quasi-single crystalline manner (contact spacing less than average grain size) have shown unprecedented performance levels as shown in Figure 12.1 [McKeag, 1996]. In the photodiode mode, rectifying contacts employing material of a dopant concentration based on the results in Chapter 8 have also been engineered to respond to UV in a visible-blind manner; sub-picoampere leakage currents have been obtained [Whitfield, 1996].

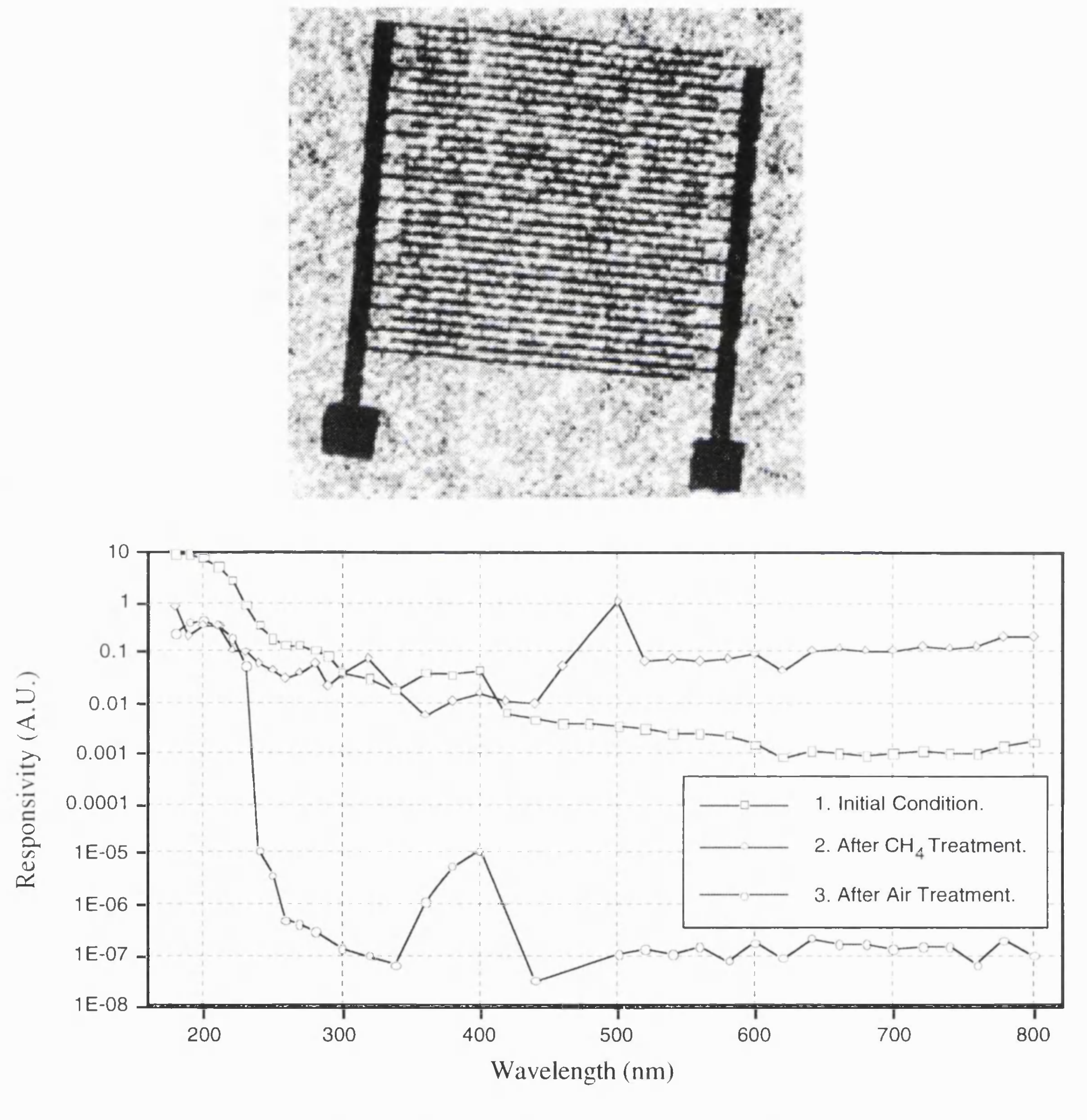

Figure 12.1 Photoconductor fabricated from polycrystalline diamond film and associated performance. Optimal performance is only obtained after gas treatments as described in [McKeag, 1996].

The improving characteristics of many classes of electronic devices from thin film diamond is encouraging for the commercial realisation of applications based on this material. The improvements achieved over the past years have primarily arisen from advances in the quality of the material such as the intrinsic diamond content to the availability of thick films where the grain sizes may be an order of magnitude greater. In order to obtain reliable characteristics in a routine fashion, all aspects of the device fabrication procedure have to be optimised and controlled; this thesis has addressed many of these issues to a point where such devices may be produced. For continued progress in the performance of diamond based devices, further investigations have to be made into areas such as selective doping by ion implantation, insulating diamond layers, and polishing/ smoothening of as-deposited diamond films. At present, the rough nature of as-deposited films places strict demands on the photolithographic process during device fabrication, and as such, limits the grain size of the material which may be employed (grain size directly corresponds to thickness and hence surface roughness). Promising reports by others demonstrating diamond polishing by excimer laser techniques suggests the possible integration with the etching method discussed in this thesis.

Although heteroepitaxial growth and n-type doping would represent significant achievements in the proposal for diamond-based electronic applications, Fox and co-workers [1994] have recently revealed carrier transport properties in homoepitaxial films within a factor of two of single-crystalline material. Corresponding advances in the thin film form diamond both in basic material quality, and in the eradication of defects present in doped material as identified in this thesis, will allow the commercialisation of diamond electronic devices to be considered. Understanding the specific characteristics of this material such as the high dopant activation energies will enable device designs and intended applications to be judged accordingly for the introduction of diamond as a wide energy bandgap semiconductor.

REFERENCES

Fox, B.A., Hartsell, M.L., Malta, D.M., Wynands, H.A., Kao, C.T., Plano, L.S., Tessmer, G.J., Henard, R.B., Holmes, J.S., Tessmer, A.J. and Dreifus, D.L., [1995]. *Diamond & Relat. Mater.*, 4, 422.

McKeag, R.D., Chan, S.S.M. and Jackman, R.B., [1995]. *Appl. Phys. Lett.,* **67**, 2117.

Whitfield, M.D., Chan, S.S.M. and Jackman, R.B., [1996]. *Appl. Phys. Lett.,* **68**, 290.

(A) GLOSSARY

AES	auger electron spectroscopy
BFOM	baliga figure of merit
BHFFOM	baliga high frequency figure of merit
CVD	chemical vapour deposition
DCCVD	direct current chemical vapour deposition
DLC	diamond-like carbon
ECR	electron cyclotron resonance
FWHM	full width at half maximum
HFCVD	hot-filament chemical vapour deposition
homo	homoepitaxial diamond film
HPHT	high-temperature high-pressure
I-V	current-voltage
JFOM	johnson figure of merit
KFOM	keyes figure of merit
MEMS	micro-electromechanical systems
MESFET	metal semiconductor field effect transistor
MISFET	metal-insulator semiconductor field effect transistor
MPCVD	microwave plasma enhanced chemical vapour deposition
poly	polycrystalline diamond possessing non-oriented and non-textured grains
RFCVD	radio frequency chemical vapour deposition
RIE	reactive ion etching
SEM	scanning electron microscopy
SIMS	secondary ion mass spectroscopy
T&O	polycrystalline diamond possessing grains of a textured and oriented nature
T&R	polycrystalline diamond with textured and randomly oriented grains

(B.1) De-grease formulation

Reagents:
- (i) 1,1,1-trichloroethane
- (ii) acetone
- (iii) 2-propanol (IPA)
- (iv) de-ionised (DI) water

Procedure:

(i) Place sample in 1,1,1-trichloroethane (40 °C) for 5 mins.
(ii) Transfer to acetone at room temperature for 2 mins.
(iii) Transfer to 2-propanol at room temperature for 2 mins.
(iv) Transfer to DI water at room temperature for 2 mins.
(v) Remove excess water with blowing nitrogen.
(vi) Dry sample in oven at 120 °C for 2 mins.

N.B. When transferring samples between solvents it is important to prevent the samples from drying out, as surface residue precipitated from one solvent may be insoluble in the next.

(B.2) Acid treatment formulation

Reagents:
- (i) concentrated sulphuric acid (H_2SO_4)
- (iia) ammonium persulphate ($(NH_4)_2S_2O_8$)
- (iib) chromium trioxide (CrO_3)
- (iii) hydrogen peroxide (H_2O_2)
- (iv) ammonium hydroxide (NH_4OH)

Procedure:

(i) Measure a saturated solution of c-H_2SO_4 with the oxidising agent *i.e.* ammonium persulphate or chromium trioxide; this is the ETCH solution.
(ii) Make up a RINSE solution which consists of a 1:1 mix of hydrogen peroxide and ammonium hydroxide.
(iii) Heat the samples in the ETCH solution at 200 °C for 20 min; white fumes of SO_3 will be evident from temperatures of 140 °C.
(iv) Transfer the samples from the ETCH solution when it cools from 200 °C to 50 °C to the RINSE solution which is heated to a bubbling state (~50°C).
(v) Transfer the sample to DI water after 10 mins in the RINSE solution.
(vi) Rinse samples throroughly and place into oven at 120 °C for 5 min to remove surface moisture.

(C) Fabrication of contact metallisation test structures

(a) Central contact definition Al (etching technique), Ni (lift-off) technique

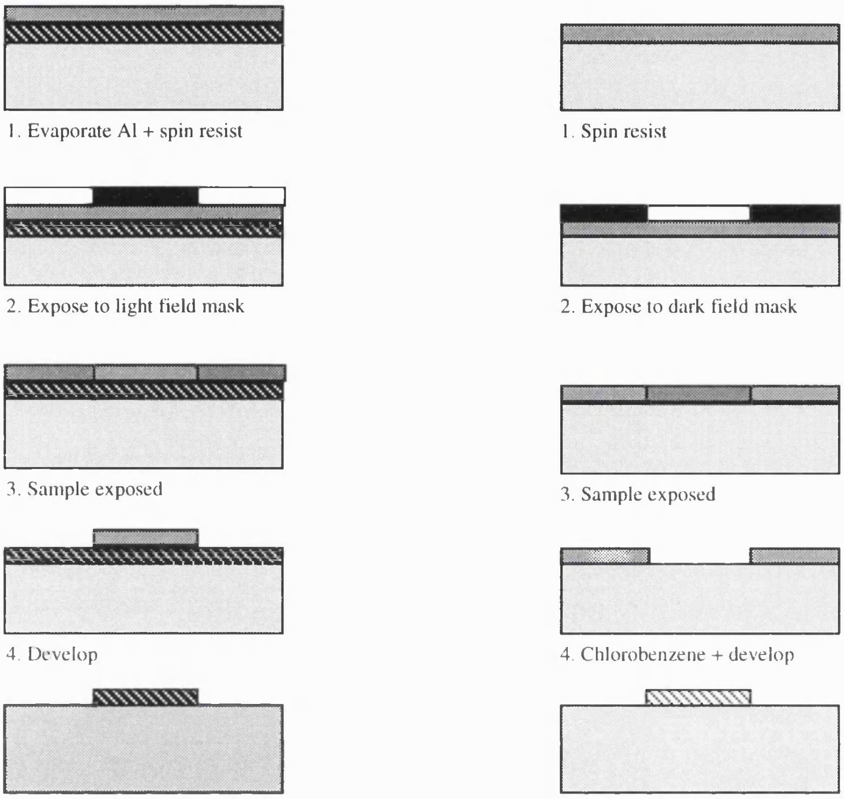

1. Evaporate Al + spin resist
2. Expose to light field mask
3. Sample exposed
4. Develop
5. Etch Al + get rid of photoresist

1. Spin resist
2. Expose to dark field mask
3. Sample exposed
4. Chlorobenzene + develop
5. Evaporate Ni + lift off

(b) Fabrication procedure for metal overlayer

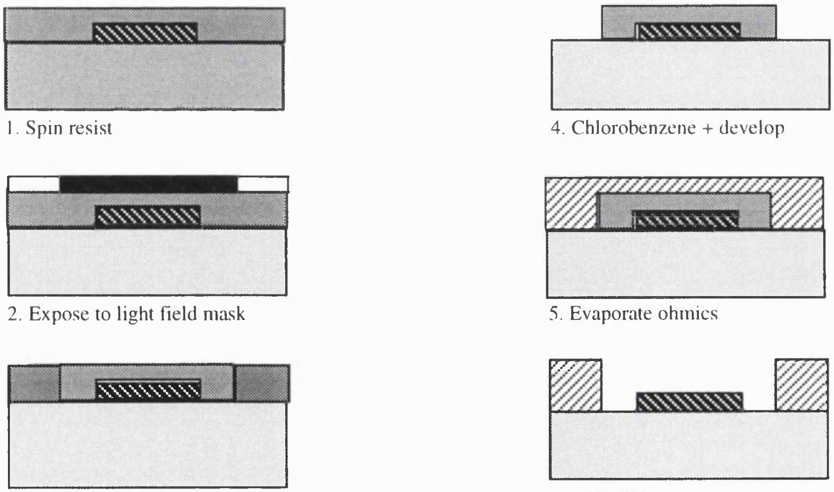

1. Spin resist
2. Expose to light field mask
3. Sample exposed
4. Chlorobenzene + develop
5. Evaporate ohmics
6. Lift off in acetone

(D) Thermionic-field emission

Current transport by tunnelling across a potential barrier in the thermionic-field emission regime has been approximated by previous authors including Padovani and Stratton: their work has been summarised in the book by Rhoderick and Williams [1988]. The reverse chracteristics are given as:

$$J = -J_s \exp\left(\frac{V_R}{E^*}\right) \tag{D.1}$$

where

$$E^* = \frac{E_{00}}{\left\{\left(\frac{qE_{00}}{k_B T}\right) - \tanh\left(\frac{qE_{00}}{k_B T}\right)\right\}}; \tag{D.2}$$

V_R is the applied reverse voltage and the saturation current Js is given by:

$$J_s = \frac{A^* T\left(\pi q E_{oo}\right)^{1/2}}{k_B}\left\{q\left(V_R - \xi\right) + \frac{q\phi_b}{\cosh^2\left(\frac{qE_{oo}}{k_B T}\right)}\right\}^{1/2} \exp\left(-\frac{\phi_b}{E_0}\right). \tag{D.3}$$

The characteristic energy parameter E_{OO}, and E_O is given as:

$$E_{oo} = \frac{\hbar}{2}\left[\frac{N_A}{m^* \varepsilon_s}\right]^{1/2} \quad ; E_o = E_{oo}\coth\left(\frac{qE_{oo}}{k_B T}\right); \tag{D.4; D.5}$$

and

$$\xi = E_{FS} - E_V = k_B T \ln\left(\frac{N_V}{p}\right) \quad ; N_V = 2\left(\frac{2\pi m^* k_B T}{h}\right)^{3/2}. \tag{D.6; D.7}$$

k_B is Boltzmann constant, T is the absolute temperature (300 K), A^* is the Richardson constant (Equation 8.2c), q is the electronic charge, ϕ_b is the barrier height, $\hbar = h/2\pi$, N_A is the acceptor concentration, m^* is the effective mass, ε_s is the semiconductor permittivity, ξ is the difference between the fermi level within the semiconductor and the top of the valence band, N_V is the effective density of states within the valence band and p is the carrier concentration.

(For the calculation of Figure 8.6, the following constants have been used: V_R = 2 V, m^* = 0.75 m_O and ϕ_b = 1.22 eV.)

(E) Fabrication of insulated-gate field effect transistor

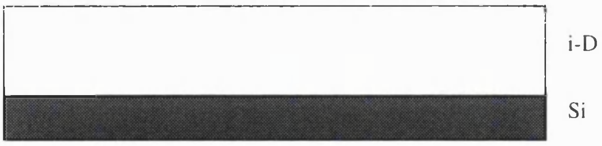

(a) Intrinsic diamond layer on silicon

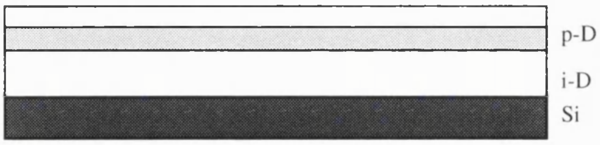

(b) Ion implantion of channel layer

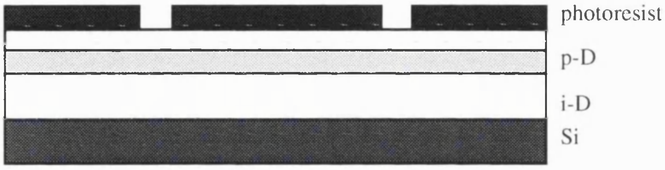

(c) Photolithography to define SOURCE and DRAIN

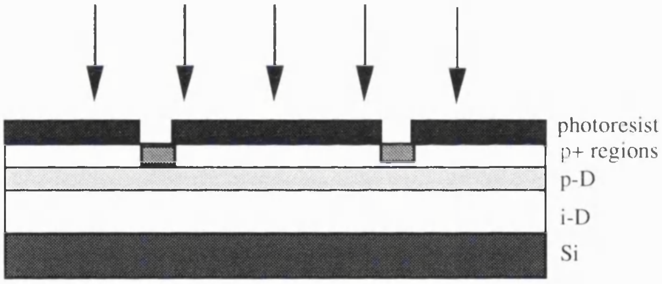

(d) Ion implantation of SOURCE and DRAIN regions

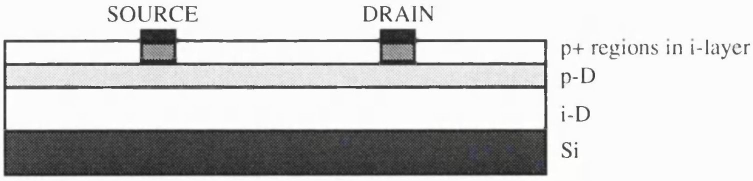

(e) Photolithography and deposition of OHMIC contacts

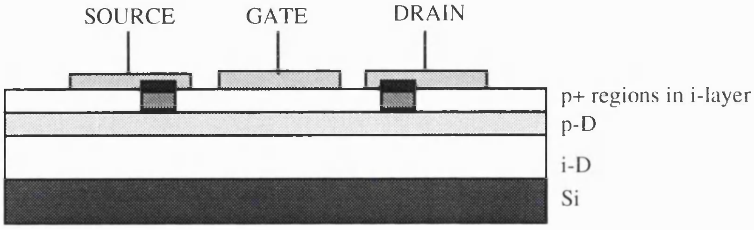

(f) Photolithography and deposition of GATE contact

(F) Publications related to this thesis:

[1] "Al and Ni contact metallisations on thin film CVD diamond"
SSM Chan, C Peucheret, RD McKeag, RB Jackman, C Johnston, PR Chalker.
J. Appl. Phys. **78** (1995) 2877.

[2] "High temperature stability of chemically vapour deposited diamond diodes"
RD McKeag, SSM Chan, RB Jackman, C Johnston and PR Chalker.
Mater. Science. Eng. **B29** (1995) 223.

[3] "Polycrystalline diamond photoconductive device with high UV-vis discrimination"
RD McKeag, SSM Chan and RB Jackman.
Appl. Phys. Lett., **67** (1995) 2117.

[4] "Thin film diamond microstructures by excimer laser projection patterning"
SSM Chan, RB Jackman, G Arthur, F Goodall and RA Lawes.
Diamond Films & Technol., **5** (1995) 291.

[5] "Laser projection patterning for the formation of thin film diamond microstructures"
SSM Chan, RB Jackman, F Raybould, G Arthur and F Goodall.
Diamond & Related Materials., **5** (1996) 317.

[6] "Thin film diamond photodiode"
MD Whitfield, RD McKeag, SSM Chan and RB Jackman.
Appl. Phys. Lett.. **68** (1996) 290.

[7] "Thin film diamond UV photodetectors: photodiodes compared to photoconductive devices for highly selective wavelength response"
MD Whitfield, RD McKeag, LYS Pang, SSM Chan and RB Jackman.
Diamond & Related Materials., **5** (1996) 829.

[8] "Cleaning thin film diamond surfaces for device fabrication: an Auger electron spectroscopic study "
B Baral, SSM Chan and RB Jackman.
J. Vac. Sci. Technol. **B**. In press (August 1996).

[9] "Diamond UV Photodetectors"
SSM Chan, MD Whitfield, RD McKeag and RB Jackman
Physica Status Solidi (a), **154** (1996)445.

[10] "High performance thin film diamond UV photodetectors"
RD McKeag, MD Whitfield, SSM Chan and RB Jackman.
Mater. Res. Soc. Symp. Proc. In press.

[11] "Characterisation of excimer laser modified thin film diamond"
SSM Chan, MD Whitfield and RB Jackman.
J. Appl. Phys.. Submitted.

[12] "Carrier transport within p-type highly oriented (100) textured diamond films"
SSM Chan, PR Chalker, C Johnston and RB Jackman.
J. Appl. Phys.. Submitted.

[13] "Thin film diamond transistors for high temperature applications"
LYS Pang, SSM Chan, RB Jackman, C Johnston and PR Chalker.
Mater. Sci. Eng. Accepted for publication.

[14] "A thin film diamond p-channel field-effect transistor"
LYS Pang, SSM Chan, RB Jackman, C Johnston and PR Chalker.
Appl. Phys. Lett. Submitted.